Covalent funtionalization of carbon nanomaterials for bioelectrochemical applications

Naoual Allali

UNIVERSITÉ DE LORRAINE

COLLEGIUM SCIENCES ET TECHNOLOGIE

Ecole Doctorale Chimie, Mécanique, Matériaux, Physique (C2MP)

PhD thesis

submitted on the 6th of February 2019 to obtain the grade of:

DOCTOR of the University of Lorraine

in **Chemistry**

by

Naoual Allali

Covalent functionalization of carbon nanomaterials for bioelectrochemical applications

---

Referees:
Dr. Cécilia Menard-Moyon, Institut de Biologie Moléculaire et Cellulaire, CNRS UPR 3572, Strasbourg, France.
Pr. Thomas Wagberg, Physics Department, Umeå University, Umeå, Sweden.

Examiners:
Pr. Alexander V. Soldatov, Department of Engineering Sciences and Mathematics, Luleå University of Technology, Luleå, Sweden (co-supervisor).
Dr. Manuel Dossot, LCPME, UMR CNRS-University of Lorraine n° 7564, Villers-lès-Nancy, France (co-supervisor).

Invited:
Dr. Victor Mamane, Institut de Chimie de Strasbourg, UMR CNRS-University of Strasbourg n° 7177, Strabourg, France (co-supervisor).
Pr. Mikael Sjödahl, Department of Engineering Sciences and Mathematics, Luleå, Sweden.

UMR CNRS-Université de Lorraine n°7053 L2CM et UMR CNRS-Université de Lorraine n°7564 LCPME
Faculté des Sciences et Technologies
Université de Lorraine

Preface

“No one succeeds without effort... Those who succeed owe their success to perseverance.”

Ramana Maharshi

Abstract

Carbon nanotubes (CTNs) are renowned for their exceptional electronic and mechanical properties. Their structure can be considered as rolling up a graphene sheet along a specific crystallographic direction, leading to a 1D confinement of the electronic wavefunction of the π delocalized electrons along the perimeter of the cylindrical structure thus obtained. This confinement produces the existence of defined spikes of high intensity in the electronic density of states, called van Hove singularities. These singularities are primordial to understand both the optical and electronic properties of CNTs through electron-phonon coupling processes. If the electronic density of states (DoS) is non-zero at the Fermi level the nanotube is metallic, otherwise the nanotube is semiconducting. The synthesis of CNTs always produces a mixture of both metallic and semiconducting nanotubes, and this material can be useful to be incorporated at the surface of electrodes for electrochemical devices. The high specific surface area, the high mechanical and thermal stability of CNTs and the low percolation threshold for electron transport in a mat of CNTs render them very attractive for such kind of applications. There is yet a drawback of using raw CNTs: they are not compatible with solvents and modification of their surfaces by chemistry is required to make good suspensions for easy deposition at the electrode surface and to introduce specific functional groups for promoting electron transfer, called electron shuttles.

The final aim of this thesis is therefore the covalent functionalization of CNTs by electron shuttles and their incorporation at the surface of glassy carbon electrodes for electrochemical devices application. A strategy of chemical grafting in three steps has been chosen: i) a controlled oxidation step in acidic media assisted by microwave irradiation in order to keep the structural integrity of CNTs, so as to save their useful electronic properties; ii) a chloration step to produce acid chloride groups and iii) reaction of these groups with electron shuttles modified by specific linkers. The study was first conducted on very clean HiPCO single-walled CNTs (SWCNTs). This enabled to avoid any disturbing effects of carbonaceous impurities or residual catalytic particles, since their possible effects are extremely controversial in the literature. Once validated, this approach was then conducted with cheaper material including few-walls carbon nanotubes (FWCNTs). The use of FWCNTs compared to SWCNTs was not only beneficial for the production of cost-effective electrochemical devices but also for a better durability of the final device, the inner nanotubes being not functionalized.

The challenge was to obtain a functionalization process with enough grafted electron shuttles to obtain a good electrocatalytic activity but maintaining CNTs integrity. The first step is predominant to reach this goal, and requires a very accurate understanding of the nature and the number of defects created in the CNTs structure versus the physico-chemical conditions used. The introduction of defects in the crystallographic structure of CNTs has strong consequences both for the electronic DoS and for the phononic properties of the material. Spectroscopic methods are essential in

probing these consequences. UV-visible-near IR absorption spectroscopy is the method of choice to directly probe the existence of van Hove singularities and the oscillator strength associated with the authorized electronic transitions between these singularities. Covalent grafting of chemical groups at the surface of CNTs changes both the energy and the intensity of these transitions. However, this spectroscopic method requires solubilizing CNTs in non-absorbing solvents using adequate surfactants. Interactions between surfactant molecules and CNT sidewalls may also alter the position and intensity of electronic transitions between van Hove singularities unrelated to the chemical groups covalently grafted.

Raman spectroscopy of CNTs involves the electron-phonon coupling processes through the resonant electronic enhancement of Raman modes. Double resonance processes are also observed in Raman spectrum of CNTs, for instance with the D-band mode that is actually related to the existence of defects in the graphene structure of CNTs. Therefore, Raman spectroscopy is a widespread analytical method to characterize the structural defects created by covalent functionalization processes. Indeed, the intensity ratio of the D and G bands in the Raman spectrum is correlated to the number of defects. However, CNTs are used as bundles when chemical functionalization is performed, which produces a heterogeneous distribution of chemical species grafted on CNTs. Therefore, we have developed a new protocol to obtain statistically significant data for most of the samples made in this thesis. Nevertheless, this statistical approach is still limited for samples slightly functionalized, whence the idea to use spectroscopic ellipsometry as an alternative method to characterize these samples.

More specifically, ellipsometric data were collected from UV to the IR part of the electromagnetic spectrum for CNTs functionalized in different conditions. The complex dielectric function was retrieved from the experimental data. A Drude model was used to model the infrared part of the data for raw and acid oxidized CNTs. The optical conductivity of the samples was obtained. These results, combined with other information collected using a set of complementary analytical techniques (Raman scattering, UV-visible-NIR absorption, X-ray photoelectron spectroscopy, thermogravimetric analysis coupled to mass spectrometry, transmission electron microscopy and rare gas volumetric adsorption), show that the microwave-assisted oxidation process actually consists in removing amorphous carbon deposits away from the surface of CNTs and transforming the already existing defects in the CNT structure to oxygen-containing groups such as carboxylic acids .

Rare gas volumetric adsorption was also used to compare the distribution of chemical groups at the surface of CNT bundles when two different acids are used (HNO_3 and H_2SO_4). The chloration step was also studied by these methods, as well as the final grafting of electron shuttles. Finally, these functionalized CNTs were deposited at the surface of glassy carbon electrodes and used as electron mediators for diaphorase-catalysed oxidation of nicotinamide adenine dinucleotide (NADH). This was a good example of mediated electron transfer for development of electrochemical devices based

on NADH recycling and it validated the good electrocatalytic properties of functionalized CNTs for making electrochemical sensors and actuators, opening new perspectives with potential market applications.

Keywords: Carbon nanotubes (CNTs); Functionalization/chemical modification; Raman; ellipsometry; volumetric adsorption.

Acknowledgements

My first thanks go of course to my three thesis supervisors, Victor MAMANE, Manuel DOSSOT and Alexander V. SOLDATOV. I am deeply grateful to them for having made me benefit throughout this thesis from their great competence, their intellectual rigor, their dynamism, their effectiveness, their complementarity and their certain humanity that I will never forget and that gave me the hope to continue every time when I felt demotivated. It is through these qualities that they have made these years pleasant and enriching. Be assured of my attachment and deep gratitude.

I would like to warmly thank our "scientific sponsor" Dr. Edward McRAE, for his support, his time, his valuable advice, but beyond his undeniable scientific knowledge, for his human qualities and his constant and unconditional encouragement.

I would like to thank all the collaborators of this project, Alain WALCARIUS, Yves FORT, Mathieu ETIENNE, Martine MALLET, Brigitte VIGOLO, Chris EWELS, Yann BATTIE and Xavier DEVAUX, who marked my learning of the characterization techniques used in this work. I would therefore like to thank them for their efficiency, their invaluable help in interpreting the results and, above all, for the time they have devoted to the success of this project.

I am much honored to thank Dr. Cecilia MENARD-MOYON and Pr. Thomas WAGBERG, for having kindly done me the honor of reporting and examining this work and participating in the thesis jury.

On a more personal note, I would like to thank my husband, Youssef, very warmly for the great patience, encouragement and trust he has shown me. I would like to thank him especially for his uninterrupted moral support. Many thanks to my mother, my daughters and all my big family, for their support, encouragement, and love that was very useful to me during my thesis.

Finally, a special and posthumous thank you to my father, who passed away too early, who always motivated me in my studies, and dreamed of seeing me as a Doctor one day.

List of papers

1. **Accurate control of the covalent functionalization of single-walled carbon nanotubes for the electro-enzymatically controlled oxidation of biomolecules**
By Allali, Naoual; Urbanova, Veronika; Etienne, Mathieu; Devaux, Xavier; Mallet, Martine; Vigolo, Brigitte; Adjizian, Jean-Joseph; Ewels, Chris P.; Oberg, Sven; Soldatov, Alexander V.; et al
Beilstein Journal of Nanotechnology (**2018**), 9, 2750-2762. DOI:10.3762/bjnano.9.257

2. **Mild covalent functionalization of single-walled carbon nanotubes highlighted by spectroscopic ellipsometry**
By Battie, Yann; Dossot, Manuel; Allali, Naoual; Mamane, Victor; Naciri, Aotmane En; Broch, Laurent; Soldatov, Alexander V.
From Carbon (**2016**), 96, 557-564. DOI:10.1016/j.carbon.2015.09.066

3. **Covalent Functionalization of HiPco Single-Walled Carbon Nanotubes: Differences in the Oxidizing Action of H2SO4 and HNO3 during a Soft Oxidation Process**
By Devaux, Xavier; Vigolo, Brigitte; McRae, Edward; Valsaque, Fabrice; Allali, Naoual; Mamane, Victor; Fort, Yves; Soldatov, Alexander V.; Dossot, Manuel; Tsareva, Svetlana Yu.
From ChemPhysChem (**2015**), 16(12), 2692-2701. DOI:10.1002/cphc.201500248

4. **Functionalized carbon nanotubes for bioelectrochemical applications: Critical influence of the linker**
By Urbanova, Veronika; Allali, Naoual; Ghach, Wissam; Mamane, Victor; Etienne, Mathieu; Dossot, Manuel; Walcarius, Alain
From Journal of Electroanalytical Chemistry (**2013**), 707, 129-133. DOI:10.1016/j.jelechem.2013.08.029

5. **Electrocatalytic effect towards NADH induced by HiPco single-walled carbon nanotubes covalently functionalized by ferrocene derivatives**
By Allali, Naoual; Urbanova, Veronika; Etienne, Mathieu; Mallet, Martine; Devaux, Xavier; Vigolo, Brigitte; Fort, Yves; Walcarius, Alain; Noel, Maxime; McRae, Edward; et al
From MRS Online Proceedings Library (**2013**), 1531(Low-Voltage Electron Microscopy and Spectroscopy for Materials Characterization), 2013.84/1-2013.84/6. DOI:10.1557/opl.2013.84

6. **Few-wall carbon nanotubes covalently functionalized by ferrocene groups for bioelectrochemical devices**
By Allali, Naoual; Urbanova, Veronika; Mamane, Victor; Waldbock, Jeremy; Etienne, Mathieu; Mallet, Martine; Devaux, Xavier; Vigolo, Brigitte; Fort, Yves; Walcarius, Alain; et al
From MRS Online Proceedings Library (**2012**), 1451(Nanocarbon Materials and Devices), No pp. given. DOI:10.1557/opl.2012.1337

7. **Covalent functionalization of few-wall carbon nanotubes by ferrocene derivatives for bioelectrochemical devices**

By Allali, Naoual; Urbanova, Veronika; Mamane, Victor; Waldbock, Jeremy; Etienne, Mathieu; Mallet, Martine; Devaux, Xavier; Vigolo, Brigitte; Fort, Yves; Walcarius, Alain; et al

From Physica Status Solidi B: Basic Solid State Physics (**2012**), 249(12), 2349-2352. DOI:10.1002/pssb.201200098

Contents

Abbreviations

All abbreviations are defined in the text but here are reproduced the most useful ones:

CNT: Carbon nanotubes
f-CNT: Functionalized carbon nanotubes
SWCNT: Single-walled carbon nanotubes
FWCNT: Few-walled carbon nanotubes (3-5 walls)
MWCNT: Multi-walled carbon nanotubes
CVD: Chemical vapor deposition
DOS: Density of (electronic) states
GCE: Glassy carbon electrode
HR-TEM: High-resolution transmission electron microscopy
SEM: Scanning electron microscopy
STEM: Scanning transmission electron microscopy
EELS: Electron energy loss spectroscopy
EDS: Energy-dispersive X-Ray spectroscopy
TGA: Thermogravimetric analysis
FTIR: Fourier-transform infrared spectroscopy
DRIFT: Diffuse reflectance infrared Fourier-transform spectroscopy
ATR: attenuated total reflection
UV-vis: Ultraviolet and visible absorption
XPS: X-ray absorption spectroscopy
MS: Mass spectrometry
NADH: nicotinamide adenine dinucleotide (reduced form)
NAD^+: nicotinamide adenine dinucleotide (oxidized form)

1 General introduction to the research project.

1. Carbon Nanotubes (CNTs): an allotropic family of carbon materials with remarkable properties.

1.1. Structure, mesh, reciprocal lattice and chiral indices.

Carbon nanotubes (CNTs) constitute a tubular allotropic variety of the element Carbon. These filament-shaped structures have been observed several times through electron microscopy since the 1960s, (Boehm, 1997; Monthioux, 2006) but Iijima's article of 1991 (IIjima, 1991) is considered as the first article describing the interest of these structures. CNTs are formed of hexagons of sp^2 hybridized carbon atoms, thus forming delocalized electronic π-bonds on the hexagonal rings. As a result, the structure of these nanotubes can be described formally as a rolling up of a graphene sheet (an isolated plane of hexagons of sp^2 hybridized carbon atoms) along a given axis, with a perfect edge-to-edge matching of each carbon atom so as to maintain a hexagonal structure all along the resulting tube. Rolling of a single sheet leads to a single-walled CNT (SWCNT). During the synthesis of these structures, it is possible to SWCNTs. It is also possible to obtain several tubes embedded concentrically within each other: double-walled for two tubes, triple-walled for three tubes, and multi-walled as soon as the number of tubes is greater than 3 (MWCNT).

Figure 1 shows some transmission electron microscopy (TEM) images obtained with samples of mono, double and multi-walled CNTs.

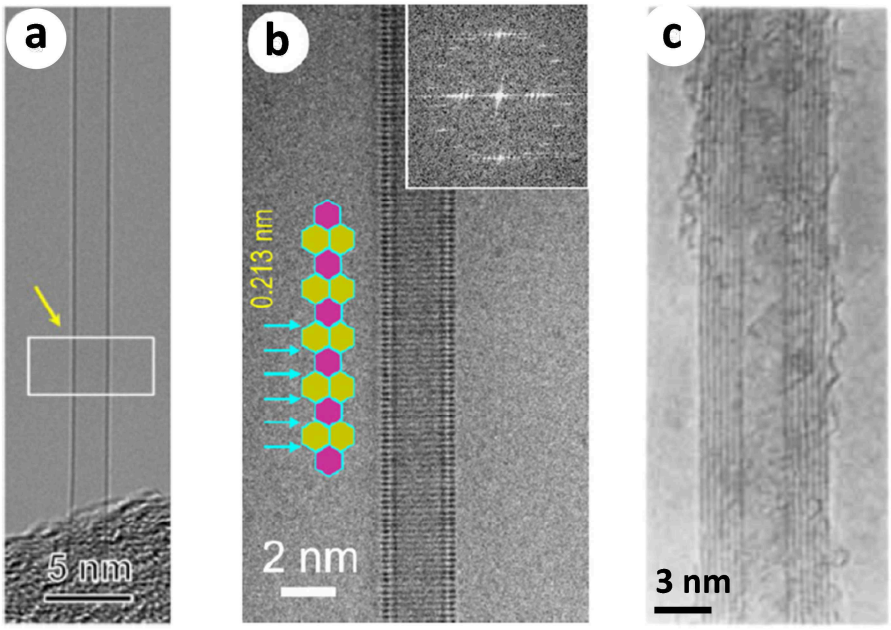

Figure 1: some examples of carbon tubular structures observed in transmission electron microscopy: a) single-walled nanotube, b) double-walled nanotube, the insert at the top right shows the Fourier transform of the image, and c) multi-walled nanotubes. a and b: Adapted from the reference (Jang, et al., 2012); c: adapted from the reference (IIjima, 1991)

The formation of a SWCNT can be pictured as illustrated in Figure 2. Doing so, it is possible to define a rolling vector, denoted C_h in Figure 2, and which will be equal in norm to the circumference of the obtained nanotube.

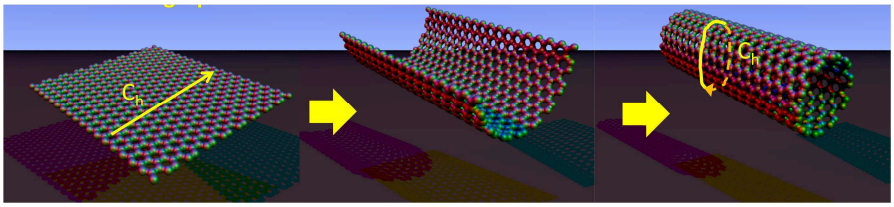

Figure 2: a SWCNT can be structurally described from a graphene sheet which is rolled on itself in a given direction. Adapted from https://en.wikipedia.org/wiki/Carbon_nanotube#.

The crystallographic description of a CNT can therefore be based on the crystalline lattice of graphene. Figure 3 represents in a) the direct network with a possible choice of two vectors $\overrightarrow{a_1}$ et $\overrightarrow{a_2}$ of the primitive mesh and in b) the corresponding reciprocal lattice, with in gray the corresponding Brillouin zone (Wigner-Seitz mesh of the reciprocal network). The mesh of the direct network contains 2 carbon atoms which have been represented in two different colors in the figure. The vectors $\overrightarrow{b_1}$ et $\overrightarrow{b_2}$ of the reciprocal network are such that:

Equation 1

$$\vec{b}_i . \vec{a}_j = 2\pi\delta_{ij}$$

With δ_{ij} the Kronecker symbol (δ_{ij} = 1 if i = j, 0 if not).

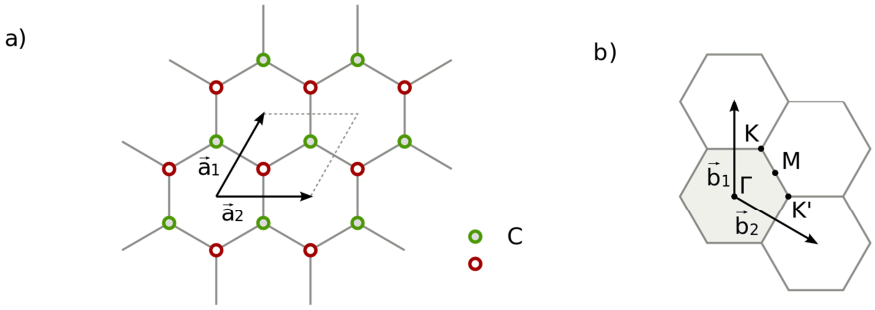

Figure 3: a) the direct network of graphene with two vectors $\boldsymbol{a_1}$ *and* $\boldsymbol{a_2}$ *of the primitive mesh, and the two atoms per mesh illustrated in red and green. B) The reciprocal lattice of graphene with the two basic vectors* $\boldsymbol{b_1}$ *and* $\boldsymbol{b_2}$*, as well as the points of high symmetry Γ (center of zone), K/K' et M.*
Credit : https://commons.wikimedia.org/wiki/File:Real_and_reciprocal_space_unit_vectors_of_graphene_lattice.svg

Points Γ (the center of the Brillouin zone), K/K' and M are points of high symmetry of the Brillouin zone of graphene, and it is interesting to represent the evolution of energy densities (electronic or phononic) on the lines connecting these different points, in order to understand the electronic and vibrational properties of graphene. It will then be necessary to adapt this description to the fact that the CNTs are rolled graphene structures, which will introduce a condition of quantification of the electronic wave vectors along the diameter of the nanotubes (see section 1.3).

We decompose the rolling vector $\mathbf{C_h}$ of the graphene sheet, which will define a given type of nanotube, on the basis vectors of the direct network. It uses two indices (n, m) called the chirality indices or chiral indices of the CNT:

Equation 2

$$\boldsymbol{C_h} = n\overrightarrow{a_1} + m\overrightarrow{a_2}$$

Figure 4 gives the example of a (4,2) nanotube. We can also define the translation vector **T** so that its scalar product with $\mathbf{C_h}$ is zero. The parallelepipedal space delimited by the vectors $\mathbf{C_h}$ and **T** on the graphene network represents the elementary cell of the CNT, which can be reproduced "forever" via the translation vector **T**. We can also define the "angle of chirality" θ , which is the angle between the basis vector $\overrightarrow{a_1}$ and the vector $\mathbf{C_h}$.

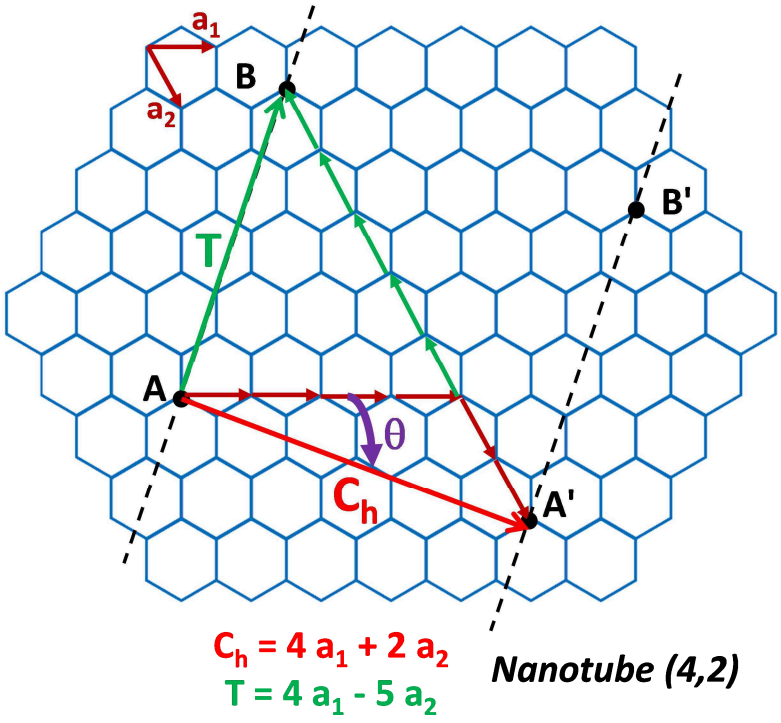

*Figure 4 : definition of rolling and translation vectors $\boldsymbol{C_h}$ and **T** with chirality indices (n,m) for the example of a (4,2) nanotube. The nanotube is formed by folding the graphene sheet and joining for example points A and B at the respective points A 'and B', and sticking seamlessly the carbon atoms side by side.*

Figure 5 shows the three types of SWCNTs that can be obtained depending on the value of the angle of chirality θ. If θ = 0° (zig-zag nanotube) or θ = 30° (armchair nanotube), the resulting tube is not chiral because a plane perpendicular to the nanotube becomes a plane of symmetry, and the image of the nanotube in a mirror is then exactly superimposed on that of the starting nanotube. If 0° < θ < 30°, this plane of symmetry disappears and the nanotube becomes chiral. We will also see in section 1.3 that, depending on the values of the chiral indices (n, m), the CNTs can have either a metal-type conductivity or behave like semiconducting materials (but one-dimensional, which

offers very interesting prospects in molecular electronics for the fabrication of nanoscale transistors).

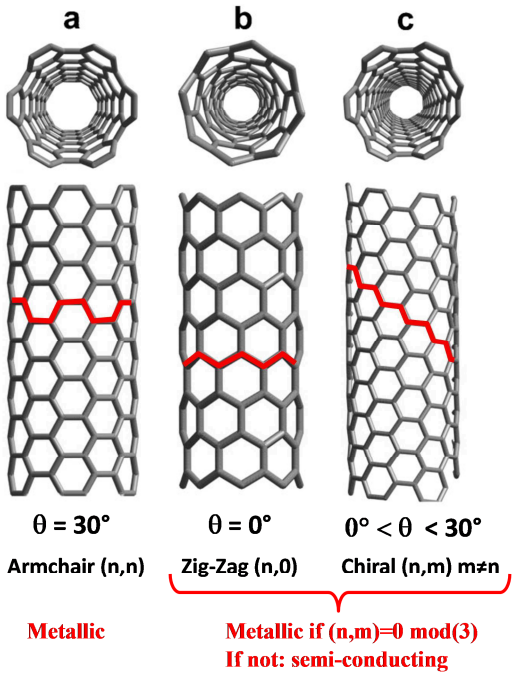

Figure 5: the three main types of possible structures for CNTs: the chair structure (armchair), the zig-zag structure and the chiral structure, with the associated values of the chirality angle θ and chiral indices (n, m).

1.2. Some generalities on the synthesis methods of SWCNTs

The synthesis of carbon nanostructures such as graphene or CNTs is based on very specific conditions and generally out of equilibrium: a flow of carbon species is sent to a surface, and can undergo a reduction on a specific catalyst at relatively high temperatures (550-1100 ° C). Three major synthetic methods have historically been used to synthesize single- or multi-wall CNTs: electric arc synthesis (IIjima, et al., 1993; Bethune, et al., 1993), laser ablation (Thess, et al., 1996) and chemical vapor deposition (CVD) (Dai, et al., 1999), the last method (performed under various physicochemical conditions) having become the most widespread.

The electric arc synthesis consists of producing an electric arc between two graphite electrodes in a controlled atmosphere chamber (helium, H_2, CH_4, etc.). If the anode is a composite material of graphite and a transition metal such as Ni, Fe, Co ... (or alloys of these metals), the formation of SWCNTs is favored over that of MWCNTs. On the other hand, the sample thus synthesized contains many impurities: amorphous carbon, residual catalytic particles often forming metal carbides, etc. Journet et al. showed in 1997 that the use of a catalyst containing 1atomic % Yt and 4.2 at. % Ni (mass % with respect to the carbon element) allowed a SWCNT production yield between 70% and 90% (Journet, et al., 1997).

Laser ablation synthesis was developed by R. Smalley's group at Rice University in 1995 (Guo, et al., 1995). The principle, shown in Figure 6, is to vaporize the atoms of a

graphite target via a nanosecond laser pulse of high energy at 532 nm wavelength (by doubling the frequency of a pulse at 1064 nm of a Nd: YAG laser). The graphite target containing a catalyst (eg, a 50:50 at. .Co / Ni mixture) is placed in the center of a tubular furnace heated to 1200 ° C. At this temperature, the laser pulse vaporizes the carbon atoms that react on the catalyst particles to grow nanotubes. The use of transition metals favors the synthesis of SWCNTs. An argon stream entrains the chemical species formed on a water-cooled copper collector. The main interest of the method compared to the electric arc synthesis is to greatly reduce the impurity content, especially carbonaceous impurities.

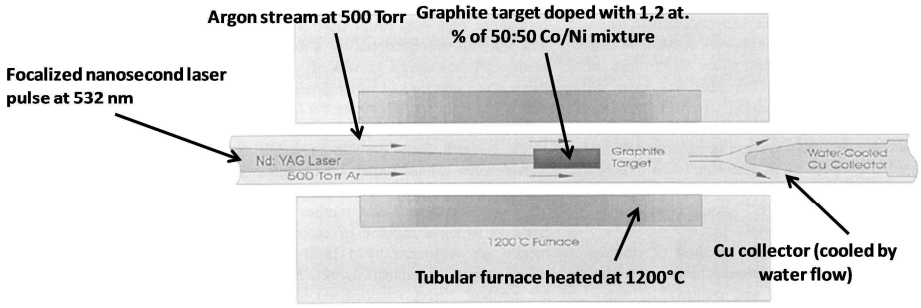

Figure 6: Principle of the synthesis of SWCNTs by laser ablation. Adapted from (Guo, et al., 1995).

The two previous methods of synthesis are very energy-consuming and are not well adapted to industrial production necessary for the large-scale use of CNTs in materials. Moreover, they do not make it possible to achieve spatially controlled growth like bundle alignment, synthesis of individual nanotubes, etc. ... By the end of the 1990s, chemical vapor deposition (CVD) synthesis made it possible to circumvent these obstacles (Kong, et al., 1998; Dai, et al., 1999). At present, there is a great diversity of methods based on the principle of CVD, using many catalysts, optimally-adjusted temperatures and pressures, diverse carbon source molecules and so on. ... This profusion of methods does not necessarily help to build a unified vision of the growth of single-walled CNTs. At the present time, there is still no clear and universal vision of the parameters controlling the growth of nanotubes in order to establish the links between the characteristics of the catalyst and those of the obtained CNTs. However, real progress has been made over the past five years, and CVD synthesis is becoming more and more specific in that it allows for better control of the CNT diameter distribution. The objective of this work is to synthesize one or a few specific CNT chiralities. We will see in the following paragraph that depending on the indices (n, m) of the CNTs, they can be conductors with a metallic behavior, or behave rather like semiconductors. The use in electronics of these materials, either for the purpose of molecular electronic connectors or for the production of nanoscale transistors, therefore requires the use of nanotubes respectively metallic or semiconducting. A possible approach is based on the specific synthesis of tubes of one type or the other, thus on a growth controlling the CNT indices (n, m). One of the approaches envisaged consists in optimizing the formation of catalytic particles in terms of size dispersity and crystallinity, so that the produced CNTs have a narrow-range set of diameters. (Zhang, et al., 2016).

While there are many other less common synthetic methods, we will close this paragraph by citing only a bottom-up approach based on the synthesis of nanotubes of specific indices (n, m) using elementary assemblies of molecular precursors (Sanchez-Valencia, et al., 2014). These current works do not however concern this thesis, we will not make a bibliographical report on this work.

1.3. Electronic and mechanical properties of carbon nanotubes.

SWCNTs have a diameter of the order of one nanometer. At this scale, the quantum effects on the electronic wave function are very important, and this confinement of the electronic waves along the circumference imposes that the wavelength λ for the standing waves is such that:

Equation 3

$$l \times \lambda = 2\pi R = \pi d$$

where l is an integer, R is the nanotube radius and d its diameter which is calculated by the relation:

Equation 4

$$d = \frac{a_0}{\pi}\sqrt{n^2 + m^2 + mn}$$

Thus, the only possible wavelengths for the electronic wave function for a chiral index tube (n, m) are given by:

Equation 5

$$\lambda = \frac{a_0}{l}\sqrt{n^2 + m^2 + mn}$$

Take the example of a nanotube of indices (10,0). Figure 7A indicates in real space the elementary mesh of the nanotube and positions in this mesh a stationary wave along the circumference. In this figure, a wave with 3 extrema, l = 3 was taken (schematically on the left of the figure). A standing wave is indicated on a circle with these three extrema. In reciprocal space, we have positioned the different waves of wave vectors k = 2π/λ, and in red are the corresponding wave vectors. We see that in the case of a CNT of chiral indices (10,0), none of these stationary waves has a wave vector k passing through one of the points K or K' (Dirac cones) of the Brillouin zone of the CNT. This means that there is no possible electron density in these Dirac cones and the CNT is a semiconductor with a gap between the valence band and the conduction band. For a metallic CNT, on the contrary, these standing waves have wave vectors, at least one of which passes through a Dirac cone. Figure 8 shows this difference between metallic and semiconducting CNTs in a three-dimensional representation, the standing waves corresponding to planes intersecting the energy bands vertically.

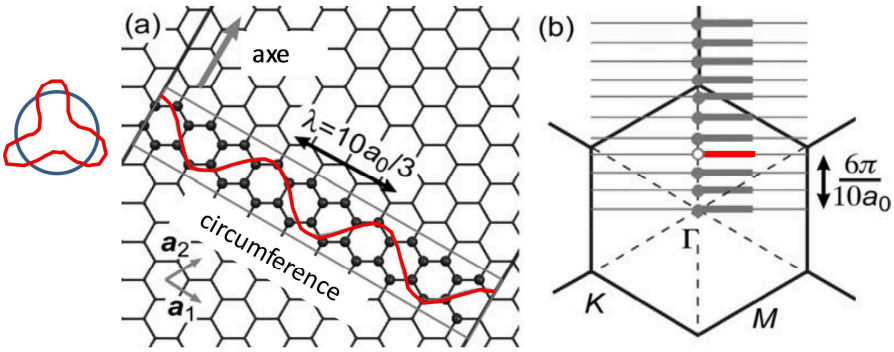

Figure 7: description of the winding of the graphene sheet in terms of folding of the Brillouin zone of graphene. For example, a nanotube (10.0) is considered. The stationary electronic wave condition along the circumference of the nanotube imposes a quantification of the wavelength of the wave, indicated schematically on the circle to the left of the part A for the example of a wave with 3 extrema. The gray rectangle shows the elementary cell of the nanotube (10,0) with this three-extrema wave unfolded along the circumference of the tube. All wavelengths are given for this tube by $10a_0/l$, l being an integer. Part B of the figure places this particular wave in the diagram of the Brillouin zone using the wave vectors $k=2\pi/\lambda=2\pi l/(10a_0)$. In red figure our particular wave example with l=3. None of the stationary electronic waves pass through the Dirac K-points of the Brillouin zone: the nanotube (10,0) does not have an electron density at this point, it is a semiconductor nanotube. Adapted from reference (Thomsen, et al., 2007) .

It can be shown that only the CNTs for which the difference (n-m) is a multiple of 3 are metallic. This approach relies only on the Brillouin zone of graphene and the reasoning neglects the folding of bands and the effects due to the curvature which modifies the overlap of the 2p orbitals of carbon (in particular for small diameter CNTs with high curvature rate). However, this approach is sufficient to show that different-diameter CNTs have different electronic properties. It can thus be expected that the chemical reactivity of CNTs will be influenced by their metallic or semiconducting nature and also by the diameter. Smaller diameter tubes are indeed less chemically stable due to a less efficient overlap of the 2p orbitals of carbon atoms.

The stationary wave condition around the CNT circumference thus imposes specific wave vectors for which the electronic density of states is very high. When we examine the energy of the electronic levels according to this DOS, we obtain singular peaks of high density called "van Hove singularity". Figure 9 illustrates two examples for a metallic CNT and a semiconducting CNT. The density peaks corresponding to the valence bands are denoted $\mathbf{v_n}$, those of conduction are denoted $\mathbf{c_n}$. The figure further shows two examples of possible electronic transition between these peaks; as we will see later, these will play a crucial role in understanding the spectroscopic properties of CNTs, in particular their visible and near-IR light absorption as well as inelastic Raman scattering.

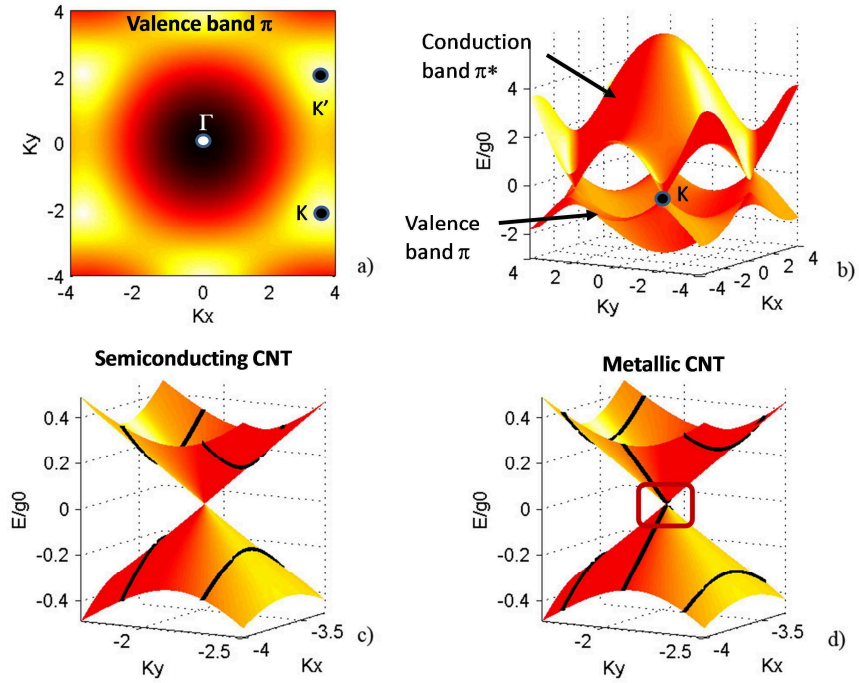

Figure 8: a) Electronic energy in the first graphene Brillouin zone for the valence band π seen in projection in the plane of the wave vectors (k_x,k_y), ranging from the lowest to the highest energy of black to white. Point Γ thus represents a minimum of energy for the valence band, and the points of symmetry K and K 'of the higher energy points. B) Representation of valence and conduction energy bands of graphene in three dimensions. c) and d) Zooms on a Dirac point (symmetry point K) of the graphene bands. In c), the allowed wave vectors for a carbon nanotube of a given diameter trace black curves on the energy layer of the bands, corresponding to the intersection of a plane with the layer. These lines correspond to the wave vectors allowed by the standing wave condition along the circumference of the CNT. We see that these lines do not pass through the Dirac point. It is a CNT semiconductor. In d), these authorized lines pass through the Dirac point. The energy density at this point is therefore non-zero and the nanotube is metallic. The position of the black lines depends on the chirality indices (n, m) of the nanotubes. Adapted from Wikicommons.

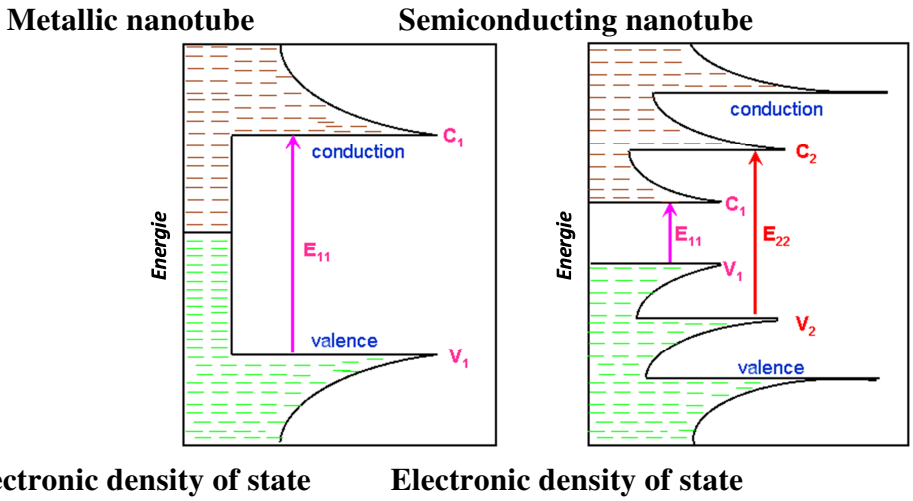

Figure 9: energy versus density of electronic states for a) a metal CNT, showing two density peaks called van Hove singularities, and b) a semiconductor CNT. We note v_n van Hove peaks of the valence band and c_n those of the conduction band. E_{11} represents the first van Hove transition allowed for optical absorption, E_{22} the second transition, etc.. ... Adapted from https://commons.wikimedia.org/wiki/File:SSPN41.PNG.

1.4. Importance of separation of metallic and semiconducting nanotubes.

As seen above, the electronic structure of CNTs is strongly influenced by the chiral indices (n, m). Under conventional synthesis processes, a mixture of semiconducting and metallic CNTs is obtained. For certain potential uses, this is undesirable: for example, the applications of semiconducting CNTs for the fabrication of molecular transistors or for applications for photovoltaic cells, the presence of metallic tubes is a major drawback because the leakage of charges caused by these conducting tubes would drastically reduce the device efficiency of such nanomaterials. On the contrary, if we seek to introduce conductive CNTs into a material, in order to increase its electrical conductivity, metallic CNTs would obviously be best suited. We therefore see that the separation between the two species of CNTs is a major issue in terms of applications.

This separation can be carried out either via non-covalent interactions, for example by developing preferential interactions with the semiconductor nanotubes, or covalently (differential chemical functionalization). We will first present a brief summary of some non-covalent methods, which have the merit of maintaining the structure of the CNTs since they do not introduce new defects via the formation of covalent bonds. Ultra-centrifugation with its density gradient was one of the first separation methods used with real success since 2006 (Arnold, et al., 2006). A specific medium (iodixanol forming an aqueous solution with a density gradient) makes it possible to generate a density gradient gel in a test tube. The sample of CNTs is placed in aqueous suspension in the presence of a surfactant (for example, sodium cholate) or a mixture of surfactants and the suspension is subjected to ultrasound to promote the passage of the CNTs from their bundled state into an individualized state. This suspension is injected at the top of the gel, and the test tube is subjected to ultracentrifugation between 150,000 and 250,000 g typically. The CNTs are then separated according to their mass and thus their diameter, the bundles being found at the bottom of the gel, and the nanotubes of smaller diameter at the top of the gel. The method can also be optimized not for sorting according to diameter, but in terms of differential chemical interactions between the tubes surrounded by surfactant and the gel. This then makes it possible to separate the metallic from the semiconducting CNTs. Figure 10 shows two examples of results obtained by this method.

The use of surfactant molecules or polymer covering of the CNT walls via van der Waals interactions makes it possible to promote the dissolution in some solvents of CNTs of one electronic type and not of the other. Much research has been conducted over the past decade in this field, and there are many methods using, for example, DNA molecules (Zheng, et al., 2003; Tu, et al., 2008; Tu, et al., 2009) or polymers (Nish, et al., 2007; Antaris, et al., 2010; Toshimitsu, et al., 2014). Gel chromatography, electrophoresis or phase separation techniques can then be used to separate the CNTs.

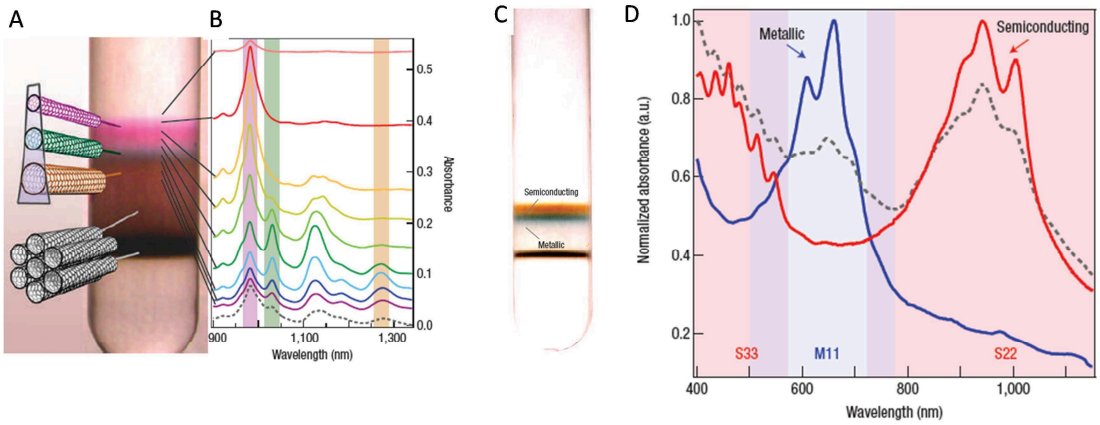

Figure 10: Principle of CNT separation by ultra-centrifugation on density gradient gel. A) The nanotubes are sorted according to their diameter in fractions ranging from the smallest diameter at the top of the gel to the residual bundles at the bottom. In B) are indicated the near-IR absorption spectra of the corresponding fractions. C) and D) represent the case where the process is optimized to separate the metallic nanotubes from the semiconductors. This time, it is not the diameter, but the differential interaction of the tubes with the surfactant and the gel, which allows the separation, shown in D by the visible-near-IR absorption spectra. From (Arnold, et al., 2006).

The current challenge is even to go beyond the metallic / semiconducting separation, in order to provide CNT samples strongly enriched in a given chirality. Recent work has made it possible to carry out the separation of chiral enantiomers within a given CNT sample of indices (n, m), as well as for semiconductor-type tubes (Liu, et al., 2014) and metallic tubes (Tanaka, et al., 2015). These processes are currently limited to the laboratory scale, but industrialization does not present any particular technical problem; however the use of specific molecules is sometimes relatively expensive or potentially toxic organic solvents in large quantities may be required. This work opens the way not only to practical applications of CNTs, but also to fundamental studies on the physico-chemical properties of a given-chirality sample, or even pure enantiomer sample.

Separation can also be achieved via covalent chemical functionalization of the tubes. In this case, it is a question of developing selective chemical transformation processes between metallic and semiconducting CNTs. It is even possible to explore selective reactivity based on chiral indices and diameter, which raises the possibility of reactions with only a relatively small subset of CNTs in the overall sample. (Hodge, et al., 2012). Works in this area are numerous. Examples include the addition of diazonium salts, a reaction that has been widely used and characterized in the literature. Generally, the effectiveness of the addition of these salts is clearly favored in the presence of metallic CNTs (Strano, et al., 2003). The mechanism of this addition is complex and takes place in several stages (Usrey, et al., 2005; Schmidt, et al., 2009), involving a radical chain transfer reaction in which the CNTs play a catalytic role via an electron transfer mechanism. Metallic CNTs play this role much more efficiently than the semiconducting. Thus the use of diazonium salts bearing on the aryl group an electron-withdrawing group such as NO_2 promotes the reactivity towards the metallic CNTs and greatly increases the selectivity of the reaction. This is due in part to the fact that the metallic CNTs have a non-zero electron density at the Fermi level which promotes the creation of aryl-CNT

radical intermediates. Other reactions are also more or less selective. We can mention for example the work of our group on the radical addition of a methoxyphenyl radical which has also shown some selectivity between smaller diameter metallic and semiconducting CNTs (Liu, et al., 2008).

We therefore see that there are two main methods for separating CNTs according to their chirality: the non-covalent methods, which unfortunately have not yet produced a large amount of sample, and the covalent functionalization methods that make it possible to treat more significant CNT quantities, but which create defects (carbon atoms of sp^3 hybridization) in their structure. There is thus a still-open field of investigation towards developing softer selective functionalization methods, introducing only a small number of atomic defects in sp^3 hybridization, or reversible functionalization after separation to reconstitute the integrity of the CNT structure once sorted.

1.5. Why functionalizing CNTs? The problem of their compatibility with an external environment and their aggregation into bundles.

The excellent mechanical, thermal and electrical conductivity properties of CNTs allow these nanomaterials to be used as reinforcing agents or as fillers in various matrices. Work to incorporate CNTs into polymer matrices to form new generation composites is plethoric, but all highlight the difficulty of obtaining a truly exceptional mechanical reinforcement. Indeed, the van der Waals interactions between the CNTs cause their aggregation into bundles whose mechanical properties are significantly degraded compared to those of individual tubes, because of the possible sliding of tubes within the bundles upon applying stresses to the composite.

Covalent or non-covalent chemical functionalization is also a possible way to breakdown the CNT bundles and produce isolated tubes. The use of surfactant-type molecules can help disperse the CNTs in order to obtain stable suspensions of individual tubes in solution. The major disadvantage of this method is the introduction of external molecules on the CNT walls which can prevent a good subsequent incorporation into the polymer matrix, or simply make it impossible for subsequent chemical treatments for grafting chemical functions on the CNTs. One approach may be to use, for example, a CNT reduction reaction with an alkali metal such as potassium, which will negatively charge the CNT wall and promote dispersion by electrostatic repulsion (Gebhardt, et al., 2017). In a second step, it then becomes possible to use these reduced CNTs to perform a covalent grafting. These CNTs do not re-aggregate and it is possible to consider their incorporation into different environments compatible with such grafted groups.

1.6. Examples of applications of functionalized SWCNTs.

Current applications of functionalized CNTs – but which remain to be more developed over the years to come - can be divided into two main classes (Loiseau, et al., 2006):

- The incorporation of modified CNTs into matrices, for example polymers, in order to produce composite materials making use of the good thermal or electrical conductivity of the CNTs or their mechanical strength.
- The use of modified CNTs for the production of electrochemical sensors through their incorporation on the surface of working electrodes.
- Applications in molecular electronics, for example the production of transistors or the use of metal CNTs as electronic wires of very small size. Their use might call upon isolated rather than bundled CNTs. It is also possible to reconcile this electronic application with the incorporation of CNTs into a flexible polymer matrix, as shown very recently in reference (Lei, et al., 2017).

We will show in this thesis all the interest of incorporating functionalized CNTs with ferrocene derivatives to make bioelectrodes capable of having an enzymatic co-factor such as nicotinamide adenine dinucleotide (NADH) to interact with enzymes such as glucose oxidase.

2. Characterization methods for functionalized carbon nanotubes.

2.1. Electronic absorption and emission spectroscopies.

In order to understand the electronic absorption spectra of CNTs, it is necessary to return to the description of their electronic energy levels: the electronic DOS shows the existence of singular peaks, called "van Hove singularities" (Figure 9). The possible transitions between the peaks corresponding to the valence and conduction bands account for the possible absorptions of the CNTs. However, the position of these peaks depends on the chiral indices (n, m) of the tubes. We thus see that electron absorption spectroscopy is a technique of great interest because it makes it possible to analyze the types of CNTs present in a sample, each absorption peak characterizing a given chirality.

S_{ii} denotes the transitions $v_i \rightarrow c_i$ of the semiconducting CNTs, and M_{ii} the corresponding transitions for the metallic CNTs. Note that it is the quantum selection rules that indicate (via the Fermi golden rule) that only the transitions $i \rightarrow i$ are possible in absorption, the transitions $i \rightarrow j$ (with $j \neq i$) being forbidden. These transitions are revealed by narrow peaks in the UV-visible-near-IR absorption spectra of a CNT sample (see Figure 11A). The difference in energy between these singularities depends on the diameter of each CNT present in the sample analyzed. It is thus possible to present the energy of these transitions as a function of the diameter of the nanotubes, in what is termed the Kataura diagram, as is shown in Figure 11B.

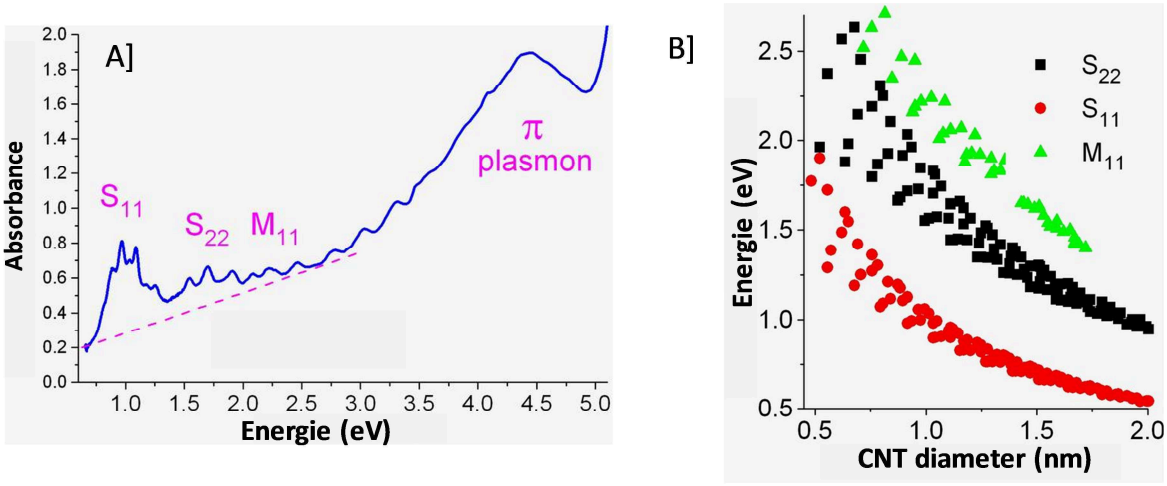

Figure 11: A] Electron absorption spectrum of a sample of carbon nanotubes showing the S_{ii} and M_{ii} absorption peaks related to van Hove singularity transitions; B] Kataura diagram connecting the position of the resonance energy to the diameter of the nanotubes for the different S_{ii} and M_{ii} transitions.

The difficulty of such an experiment lies in the suspension of the CNT samples (Weisman, 2008). We chose to work in deuterated water, which offers a spectral window through which to analyze our samples easily up to 1900 nm wavelength. The procedure generally consists of dissolving about 0.1 to 1 mg / mL of nanotubes by adding 2% by weight of a surfactant, then subjecting the suspension to sonication with a sonotrode at 300 W for ten two thirty minutes, and then centrifuging at 4000 rpm to recover only the supernatant. We tested different surfactants, and finally we chose sodium dodecyl sulfate (SDS). The problem with this technique is that the CNTs that remain agglomerated in bundles are removed from the analysis because they are located in the pellet centrifugation.

The CNT suspensions thus prepared can also be used to make luminescence experiments (electron emission). In this case, only the semiconducting tubes give rise to this luminescence phenomenon, which is inhibited for metallic CNTs (Bachilo, et al., 2002).

2.2. Raman scattering spectroscopy.

Inelastic scattering of light by a molecule involves an exchange of energy between the incident photons and the molecules in the sample. This exchange of energy makes it possible to observe the vibrational transitions and the corresponding phenomenon is called Raman scattering in honor of Sir Chandrasekhara Raman, who received the Nobel Prize in physics in 1930 for this discovery. The oscillating electric field of an electromagnetic wave will interact with the electronic cloud of the molecule. If the interaction is inelastic, a change in the vibrational level of the molecule is observed. In the case of a Stokes type interaction, the transition is to an excited vibrational level: the energy of the electromagnetic wave is lower after diffusion, and its wavelength is greater. It is this Raman Stokes scattering process that we will use to analyze the vibrations of the CNTs. However, because of the particular structure of the electronic DOS with its van

Hove singularities, we will see that the Raman scattering process is enhanced by electron resonance.

When using a given laser wavelength for Raman scattering, the CNTs having electronic transitions between van Hove singularities for which the transition energy is within a few dozen meV from the energy of the incident (laser) photons will give rise to a Raman effect exalted by electron resonance. The Raman spectrum will therefore contain information on the CNTs in resonance with the incident laser, because their contribution from diffusion will cover the much smaller contribution of the other CNTs present in the sample. A resonance Raman spectrum typical of a CNT sample is shown in Figure 12.

It consists of:

- low frequency peaks related to the radial vibration of the tubes ("Radial breathing mode", RBM) whose vibration wave numbers are inversely proportional to the diameter. These peaks make it possible to determine which CNT diameters are in resonance with the incident photons of the laser being used. Typically, thanks to the Kataura diagram, we can distinguish the metallic from semiconducting CNTs, and study whether the respective populations are affected in the same or differential ways by the chemical grafting treatment that they have undergone.

- a so-called defect band (D band), around 1350 cm^{-1}. This band is related to diffusion processes by the defects of the crystalline structure of the CNTs. Its intensity increases (without being proportional) with the number of structural defects, these being vacancies, Stone-Wales defects (two cycles with 6 carbon atoms replaced by contiguous 5- and 7-cycles, for example), pendant bonds and/or a sp^2 to sp^3 hybridization of a carbon atoms due to the covalent grafting of a molecule. Thus, when the covalent grafting is large enough to increase the number of carbon atoms in sp^3 hybridization, the D band increases significantly in the Raman spectrum compared to the other bands of the spectrum. It is therefore a good indicator of the success of a covalent graft carried out in a significant extent (typically better than 1 carbon atom statistically functionalized for 60 to 80 atoms).

- two bands, denoted G^- and G^+, around 1500-1600 cm^{-1}, which correspond to lateral displacements of the carbon atoms along the major or minor axes of the structure and which also exist in the Raman spectrum of graphite (hence the symbol used for these modes).

- other modes related to some electronic resonance process, for example, the G' mode linked to a double resonance process around 2600 cm^{-1}.

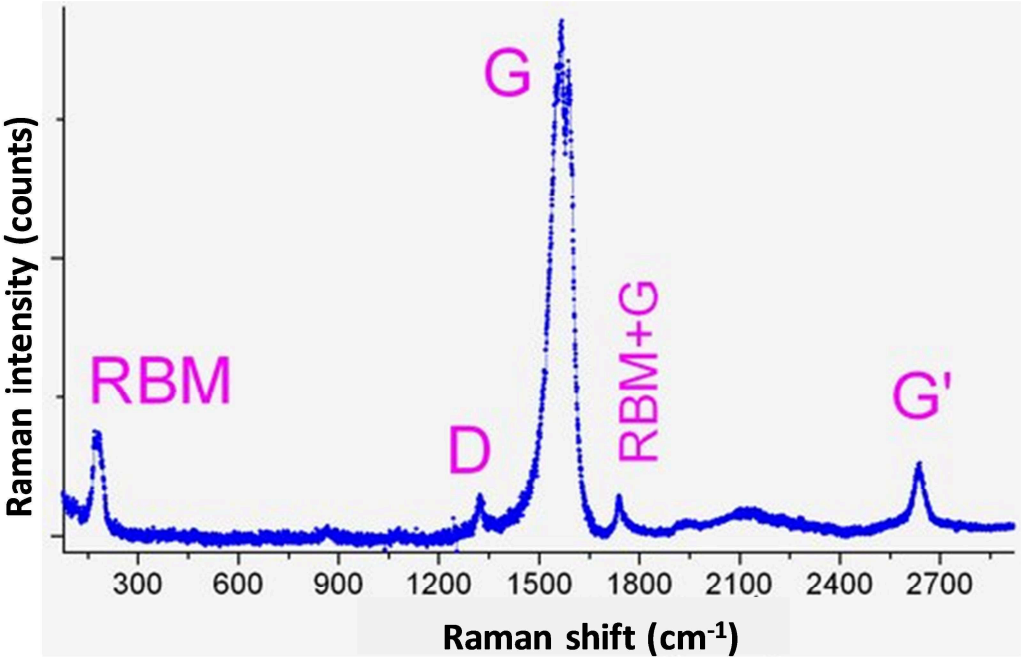

Figure 12: a Raman scattering spectrum typical of a sample of carbon nanotubes.

2.3. Spectroscopic ellipsometry.

Ellipsometry measures over a defined spectral range the intensity resulting from the reflection of a polarized light beam on a surface. Light being an electromagnetic wave, we can decompose the electric field vector $\overrightarrow{E_i}$ of the incident wave in two directions ⊥ to each other *(Figure 13)*: $\overrightarrow{\boldsymbol{E_i^p}}$, the component parallel to the incidence plan and $\overrightarrow{\boldsymbol{E_i^s}}$, perpendicular to this plane. The incidence plane is that containing the incident wave vector and the perpendicular to the surface of the sample. In general, electric fields are represented by complex quantities of the type $\boldsymbol{E_i^p(t,\vec{r}) = E_i^{p,0} e^{-i(\omega t - \vec{k}.\vec{r})}}$ for a wave ω, of wave vector $\vec{\boldsymbol{k}}$. After reflection on the sample surface, the modification of the electric field is represented by two coefficients of reflection in amplitude r_p and r_s, which are numbers called the Fresnel coefficients. In this work our samples are CNT films several hundred nanometers thick, which can be modeled by a homogeneous semi-infinite medium (the CNTs being randomly oriented). In this context, the Fresnel coefficients are defined by (Battie, et al., 2016):

Equation 6

$$r_s = \left(\frac{|E_r^s|}{|E_i^s|}\right) = \frac{n_i \cos\theta_i - n_t \cos\theta_t}{n_i \cos\theta_i + n_t \cos\theta_t}$$

$$r_p = \left(\frac{|E_r^p|}{|E_i^p|}\right) = \frac{n_i \cos\theta_i - n_t \cos\theta_t}{n_t \cos\theta_i + n_i \cos\theta_t}$$

n_i represents the refractive index of air and n_t that of the film being analyzed, i.e., here the CNTs. If we denote by δ_s and δ_p the optical path differences between the incident and reflected beams for the two states of polarization, we have:

Equation 7

$$r_s = |r_s|e^{i\delta_s}$$

$$r_p = |r_p|e^{i\delta_p}$$

which makes it possible to define the two ellipsometric angles Ψ and Δ that are measured in practice by:

Equation 8

$$\rho = \frac{|r_p|e^{i\delta_p}}{|r_s|e^{i\delta_s}} = \frac{|r_p|}{|r_s|}e^{i(\delta_p - \delta_s)} = (\tan\Psi)e^{i\Delta}$$

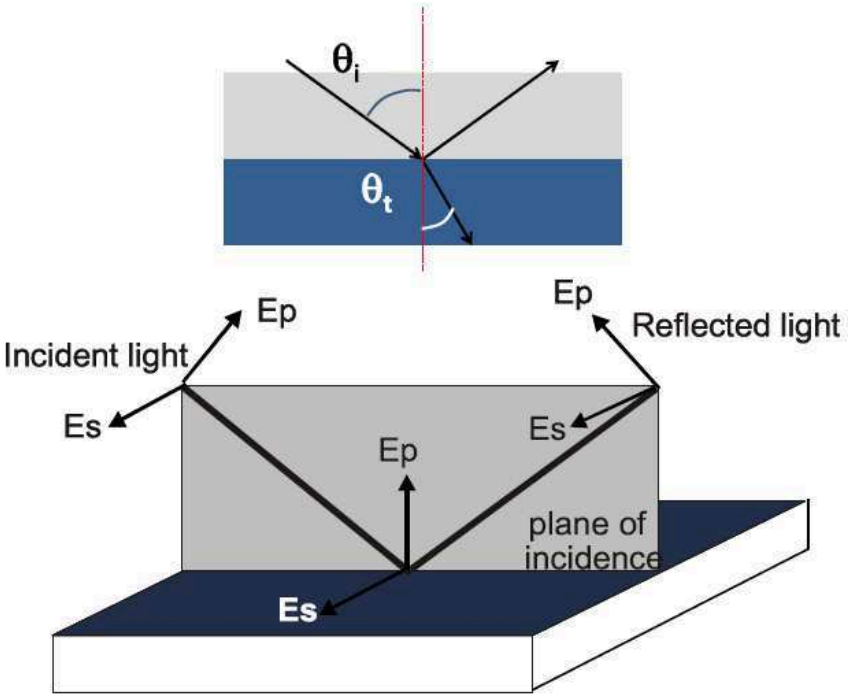

Figure 13: Principle of Ellipsometry

An ellipsometric spectroscopy experiment therefore consists in recording the value of the angles Ψ and Δ depending on the wavelength (or energy) of the incident beam. From the measurement of ellipsometric angles, a physical model can be used to calculate the dielectric function of the CNT film. One of the difficulties of this technique is defining and applying a suitable model to the nature of the sample which is necessary to fully make use of the data. In the framework of the model of a homogeneous semi-infinite film, the dielectric function is calculated as a complex function by (Battie, et al., 2016):

Equation 9

$$\varepsilon = (\sin^2\theta_i)\left\{1 + \left(\frac{1 - (\tan\Psi)e^{i\Delta}}{1 + (\tan\Psi)e^{i\Delta}}\right)^2 (\tan^2\theta_i)\right\}$$

This model of a homogeneous semi-infinite medium, in which the CNTs are supposed to be randomly oriented in the film, can be verified by varying the angle of incidence θ_i and applying the transformation given by Equation 9. The data must fit perfectly, otherwise the model is not adapted to the nature of the sample.

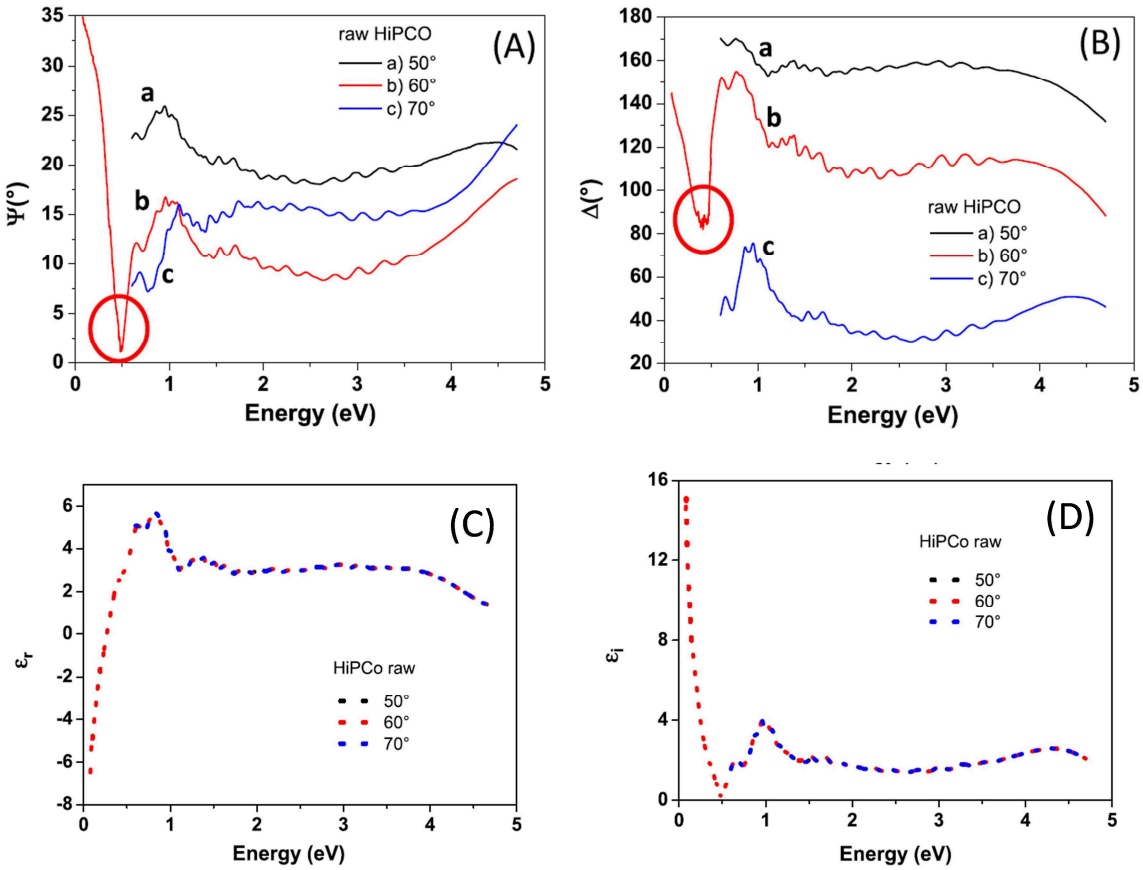

Figure 14: ellipsometric spectroscopy of purified HiPCo carbon nanotube films. A) and B): measurements of ellipsometric angles Ψ et Δ according to the angle of incidence θ_i on a spectral range from infrared to ultraviolet.C) and D) : values of the real part and the imaginary part of the dielectric function of the carbon nanotube film deduced from Equation 9 for the three incidence angles studied. Adapted from (Battie, et al., 2016).

Figure 14 shows an example of this type of analysis for a purified HiPCo CNT film ("superpure" Nanointegris reference, 95% SWCNTs, < 5% residual catalytic particles and carbonaceous impurities). A film with a thickness of the order of 400-500 nm was deposited on a nitrocellulose membrane. Three angles of incidence were used, and ellipsometric angles Ψ and Δ were measured over a wavelength range from infrared to ultraviolet. The transformation given by Equation 9 was then applied to this data set, and then we plotted the real and imaginary parts of the complex dielectric function (Battie, et al., 2016). The results of this study are shown in Figure 14.Figure 14: ellipsometric spectroscopy of purified HiPCo carbon nanotube films. A) and B): measurements of ellipsometric angles Ψ et Δ according to the angle of incidence θ_i on a spectral range from infrared to ultraviolet.C) and D) : values of the real part and the imaginary part of the dielectric function of the carbon nanotube film deduced from Equation 9 for the three incidence angles studied. Adapted from . We see that the values of the dielectric functions are identical (within the limits of the experimental measurement

errors) for the three angles of incidence studied. This reinforces the choice of the semi-infinite isotropic and homogeneous medium model. A similar study was then applied to chemically functionalized CNTs, and conductivity properties were deduced from the data. We were able to confirm the covalent grafting of certain functions on CNTs via characteristic absorptions in the infrared part of the ellipsometric data. This work has shown the full potential of this technique for the study of functionalized CNTs (Battie, et al., 2016).

2.4. X-ray photoelectron spectroscopy

The principle of X-ray photoelectron spectroscopy (XPS) is to irradiate a sample with a very energetic radiation in the range of X-rays. An electron is removed from the atom by absorption of the photon, it migrates to the surface of the material and an acceleration voltage allows extracting it in a high vacuum and focused towards a detector that will analyze its kinetic energy. Figure 15 indicates the essential elements of an XPS spectrometer.

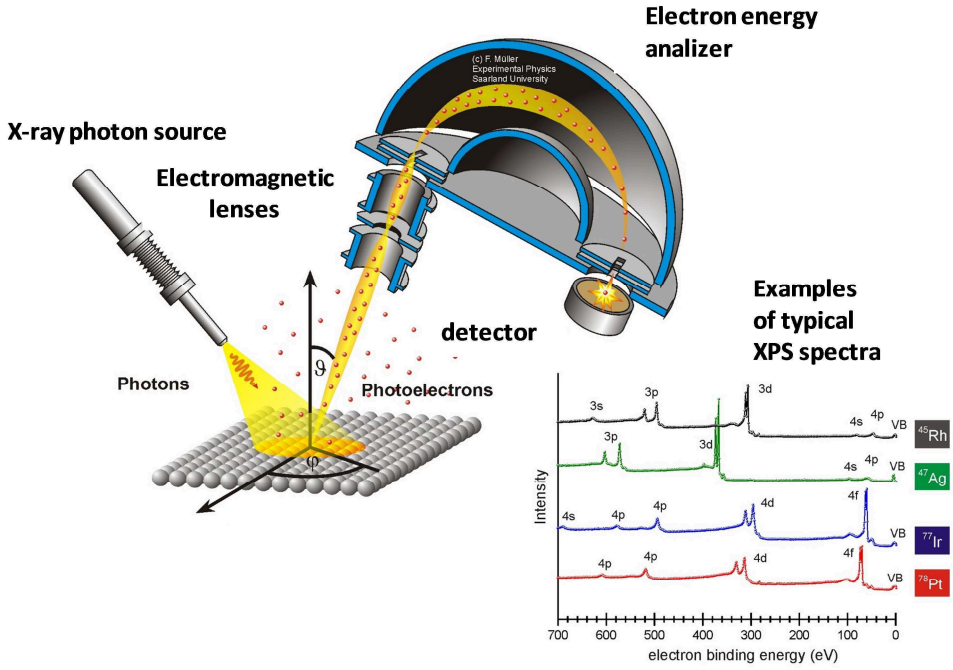

Figure 15: principle of a XPS spectrometer. Adapted from http://jacobs.physik.uni-saarland.de/instrumentation/uhvl.htm

Knowing the energy of the incident X-ray photon E_X, measuring the kinetic energy of the electron E_{cin}, we deduce the binding energy of the electron E_l by simple conservation of energy:

Equation 10

$$E_X = E_{cin} + E_l \rightarrow E_l = E_X - E_{cin}$$

We see that the resolution of the energy measurement depends both on the resolution of the electron energy analyzer and on the spectral width of the X-ray source which

determines the uncertainty of E_X. The best current spectrometers ultimately provide a resolution of the order of 0.4-0.6 eV in energy, using monochromatic X-ray sources by reflection on crystals at well-defined angles.

XPS spectra provide characteristic peaks of the core orbitals of the atoms constituting the sample. Since the average free path of electrons in solids is very short, the probed depth of the material is of the order of a few nanometers depending on the nature, the surface state and the elemental composition of the sample. To analyze CNTs, we have prepared suspensions in tetrahydrofuran (THF) at a level of 0.1 mg/mL. The suspension was sonicated for 10 minutes in an ultrasonic bath, then a drop of 100 µL was deposited on a glass slide covered by plasma evaporation of a layer of 100 nm of gold. This layer makes it possible to give a conductive character to the substrate, which thus evacuates the surface charges of the sample. This also makes it possible to provide an internal reference thanks to the Au 4f peak. Finally, this avoids carbon contamination and the O 1s and Si 2p signals of the glass slide. THF was chosen because it is a solvent that evaporates very quickly. Thus, depending on the quality of the suspension, another drop could be deposited on the first one to increase the thickness of the deposited nanotubes. The analysis is therefore performed on bundled nanotubes, but only for the first 10 nanometers of the deposited heterogeneous film. The analysis ellipse (the size of the x-ray spot) was about 700 × 400 μm^2, so for each sample we have two analysis points at different locations. Each time, the results showed great consistency, the spectra being very similar. The statistical validity of this analysis is therefore proven.

The interest of XPS spectroscopy, in addition to an elemental surface analysis of the samples, lies in the small energy shifts of the XPS peaks as a function of the degree of oxidation of the element. Thus for carbonaceous materials, the peak of the 1s orbital of the carbon element (simply designated by C 1s) is generally composed of several contributions:

- A signal around 284.4-285.7 eV attributed to C atoms in sp^2 hybridization in the CNTs.
- A signal around 285.3-285.6 eV attributed to C atoms in sp^3 hybridization, involved in C-C or C-H type bonds, for example.
- Multiple signals with higher binding energies corresponding to defects, for example oxygenated, either in sp^3 hybridization (single C-O bonds at 286.5 eV) or in sp^2 hybridization (C=O double bonds at 289 eV).
- A very wide band of low intensity centered at 291 eV, which corresponds to the interactions of the photoelectrons with the π plasmon bands of metallic CNTs in the sample.

Figure 16 furnishes an example of the XPS spectrum of an unpurified SWCNT sample after synthesis (Liu, et al., 2008). Peaks of Csp^3 and oxygenated defects are significant here because the sample also contains highly defective carbonaceous impurities. This is a good example of the expected positions for C 1s peaks of the defects that we will find in this thesis work.

We therefore see the interest of XPS spectroscopy: it allows studying the covalent functionalization of CNTs. The quantification of sp3-type defects with respect to the sp^2 hybridized atoms of the intact structure makes it possible to estimate the level of covalent defects. Coupled with another quantitative technique such as thermogravimetric analysis, XPS is therefore an important technique for quantitatively estimating the level of functions grafted onto the CNT surface.

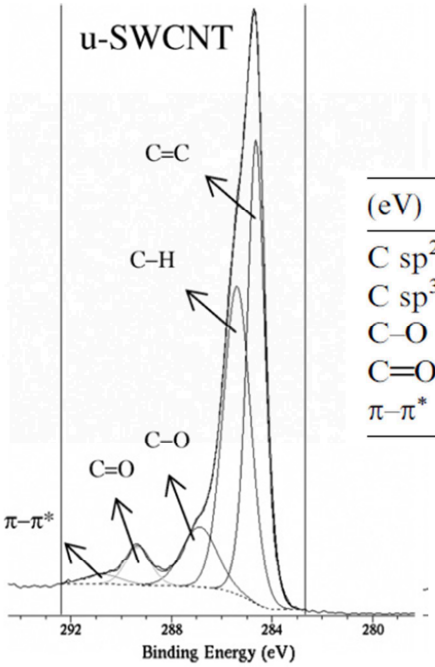

(eV)	u-SWCNTs
C sp^2 284.6 ± 0.1	41.8
C sp^3, CH_x 285.3 ± 0.1	41.3
C–O 286.5 ± 0.1	10.5
C=O 288.9 ± 0.2	4.7
π–π* 290.8 ± 0.2	1.7

Figure 16: example of the XPS spectrum of the orbitals C 1s of a sample of unpurified CNTs. The different contributions are quantified and reported in the table on the right of the spectrum. Adapted from (Liu, et al., 2007).

2.5. Thermogravimetric analysis coupled with mass spectrometry.

The principle of thermogravimetry, or thermogravimetric analysis (TGA), is to gradually heat a sample with a given mass from ambient temperature to a high temperature under a controlled atmosphere that can be neutral, reducing or oxidizing. The mass of the sample is continuously recorded as a function of its temperature. The recorded mass losses are generally indicative of the loss of particular chemical groups. Thus for carbonaceous materials, the different chemical defects in the structure have rather characteristic starting temperatures. It should be noted that the thermal transformations without any mass loss, such as a change of crystalline structure, cannot be detected by this method (Wirth, et al., 2014).

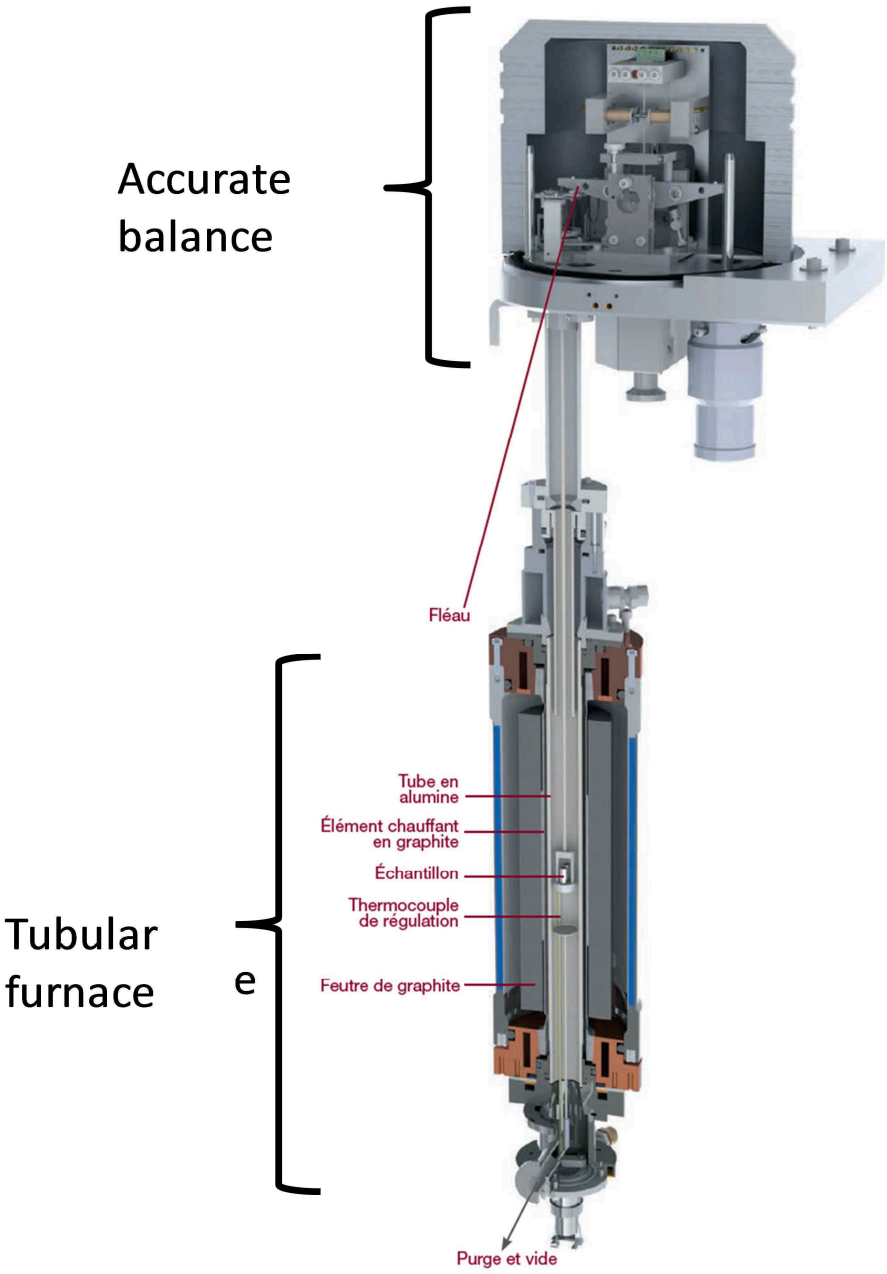

Figure 17: principle of the thermogravimetric analysis apparatus Setaram SETSYS Evolution 1750

A thermogravimetric apparatus consists of a high-precision balance, an oven and a controlled atmosphere sample-holder system. Figure 17 shows a schematic diagram of the Setaram Evolution 1750 device that we used in our studies. The balance is accurate to within 2 ng, with a drift of only 0.1 µg per hour. The CNT powder (generally 5 to 10 mg) is deposited in an alumina or platinum crucible. The tubular oven is designed to operate without damage up to temperatures of 1350°C for several hours. The temperature ranged from room temperature to 1000°C at a heating rate of 3°C per minute under a helium atmosphere. Via a connection tube thermostated at 300°C on the purge output, the gases emitted are analyzed through coupling the TGA instrument to a Pfeiffer GSD 301C Vacuum OmniStar mass spectrometer. The mass spectrometer parameters were such that the ions formed were with a z=1 charge, thus facilitating the tuning of the m/z analysis

channels. Systematically, two analyses were conducted on each sample, in order to study the reproducibility of the experiments. Thus about 10-20 mg of sample was needed for each study.

Figure 18 shows an example of this type of study for HiPCo CNTs purified then oxidized by two different oxidation methods in acidic media and assisted by microwave irradiation (Devaux, et al., 2015). Both oxidation processes increase the amount of oxygen functions present in the CNT structures. The mass loss curve of the sample oxidized by H_2SO_4 (oxH_2SO_4-SWCNT) is almost identical to that of the purified sample up to about 700°C. The sample oxidized by HNO_3 (oxHNO_3-SWCNT) stands out significantly from the other two samples with a greater mass loss above 200°C. We also indicate in Figure 18B the curves obtained by mass spectroscopy on different m/z channels for the raw sample. Emissions of CH_3 and C_2H_2 type fragments correspond to the sp^3 type defects present during the synthesis of CNTs, whereas the peaks of CO and C starting around 650°C probably result from the loss of oxygenated phenol moieties. Indeed, the initial sample was purified by an industrial process to remove the catalytic particles; it can be assumed that part of the process included an oxidizing treatment. The CNT sample therefore certainly contains oxygenated defects due to this purification treatment. A similar study was conducted with the oxidized CNTs (Devaux, et al., 2015).

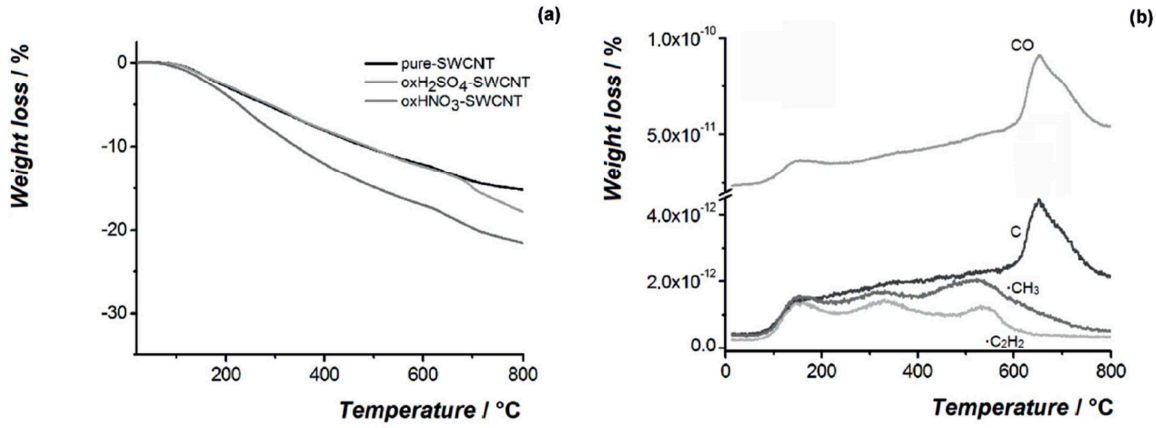

Figure 18: a) Thermograms obtained under Helium of purified HiPCo carbon nanotubes (raw), oxidized under microwaves with diluted H_2SO_4 (oxH_2SO_4-SWCNT) or with concentrated HNO_3 at 65% weight (oxHNO_3-SWCNT). B) Mass spectrometry curves for the channels C (m/z 12), CH_3 (m/z 15), C_2H_2 (m/z 26) et CO (m/z 28) for the raw sample. Adapted from (Devaux, et al., 2015).

3. Covalent chemical functionalization of single-walled carbon nanotubes.

3.1. The interest of the covalent approach.

Covalent functionalization allows the formation of a covalent bond between functional entities and the carbon skeleton of the CNTs. Its goal is to permanently graft the functional molecules on the surface of CNTs so that they can then be better dispersed in polar solvents such as water, acetone or an alcohol as well as in polymer matrices. The application of a targeted functionalization makes it possible to obtain CNTs having required physicochemical properties, such as mechanical strength, solubility or electrical conductivity.

These functions can be attached to tube ends or sidewalls. The sites of higher chemical reactivity in the CNT structure are the extremities, which have a structure identical to that of hemi-fullerenes. The curvature of the CNT side walls makes the addition reactions more favorable than on a graphene sheet (Hamon, et al., 2001) (Srivastava, et al., 1999). Furthermore the exoedric chemical reactivity increases with increasing curvature of the side walls; this has been attributed to the pyramidization of the sp^2 hybridized carbon atoms and to the misalignment of the π orbitals (Gebhardt, et al., 2010). Another parameter that profoundly modifies the chemical reactivity of the CNTs side walls is the presence of defects. About 2% of the carbon atoms in CNTs are in non-hexagonal rings. The presence of defects such as vacant positions or pentagon-heptagon pairs (Stone-Wales defects) results in improved local chemical reactivity. The covalent functionalization of the side wall generates carbon atom sites in sp^3 hybridization which can cause the loss of their properties, such as their high conductivity and good mechanical properties. With an increasing degree of functionalization, the tubes can possibly be transformed into almost insulating materials with a poor electric conductivity. The partial restoration of the structural integrity of the starting material can be achieved by thermal annealing of the modified tubes at temperatures between 300 and 500 °C. It is therefore important to be able to control the level of functionalization in order to maintain their conduction properties for the envisaged applications.

The covalent modifications can be classified in two categories: direct functionalization of the side walls and indirect chemical modification via functions (most often carboxylic acids) already present on the surface of the CNTs. These functions can then be used as chemical anchors for further functionalization.

3.2. The main classes of chemical reactions used for CNTs.

Several reactions allowing a direct functionalization of the walls have been described since the discovery of CNTs (Singh, et al., 2009) (Figure 19).

Fluorination of CNTs was one of the first methods of covalent functionalization described in the literature. It is carried out efficiently in the presence of F_2 at temperatures between 150 and 400 °C. (Adamska, et al., 2017). The interest is that the fluorine atoms can then be substituted by alkyl groups or by amines (Khabashesku, et al., 2002).

Cycloaddition reactions, well known with fullerenes, have been successfully used by different research groups (Kumar, et al., 2011). Thus, the reaction of carbenes with CNTs by a [2 + 1] process led to substituted cyclopropanes (Hu, et al., 2003). Similarly, nitrenes

have been used for the formation of aziridines (Holzinger, et al., 2003). A simple method for obtaining soluble CNTs has been described by Prato et al. (Georgakilas, et al., 2002), (Tagmatarchis, et al., 2004). In this reaction, also known as the Prato reaction, azomethine ylides thermally generated in situ by condensation of an amino acid with an aldehyde, add up in a [2 + 3] cycloaddition process on the walls and ends of the tubes, to form fused pyrrolidine rings.

CNTs can also be efficiently functionalized by radical addition. Electrochemically or chemically generated aryl radicals from diazonium salts add to the tube walls to yield soluble CNTs in different solvents. (Dyke, et al., 2003). We have shown in previous work that aryl radicals can also be generated from hydrazines in the presence of oxygen (Liu, et al., 2006).

Nucleophilic addition of heterocyclic carbenes led to the formation of zwitterionic species rather than cyclopropanes (Holzinger, et al., 2001). The latter are however obtained by addition / substitution of the base of bromomalonates on the double bonds of the tubes (Bingel reaction) (Coleman, et al., 2003).

Another class of reactions that has been widely used is the reduction and reductive alkylation of CNTs. (Pekker, et al., 2001), (Liang, et al., 2004). These methods involve injecting electrons onto the CNTs to make them carbanionic. These CNT-carbanions can then be trapped by different electrophiles.

Oxidation reactions have been widely studied. They are often used during CNT purification processes to remove metal nanoparticles and amorphous carbon. However, even after annealing, a certain number of oxygenated functions, such as epoxides, ketones or carboxylic acids, remain present in the purified CNTs. These functions can then be converted to esters or amide either directly or after chlorination.

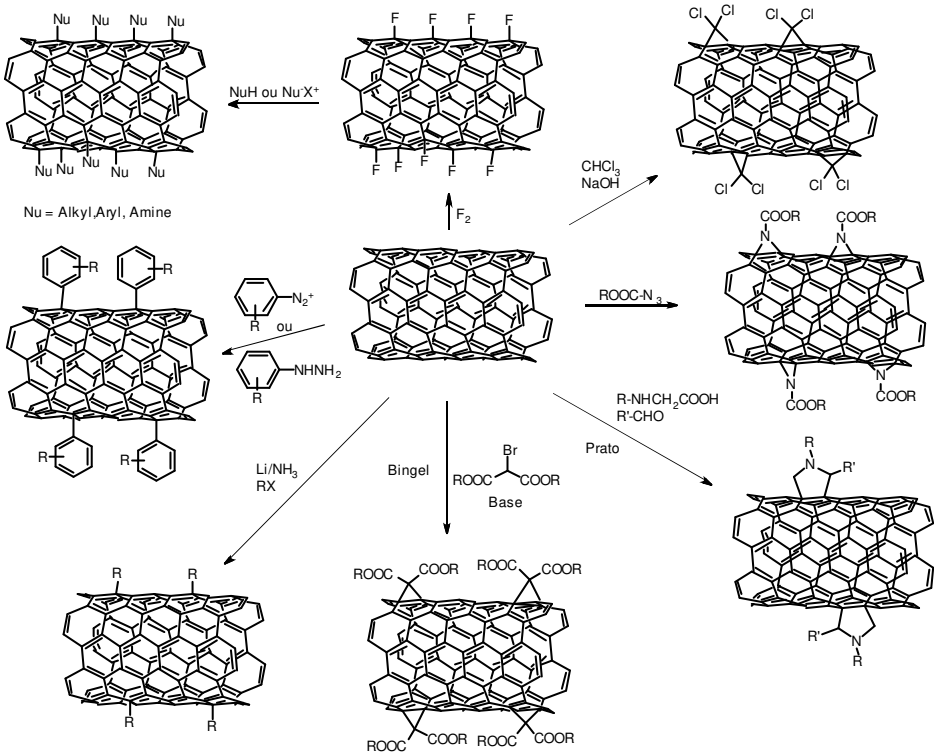

Figure 19: Common Reactions for Covalent Functionalization of CNTs

It is this path that we have chosen to carry out the grafting of our electro-active molecules (EA) on tube sidewalls: mild oxidation under microwaves makes it possible to transform practically all the oxygenated functions into carboxylic acids. The CNT-COOH obtained are converted into CNT-COCl in the presence of thionyl chloride ($SOCl_2$). The latter are reacted with EA molecules having an alcohol function, to lead to ester-linked CNT-EAs (CO-O) (Figure 20).

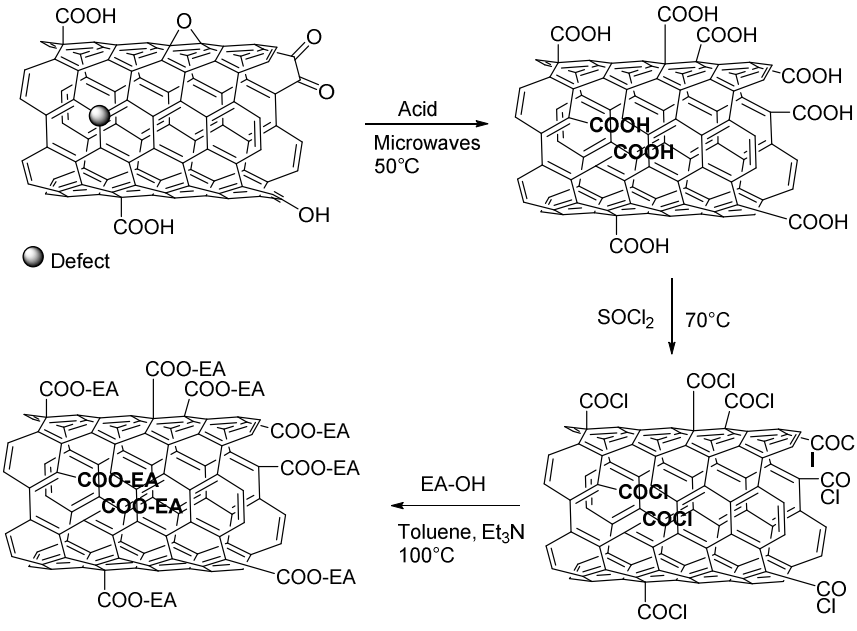

Figure 20: Synthetic route used in this work

In the next part, we will examine the most common oxidation processes and their impact on the CNT structure. We will also describe the interest of using microwaves to control the level of functionalization.

3.3. Oxidation processes and microwave irradiation

The effects of various conditions using oxidative reagent solutions such as H_2SO_4 (Chen, et al., 2006) or HNO_3/H_2SO_4 mixtures (Rao, et al., 1996), hydrogen peroxyde (piranha mixture) (Datsyuk, et al., 2008) or HNO_3 (Darmstadt, et al., 1998) have been extensively studied to functionalize CNTs. However, a significant increase in the number of defects and possibly a shortening of the CNTs have also observed. In order to reduce chemical attack, the oxidation of carbon materials can also be applied with more dilute nitric acid (Avilès, et al., 2009) or by using $KMnO_4$ (Zhang, et al., 2003). It has been regularly observed that the oxygen content is not increased in the treated CNTs. Indeed, the carboxyl functional groups introduced by the wet oxidation treatment were present in large amounts in carboxylated carbonaceous fragments (CCF) formed from the CNTs. These undesirable CCFs are polycyclic aromatics with COOH groups. They are removed during the basic washing so that the amount of COOH on the oxidized CNTs does not vary. (Salzmann, et al., 2007).

In order to obtain CNTs weakly but homogeneously oxidized (along the walls and not only at the ends), we have proposed the use of microwaves at low temperatures. Indeed, microwaves are known to greatly reduce reaction times (from several hours to minutes) (de la Hoz, et al., 2005). In recent years, many studies have described their use for the functionalization of CNTs (Vázquez, et al., 2009). For example, we can mention cycloaddition reactions (Brunetti, et al., 2007), addition of aryl radicals (Mamane, et al., 2014) & (Brunetti, et al., 2008), oxidation (Wang, et al., 2006), bromination (Colomer, et al., 2009) and alkylation (Xu, et al., 2008).

In our case, the use of a low temperature (50 °C) makes it possible to avoid over-oxidation phenomena and to greatly reduce the reaction times and thus to better control functionalization. Controlling the level of functionalization is of great importance to benefit from the properties of CNTs in materials or devices. High levels lead to both excessive degradation of the CNT structure and disruption of the conjugate system which have a negative impact on the intrinsic CNT properties (conductivity, mechanical properties). Low functionalization levels are indisputably preferred for CNT-based composites.

3.4. Functionalization by electro-active molecules: the interest of functionalized CNTs for the modification of electrodes.

One of the most promising applications of functionalized CNTs is the development of sensors. Conductive carbon materials have good prospects as electrode materials because of their good conductivity, high surface area to volume ratio, and thermal stability. Thus, CNTs have excellent potential for the fabrication of electrochemical sensors working for instance with biomolecules like NADH (Wang, et al., 2002), glucose

(Perez-Lopez, et al., 2005), phenolic compounds (Pumera, et al., 2006), dopamine (Angeles, et al., 2008), proteins (Kara, et al., 2010), etc... An essential prerequisite for the development of sensors is the establishment of good electron transfer between the analyte and the electrode. However, most detectable species are non-conductive and the direct electron transfer of some analytes is generally not reproducible. The introduction of electrochemical mediators is therefore crucial to improve the transfer of electrons in the detection process: bioelectrochemical sensors are thus obtained. These can be easily prepared and have often proved to be very sensitive. Organometallic mediators such as cobaltocene and nikelocene (Li, et al., 2014), organic compounds such as tetrathiafulvalene derivatives (Perez, et al., 2009), phtalocyanines (Bottari, et al., 2010) and even some organic dyes such as methylene blue (Li, et al., 2013) have been used. Ferrocene is one of the most exploited organometallic molecules in the development of bioelectrochemical sensors because it has good electrochemical characteristics such as fast electron transfer rate, low oxidation potential and stability of two redox states (Martic, et al., 2011) & (Saleem, et al., 2015). Thus, the ferrocenyl moiety is generally used as a model redox molecule to characterize the effectiveness of modified carbon nanomaterials, as it has both chemical and electrochemical stability (Rabti, et al., 2016).

4. Motivation and novelty of the work presented in this thesis.

4.1. A covalent functionalization method that preserves the structural integrity of CNTs.

In the context of the use of functionalized nanotubes within electrochemical devices, it is important to preserve as much as possible the electronic properties of the nanotubes, and therefore their structural integrity. Indeed, the covalent functionalization methods are of interest in that they immobilize the grafted functions via covalent chemical bonds, thus furnishing resistance to leaching, diffusion in the medium into which the electrode plunges, etc. But in return, they induce defects by modifying the hybridization of the carbon atoms constituting the wall of the CNTs from sp^2 to sp^3. The defects thus created can, when their number becomes sufficient, disturb the electrical and mechanical properties of the CNTs.

Our motivation is therefore to develop covalent grafting methods that make it possible to control as best as possible the number of carbon-type defects in sp3 hybridization in the structures. The idea is to graft enough electroactive functions to obtain a material that is electrocatalytic when deposited on an electrode, but without affecting too much CNT electrical properties (including electron transfer). For this purpose, we will use a soft and fast oxidation method in an acidic medium assisted by microwave irradiation. Our previous studies have indeed shown that these conditions make it possible to control the number of oxygenated defects resulting from the oxidation of the carbon atoms of the CNT sidewall by varying the irradiation time of a suspension of raw CNTs. The acidic medium favors the oxidation reaction, and the microwave irradiation causes local heating of the nanotube bundles which accelerate the reaction. We will test in this work two particular acidic media:

- A concentrated nitric acid medium at 65% (by weight), which is a fairly conventional medium in purely thermal oxidation. Using these acidic conditions with ourely thermal process requires refluxing for several hours. We will show that a few tens of minutes of microwave irradiation in such a medium are sufficient to obtain a sufficient number of COOH-type defects on the CNT surface and then graft electroactive functions using these functions.
- We have also tested even milder conditions with a sulfuric acid medium diluted to 2.5 mole.L^{-1}. This reduces the danger of the oxidation process, as the work is done in an acid solvent but mainly composed of water. Applications on an industrial scale might then be possible.

Once this oxidation step has been performed, the surface of the CNT bundles comprises oxygenated defects including carboxylic acid groups COOH which will be converted into a more reactive COCl group by reaction with $SOCl_2$, then brought into contact with our electroactive molecules carrying spacer alcohol function. The subsequent esterification reaction enables the electroactive groups to be covalently bonded to the surface of the CNTs (see Figure 20). We have developed two types of spacers connecting ferrocene electroactive groups to the CNT walls:

- Spacers with a polyethyleneglycol chain.
- A spacer with a C6-alkyl chain.

The molecules were synthesized as part of a master's degree work preliminary to this thesis (Allali, et al., 2012).

4.2. An advanced analytical approach for the characterization of the obtained materials.

Too often in the literature the covalent nature of the bonds connecting the CNT walls and the chemical group of interest are poorly or badly characterized. We chose to work on extremely pure HiPCo type CNTs, purchased from Nanointegris, in order to minimize the impurity content and considerably improve the quality of the information obtained with the different analytical characterization techniques we used. These complementary techniques are described in Chapter 2 and have also been associated with transmission scanning electron microscopy (STEM) studies carried out by our colleague Xavier Devaux on a microscope corrected for optical aberrations available at the same time in Jean Lamour Institute. We were able to obtain images with an atomic resolution of the sidewall of the nanotubes. Coupled with electron energy loss spectroscopy (EELS), we were able to observe the iron of the ferrocene group of our electroactive functions and show that these groups were covalently attached to the CNT sidewalls.

The success of this analytical approach is based on the complementarity of the techniques employed. This work was often done in collaboration, the analytical effort being particularly important, but this thesis work takes a big part in these data collection. Particularly, we carried out numerous spectroscopic analyzes (UV-visible absorption, Fourier-Transform InfraRed (FTIR) absorption, Raman scattering, XPS).

4.3. Choice of the electro-active groups.

The final goal of this work being to carry out enzymatic electrochemical devices, we wanted to graft electro-active functions allowing to promote oxidation-reduction reactions with active biomolecules and in particular NADH (dihydronicotinamide adenine dinucleotide, reduced form). The NADH/NAD^+ molecular system is a co-enzymatic system involved in many enzymatic reactions involving electron and/or proton transfers. For example, it makes it possible to operate oxidase or dehydrogenase enzymes and, as such, is particularly interesting for the development of either bioelectrochemical devices, sensors or synthetic bioreactors. The NADH/NAD^+ system is shown in Figure 21. We see that we move from the oxidizing form NAD^+ to the reduced form NADH by transferring one proton and two electrons onto the pyridine ring circled in red on the figure. The addition of an electron and a proton in the form of a hydrogen atom is carried out on the carbon atom located in the para position to the nitrogen atom of this ring, while the second electron neutralizes the positive charge of the nitrogen atom. Of course, this Lewis schematic representation is only an indication of the most reactive part of this molecular system at the electrochemical level.

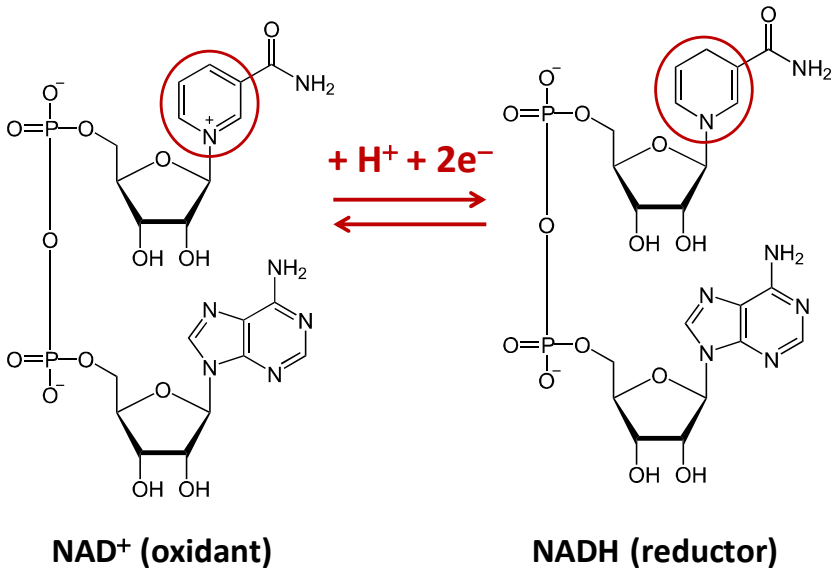

Figure 21 : the NAD^+/NADH ox-red system used as a co-enzyme in this work.

To be able to transfer electrons efficiently between an electrode and the NAD^+/NADH system, it is useful to use electroactive mediators that will take care of transporting the electrons from the electrode to the NAD^+/NADH system. Indeed, whether it is the electrochemical oxidation of NADH or the reduction of NAD^+, these processes require significant overpotentials to most conventional electrodes (Elving, Bresnahan, Moiroux, & Samec, 1982) (gold, platinum, graphite, glassy carbon electrode (GCE)). These overpotentials tend not to make the reaction sufficiently specific in the presence of other electroactive molecules in the same range of potentials. In addition, the reaction products accumulate and adsorb on the electrode surface, causing a rapid loss of efficiency and passivation of the surface. A very large number of ways have been followed for more than thirty years to solve this problem, using electrodes modified by materials that

increase the specific area, allow a transfer of electrons mediated by electron shuttles, and on the surface of which the products of the reaction do not accumulate.

Carbonaceous materials such as carbon black, multiwall or single-wall carbon nanotubes or graphene have been studied as materials with a high specific surface area. The oxygenated defects of these materials (carboxylic acids, ketones, quinones) seem to play a weak catalytic role on the oxidation of NADH, as well as locally mediating electron transfer sites (Blandon-Naranjo, Hoyos-Arbelaez, Vazquez, Della Pelle, & Compagnone, 2018). However, carbonaceous materials alone are not sufficient to achieve effective recycling of the NADH/NAD^+ system. The use of electron transfer mediating molecules, either grafted non-covalently onto nanotubes via π–π type interactions (Giroud, Sawada, Taya, & Cosnier, 2017), or deposited as electro-generated films on the surface of the nanotubes (Saleh, Okajima, Kitamura, Mao, & Ohsaka, 2018) greatly improves the electrocatalytic efficiency of the device. However, the possible release of these mediators into the environment encourages a covalent grafting approach of the mediators on carbon nanomaterials, a strategy that we will follow in this thesis work.

Our goal is therefore to graft electro-active molecules that act as electron transfer mediators on the surface of carbon nanotubes. To improve the recycling of the NADH/NAD^+ system and avoid adsorption of degradation products on the surface of the modified electrode, we will use diaphorase as an intermediate for the oxidation of NADH. The principle of our approach is shown in Figure 22.

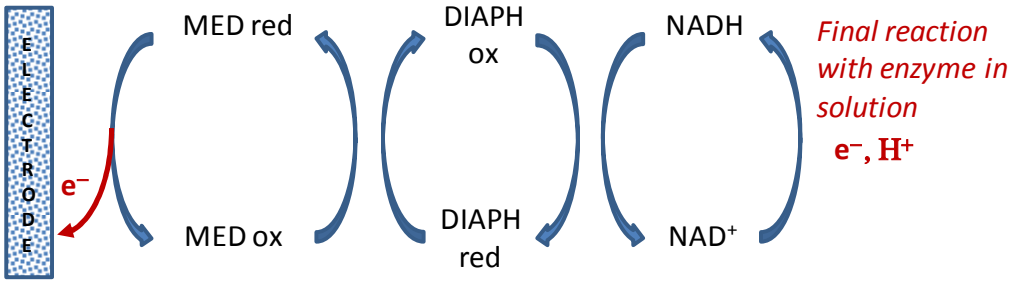

Figure 22 : Use of diaphorase in electro-catalytic processes involving NADH. MED is the electron transfer mediator material (in our case, carbon nanotubes chemically grafted by electro-active functions). DIAPH is the diaphorase.

In this thesis work, we examined different possibilities of electroactive functions allowing us to work either in NADH oxidation or in NAD^+ reduction. Our attention was focused on the following mediators:

- For the oxidation of NADH in the presence of diaphorase: ferrocene derivatives, an osmium complex or a K3 vitamin derivative.

- For the reduction of NAD^+ in the presence of diaphorase: methylviologen.

- For the reduction of NAD^+ without diaphorase: a ruthenium complex based on bi-pyridine.

The different mediators have been grafted as explained above, i. e. via a spacer with an alcohol function, which will react on activated acid functions formed on the surface of the CNTs by a controlled oxidation process. Two types of spacer arms were tested: a hydrophobic alkyl chain spacer, and a much more hydrophilic polyethylene glycol chain spacer. We will see in the rest of this work that the hydrophilic or hydrophobic nature of the spacer arm will have a crucial influence on the electrochemical results. Figure 23 shows the five mediators used and the two types of spacers (not all combinations are shown in this figure!).

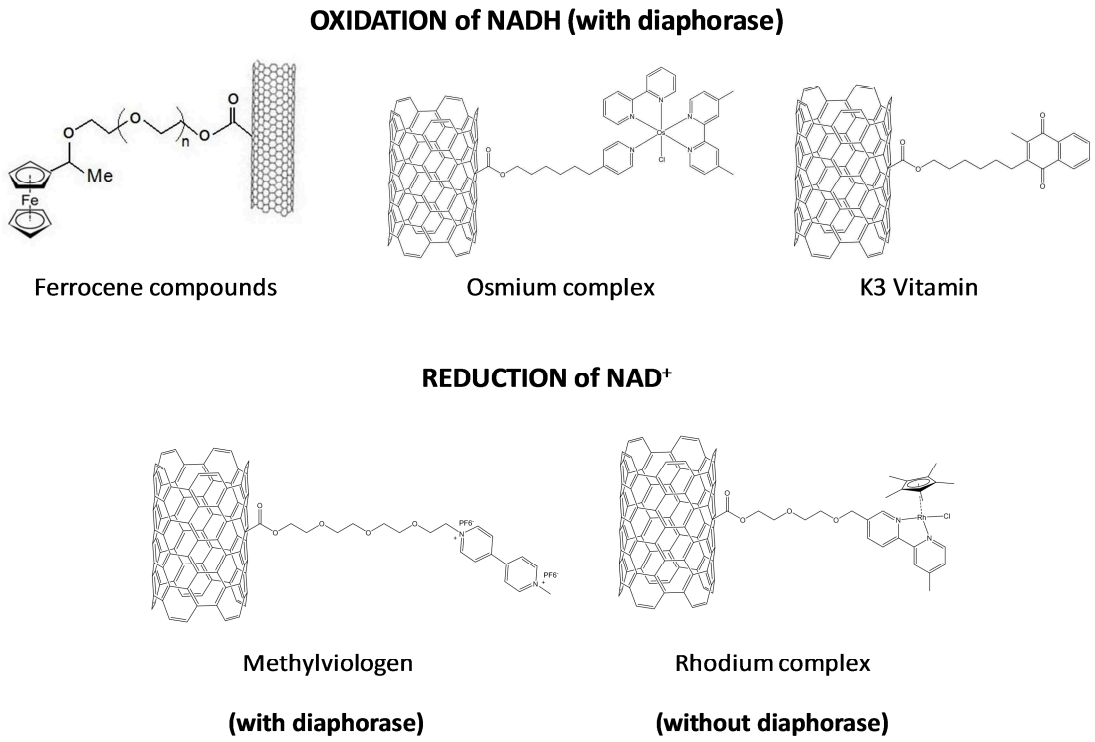

Figure 23 : the different electrochemical mediators that have been tested in this thesis work. Only ferrocene derivatives have led to significant electro-catalytic activity, so we will only present the work done on these mediators.

We carried out the covalent grafting of each of these compounds on CNTs with a low number of walls (manufacturer: Nanolab) or on single-walled CNTs synthesized by the HiPco process and purified (manufacturer: NanoIntegris). The preliminary study of the electrochemical reaction with NADH or NAD^+ of these grafted nanotubes was carried out by depositing on the surface of a glassy carbon electrode (GCE) a layer of grafted nanotubes from an aqueous suspension, then immobilizing the layer with either a chitosan gel or a silica gel formed by condensation of tetra-ethoxysilane (TEOS). If necessary, the diaphorase was co-immobilized with the carbon nanotubes. The electrode thus formed was used in a conventional three-electrode assembly with an Ag/AgCl reference electrode and a platinum counter electrode. A solution containing NADH or NAD^+ as appropriate was oxidized or reduced by cyclic voltammetry. The electrochemical scanning rate was varied from 5 to 20 mV/s, the solution concentrations of NADH or NAD^+ were varied, and the overall electrochemical behaviour was studied to reveal a significant or negligible electro-catalytic effect. This preliminary work was conducted in close interaction with

Mrs Veronika Urbanova, in charge of the electrochemical study, while the syntheses of mediators modified by spacer arms and covalently grafted to the surface of the CNTs were carried out as part of this thesis work.

At the end of this systematic study, ***we obtained clear electro-catalysis results only when the mediator used was a ferrocene derivative***. This is why the whole rest of this work consisted in developing this approach in a systematic way, by studying in particular the possible effect of the spacer connecting the molecules of electrochemical mediator to the CNTs, and by characterizing in a particularly detailed way the different chemical steps carried out on the CNTs and the covalent nature of the complete grafting process.

4.4. The use of electrodes modified by functionalized nanotubes for the development of bio-electrochemical devices.

Functionalized CNTs have been used in this thesis for the electro-catalytic detection of biological molecules such as NADH and glucose. In particular, the functionalization of CNTs by ferrocenic groups makes it possible to greatly reduce the potential associated with the electrochemical oxidation of NADH and thus promotes its detection and regeneration at low potentials.

Figure 24 shows the bioelectrochemical device used for the electrocatalytic regeneration of NAD^+. The electronic mediator (Fc = ferrocene) is immobilized on the surface of the CNTs which are then mixed with the enzyme GDH (glucose dehydrogenase) and deposited on a glassy carbon electrode. The electrode is introduced into the electrochemical cell containing the co-factor. The mediator is covalently linked to the CNT in order to avoid detachment and thus to increase the stability of the bioelectrochemical cell.

The electrochemical results for ferrocene functionalized CNTs with the diethylene glycol linkage show that the anodic current increases with the gradual addition of NADH. Since the oxidation of NADH starts at higher potentials when the functionalized CNTs are absent or when the oxidized but not functionalized CNTs are used, a very clear electrocatalytic effect is obtained due to the simultaneous presence of the CNTs and the ferrocene moieties. All these results were obtained with very pure nanotubes (HiPco) to show that the electrocatalytic effect is not due to metal impurities often present in the majority of CNTs.

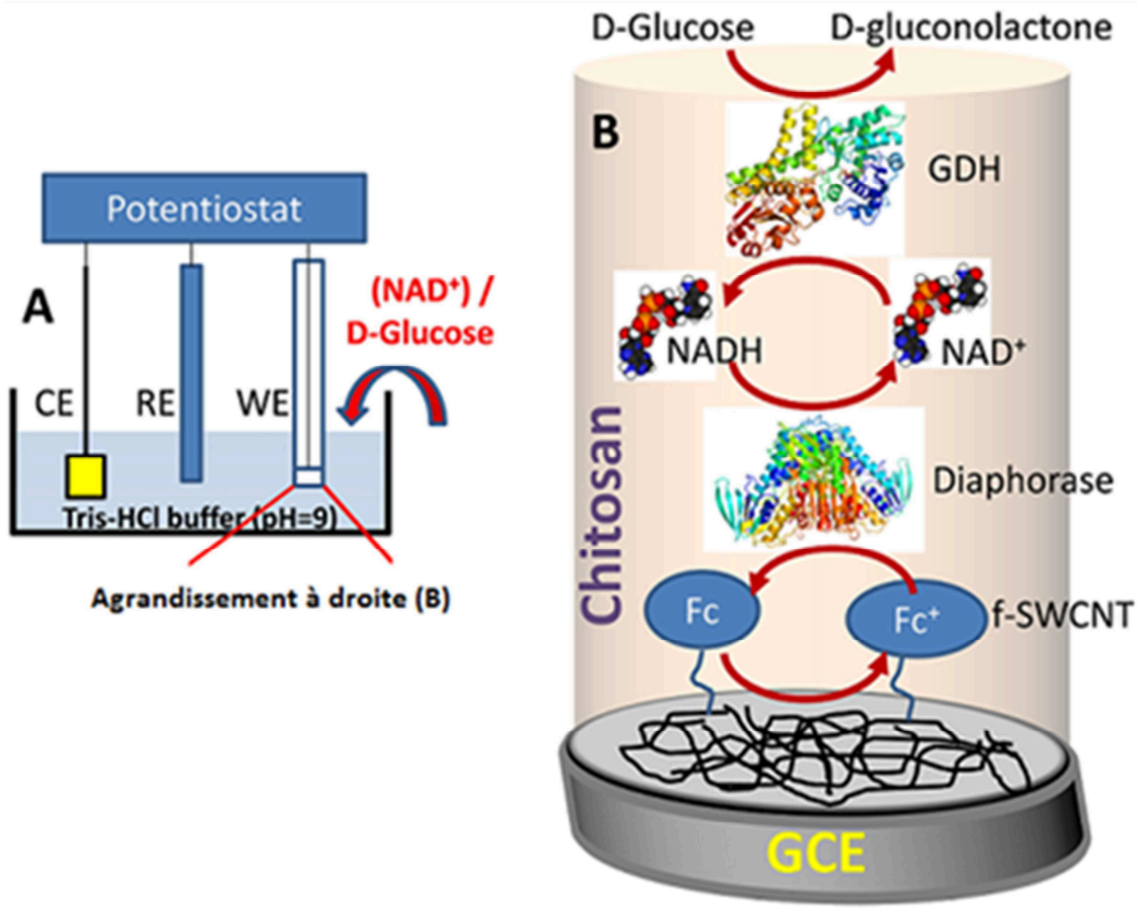

Figure 24: Our bioelectrochemical device

2 Summary of appended papers

We chose to present the peer-reviewed publications and proceedings from this thesis in an order that is not necessarily the chronological order. Figure 25 indicates the chosen order, which corresponds to the grouping of the work into three clearly defined sub-themes.

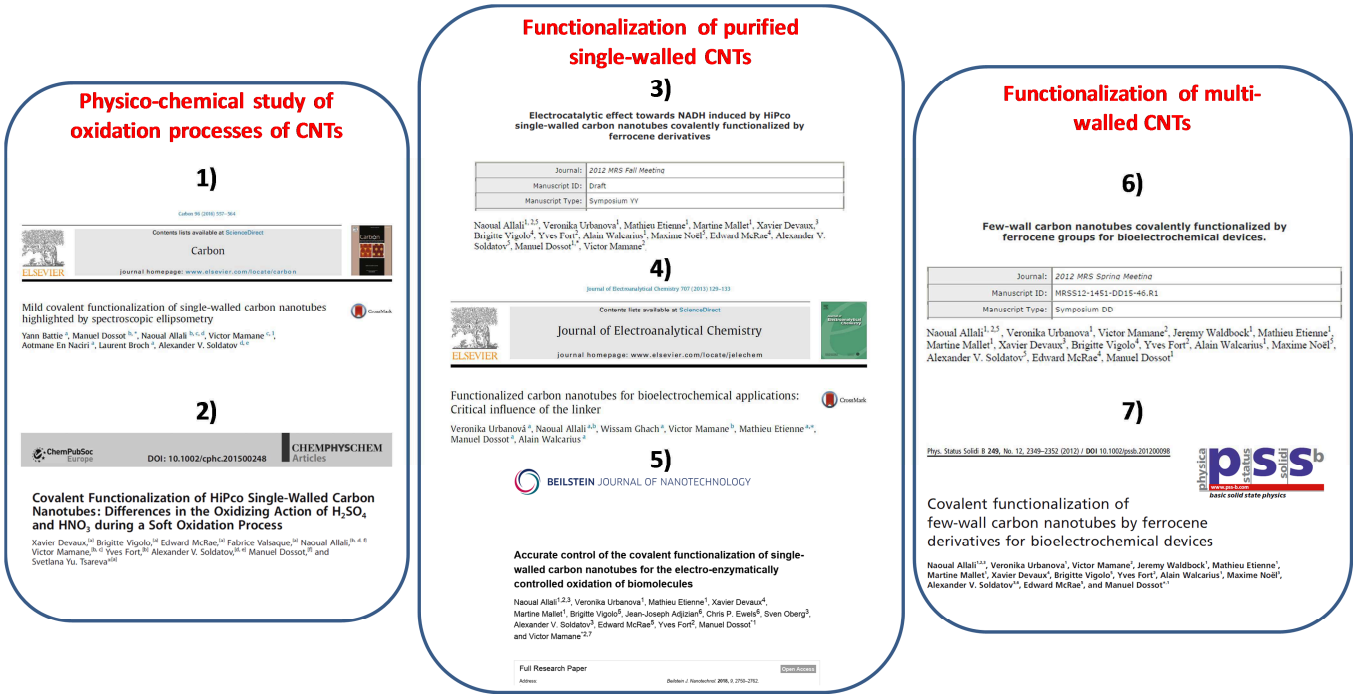

Figure 25: Organization of the presentation of the works resulting from this thesis. The first two publications mainly concern the oxidation mechanisms of CNTs. The three publications numbered 3 to 5 concern the study of the covalent functionalization of single-wall nanotubes and the effect of the nature of the spacers used on the electrochemical signals obtained at an electrode modified by these CNTs functionalized with ferrocene groups. Publications 6 and 7 extend this work to lower-quality multi-walled CNT samples, but prove that our functionalization processes are operational on much lower cost commercial samples. These systems are economically more interesting for future applications.

The first theme, which groups publications numbered 1 and 2, mainly concerns the study of the CNT oxidation stage. The first publication is devoted to the study of raw and oxidized nanotubes by Raman spectroscopy and spectroscopic ellipsometry. This publication concerns also functionalized nanotubes by the radical route, to show the interest of using ellipsometric analysis in the infrared range to show the functionalities grafted on the nanotubes. However, this technique is sensitive to grafted groups only if they are introduced in sufficient quantities. This explains the use of the radical grafting pathway, whose grafting rates are quite high. It was not possible to highlight the ferrocene groups in the context of HiPCo nanotubes grafted by the latter, because the grafting rate was too low. The second publication is a detailed study of oxidized HiPCo nanotubes in two different acid media, exploiting gas absorption volumetry, electron microscopy and vibrational spectroscopy. This is the study of the CNTs produced in the first step of our grafting process indicated in Figure 20. We show in particular that the functionalization

of the nanotube bundles is topologically different between the concentrated HNO_3 and the diluted H_2SO_4 media.

The second theme is dedicated to the covalent functionalization of single wall nanotubes, including the highly purified HiPCo nanotubes obtained from Nanointegris. This work unmistakably highlights the covalent functionalization of nanotubes, particularly thanks to our advanced analytical approach based on a range of highly complementary techniques. They also show that our three-step process works well on the walls of the CNTs with ferrocene groups, while maintaining excellent structural integrity because Raman scattering spectroscopy does not show a significant increase in the sp^3-like defects around of 1350 cm^{-1}. These functionalized CNTs are then used in bioelectrochemical devices, notably using electron (and proton) exchanges with NADH (nicotinamide adenine dinucleotide in reduced form). A very clear electrocatalytic effect is obtained, which is extremely interesting since NADH is the co-factor of more than 400 different enzymes. The dilute sulfuric acid oxidation process is just as good as that in the concentrated nitric acid, which allows us to propose a soft oxidation route, in an essentially aqueous medium, and fast thanks to the assistance microwave.

The very high purity of the nanotubes used makes it possible to eliminate any effect of the impurities (residual catalytic particles, amorphous carbonaceous particles). Finally, the study of the effect on the electron transfer efficiency of the nature of the spacers is conducted from an electrochemical point of view (publication number 4) but also via molecular modeling carried out by our colleagues from the Nantes Institute of Materials (publication number 5, accepted in Beilstein Journal of Nanotechnology, 2018). This work shows that an alkyl chain spacer causes a refolding of the ferrocene unit towards the wall of the nanotubes, thus preventing good mobility of the electroactive group enabling it to react within the bioelectrochemical device. The problem is solved by the use of a polyethylene glycol chain spacer (PEG), which is much better chemically compatible with chitosan or the silica used to immobilize the grafted CNTs on the surface of the electrode. In this case, the length of the chain does not seem to play a significant role from the point of view of the results obtained in electrochemistry, even if an optimum is found for a 6-pattern PEG spacer. Theme 2 includes a presentation of an oral presentation at the Fall Material Research Society (MRS fall meeting 2012), and two publications.

Finally, theme 3 extends the interest of our grafting method to nanotubes with several walls, much less "clean" than the purified HiPCo nanotubes. The interest here is to use low-cost commercial sources of CNT, and to show that these CNTs, once grafted by ferrocene groups with PEG spacers, work very well within bioelectrochemical devices. This makes it possible to envisage concrete applications of these nanotubes in devices of the sensor type, or of the bioelectrochemical reactor type. This theme 3 contains the proceedings of a poster presented at the Spring Material Research Society (MRS Spring meeting 2012) and one publication.

Summary of Paper n°1

(Carbon 96 (2016) 557-564)

Title: Mild covalent functionalization of single-walled carbon nanotubes highlighted by spectroscopic ellipsometry.

Authors: Yann Battie, Manuel Dossot, Naoual Allali, Victor Mamane, Aotmane En Naciri, Laurent Broch and Alexander V. Soldatov.

Summary:

Context.

This first publication concerns the joint study by Raman scattering spectroscopy and spectroscopic ellipsometry of functionalized single-walled carbon nanotubes. Our own experience with functionalized CNTs analysis in the laboratory suggested that we should indeed find new analytical methods for characterizing the functions grafted onto the wall of CNTs. It is common to use Raman scattering spectroscopy to show an increase in sp^3 defects (via the increase in D-band intensity around ~1350 cm^{-1}) when covalently grafting chemical functions onto CNT sidewalls or extremities. However, it has been found that in the case of our microwave-assisted acid oxidation protocol, we do not have a significant increase in this D-band. In addition, the literature also reports other spectroscopic techniques, including UV-visible absorption spectroscopy or fluorescence spectroscopy. But in the first case, the suspension protocol for functionalized CNTs requires the presence of a surfactant that is retained during analysis, and there is always a concern that the surfactant may play a role and disturb the analysis of absorption peaks related to van Hove's singularities. In the second case, only semiconductor CNTs emit fluorescence, which is inhibited for metal tubes, and we thus lose knowledge of an important part of the sample. It is also important to be able to analyze all nanotubes, including those that remain bound in bundles, and most light absorption methods require suspension followed by ultracentrifugation to analyze only individualized CNTs.

The advantage of a spectroscopic method is to be non-destructive and to be able to analyze the sample as a whole, with a certain statistical significance. In this way, we obtain very complementary information from electron microscopy or thermogravimetric analysis techniques, for example. We were therefore looking for a technique based on light-matter interaction, allowing us to analyze a significant portion of our functionalized nanotubes, and providing interesting physico-chemical information to partially characterize the covalent functionalization of CNT. Spectroscopic ellipsometry has proven to be a wise choice. We had the chance to get in touch with our colleague Yann Battie, who had already used this technique on non-functionalized CNTs and who had developed the necessary protocols as part of his thesis before being appointed Lecturer at the University of Lorraine. In this context, it was natural to check whether this technique could provide interesting information for functionalized CNTs.

We chose to study first the raw HiPCo nanotubes from Nanointegris, then the oxidized nanotubes according to one of our protocols (microwave assistance in HNO_3 65% in weight), but also functionalized by a radical attack process to increase the number of created sp^3 carbon atoms on CNT sidewalls. Indeed, we know from previous studies conducted since 2006 in the laboratory that radical functionalization leads to relatively high grafting rates. We then had an interesting sample of CNT ranging from very clean tubes with relatively few defects to well-functionalized CNTs (typically 1 carbon atom out of 60 hybridized to sp^3).

Materials and Methods.

To demonstrate the relevance of an analytical technique, it is important that the sample be as clean as possible, and we therefore studied by spectroscopic ellipsometry nanotubes synthesized by the HiPCo procedure and purified by a proprietary process, provided by the company NanoIntegris (sample named HIPCO). These nanotubes were first oxidized in a strong acidic medium (HNO_3 65% in weight) by microwave assistance for 20 minutes (sample named HIPCO-HNO_3). We also chemically modified the starting nanotubes by covalent grafting of methoxyphenyl groups via a diazonium salt, by heating in reflux in toluene for several hours. This process enabled to attack CNT sidewalls by radicals. The sample is named HIPCO-MeOH. These different types of functionalized CNTs were studied by two complementary techniques, Raman scattering spectroscopy and spectroscopic ellipsometry.

For Raman scattering spectroscopy, the nanotubes were dispersed in tetrahydrofuran (THF) (0.1 mg/mL) with a 5% by weight surfactant, sodium deoxycholate, whose chemical structure is indicated below. The suspension was sonicated via a sonotrode at 90W for 30 minutes. We then transferred the suspension after centrifugation at 20,000 rpm to a second tube and rinsed with THF under simple sonication of an ultrasonic bath to remove much of the surfactant. Then we used a drop of the resulting nanotube suspension that we placed on a glass slide to let it evaporate.

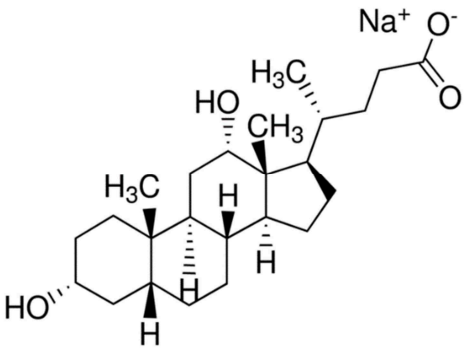

Chemical formula of sodium deoxycholate

The nanotubes re-agglomerated into bundles, but we were not trying to characterize individual nanotubes. We analyzed the samples at three different laser wavelengths: at 532 nm and 633 nm on a Witec CR200 spectrometer at the University of Lulea, equipped

with a Peletier cooled camera with a ×50 lens (0.55 digital aperture) and 1800 lines/mm grating; and at 514 nm on a Jobin-Yvon T64000 spectrometer equipped with a liquid nitrogen cooled camera, an ×50 lens (0.55 digital aperture) and 1800 lines/mm grating. We have taken care to keep the laser irradiance in all three cases below 1 kW/cm^2 to avoid any laser heating effect.

For spectroscopic ellipsometry, the analysis requires obtaining a mat of nanotube bundles as homogeneous as possible, deposited on a nitrocellulose filter. For this purpose, a relatively loaded suspension of 4 mg/mL of CNT is made in distilled water with 2% by weight of sodium cholate (formula below). The latter is better adapted to the aqueous medium than sodium deoxycholate. The suspension is sonicated for 90 minutes at 240 W while keeping the container at 5°C to avoid any heating. The suspension is centrifuged at 35,000 rpm, and the supernatant is filtered (so the pellet, which contains the largest bundles, is not analyzed) on a nitrocellulose filter. The surfactant is removed after rinsing with plenty of distilled water. This verifies the absence of foam formation, which indicates that most of the surfactant is removed.

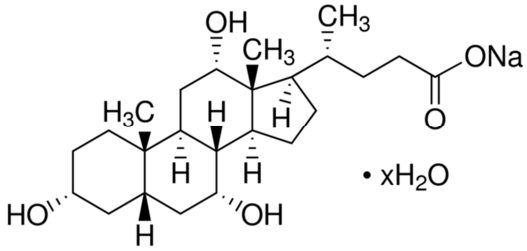

Chemical formula of sodium cholate.

Two different ellipsometers were used: between 0.6-4.96 eV (2050-250 nm wavelength), a commercial ellipsometer (Uvisel, Jobin-Yvon) was used. It is an ellipsometer using a photoacoustic modulator that modulates the phase and thus analyses the polarization of the reflected light without rotating a polarizer, thus without any mechanical movement. This allows for very fast analysis, good sensitivity and an excellent signal-to-noise ratio. The light source is a Xenon lamp, and the angle of incidence can be varied between 40 and 80 °. A photomultiplier is used for the UV-visible part up to 900 nm, then an InGaAs photodiode is used for detection in the near IR. For the infrared part between 0.07-0.6 eV (17.73 µm-2050 nm wavelength), an ellipsometer developed at the d'Alembert Institute at the Ecole Normale Supérieure de Cachan was used. It was our colleague Yann Battie who carried out the analyses in both cases.

Main results.

The publication first presents the results of Raman spectroscopy. For the HIPCO and HIPCO-MeOPh samples (Figure 5 of the publication), a clear increase in the D-band is observed at all working wavelengths used when comparing the raw and functionalized CNT D-band. On the other hand, for the HIPCO-HNO3 sample, no firm conclusion can be drawn from the Raman spectra because in one case (laser at 532 nm, figure 4A) the D

band increases very slightly, but in another (laser at 633 nm, figure 4B) it decreases after oxidation treatment!!

On the other hand, spectroscopic ellipsometry shows clearer differences between the three samples. First, the HIPCO sample was studied over the entire spectral range by varying the angle of incidence of light between 50° and 70°. An optical model of a semi-infinite and isotropic homogeneous film was used (see the first part of this thesis manuscript or the publication). This model allows extracting the real and imaginary part of the dielectric function of the CNT film. We verified that this function is independent of the incidence angle (Figure 8 of the article) and thus validated the model. Then this model was used for all three samples, and Figure 9 shows the imaginary part and the real part of the dielectric function for the HIPCO, HIPCO-HNO_3 and HIPCO-MeOPh samples from the medium infrared to ultraviolet. This figure is particularly important and is reproduced below.

We can clearly see on the imaginary part (corresponding mainly to the absorption bands of the film) the van Hove singularities of the semiconductor CNTs S_{11}, S_{22} and S_{33} as well as the metallic M_{11}, in particular for the raw HIPCO nanotubes. We also see a plasmon absorption band in the ultraviolet, characteristic of these collective electron movements in metal tubes. When the CNT are oxidized (HIPCO-HNO3 sample), all these bands are slightly disturbed. It should be noted that the same absorption experiment in the UV-visible range up to 1200 nm wavelength was attempted directly on an absorption spectrometer (Cary 6000i) in a 1 cm optical path cuvette, with suspensions of CNT in heavy water and different surfactants. We had not been able to obtain good, reproducible results, due to a too weak functionalization and a lack of reproducibility of the stability of the suspensions obtained.

The film deposition technique of ellipsometry, on the other hand, allows reproducible experiments to be carried out that provide relevant information on the effects of functionalization on the oscillator strength of the CNT absorption bands.It should be noted that the plasmon band has decreased relatively significantly; suggesting that oxidation with HNO_3 still affects the metallic CNTs a little. This supports the observation of a slight decrease in Raman band intensity in RBM modes at 532 nm (Figure 4A), while metallic CNTs are mainly observed at this wavelength (based on the Kataura diagram).

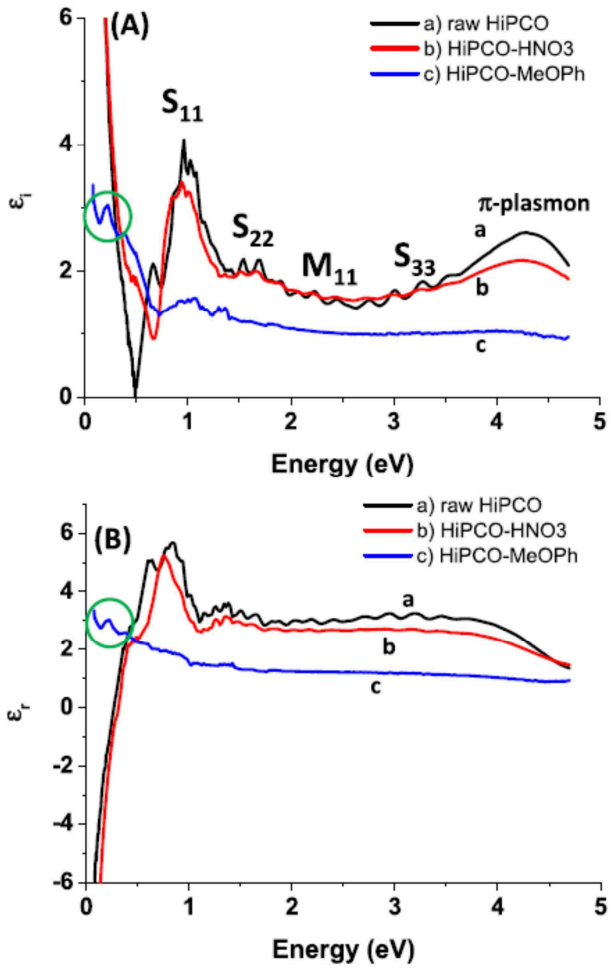

Figure 9 of the publication: A) Imaginary part and B) Real part of the dielectric function of CNT films as a function of incident light energy, derived from measurements in an isotropic, homogeneous and semi-infinite medium model.

When the functionalization process further modifies the structural integrity of the CNTs, by significantly increasing the number of carbon atoms in sp^3 hybridization, there is a very significant transformation of the imaginary and real parts of the complex dielectric function of the film. Thus for the HIPCO-MeOPh sample, the van Hove absorption peaks as well as the π-plasmon band disappear. There is also a very strong variation in the real part of the dielectric function in the infrared spectral zone (for an energy of less than 0.5 eV, the part circled in figure B above). While it is negative for HIPCO and HIPCO-HNO_3, it becomes positive for HIPCO-MeOH and shows additional absorption bands in the imaginary part of the dielectric function at 1610 and 3060 cm^{-1}, characteristic of MIR absorptions of phenyl groups. Spectroscopic ellipsometry is therefore particularly valuable in highlighting the effects of functionalization, even for a mild functionalization process such as our microwave-assisted oxidation route.

We were also able to model the IR part of the dielectric function using a coarse model (the Drude model), which allowed us to show that oxidation in HNO_3 had probably oxidized and removed residual carbonaceous impurities, while confirming the fact that

metal CNTs were slightly more affected than semiconductors in the process. This makes it possible to understand why the 532 nm Raman spectra, which are essentially derived from metal CNTs in electron resonance at this laser wavelength, show a slight increase in the D band, since these tubes are more affected.

Conclusion and perspectives.

This work validated spectroscopic ellipsometry as a new technique for functionalized CNT analysis. It has the advantage of analyzing a nanotube film, thus being statistical on the entire sample, while eliminating the potential effect of a surfactant on the electronic absorption properties of CNTs. Performing the analysis also in the infrared spectral part allows the direct detection of grafted groups if the grafting rate is not too low (in our case, typically 1 grafted C atom for 60 atoms, data from thermogravimetric analysis). It is sensitive enough to also highlight the role of residual carbonaceous impurities, and the effect of an acid treatment on these impurities. It also showed a slight preference for our microwave-assisted HNO_3 oxidation process for metallic CNTs, information that neither Raman scattering spectroscopy nor traditional UV-visible near-IR absorption could clearly establish (although in retrospect we better understood the Raman results in Figure 4). It is therefore a complementary tool to the thermogravimetric analysis technique, effective in characterizing oxidation or soft functionalization processes with low grafting rates.

In perspective to this work, we could consider testing several grafting methods by controlling the rate of grafted functions if possible, in order to further explore the observation in the field of IR medium of grafted groups, in order also to determine a grafting threshold where these functions can be detected. We could also refine the model used to interpret the results and extend these studies to few or multi-walled CNTs.

Author's contribution :

In this work, I have made the functionalization of CNTs, the analyses of CNT by Raman spectroscopy, and I participated in the interpretation of all the results, including ellipsometric spectroscopy, and the writing of the paper.

Summary of Paper n°2

(ChemPhysChem 16 (2015), 2692–2701)

Title: Covalent Functionalization of HiPco Single-Walled Carbon Nanotubes: Differences in the Oxidizing Action of H_2SO_4 and HNO_3 during a Soft Oxidation Process.

Authors: Xavier Devaux, Brigitte Vigolo, Edward McRae, Fabrice Valsaque, Naoual Allali, Victor Mamane, Yves Fort, Alexander V. Soldatov, Manuel Dossot, and Svetlana Yu. Tsareva.

Summary:

Context.

The second publication concerns the study of the chemical evolution of the surface of HiPco single-walled carbon nanotubes (SWCNT) subjected to two types of oxidation in an acid environment.

The treatment conditions used in our case, i.e. treatment with dilute H_2SO_4 acids (mild acid medium) and concentrated HNO_3 (strong acid medium), were chosen in such a way as to avoid any significant damage to the nanotube structure. During the diluted H_2SO_4 treatment used, the electrophilic reagent attacks some of the C=C bonds, producing hydroxyl groups which, in turn, can be converted into ketones (quinones or lactones), and finally into carboxylic acids. In the case of a strong oxidant or when the oxidative process is applied for a long time, there are more functional groups on the surface of the CNTs, which alter their conductive and optical properties, but also their thermal and mechanical stability. On the other hand, nanotubes can be significantly shortened. The use of a gentle oxidation process, in which acids react with existing defects without damaging the CNT sidewalls, could help us to better understand the difference in reactivity of the different oxidants.

Determining the existence and making quantitative measurement of the number of different surface functional groups created after oxidation is a real experimental challenge, as is their location on the surface of CNT bundles, especially when functionalization levels are low. To verify the presence and number of grafted functional groups, and as there is no single analytical method that provides this information, our paper reports a combination of analytical methods such as infrared spectroscopy, X-ray photoelectron spectroscopy (XPS) and thermogravimetric analysis coupled with mass spectrometry (TGA/MS).

In the present paper, we compared the oxidative action of H_2SO_4 and HNO_3 using this multi-technical approach but also by carrying out a careful study in gas volumetric adsorption, carried out by my colleague Svetlana Tsareva. The concentration of acids and the choice of treatment conditions used were made in order to achieve a mild oxidation to avoid damaging the structure of the CNTs. It is known that acids can react with impurities such as amorphous carbon, hollow carbon shells or catalyst nanoparticles; therefore,

commercial nanotubes synthesized by the HiPco process and highly purified ("Nanointegris SuperPure" grade) have been used because of their high purity level that will simplify data interpretation.

We have used a variety of analytical techniques, including TEM, STEM, energy dispersive X-ray spectroscopy (EDS), TGA-MS, diffuse reflection in infrared spectroscopy (DRIFT), rare gas adsorption volumetry, and Raman spectroscopy, to provide complete information on the type and level of functionalization, distribution of grafted functional groups and morphological changes characteristic of samples. The combined results allow us to explain the structural differences after oxidation by H_2SO_4 and HNO_3 and to suggest possible reaction mechanisms that occur on the nanotube surface.

Materials and Methods.

We therefore studied by Raman spectroscopy HiPCo Super Pure nanotubes produced and purified by NanoIntegris (sample named HIPCO). These nanotubes were oxidized by microwave assistance for 20 minutes at 50°C in an acid medium HNO_3 65% (by weight, 15 $mol.L^{-1}$) (sample named oxHNO_3-SWCNTs) and in an acid medium H_2SO_4 diluted to 2.5 $mol.L^{-1}$ (sample named oxH_2SO_4- SWCNTs).

We also treated the oxH_2SO_4-SWCNTs nanotubes with thionyl chloride $SOCl_2$, thermally refluxed under argon for 24 hours. This sample is referred to as "COCl-SWCNT". This is an intermediate step in creating acid chloride groups useful for covalent grafting of complex chemical groups, such as electroactive groups based on ferrocene derivatives, which we will use in other publications in this thesis. It was therefore interesting to study this chlorination step, despite the difficulty of placing the samples thus created in closed cells under argon to avoid reaction with ambient humidity during the various analyses carried out on this type of samples.

For Raman scattering spectroscopy, the nanotubes were dispersed in tetrahydrofuran (THF) (0.1 mg/mL) with a 5% by weight surfactant, sodium deoxycholate. The suspension was sonicated via a sonotrode at 90 W for 30 minutes. We have taken care to maintain laser irradiance for all samples at less than 1 kW/cm^2 to avoid any laser heating effect. We then transferred the suspension after centrifugation at 20,000 rpm to a second tube and rinsed with THF under simple sonication of an ultrasonic bath to remove much of the surfactant. Then we used a drop of the resulting nanotube suspension that we placed on a glass slide to let it evaporate. We analyzed the samples at 633 nm on a Witec CR200 spectrometer at the University of Lulea, equipped with a Peletier cooled camera with a ×50 objective (0.55 of numerical aperture) and 1800 lines/mm grating.

Infrared analyses of powders were performed by Fourier transform diffuse reflection mode spectrometry (DRIFT), data were collected in the high temperature chamber of the “Prying Mantis” apparatus from Harrick Corporation's, which allowed the sample to be analyzed up to 100°C under nitrogen. The reference sample is a potassium

bromide powder KBr. The diffuse reflection spectra Rs of the sample and Rr of KBr used as a non-absorbent reference powder were measured under the same conditions. The sample was prepared by mixing SWCNT powder with KBr (with a SWCNT mass fraction in KBr of 0.1%), without compaction. The reflection is defined by R = Rs / Rr. The spectra are represented on a pseudo absorbance scale (-logR).

Thermogravimetric analysis coupled with mass spectroscopy (TGA-MS) consists in measuring the mass variation of a sample as a function of temperature. The analyses were performed using a device (Setsys Evolution 1750 TGA- SETARAM/Omnistar GSF 301C-Pfeiffer Vacuum) with a helium ramp (Air Liquide Alphagaz 2) with a flow of 20 $mL.min^{-1}$ from room temperature to 1000°C at a rate of 3°C/min, on 3-4 milligrams of sample placed in an alumina crucible. The emitted gases were analyzed by a mass spectrometer (Omnistar GSD 301C). The gas was introduced into the ionization chamber of the samples. In this study, only the six intensities of the selected ions (m / z = 12, 16, 18, 18, 29, 44, 58) were monitored and correlated to the different mass losses observed in the thermograms. The parameters used for the mass spectrometer allowed a simple ionization of most species, which means the charge z = 1 for the detected mass-to-charge ratio m/z; thus, m/z or mass will be used interchangeably in the text. TGA-MS characterizations were performed on at least two samples for a given sample to ensure reproducible results.

For electron microscopy, the samples were dispersed in absolute ethanol and then deposited on a carbon film with holes deposited on a 300-mesh copper grid. Some observations of high-resolution transmission electron microscopy (HRTEM) were made with a Philips CM200 microscope with an acceleration voltage of 200 kV. The other HRTEM and STEM images were made with a JEOL ARM 200F microscope equipped with a cold field emission gun, a Cs-corrector sensor (sphericity aberration correction) and a JEOL SD30Gv detector for EDS spectroscopy. To avoid damaging the SWCNT, the microscope operated at 80 kV. High-resolution STEM images with high-angular annular dark-field detector (HAADF) were obtained for collection at half-angles of 45-180 mrad, and a pixel time of 40 ms (1024 × 1024 pixels).

The physisorption studies were carried out using a device with two pressure gauges, allowing measurement between 10^{-3} and 1100 Pa (i.e. over the entire isothermal range) with a resolution of 0.003% over the entire scale and a reading accuracy of 0.5% (over the range 10^{-3} to 1 Pa) and 0.2% (between 1 and 1100 Pa). The raw isotherms have been corrected for the effect of thermal effusion. This effect is also known as thermomolecular flux. Thus, in order not to distort the isothermal route, the pressures have been systematically corrected. Liquid nitrogen was used to maintain a constant temperature (77 K) of the sample cell containing the adsorbent under study.

The other part of the apparatus (including the pressure gauges, intake manifold, gas tank, etc., except the pumps), isolated from the cell by a valve, has been stabilized at 30± 0.5°C. The Krypton gas was introduced into this last part and then into the adsorption cell by opening the valve.

After adsorption, the cell pressure decreases and reaches an equilibrium value. The equilibration times vary from 0.3 to 1 hour per dose and were chosen experimentally. Our experimental set-up was optimized so that samples of small masses, but with a large specific surface area, could be accurately analyzed. The samples (typically a mass of 10 mg) were initially degassed outside the adsorption chamber for 7 days at 100°C to a pressure below 10^{-4} Pa. After installation in the adsorption cell, they were degassed for 1 day at 100°C at a pressure below 5.10^{-5} Pa. In addition, isothermal measurements have always started with degassing the sample at room temperature (20 °C) for 16 h at a pressure $<5.10^{-5}$ Pa. Krypton (99.998%, Fluka Analytical), was purified by pumping the condensed phase inside the device. The experiments were carried out with two adsorbent dosing protocols (AD), referred to as IAD (increase in adsorbent dosage) if the dose is increased from one injection to another or CAD (constant adsorbent dosage) if the dose is constant.

Main results.

The publication first presents the results of Raman spectroscopy. The intensity of the D-band decreases slightly after treatment with both acid treatments. For nanotubes that resonate electronically with the wavelength of the laser used, it was observed that the intensity of the band corresponding to the RBM radial breathing mode of all metallic SWCNTs decreased, while that of the semiconductor band centered at 287 cm^{-1} increased slightly after acid treatment.

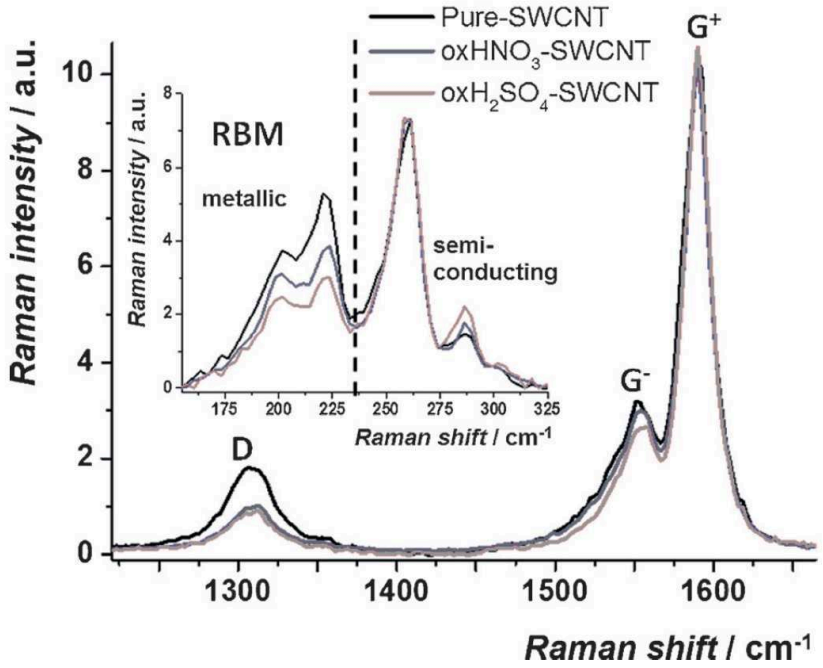

Figure 1: Raman spectra taken at 1.96 eV (633 nm) for raw SWCNT, oxH_2SO_4-SWCNT and $oxHNO_3$-SWCNT samples. The intensities have been adjusted to those of the G^+ peaks. In the insert at the top of the image: the RBM spectra taken for the same samples. The RBM intensities are normalized with respect to the intense mode at 264 cm^{-1}.

The G^- component of the G-band shows the same trend as the RBM spectrum; this means that there is a stronger impact of H_2SO_4 treatment on resonance conditions. Indeed, the two G^- contributions of metallic CNTs (including the Breit Wigner-Fano broad band which peaks at about 1530 cm^{-1}) and semiconductors (around 1550 cm^{-1}), decrease in intensity, as shown in Figure 1.

The functionalization of semiconducting CNTs modifies resonance conditions and therefore has a greater impact on the G^-band than on the RBM part of the spectrum. Interpretation of the experimental results obtained from the Raman spectroscopic analysis of SWCNT bundles is difficult. It is impossible to distinguish between the contribution of the D-band of amorphous carbon and that of defective nanotubes. However, the formation of defects in the SWCNT sample during the oxidation process changes the respective intensity of the D, G^- and G^+ bands, and the lowest frequency of the G^- part of the G-mode is reduced in intensity more significantly than the highest frequency of the G^+ part. We can therefore suggest that the decrease in the intensity of the D-band accompanied by a decrease in the intensity of the G^-band is a sign of oxidation of both amorphous carbon and nanotubes. Although the number of functionalized SWCNTs increased after acid treatments, some amorphous carbons were probably removed during oxidation. This results in a slight decrease in the intensity of the D-band of the two oxidized samples.

For raw SWCNT, the results of the coupled thermo-gravimetric analysis - mass spectrometry (TGA/MS) show that functional groups and defects are present on the surface of the purified SWCNT before oxidation treatments are performed. This result agrees with IR spectroscopy data, which showed the presence of $-C-H_n$ and -OH in the raw SWCNT sample.

The thermograms of the raw SWCNTs and the two oxidized SWCNT samples gave the following results. Raw SWCNT sample undergoes a continuous loss of mass when the temperature increases to 15.2% in loss of mass at 800°C. The TG curves of the two oxidized samples are different. Below 700°C, the weight loss of $ox H_2SO_4$-SWCNT is almost identical to that of raw SWCNT but above 700°C there is an additional weight loss. For the $ox HNO_3$-SWCNT sample, above 150°C the functions are eliminated more quickly. Processing with H_2SO_4 therefore introduces fewer functions than processing with HNO_3. The total mass loss at 800°C reaches about 18% for $ox H_2SO_4$-SWCNT and about 21% for $ox HNO_3$-SWCNT, indicating a low level of functionalization for both acids.

The TGA-MS also established a difference between the two oxidized samples concerning the thermal stability of carboxylic acids, which suggests a difference in the location of functional groups on the SWCNT surface.

Detailed TEM/STEM examinations (Figure 4 of the article) show that raw SWCNTs are aggregated in small bundles, comprising on average 25-30 nanotubes. There are also a significant number of isolated SWCNTs and very small bundles of two or three tubes. The bundles appear to be weakly bound and are a few micrometers long. The diameters of SWCNT are heterogeneous, about 0.7-1.6 nm. Triangular channels

defined by three tubes are observed, but there are other larger channels defined by four tubes.

An analysis of the HRSTEM images shows that the distance between adjacent tubes is variable. Most SWCNTs are closed. There are some diffuse metal particles or carbon impurities.

The detailed TEM-STEM examination of the oxH_2SO_4-SWCNT and oxHNO_3-SWCNT samples shows that treatment with acids leads to a significant increase in the number of open SWCNTs and that the typical lengths of SWCNTs are similar to those of raw SWCNTs. A very small increase in the number of carbon impurities was observed in both cases. The morphologies of oxH_2SO_4-SWCNT and oxHNO_3-SWCNT were, however, different.

The bundle structure of the oxH_2SO_4-SWCNT sample is similar to that of raw SWCNT but, in the case of oxHNO_3-SWCNT, the morphology changes due to some alignment of the bundles (Figure 4 (c) of the paper).

Through DRIFT analysis, we know that there are the same functional groups on the surface of the SWCNT bundles of both samples.

For oxHNO_3-SWCNT, carboxylic acids are probably uniformly dispersed on the lateral surfaces of the bundles, which could explain the alignment of the bundles by electrostatic attraction between the different bundles. This could be due to the formation of weak hydrogen bonds between functional groups on the surface of the CNT. The bundles in the oxH_2SO_4-SWCNT would then not be aligned because there are fewer COOH groups - on the side faces of the bundles; they are probably densely located mainly at the ends of the SWCNT bundles.

In addition, the volumetric adsorption study established a difference between the two oxidized samples in terms of the number of carboxylic acid groups on the ends of the SWCNTs. For the two oxidized samples, the second part of the overall isotherm is consistent with that of the raw SWCNT sample, which implies that the number of functions on the surface is insufficient to influence the adsorption of Kr on the outside surface of the bundles.

Conclusion and perspectives.

We presented the results of a study on the covalent functionalization of SWCNT HiPco. TEM/STEM, EDS, TGA-MS, Raman scattering, DRIFT spectroscopy and noble gas adsorption volumetry techniques were used and provided important information about the level of functionalization, the type of functionalization groups, and their location on the nanotube surface.

H_2SO_4 and HNO_3 treatments introduce the same functions on SWCNT bundle surfaces, but the number of -COOH groups at the end of SWCNT bundles is different, due to significant differences in properties. For the oxH_2SO_4-SWCNT sample, the

quinone or carboxylic acid groups grafted to the ends of the bundle can block the entry ports in the internal channels of the open tubes or in the interstitial channels of the bundles through the formation of dimers. In the case of the oxHNO3-SWCNT sample, the -COOH functions are well dispersed on the SWCNT surface and may form weak bonds either with -COOH, or with other groups such as -OH or quinone C=O located on adjacent bundles. These interactions lead to the alignment of the bundles.

Author's contribution:

In this work, I have made the functionalization of CNTs, the characterization of CNTs by Raman spectroscopy, and I participated in the interpretation of all the results, and the writing of the paper.

Summary of Paper n°3

(Proceeding of the 2012 MRS fall meeting in Boston)

Title: Electrocatalytic effect towards NADH induced by HiPco single-walled carbon nanotubes covalently functionalized by ferrocene derivatives.

Authors: Naoual Allali, Veronika Urbanova, Mathieu Etienne, Martine Mallet, Xavier Devaux, Brigitte Vigolo, Yves Fort, Alain Walcarius, Maxime Noël, Edward McRae, Alexander V. Soldatov, Manuel Dossot, Victor Mamane .

Summary:

Context.

The third publication reports the covalent functionalization of single-walled carbon nanotubes by ferrocene derivatives with polyethylene glycol chains of variable length. The objective is to examine whether covalent grafting of electroactive functions allows an electrocatalytic effect to be observed when the grafted nanotubes are incorporated into the surface of a glassy carbon electrode (CGE) used as a working electrode to transfer charges to biomolecules, such as adenine dinucleotide dihydronicotinamide, NADH. In order to avoid as much as possible a catalytic effect of residual metal particles from the growth catalysts used to produce the nanotubes, we chose to work with an initial commercial sample of single-walled nanotubes synthesized according to the HiPco process, of the highest purity available ("super pure" grade from NanoIntegris). This sample contains less than 5% of metallic and carbonaceous impurities. Functionalized CNTs are deposited on the surface of GCE and this modified electrode is used to oxidize the NADH cofactor in the presence of diaphorase. We will indeed show in this work that a clear electro-catalytic effect is highlighted, which can only be attributed to functionalized CNTs.

HiPco nanotubes are covalently functionalized by a three-step process with ferrocene derivatives (scheme 1):

- Oxidation in an acidic environment using microwave irradiation to control the number of defects on the side walls of the CNT.

- Chlorination step by $SOCl_2$.

- Grafting of ferrocene derivatives using an alcohol function carried by a polyethylene glycol chain, whose length can be varied.

The previous studies showed the value of using microwave assistance in oxidation step 1. It allows enough defects to be transformed into COOH-type chemical groups to allow subsequent grafting of electroactive groups, while respecting the integrity of the mechanical and electronic structure of the nanotubes. The polyethylene glycol spacer was chosen to promote the dispersion of functionalized CNTs in water. Spectroscopic, thermal

and microscopic techniques are used to quantify the number of grafted ferrocene derivatives per carbon atom of the CNTs. Finally, a biosensor is manufactured by modifying the surface of the glassy carbon electrode with functionalized CNTs, this biosensor is tested for oxidation catalyzed by the diaphorase of the NADH cofactor.

Materials and Methods.

All compounds used in the steps in scheme 1 were of high purity and used as received. HiPco single-walled CNTs contain less than 5% impurity (residual catalyst) and have a diameter distribution between 0.8 and 1.2 nm. The dispersion is carried out in concentrated nitric acid (65%) and subjected to microwave irradiation for 20 min at 50°C. The conversion of COOH to COCl is carried out by treatment with $SOCl_2$ at 70°C for 24 hours. Ferrocene groups (Fc-ETG-n) react with COCl groups by their terminal alcohol function, allowing the mediator to be covalently attached to the side walls of the CNT. Functionalized CNTs (f-CNTs) are noted: HiPco-FcETGn, n being the number of additional ethyleneglycol units. Two different chain lengths are chosen for the spacers in the present paper, n=1 and n=7. The analysis of functionalized CNTs is performed by a complete set of techniques: Raman spectrometry (wavelength of the laser used 514 nm), visible and near-infrared absorption (Vis-NIR), X-ray photoelectron spectroscopy (XPS), high-resolution transmission electron microscopy (HRTEM) coupled with energy-dispersive X-ray spectroscopy (EDS), and finally thermogravimetric analysis (TGA) coupled to mass spectrometry (MS).

The f-CNTs were suspended in water using a chitosan solution and co-deposited on the surface of the GCE electrode with diaphorase to regenerate the NADH molecules. Chitosan allows a good immobilization of electroactive species on the surface of the CGE, while being very easy to use. Cyclic voltammetry measurements were performed in a conventional three-electrode cell configuration, including the working electrode (GCE modified by f-CNT films and NADH and diaphorase molecules), an Ag / AgCl reference electrode (with internal KCl 3M electrolyte) and a platinum wire auxiliary electrode. All measurements were recorded in a Tris-HCl buffer (pH 9.0) at a scanning rate of about 5 mV/s.

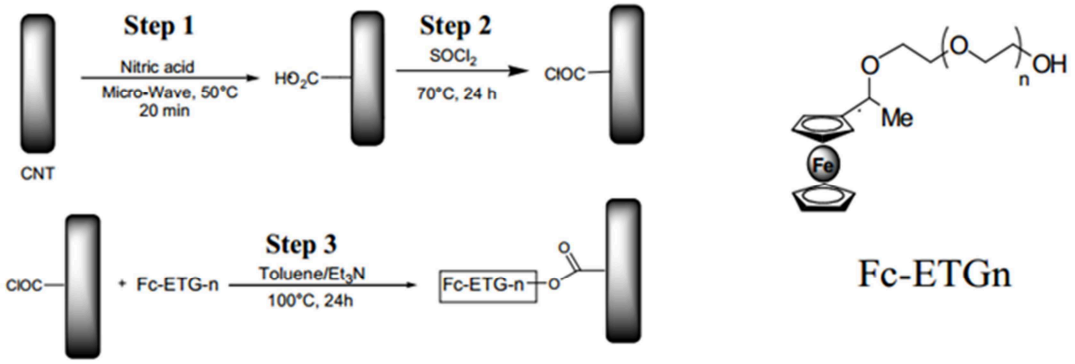

scheme 1: The three steps of functionalization of HiPco SWCNTs by ferrocene derivatives.

Main results.

Analyses of the raw HiPco sample by HRTEM showed some metallic impurities but in small numbers, and all surrounded by some carbon gangues. There is also a remarkable absence of nanographite-type impurities. Some amorphous carbon shells/deposits are observed on the outer tubes of the beams, but this can be produced under the electron beam in the microscope, and this does not necessarily come from the original sample.

The results of thermogravimetric analyses performed under helium flow are shown in Figure 1 for three samples: raw HiPco CNTs (i.e. the commercial product as received), HNO_3 oxidized HiPco CNTs and HiPco-FcETG1 CNTs. The raw sample shows a monotonous mass loss up to 1000°C, this loss is related to the desorption of chemical molecules existing on the surface or solvent molecules physisorbed during purification by the manufacturer. The mass loss slope of the oxidized HiPco sample is greater between 200°C and 300°C, then beyond 300°C, the curve shows the same rate as the raw sample. Oxidation by HNO_3 under 20 min of microwave irradiation does not introduce many new defects, unlike thermal oxidation processes during several hours of treatment. If the difference in mass loss between the raw HiPco sample and the oxidized HiPco sample is due to the desorption of the COOH functions, a COOH function is formed every 120 carbon atoms. For HiPco-Fc-ETG1, the rate of mass loss is significant between 200 and 600°C. We attribute this significant mass loss to the desorption of the ferrocene compounds grafted onto the side walls of the CNT.

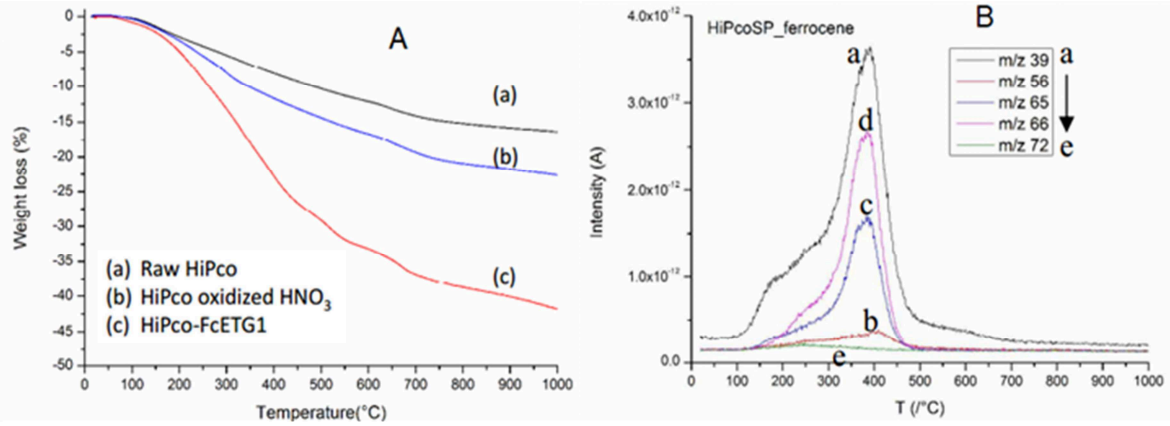

Figure 1: TGA analyses under helium flow of a) raw HiPco sample, b) oxidized HiPco sample and c) HiPco-Fc-ETG1, B : m/z channels of the mass spectrometer as a function of temperature for the detachment of 1,3-cyclopentadienyl fractions and iron atoms for the HiPco-FcETG1 sample.

Coupling mass spectroscopy to TGA confirms that iron atoms and 1,3-cyclopentadiene groups in the ferrocene group are desorbed between 200 and 500°C (Figure 1, B). Assuming that the difference in mass loss between oxidized HiPco and HiPco-Fc-ETG1 comes from the ferrocene derivative, it can be calculated that 1 per 130 C atom is grafted by the FcETG1 group. Therefore, 92% of COOH functions are grafted

by ferrocene derivatives according to these results. Obviously, this conversion rate may be a little overestimated, but it is clear that steps 2 and 3 (in Figure 1) are very effective for HiPco CNTs. **This is a really important result of the thesis: we have developed an efficient method of grafting a moderate number of electroactive groups, allowing the electronic structure of the CNTs to be maintained, while adding the desired electro-active function as we will see.**

In order to confirm these conclusions, an XPS analysis is performed on the raw, oxidized and functionalized HiPco samples. The results obtained showed the detection of iron atoms for functionalized samples, this iron comes from grafted ferrocene groups, which confirms functionalization. On the other hand, the iron atoms of the residual catalytic particles are not detectable by XPS in the raw and oxidized samples, due to the carbon layers covering these particles as seen in HRTEM. There is therefore clearly very little chance that these few metallic impurities can contribute to a significant charge transfer with NADH.

HRTEM analyses and the EDS spectrum of the HiPco-FcETG7 sample (Figure 2) clearly show the presence of iron atoms in the middle of a CNT bundle. This presence of iron atoms is attributed to ferrocene (the catalytic particles are not visible in the image). This confirms that the grafted functions are on the walls of the bundles and not only at the ends of the nanotubes. This is self-consistent with paper n°2 that has shown the fact that HNO_3 treatment enables to produce COOH groups all along CNT sidewalls.

Figure 3 reports the visible-NIR absorption and Raman scattering spectra for samples suspended in a 5% aqueous solution of sodium deoxycholate (DOC). The solution is briefly sonicated (30 min) and then centrifuged in order to remove the CNTs clusters. The functionalized samples clearly show a decrease in intensity for the Van Hove singularities of the metallic (E^{m}_{11}) and semiconductor (E^{sc}_{11} and E^{sc}_{22}) CNTs.

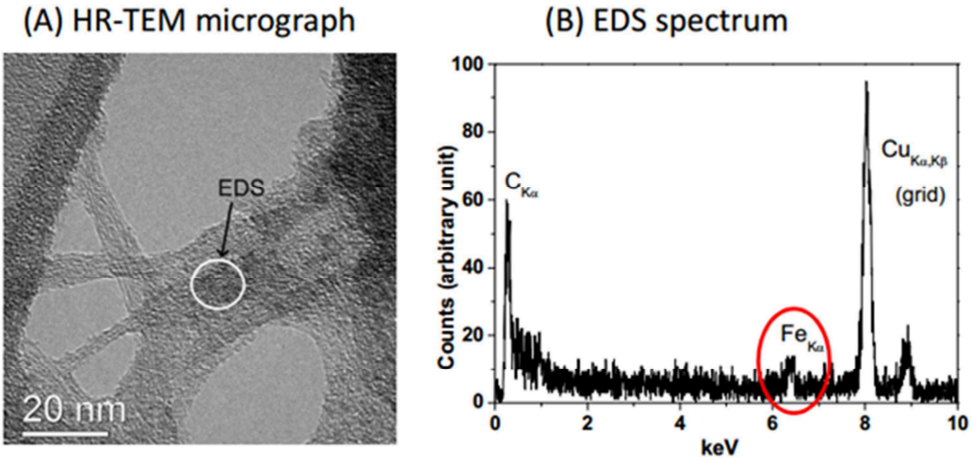

Figure 2: HR-TEM (A) and EDS (B) analysis of the HiPco-FcETG7 sample.

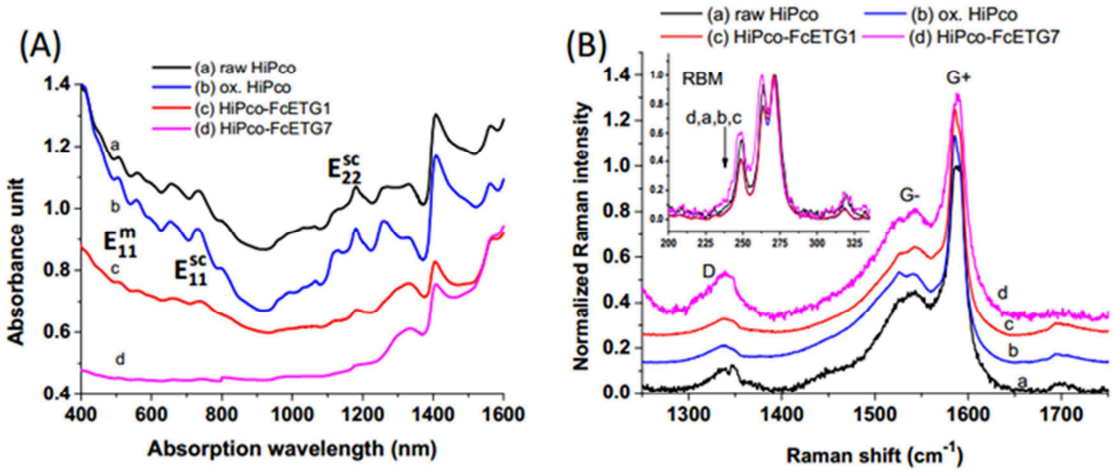

Figure 3: A)Visible-NIR absorption spectra and B) Raman scattering spectra of raw, oxidized and functionalized HiPco samples.

This is surprising that visible-NIR spectra seem more sensitive to functionalization than Raman spectroscopy; However, Raman spectroscopy only probes CNTs that are electronically resonant with the laser wavelength, while absorption spectroscopy probes all the suspended CNTs. Besides, the protocol in absorption spectroscopy essentially selects the more functionalized CNTs (that are present in the supernatant of the suspension).

All these results are a strong indication of the covalent nature of the functionalization process. Raman analyses (Figure 3B) showed that the intensity of the D-band related to covalent defects does not vary much between samples. Oxidation by microwave irradiation in the presence of HNO_3 did not introduce many new defects, which is consistent with TGA analyses. This chemical treatment promotes the conversion of existing defects into COOH functions but does not reduce CNT or destroy their side walls. By normalizing the spectra to 270 cm^{-1}, the intensities of the radial breathing peaks (RBMs) do not change much despite the decrease in electron resonance in the absorption spectra. **This change in resonance is certainly due to a charge transfer character to the ferrocene groups, in sufficient number to cause the loss of resonance in the optical domain, but insufficient to increase the diffusion process by the sp3 covalent defects characteristic of the D band of the Raman spectrum. No preferential functionalization between metallic CNTs or semiconductors is clearly observed.**

Electrochemical tests obtained with oxidized and functionalized HiPco samples deposited on GCE in the presence of increasing amounts of NADH are shown in Figure 4. The results show that the oxidized HiPco CNTs do not give any electro-catalytic effect, while for the HiPco-FcETG1 and HiPco-FcETG7 samples, the oxidation peak increases significantly with the addition of NADH, indicating effective electro-catalytic behavior. These results confirm that covalently modified HiPco samples lead to electro-catalytic effects towards NADH in solution, but that residual metal or carbon impurities show no electro-catalytic effects. **The latter therefore comes exclusively from the grafted electro-active groups**.

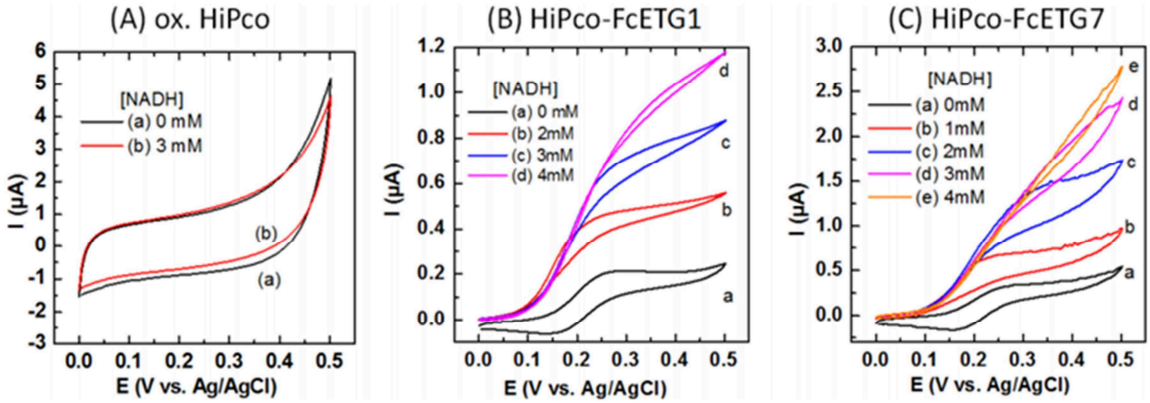

Figure 4: Voltammetric response to NADH concentrations measured on modified GCE with A)oxidized HiPco, B) and C) HiPco functionalized.

Conclusion.

The covalent functionalization of HiPco's own CNTs by ferrocene derivatives was confirmed by a set of additional analyses. The cyclic voltamperometry of a GCE modified by these functionalized CNTs in the presence of NADH showed a clear electro-catalytic effect of these covalently modified CNTs against NADH oxidation. The role of impurities or only the oxidized edges at the ends of the CNTs can be excluded to explain this effect.

Author's contribution :

In this work, I have made the functionalization of CNTs, the characterization of CNTs by Raman, visible-NIR and XPS spectroscopies, and TGA-MS analyses. I participated in the interpretation of all the results, and the writing of the paper.

Summary of Paper n°4 (Journal of Electroanalytical Chemistry 707 (2013) 129–133)

Title: Functionalized carbon nanotubes for bioelectrochemical applications: Critical influence of the linker.

Authors: Veronika Urbanová , Naoual Allali, Wissam Ghach , Victor Mamane , Mathieu Etienne, Manuel Dossot, Alain Walcarius.

Summary:

Context.

The effective electron transfer between an electrode surface and enzymatic active centers is a prerequisite for the construction of biosensors and bio batteries. For this purpose, the use of electron relays that transport electrons between the redox center of the enzyme and the conductive surface is essential. We can consider two general approaches to establishing such electronic communication. The first includes "electroactive-enzymes", in which the protein itself is modified by covalently linked redox mediators. The chemical modification of proteins by an electronic relay has been successfully applied in oxidations, for example with glucose oxidase, dehydrogenase and lactate oxidase. A second approach concerns the covalent attachment of the redox mediator via a long and flexible spacer arm leading to an electrical relay between an enzymatic active site and the surface of the electrode.

The electrochemical oxidation of nicotinamide adenine dinucleotide (NADH) has received much attention because of its importance for the design of novel biosensors, since NAD-dependent dehydrogenases are one of the most important groups of redox enzymes. Direct electrochemical oxidation of NADH and NAD^+ reduction reactions require the application of a high overvoltage, often leading to electrode poisoning; in addition, direct electrochemical reduction of NAD^+ leads to species lacking enzymatic activity. These disadvantages can be overcome by using electron transfer mediators as electro-catalysts which can lower the over-potentials usually observed for the NADH / NAD^+ redox couple.

Carbon nanotubes (CNTs) are widely used to improve electron transfer between enzymatic redox sites and an electrode surface and are also promising platforms for the immobilization of various redox mediators. CNTs have attracted increasing interest in the field of biosensors because of their interesting characteristics in terms of improving sensitivity and/or selectivity to chemical or biological compounds.

Ferrocene derivatives are often used to modify bioelectrodes because they act as a redox mediator between the electrode and the redox active center of an enzyme. To avoid

any loss of mediator in solution, different matrices for the encapsulation of ferrocene (e. g. chitosan, conductive polymers, hydrogels, sol-gel, etc.) have been used in the literature.

In this work, we used our original grafting strategy to covalently bind ferrocene derivatives to carbon nanotubes (CNT-Fc) via an alkyl spacer (CNT-(CH_2)n-Fc) or a polyethylene glycol PEG (CNT-$(EtG)_n$-Fc) and studied their behavior towards electro-catalytic oxidation of NADH. First, glassy carbon electrodes modified with CNT-Fc (dispersed in a chitosan matrix) were tested for diaphorase-catalyzed (DI-catalyzed) oxidation of NADH. In a second step, the NTCs-Fc were successfully incorporated into silica-based gels for co-immobilization with glucose dehydrogenase, DI and the NAD^+ cofactor, in order to evaluate their interest in electrochemical biochemical devices.

Materials and Methods.

Preparation of the electrode:

The glassy carbon electrodes (GCE, 5 mm in diameter) were polished with aluminum oxide (1 and 0.05 μm), sequentially, and then washed with water. The 0.5% chitosan solution was prepared by dissolving chitosan in a 1% acetic acid solution. The chitosan film with functionalized nanotubes (CNT-Fc) was prepared by mixing 2 mg of CNT-Fc, with 1 mL of chitosan under agitation overnight. 5 μL of this suspension was deposited on the surface of the GCE electrode to obtain a very thin and stable film after drying. Chitosan films containing the DI (5mg.mL^{-1}), alone, or the DI with GDH (1,000 U.mL^{-1}), are prepared by mixing 10 μL of the chitosan solution with 5 μL of DI or 15 μL of the chitosan solution with 10 μL of GDH and 5 μL of DI. Then, 5 μL of the mixture was deposited on the GCE modified by a chitosan/CNT-Fc film and dried.

The bio-doped silica sol-gel layer was prepared by dissolving 0.18 g of tetraethoxysilane (TEOS), 0.13 g of 3-glycidoxypropyl-trimethoxysilane (GPS), 0.5 mL of water and 0.625 mL of hydrochloric acid (HCl 0.01 mol.L^{-1}), which were shaken for 12 hours, then diluted 15 times with water for later use. The NAD-GPS solution was typically prepared by mixing 6 mg of NAD^+ and 37.5 mg of GPS in a Tris-HCl buffer solution at 100 μL (pH 7.5) with 14 h of agitation. Finally, 7.5 μL TEOS/GPS were mixed with 7.5 μL CNTs-Fc, 2.5 μL PEI (10% by weight, pH 9.0), 5 μL NAD-GPS solution, 7.5 μL GDH (1,000 U.mL^{-1}) and 5 μL DI (5 mg.mL^{-1}) applied drop by drop to the electrode surface.

Electrochemistry:

All electrochemical experiments were performed using a PGSTAT12 Metrohm-Autolab potentiostat controlled by GPES software. Measurements were made in a three-electrode cell, the measuring electrode is modified GCE, the reference electrode is Ag /AgCl (internal electrolyte KCl 3 mol.L^{-1}) and the auxiliary electrode is made of platinum wire.

Main results.

The publication first presents the results of the study of the electro-catalytic behavior of CNT-Fc with respect to the oxidation of NADH in the presence of a DI / chitosan overlay. A first experiment was carried out with SWCNTs functionalized with carboxylic acids before modification with ferrocene fragments. As can be seen in successive cyclic voltammograms, only a limited current increase was observed between 0.2 and 0.3 V when 1-6 mM NADH was added, without a well-defined redox peak. Good electrocatalytic behavior was observed for all ETG linkers tested here. On the other hand, very weak anode currents were observed using CNT-$(CH2)_6$-Fc modified GCE (i.e., an alkyl arm) in the presence of NADH (Fig. 1E of the publication), and such a poor result was obtained independently of the alkyl chain length.

The effect of the spacer arm on the electro-catalytic response can be explained by different hydrophobic / hydrophilic equilibria. The hydrophobic alkyl spacer may interfere with the good mobility of the Fc fragments between the surface of the electrode and / or the active center of the DI. In contrast, PEG is known as a flexible and biocompatible linear polymer with excellent solubility in water and thus PEG spacers provide the Fc fragment with more freedom to act as an electron shuttle, which increases the electron transfer frequency of the reactions with the redox centers of the DI.

In order to evaluate the effect of the length of the PEG spacer on the electrochemical response of the CNT- (EtG) n-Fc as well as their dispersing efficiency in water, six different lengths of PEG chain were synthesized, that is, mono, di-, tri-, tetra-, penta- and octaethyleneglycol (n = 1, 2, 3, 4, 5, 8). Figure 2 of the paper reports the electrochemical responses measured by cyclic voltammetry with a PEG chain of two (Figure 2A) and eight ethylene glycol (Figure 2B). While the electrochemical response of the ferrocene group in the absence of NADH was poorly defined in the experiment reported in Figure 1F, an increase in the chain length led here to a better electrochemical response with oxidation peaks and clearly visible reduction of ferrocene respectively at 0.26 and 0.16 V relative to Ag/AgCl. The number of ethylene oxide units does not appear to dramatically influence the intensity of the current for the oxidation of NADH. This is particularly interesting for using such functionalized nanotubes as potential biomedical materials since the PEG chain prolongs their biocompatibility.

With respect to the possible application of a CNT-Fc modified electrode as a bioelectrochemical component, glucose dehydrogenase (GDH) was chosen to examine the bioelectrocatalytic oxidation of glucose in the presence of NAD^+ cofactor. One of the most challenging aspects in the development of dehydrogenase-based biosensors is the immobilization of all biocatalyst components (ie, enzymes, cofactors and mediators) in a sustainable and active form. the surface of the electrode. In this work, thanks to the hydrophilic character of the PEG arms, CNT (EtG)n-Fc were incorporated in a sol-gel thin film to co-immobilize all the components necessary for the enzymatic electro reaction (Figure 5 of the paper).

The results clearly demonstrate that the electro-catalytic oxidation of NADH to NAD^+ takes place by electron transfer mediated by such a multi-component system and it can therefore be concluded that ferrocene clearly plays the role of electron mediator in our system.

Conclusions and perspectives:

In this work, we have shown the interest of the PEG (polyethylene glycol) linkers for the functionalization of carbon nanotubes with ferrocenes (Fc). It allows an effective relay of the DI for electro-catalytic oxidation of NADH. The good dispersion of the functionalized CNTs in the aqueous solutions allows their incorporation into sol-gel bioelectrocatalytic devices including glucose dehydrogenase, DI and bound NAD^+. Such a strategy for the covalent functionalization of carbon nanotubes should be useful for the design of various other devices such as biosensors, fuel cells or bioreactors. We are currently exploring ways to increase the number of clusters to be grafted onto CNTs, which would also improve the dispersion of the material in aqueous solution.

Author's contribution:

In this work, I have made the functionalization of CNTs, the characterization of CNT, and I participated in the interpretation of all the results, and the writing of the paper.

Summary of Paper n°5 (Beilstein J. Nanotechnol. 2018, 9, 2750–2762).

Title: Accurate control of the covalent functionalization of single walled carbon nanotubes for the electro-enzymatically controlled oxidation of biomolecules

Authors: Naoual Allali, Veronika Urbanova, Mathieu Etienne, Xavier Devaux, Martine Mallet, Brigitte Vigolo, Jean-Joseph Adjizian, Chris P. Ewels, Sven Oberg, Alexander V. Soldatov, Edward McRae, Yves Fort, Manuel Dossot and Victor Mamane.

Summary:

Context

In the study conducted for the publication n°4 with Nanolab nanotubes, we have demonstrated a rather unexpected effect of the role of the spacer used between the wall of the nanotubes and the electro-active ferrocene group by comparing alkyle spacers and polyethyleneglycol spacers. We wanted to examine in more depth the role of this spacer by returning to ultra-high purity single-wall HiPCo nanotubes, which make it possible to obtain much more precise data concerning the covalent nature of chemical grafting. In particular, the electron microscopy study of highly purified single-walled nanotubes is much simpler than in the case of multiwall with carbonaceous impurities. We therefore examined again the role of the nature of the carbon chain of the spacer (alkyl or polyethylene glycol, PEG) and its length (in the case of the PEG chain) on the grafting reactions and the efficiency of the electrocatalytic charge transfer with NADH, exploiting Nanointegris "SuperPure" grade HiPCo nanotubes. Moreover, we have taken up the two acid oxidation modes used in the publication No. 2, to see if the acid phase oxidation step played a role. We will show that the oxidation in dilute H_2SO_4 medium allows a covalent grafting as interesting as the concentrated nitric acid medium, which is unexpected in view of the results of paper n°2. This will allow us to propose a less dangerous protocol and more respectful of the environment. This smooth and fast oxidation process is essential to preserve the mechanical and electronic properties of CNTs. This oxidation step will be followed by two chemical steps in order to graft covalently ferrocene derivatives on the side walls of SWCNTs via chains of different lengths and different chemical nature. These functionalized tubes (f-SWCNT) were deposited on the surface of glassy carbon electrodes (GCE) using chitosan molecules to form a homogeneous film. These electrodes were used to oxidize the reduced form of the cofactor nicotinamide adenine dinucleotide (NADH) and the results clearly demonstrated an electro-catalytic effect due to the presence of the grafted ferrocene acting as a mediator. This system can be applied to bio-detection, as illustrated by glucose detection.

This work presents our strategy for covalently grafting certain ferrocene derivatives on the walls of highly purified HiPco SWCNTs and to study their electrochemical efficiency, for the oxidation of NADH in the presence of redox proteins.

In addition to the different analysis techniques, this study confirms the covalent nature of the chemical bonds formed on the surface of nanotubes.

Indeed, if we can establish that our strategy is useful for making a well-designed electrochemical device to oxidize NADH, many applications would be possible, since NADH is the co-factor of hundreds of enzymes. The functionalized nanotubes (f-SWCNTs) will be deposited on the surface of a GCE electrode and immobilized by a layer of chitosan, which will also include diaphorase, a redox protein catalyzing the oxidation of NADH in the presence of a redox mediator. The use of highly purified SWCNTs samples rules out any potential role of impurities, in particular the possible direct electron transfer between them and the NADH molecules. Figure 1 below summarizes the context and approach of this study.

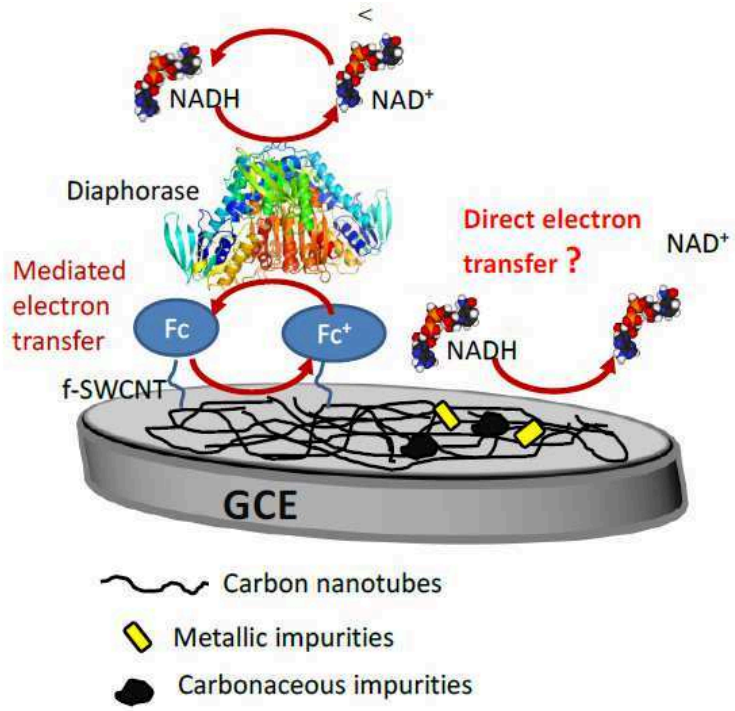

Figure 1: The working electrode incorporating the f-SWCNTs deposited on the surface of the GCE. The main objective is to use ferrocene (Fc) derivatives to transfer electrons to diaphorase, to allow electro-catalytic oxidation of NADH to NAD^+.

Materials and methods

The oxidation, chlorination and functionalization steps are previously detailed in Publications 2, 3 and 4. Samples were kept under argon to avoid moisture contamination and analyzed directly by HR-TEM, XPS and TGA-MS. Once opened to air, the samples were analyzed by Raman spectroscopy.

Analysis techniques

High resolution transmission electron microscopy (HRTEM) and high-resolution scanning transmission electron microscopy (HRSTEM) were performed using a JEOL

ARM200 microscope equipped with a cold field emission gun, a Cs-sensor corrector (spherical aberration correction), a JEOL JED2300T energy dispersion spectrometer for EDS energy dispersive X-ray spectroscopy, and a Gatan GIF filter for electron energy loss spectroscopy (EELS). The microscope was operated at 80 kV acceleration voltage to minimize damage to the samples. HRSTEM images were recorded using an electron beam with a probe size of about 0.12 nm. The images on the HAADF and the bright field detector (BF) were recorded simultaneously with a half-angle of collection of 45-180 mrad and 11 mrad respectively for image resolution.

The STEM-EDS and STEM-EELS experiments were performed with an electron probe of about 0.17 nm and a half-angle of convergence of 24 mrad. The energy resolution was about 0.45eV. The collection angle of the EELS spectrometer was 30 mrad. The samples were dispersed in absolute ethanol and then deposited on a perforated carbon film supported by a mesh grid. STEM image simulations were performed using Nanotube Modeler (JCrystalSoft) and Vesta 3 software for atomic model generation and QSTEM for STEM image simulations. The SWCNT chiral indices were assigned by analyzing the Fourier transform of the HRSTEM images and comparing the images to simulations.

The Raman spectra were recorded with a T64000 spectrometer (Horiba Jobin Yvon) equipped with a confocal microscope (Olympus BH2-UMA, laser wavelengths λ = 514 nm and λ = 458 nm). A 80× magnification objective with a 0.90 numerical aperture was used to collect the spectra in the backscattering mode. The spectral resolution was 1 cm^{-1}. The laser spot had a diameter of 1 μm and the irradiance was kept below 1 kW/cm^2 to prevent heating of the samples. At least 20 spectra were collected and averaged for each sample to obtain a statistically representative spectrum.

The XPS analysis was performed using a spectrometer equipped with a monochromatic Al Kα X-ray source ($h\nu$ = 1,486.6 eV), operating at 150W (KRATOS Axis Ultra, Kratos Analytical, UK). The spectra were collected at a normal angle (90 °) and the analysis zone was an ellipse of 700×300 μm^2. XPS survey spectra were recorded with an energy step of 1.0 eV and a 160 eV bandwidth analyzer, while the detailed spectra for each element were recorded with a step of 0.05 eV and a band energy pass of 20 eV. The XPS spectra were then analyzed with Kratos Vision Software (Vision 2.2.0) after subtraction of Shirley baseline. The Gaussian-Lorentzian functions (70/30) were used for decomposition of peaks. Charge correction was performed using the C1s signal and adjusting the signal for carbon contamination (H-C signal) to 284.6 eV.

For thermogravimetric analyzes coupled with mass spectrometry (TGA-MS), 5-6 milligrams of the powder sample were placed in an alumina crucible. The analyzes were carried out using a device (Setsys Evolution 1750 TGA - SETARAM / Omnistar GSF 301C - Pfeiffer Vacuum) with a helium ramp (Air Liquide Alphagaz 2) with a flow of 20 $mL.min^{-1}$ from room temperature to 1000 ° C at a rate of 3 °C/min. The parameters used for the mass spectrometer allowed simple ionization of most species, which means that z = 1 for the mass-to-charge ratio m/z detected.

All electrochemical experiments were performed using a PGSTAT12 Metrohm-Autolab potentiostat controlled by the GPES software. The measurements were made in a three-electrode cell, the measuring electrode is the modified GCE, the reference electrode is an Ag/AgCl electrode (3M KCl internal electrolyte) and the auxiliary electrode is a platinum wire.

Main results.

Oxidation and chlorination:

The first step necessary for grafting ferrocenes to SWCNT is in a strong acid medium, by microwave irradiation. Microwaves indeed promote oxidation by rapid thermal activation, which allows the oxidation step to be carried out in just a few minutes and makes it possible to control the number of defects introduced.

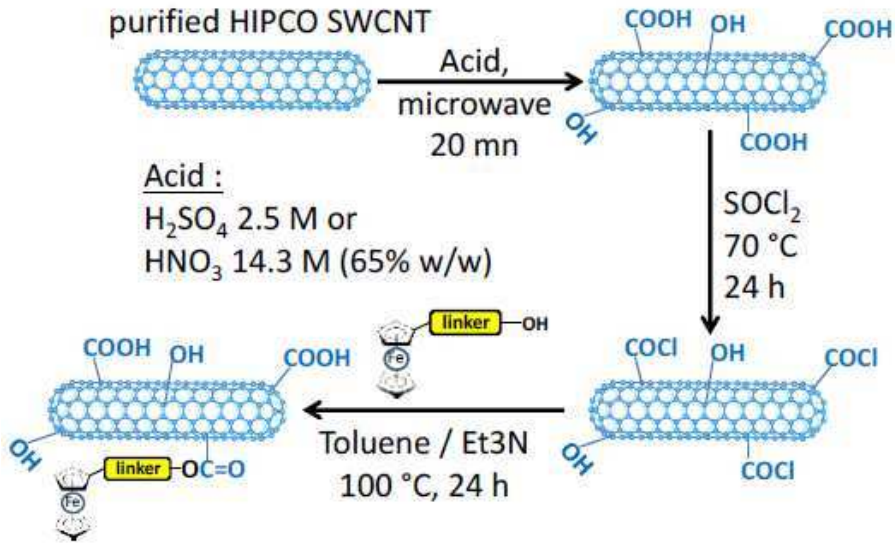

Scheme 1: the three steps of the covalent functionalization of HIPCO SWCNT using two different oxidations.

Functionalization of CNTs by ferrocene derivatives:

We rely on the work of publications 2, 3 and 4 to carry out a synthesis in three steps, as before. The only change comes from the oxidation stage where two modalities were explored (scheme 1 below); the first is based on dilute sulfuric acid (2.5 M H_2SO_4) to give oxidized CNTs (HIPCO-H_2SO_4) and then functionalized with ETGn ferrocene (HIPCO-H_2SO_4-FcETG_n). And the second is based on concentrated nitric acid, to give CNTs oxidized by 65% HNO_3 (HIPCO-HNO_3), then functionalized (HIPCO-HNO_3-FcETG_n). Thus, an alkyl chain and polyethylene glycol (ETG_n) bonds of different chain sizes were used in this study (Scheme 2). XPS analyzes were performed on CNT powders to see if the ferrocene groups were indeed present on the surface of the CNT beams, but they can't confirm the covalent nature of the functionalization process. For this, we

performed TGA-MS analyzes of our samples under (He). Figure 4A of the paper shows TGA curves obtained for raw samples, HiPCO-HNO_3 and HIPCO-HNO_3-$FcETG_2$.

The mass spectrometer coupled with the thermal analysis made it possible to examine the nature of the leaving groups. The cyclopentadienyl groups, which are expected from the decomposition of ferrocenes, can be monitored by detecting the main fragment at m/z = 66 and also at m/z = 39. Iron ions at m/z = 56 were also detected, as shown in Figure 5 of the paper. The TGA curves clearly show an increase in mass loss above 300 ° C for the oxidized sample, and an even greater increase for the HNO_3-$FcETG_2$ sample. This is consistent with the greater number of oxidized defects detected by XPS as well as the presence of ferrocene derivatives. Figure 5 also indicates that the ferrocenes are mainly detached above 300 °C, too high temperature to match physisorbed molecules. TGA-MS experiments thus confirm the covalent grafting of ferrocene derivatives on CNTs.

As already mentioned in the previous papers of this thesis, the intensity of the D band at 1350 cm^{-1} (associated with the presence of structural defects) remains essentially constant when compared to the G^+ and G^- bands for all samples. Radial breathing modes (RBM) are also barely affected by chemical steps. The structural integrity of the CNTs in resonance with the laser energies used in this study (514 and 458 nm) remains quite good. However, the XPS and TGA-MS experiments have shown an increase in oxidized functions, which generally involve the creation of sp^3 hybridized carbon atoms on the walls of the CNTs. To explain this contradiction, it can be hypothesized that microwave irradiation in acidic media mainly converts existing sp^3 defects in raw CNTs into oxidized hydroxyl and carboxylic acid functions but does not present many new defects such as the purely thermal process (reflux heating). In addition, our functionalization process uses CNT beams, and probably most of the tubes in the beams are unaffected by the chemical process.
The absence of a significant change in the intensity of the D band in the Raman spectra is consistent with the low atomic percentage value of Fe detected in XPS.

HRSTEM and EELS analyses confirm the presence of ferrocene derivatives at the bundle surface. The intensity of the signal on the HAADF images is related to the average Z number of the atoms. In the image shown in Figure 1 next page (Figure 7 of the paper), in HAADF images taken at high magnification, bright spots at the end of the short gray lines can be seen on the walls of the insulated tubes or on the outer tubes of the bundles. A second, less brilliant point is systematically seen at the other end of these objects. The length of these kind of objects was systematically measured between 1.2 and 1.4 nm, which are consistent with the presence of a grafted $FcETG_2$ groups. Figure 8 of the paper (Figure 2 of this summary) illustrates this fact by presenting micrographs of high-resolution STEM images recorded on the HIPCO-HNO_3-$FcETG_2$ sample. In the HAADF micrograph (Figure 2a) the arrows point to both sides of the typical object. The CNT structure that is present at the outer edge of a beam has been determined from the Fast Fourier Transform (FFT) of the BF image shown in Figure 2b, the zones containing

atoms heavier than the carbon appear like white areas. The signals are compatible with the presence of grafted ferrocenes through ETG bonds.

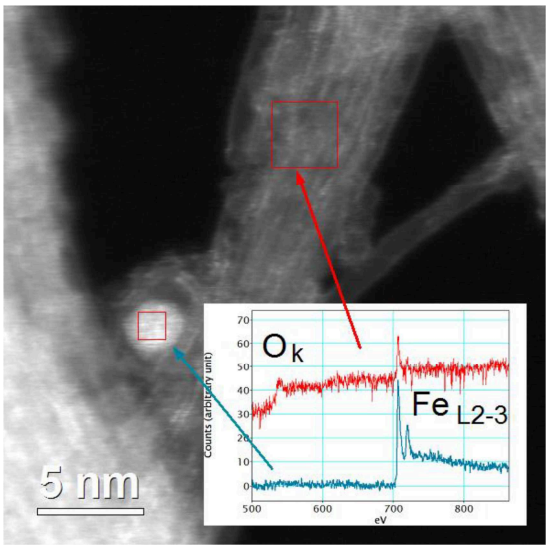

Figure 1: Example of a STEM HAADF image of the HIPCO-HNO3-FcETG2 sample. Insert: EELS spectra of the catalyst particle (blue arrow) and beam recorded in the red square area.

To reinforce the interpretation of the images obtained on the small object at the surface of the tube, simulations were carried out for a SWCNT grafted with a $FcETG_2$ group. A structural model of SWCNT with (11,6) chiral indices was used for the simulation (structure and diameter close to that of (11,5)). The $FcETG_2$ molecule grafted onto the surface of the SWCNT model has been oriented to simulate a ferrocene group in a π-stack interaction. The distance between the tube and cyclopentadiene was set at 0.35 nm.

Simulations were performed at each nanometer for focal lengths from -12 nm to 12 nm for the HAADF and BF detectors. For the HAADF simulations, the contrast obtained correspond to that detected experimentally (Figure 2c and 2d, compared to the inset of Figure 2a). The bright spot corresponds to the ferrocene group, the gray line to the polyethylene glycol linker, and the lighter point at the other end to the ester bond between the CNT and the spacer. For BF images, the contrast obtained is highly dependent on focus and contrast reversal can occur, as shown in Figures 2d and 2f.

Image simulation can be used to estimate the focus of images by comparing the recorded image with simulations for different foci. For example, the focus of the BF image shown in Figure 2b was estimated slightly over-focused by 1 or 2 nm. Many STEM images have been analyzed for different samples, and the functionalization of the sidewalls has been observed for metal and semiconductor tubes oxidized under HNO_3 or H_2SO_4 acidic conditions. Therefore, these results strongly support the hypothesis that the outer tubes of the bundles have been covalently grafted with $FcETG_n$ groups.

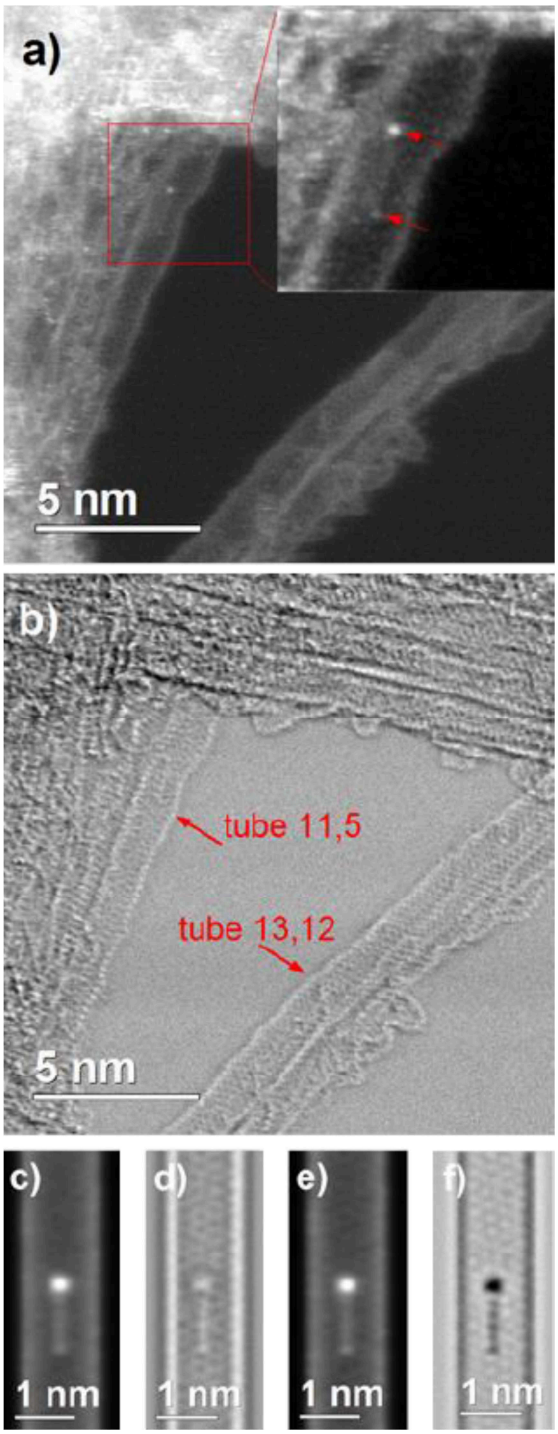

Figure 2: HIPCO oxidized with HNO_3 functionalized with $FcETG_2$ a) HAADF image. The insert is on the FcETG molecule, the top arrow points to the ferrocene and the down arrow points to the ester link. b) Simultaneously recorded BF image for assignment of a chiral index. c), d) and e), f): simulated images of HAADF (and others) and BF (d and f) of an SWCNT of 11.6 with a molecule of $FcETG_2$ for 1.7 nm (c and d)) and sub-focus of - 6.3 nm.

As a conclusion to this analytical part, we succeeded in covalently grafting ferrocene derivatives on HIPCO SWCNTs, in a manner sufficiently weak to preserve the structural integrity of the nanotubes. The complete set of data is consistent with the oxidation of pre-existing defects under microwave irradiation in an acid medium. The

isolated CNTs or those constituting the outer tubes of the bundles are covalently functionalized with ferrocene derivatives on their sidewalls. Both acid conditions give similar results. Diluted H_2SO_4 is therefore very interesting since it avoids the use of concentrated acid solution. **The use of H_2SO_4 with microwave irradiation therefore represents a fast, ecological, safe and energy-efficient process if one is interested in the development on a semi-industrial scale**.

These functionalized samples were then used to modify a GCE subsequently incorporated into the bio electrochemical device, to test their capacity in electrochemical devices. Even if the number of grafted groups is small, as shown by the TGA-MS and XPS analyzes, the electro-catalytic effect is well observed towards the NADH molecules in solution and within the complete bio electrochemical device.

The electrochemical response was most likely controlled by the availability of ferrocene at the surface which depended mainly on the dispersion of the tubes in the chitosan layer. This confirms the catalytic role of the ferrocene units, while our weak functionalization process avoids attacking the structural integrity of the CNTs and provides a good electron transfer efficiency between the modified GCE and the enzymes.

The small amount of residual impurities in our HIPCO samples is not electroactive. The oxidized CNTs were used as a control sample to verify that the oxidation process did not activate the residual impurities or generate electroactive groups such as quinones on the surface of the CNTs. **In addition, with this test we confirmed that no direct electron transfer can be made between the diaphorase and the electrode, even in the presence of SWCNT**.

The role of spacer length on the resulting enzymatic reactivity of the ferrocene unit was studied using structural and dynamic models to simulate both $FcETG_2$ and $FcETG_8$ covalently attached to the surface of a CNT. Calculations were made with and without water (1967 water molecules are evenly distributed in the box, giving a net density of approximately 0.800 g/cm^3 with HIPCO-FcETG8 and 1.01 g/cm^3 without functionalized CNTs. Any molecule of water located at a distance of less than 3.0 Å from the tube has been removed.

In the absence of water, the ETG chain of HIPCO-$FcETG_8$ and HIPCO-$FcETG_2$, seems to interact strongly with CNT wall following a zigzag path on the surface of the CNTs. π-stacking occurs on the nanotube. We therefore used this very useful information in our vacuum HRSTEM simulation by placing the ferrocene unit in a π-stack with the tube, in the results presented in Figures 2c-f. In such a configuration, ferrocene electron transfer can take place between the ferrocene unit and the surface of the CNTs instead of interacting freely with the diaphorase biomolecule. Accordingly, this would extinguish the enzymatic activity of the modified GCE.

To explain why our device still can work, we then simulated the effect of water and we have shown that in the presence of water, the Van der Waals and dipolar interactions between the water molecules and the ETG chain are effectively strong. That bends the chain and maintains the ferrocene unit more than 6Å away from the CNT surface! Even for HIPCO-$FcETG_2$, while the water-ETG interactions are considerably

reduced, which allowed some flexion of the chain and greater interaction with the surface, the ferrocene unit is not stacked on the surface of the CNT, so the step of electron transfer with diaphorase is still possible. The simulations confirm the essential role of the PEG linker in the efficiency of the bioelectrochemical device in water, due to the favorable interaction between the ETG units and the water molecules which prevents the π stacking of the ferrocene unit to the surface of the CNT.

Conclusions and perspectives

This work has clearly demonstrated the interest of using covalently functionalized SWCNTs to make electrochemical devices. Using a very clean sample, a set of complementary analytical techniques strongly confirmed the covalent nature of the functionalization process. We have shown that microwave irradiation under acidic conditions mainly transforms pre-existing defects into oxidized functions, which can be chlorinated using $SOCl_2$ and then grafted with ferrocene derivatives. Even if the number of grafted groups is small, as shown by the TGA-MS and XPS analyzes, the electrocatalytic effect is observed with respect to NADH and in the complete bioelectrochemical device. This confirms the catalytic role of the ferrocene units, while our soft functionalization process avoids attacking the structural integrity of the CNTs and achieves good electron transfer efficiency between the modified GCE and the enzymes. The "soft" use of H_2SO_4 at 2.5 $mol.L^{-1}$ is efficient, greener and safer than using concentrated solutions of HNO_3. We have shown that the residual impurities in the case of mediated electron transfer play no role in the oxidation of NADH, contrary to what has been presented in the literature for other systems.

We also emphasize the value of using molecular dynamics simulations to evaluate the important role of the intermediate link, which certainly depends on the solvent used for electrochemistry. CNTs are indeed useful for well-designed electrocatalytic devices, thus constituting a viable alternative to graphene-based sensors provided that the samples are clean enough so that the function is not controlled by the presence of residual impurities that can lead to non-reproducible measures.

Author's contribution:

In this work, I have functionalized the CNTs, optimize a new method of oxidation, characterized the CNTs, discuss all results obtained, and participated in the writing of the article.

Summary of Paper n°6 (2012 MRS Spring Meeting, MRSS12-1451-DD15-46.R1))

Title: Few-wall carbon nanotubes covalently functionalized by ferrocene groups for bioelectrochemical devices.

Authors: Naoual Allali, Veronika Urbanova, Victor Mamane, Jeremy Waldbock, Mathieu Etienne, Martine Mallet, Xavier Devaux, Brigitte Vigolo, Yves Fort, Alain Walcarius, Maxime Noel, Alexander V. Soldatov, Edward McRae, and Manuel Dossot.

Summary:

Context

Previous publications have aimed to establish in an unmistakable way the successful covalent grafting of electroactive molecules on carbon nanotubes of very high purity. In these studies, we used single-wall CNTs, and this allowed us to establish an efficient grafting protocol, which respects the structural integrity of the CNTs, while showing the negligible role of the few percent of residual impurities on the CNTs. enzymatic charge transfer process with NADH.

However, the CNTs used in these studies are particularly expensive (of the order of 1500 to 2000 $ per gram), and if we wish to use such tubes within electrochemical devices of the sensor or bioreactor type, this cost is not reasonable. We have therefore studied the opportunity of transferring our protocol to nanotubes with a low number of walls, but whose cost is much lower, of the order of $ 150 per gram.

The last two publications (the present paper and paper n°7) therefore develop the covalent functionalization of multi-layer CNTs with ferrocene derivatives, always with the aim of improving their dispersion in water and grafting electroactive chemical groups on their walls in order to promote the transfer of electrons to biomolecules. These functionalized CNTs are used to modify a glassy carbon electrode (GCE) on the surface of which the oxidation of the NADH cofactor will be carried out.

As done in the previous papers, the ferrocene group was chosen as the electron shuttle model, attached to the CNT walls through a polyethylene glycol (ETG) link of variable chain length, as in the case of SWCNTs. The nature of functionalization is evaluated by the combined use of thermal and spectroscopic techniques. The electrochemical biosensor construction is performed by depositing a functionalized CNT film (f-CNT) on the surface of a glassy carbon electrode (GCE). The electrode is tested with a $NADH/NAD^+$ redox couple.

Materials and methods

The CNT samples used for functionalization are purchased from NanoLab. HRTEM analyzes show that the sample contained mainly double- or triple-walled CNTs, few multi-walled CNTs and few SWCNTs. The manufacturer estimates that these CNTs contain about 7% COOH from a thermal reflux in a concentrated solution of nitric acid, while our preliminary experiments with this raw batch indicate that this amount is less than 2%, which is why a second oxidation process was applied to the sample. The CNT sample was dispersed in nitric acid (65% by weight) and then subjected to microwave

irradiation for 20 min at 50 ° C. The conversion of COOH functions to COCl is carried out thanks to a $SOCl_2$ treatment. Ferrocene derivatives (Fc-ETGn) were attached as explained in the previous papers of the thesis. The raw, oxidized and functionalized CNTs were studied by Raman scattering spectroscopy, XPS, high resolution transmission electron microscopy (HR-TEM) and thermogravimetric analysis (TGA). The cyclic voltammetric analyzes of the electrocatalytic reactions observed with NADH on the surface of the GCE electrode modified with f-CNT are carried out as in Publication no. 3. A three-electrode assembly with an Ag/AgCl reference electrode is used. The f-CNTs are co-deposited with diaphorase via a suspension in a chitosan solution for immobilizing the materials at the GCE electrode.

Main results

TGA analyzes carried out under helium flux on the raw sample of few walls carbon nanotubes (raw FWCNT) show a regular mass loss up to 800 ° C (Figure 1). This may be related to the desorption of existing chemical functions on the surface of the raw sample, or to residual solvent molecules. For oxidized CNTs, the loss of mass between 300 ° C and 500 ° C is more pronounced due to many functional groups (COOH created during oxidation). The steep slope observed around 500 ° C for the functionalized CNT shows that the mass loss rate is greatly increased between 250 and 450 ° C. This significant loss of mass is attributed to the desorption of ferrocene derivatives. By analogy with the TGA-MS studies performed on functionalized HiPCo nanotubes, we attribute the significant loss of mass to ferrocene derivatives.

XPS results in this paper also confirm the presence of Fe atoms from ferrocene f-CNTs, which are not detected in raw or oxidized CNTs. These results confirm altogether the functionalization of CNTs by ferrocene derivatives. The number of ferrocene derivatives attached to the side walls of the CNTs as well as the number of COOH groups can be estimated from the loss of mass and the amount of CNT powder used for these experiments. The calculation of the oxidation rate is 2.3% (oxidation of one C atom over 43), and the degree of functionalization is of the order of 0.85% (functionalization of one C atom out of 118). About 36% of the oxidized sites (COOH) are therefore grafted by ferrocene units, a rate lower than the one obtained with HiPCO SWCNTs. **It may be since outer walls of FWCNT are of bigger diameter and therefore the oxidized sites may be less reactive.**

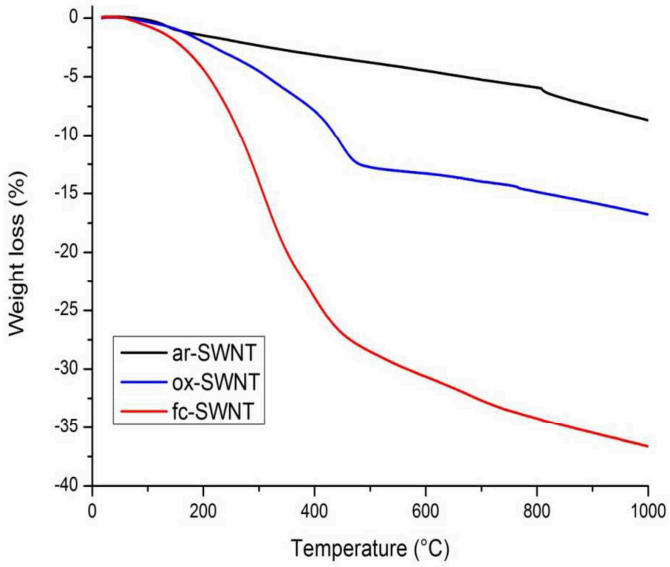

Figure 1: TGA analyzes of raw FWCNT (top, black curve), oxidized FWCNT (middle, blue curve) and FWCNT functionalized by ferrocene with a n=2 PEG linker (bottom, red curve).

To confirm the results of TGA, XPS analysis is performed on the different samples (raw, oxidized and functionalized). There was an increase in the number of C=O and HO-C=O functions on the sidewalls of the tubes after oxidation, confirming the TGA results. The presence of iron is only detected in the functionalized samples. Since the XPS is able to probe the iron elements on the surface of the analyzed samples, the iron detected is that of the ferrocene grafted on the surface of the CNTs. The low iron content grafted in the case of Fc-ETG$_4$ may be due to a larger steric hindrance effect because the spacer is larger.

A Raman analysis (514 nm laser) is performed to confirm that the CNT structure has not undergone too much alteration during the oxidation and functionalization steps. These Raman spectra show that no significant change in the intensity ratio of the D / G band is observable for the three treated samples. Other wavelengths were tested (458, 488, 532 and 632 nm) and gave the same results. The spectroscopic data and the thermogravimetric analyses confirmed the good success of the functionalization of the multi-walled CNTs by the ferrocene derivatives. These functionalized CNTs were then deposited at a GCE to allow electrochemical detection of NADH. A film was deposited on the surface of a GCE by evaporation of a drop of functionalized CNT suspension and mixed with diaphorase and chitosan molecules. The electrochemical signal of the ferrocene / ferricenium pair is visible and stable during a multiple scan (Figure 2A), this indicates that the ferrocene derivatives are immobilized on the surface of the CNTs.

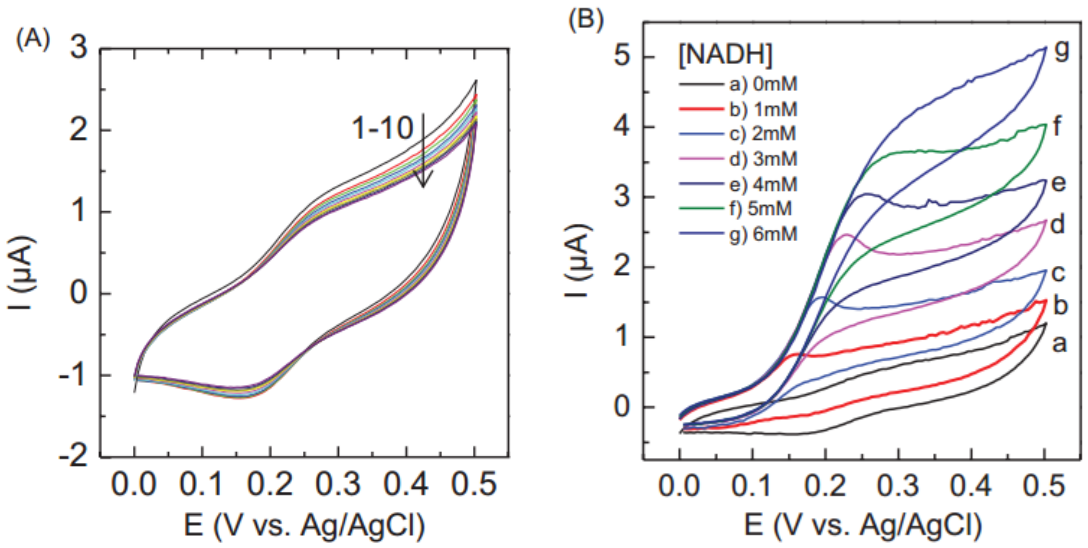

Figure 2: (A) first ten consecutive cyclic voltammograms recorded on a GCE modified with a chitosan / Fc-ETG$_1$ film. (B); cyclic voltammograms measured on a chitosan / diaphorase / f-CNT-modified GCE (FC-ETG$_4$) in the presence of increasing concentrations of NADH in the solution.

The electrocatalytic behavior of the F-CNT-modified GCE (Fc-ETG$_4$) with respect to the oxidation of NADH is studied. Figure 2B shows the corresponding evolution of the cyclic voltammograms obtained in the presence of increasing concentrations of NADH in solution. As can be seen, the oxidation peak increases significantly with the progressive addition of NADH indicating an effective electrocatalytic behavior. These results confirm the previous analyses by proving that the functionalized FWCNTs have been covalently modified by ferrocene derivatives. It should be noted that blank tests (controls) were performed with non-functionalized CNTs and no signal was detected in the presence of NADH.

Conclusion & perspectives

We have shown that few-walled CNTs have been covalently functionalized with ferrocene derivatives through the combination of thermal and spectroscopic analyses. The functionalized carbon nanotubes were used to modify a GCE and to test the oxidation of NADH in aqueous solution. The results obtained show the utility of such covalently modified CNTs for their potential application as a sustainable component of an electrochemical biosensor or bioreactor. These studies also demonstrate the value of our three-step protocol, including microwave assistance for the initial oxidation step, for the successful grafting of electro-active functions in quantities sufficient for observe a good effect of electrocatalysis, without diminishing the structural properties of the nanotubes. The fact that this protocol works equally well for single-walled and multi-walled nanotubes makes it possible to envisage a much more realistic application in terms of cost for bio-electrochemical devices, such as a glucose sensor or a bioreactors.

Author's contribution:

In this work, I functionalized the CNTs, I've made the analyses of CNT by Raman and XPS spectroscopies, and I participated in the interpretation of all the results, and the writing of the paper.

Summary of Paper n°7 (Phys. Status Solidi B 249, No. 12, 2349–2352 (2012))

Title: Covalent functionalization of few-wall carbon nanotubes by ferrocene derivatives for bioelectrochemical devices

Authors: Naoual Allali, Veronika Urbanova, Victor Mamane, Jeremy Waldbock, Mathieu Etienne, Martine Mallet, Xavier Devaux, Brigitte Vigolo, Yves Fort, Alain Walcarius, Maxime Noel, Alexander V. Soldatov, Edward McRae, and Manuel Dossot.

Summary:

This paper reports the same kind of results presented in the proceeding of the MRS Spring meeting (paper n°6) with additional characterization in Raman spectroscopy. Therefore, a complete summary is not given here. Briefly, additional Raman characterizations were presented in this paper, with a more detailed study of the RBM frequencies that showed minor modifications after oxidation and grafting of ferrocene units, but the results once again confirmed that our functionalization process works well with few-walled CNTs without introducing too many defects on CNT side-walls.

Author's contribution:

In this work, I functionalized the CNTs, I've made the analyses of CNT by Raman and XPS spectroscopies, and I participated in the interpretation of all the results, and the writing of the paper.

3 Conclusions and future work

3.1 Conclusions

The results obtained during this thesis concern the covalent functionalization of carbon nanotubes, their characterization and their integration into bioelectrochemical devices.

This thesis work clearly established the interest of using covalently functionalized single-walled CNTs for the manufacture of electrochemical devices. Using a very clean sample of CNTs, a set of complementary analytical techniques firmly confirmed the covalent nature of the functionalization process, a study that is rarely conducted in such detail in the literature.

For the first step of the functionalization process, we have shown that microwave irradiation under acidic conditions mainly transforms pre-existing defects into oxidized functions (in particular COOH carboxylic acid functions), which allows to maintain a good structure with few defects on the nanotubes (but sufficient grafted functions to obtain a valid electrochemical signal) in order not to destroy the electrical properties of the tubes. We have proven that H_2SO_4 and HNO_3 treatments result in the introduction of the same functions on SWCNT walls, but the number of COOH groups at the extremities of SWCNT bundles is different.

The application of this type of oxidation process on multiwall nanotubes has proven that this protocol also works perfectly for the latter, which makes it possible to consider a much more realistic application in terms of cost for bio-electrochemical devices, such as a glucose sensor or a bioreactor.

Once the CNTs are oxidized, they can be chlorinated using thionyl dichloride ($SOCl_2$) and then grafted with ferrocene derivatives. The ferrocene/ferrocerium couple has a reversible character in terms of electron transfer, it is particularly effective in conjunction with diaphorase enzyme to exploit the electrochemical dialogue of the NADH/NAD^+ system. The different electrochemical cycles during voltammetric studies show good stability over time of the electroactive functions. Although the number of grafted groups is low, as shown by the TGA-MS and XPS analyses, the electro-catalytic effect is observed with respect to NADH alone and in the complete bioelectrochemical device. **This strongly confirms the catalytic role of ferrocene units**.

The intermediate spacer between the wall of the CNTs and the electroactive groups has a key role in electron transfer efficiency. We have shown that with the hydrophobic alkyl spacer, the ferrocene cannot properly exchange electrons with the diaphorase. On the contrary, with a polyethylene glycol chain that has a greater affinity with the aqueous medium and chitosan constituting the film, the ferrocene group is more flexible and can be better positioned to react effectively with diaphorase. This has been confirmed by molecular dynamics calculations. We see that the simple change in the chemical nature or length of the spacer influences the effectiveness of the device, sometimes significantly since the alkyl spacer eliminates electro-catalysis. The spacer is therefore crucial for

regulating intermolecular interactions between grafted electroactive groups and the wall of nanotubes (hydrophobic and π–π type interactions), on the one hand, and the same electroactive groups and diaphorase present in a hydrophilic medium on the other. We also underline the interest of using molecular dynamics simulations to evaluate the important role of this spacer, which certainly depends on the solvent used for electrochemistry but also probably on the enzyme system used in the targeted application. Molecular dynamics can be an interesting tool for performing an *in silico* evaluation of the properties of a series of spacers, in order to synthesize only those that can bring a real benefit to electro-catalysis.

On the other hand, our soft functionalization process avoids altering the structural integrity of the CNTs and provides good electron transfer efficiency between the modified glassy carbon electrode (GCE) and the enzymes. The use of mild oxidation conditions (H_2SO_4 at 2.5 $mol.L^{-1}$) is effective, more environmentally friendly and safer compared to the use of concentrated solutions of HNO_3. It could be interesting to test alternatives to $SOCl_2$ treatment in perspective, to develop a process where all the steps would be considered under the green and sustainable chemistry aspect.

We have shown that residual impurities in the case of electron transfer using a redox mediator play no role in the oxidation of NADH, unlike what has been presented in the literature for other direct electron transfer systems. The reversible electrochemical signal of the ferrocene/ferrocenium couple is perfectly visible and stable during voltammetric cycling, which is another strong indication of the covalent nature of grafting ferrocene functions onto the surface of carbon nanotubes. We have shown that nanotubes that are not functionalized or simply oxidized and then treated with $SOCl_2$ do not lead to this electrocatalytic phenomenon.

All samples from all stages were well characterized with several CNT analytical techniques such as TEM/ STEM electron microscopy, EDS, TGA-MS, Raman scattering, DRIFT spectroscopy and noble gas adsorption volumetry, which allowed us to obtain important information about the level of functionalization, the type of grafted groups, and their location on the surface of the nanotubes. We have also used spectroscopic ellipsometry as a new technique for functionalized CNT analysis, we have shown that it can analyze a film of CNTs in a statistical way and constitutes a new tool complementary to the thermogravimetric analysis technique and Raman scattering. ***All these protocols developed as part of this thesis work now constitute a kind of standard for the analysis of covalently grafted CNTs, and this is an important step in the metrology of these functionalized nano-objects.***

The results of this thesis therefore lead us to claim that, although many people currently work with graphene, CNTs are indeed useful for well-designed electro-catalytic devices, which constitutes a viable alternative to graphene-based sensors provided that the samples used are sufficiently clean so that the function is not controlled by the presence of residual impurities that may lead to non-reproducible measurements

3.2 Future work

We have successfully tested the grafting of other electro-active functions, but these other groups have not given proven efficacy in oxidizing NADH, or in reducing NAD^+. However, as a perspective to this work, we tested an ultimate synthesis aimed at covalently grafting the NAD^+ molecule itself onto the surface of the CNTs. The idea was then to mix the NAD^+ grafted nanotubes on the surface of the glassy carbon electrode in the presence of diaphorase, all immobilized within a layer of chitosan or a silica gel. To do this, we used the grafting of an epoxy group associated with one of our PEG spacer (figure below).

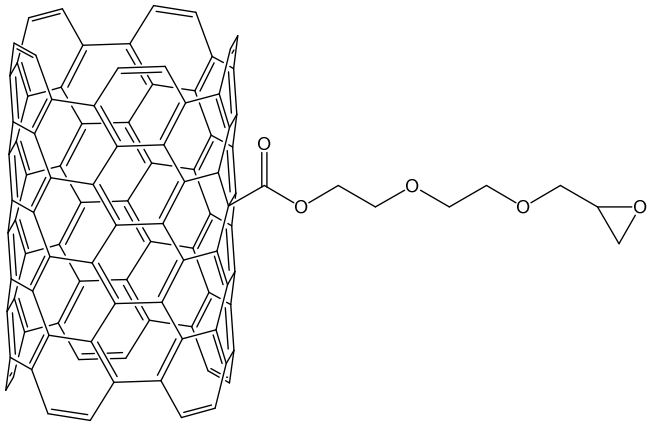

Figure 26: CNTs from Nanolab grafted by an epoxy group at the extremity of a PEG linker.

We thought that the very tight epoxy ring could react with one of the nitrogen atoms of the NAD^+ and lead to an opening of the ring and a covalent grafting of the NAD^+. We therefore suspended these chemically modified nanotubes in the presence of an NAD^+ solution, shaken overnight at room temperature. Then we co-deposited on the surface of the GCE a drop of this mixture, diaphorase, and D-sorbitol dehydrogenase (DSDH), all immobilized in a layer of chitosan. Figure 27 reports the voltammograms obtained when we placed increasing amounts of D-sorbitol in the aqueous solution. We observe a net electro-catalytic effect whereas in this experiment, there is no electro-active group other than the NAD^+ that reacted with the nanotubes. This confirms that NAD^+ is well bound to the CNTs, but at the end of the PEG spacer, giving it enough flexibility to react with the enzyme, and not just adsorbed on the walls. Indeed, the same experiment carried out in the same way but using nanotubes simply oxidized (i.e. without grafted epoxy group) does not give any electro-catalytic effect:

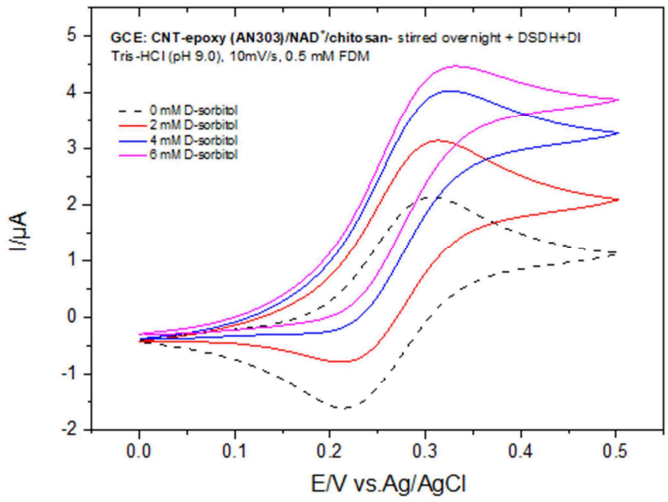

Figure 27: Cyclic voltammograms of Nanolab CNTs grafted by an epoxy group after reaction with NAD^+, in the presence of diaphorase and DSDH, depending on the solution concentration of D-sorbitol

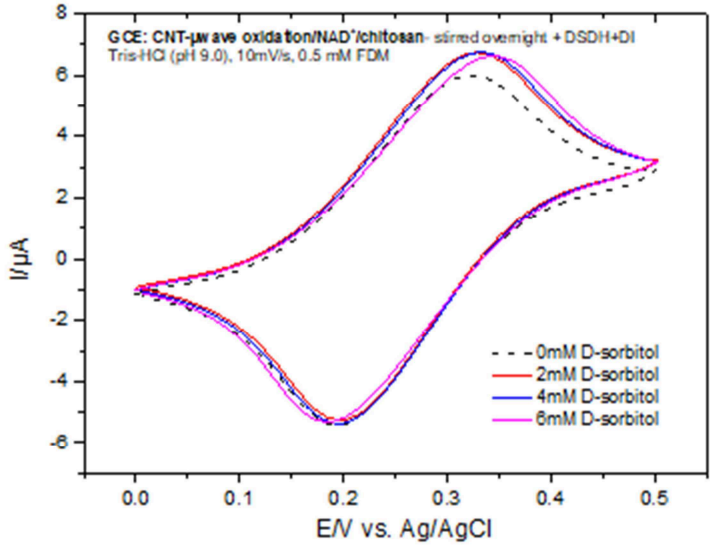

Figure 28: as in Figure 27, but with CNTs simply oxidized and not grafted with the PEG spacer and epoxide.

To test the stability of the grafting, we recorded the electrochemical signal for 20 minutes after the introduction of 2 mM of D-sorbitol in solution for the complete grafted system of Figure 27. Here is the result obtained:

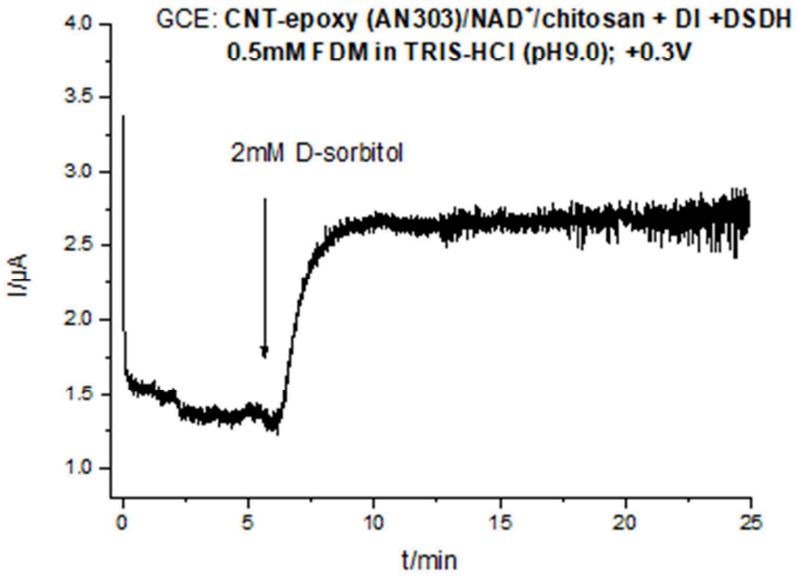

Figure 29: stability of the electrochemical signal in the presence of D-sorbitol.

This is a good argument to demonstrate that we have successfully immobilized the NAD$^+$ covalently on the surface of the CNTs ! We therefore show that our synthesis pathway is very general and particularly well suited for optimizing bioelectrochemical reactions with molecules as complex as NAD$^+$. This really opens up very interesting perspectives for this work, and these last results should be reproduced, and the way in which NAD$^+$ is grafted onto the surface of the CNTs should be analyzed in detail, using our multi-technical analysis protocol. STEM microscopy would be particularly interesting here to visualize the grafted NAD$^+$, which could well contrast on the HAADF detector via the nitrogen atoms of the heterocycles. Finally, a subsequent thesis could be devoted to the realistic evaluation of such tools for concrete applications, in the case of bioreactors in particular.

4 Bibliography

Adamska M. and Narkiewicz U. Fluorination of Carbon Nanotubes − A Review, J. Fluor. Chem. - 2017. - 200, 179-189.

Allali N. and Mamane V. Al(OTf)3 as a new efficient catalyst for the direct nucleophilic substitution of ferrocenyl alcohol substrates. Convenient preparation of ferrocenyl-PEG compounds , Tetrahedron Letters. - 2012. - Vol. 53. - 2604–2607.

Angeles G. A., Perez-Lopez B. and Paloma- Pardave M. Enhanced host–guest electrochemical recognition of dopamine using cyclodextrin in the presence of carbon nanotubes, Carbon. - 2008. - 26, 898-906.

Antaris A.L. [et al.] Sorting Single-Walled Carbon Nanotubes by Electronic Type Using Nonionic, Biocompatible Block Copolymers, ACS Nano. - 2010. - Vol. 4. - 4725–4732.

Arnold M.S. [et al.] Sorting carbon nanotubes by electronic structure using density differentiation, Nature Nanotechnology. - 2006. - Vol. 1. - 60-65.

Avilès F [et al.] Evaluation of mild acid oxidation treatments for MWCNT, Carbon. - 2009. - 47, 2970-2975.

Bachilo S.M. [et al.] Structure-assigned optical spectra of single-walled carbon nanotubes, Science. - 2002. - Vol. 298. - 2361-2366.

Battie Y. [et al.] Mild covalent functionalization of single-walled carbon nanotubes highlighted by spectroscopic ellipsometry , Carbon. - 2016. - Vol. 96. - 557-564.

Baufeld B., Brandl E. and Biesta O. van der Wire based additive layer manufacturing: Comparison of microstructure and mechanical properties of Ti–6Al–4V components fabricated by laser-beam deposition and shaped metal deposition, Journal of Materials Processing Technology. - January 2011. - Vol. 211.

Bethune D.S. [et al.] Cobalt-catalysed growth of carbon nanotubes with single-atomic-layer walls, Nature. - 1993. - Vol. 363. - 605-607.

Blandon-Naranjo L. [et al.] NADH oxidation onto different carbon-based sensors: effect of structure and surface oxygenated groups, Journal of Sensors. - 2018. - 6525919-1/6525919-9.

Boehm H. P. The first observation of carbon nanotubes, Carbon. - 1997. - 581-584.

Bottari G. [et al.] Covalent and Noncovalent Phthalocyanine−Carbon Nanostructure Systems: Synthesis, Photoinduced Electron Transfer, and Application to Molecular Photovoltaics, Chem. Rev. - 2010. - 110, 6768-6816.

Brunetti F. G. [et al.] Microwave-Induced Multiple Functionalization of Carbon Nanotubes, J. Am. Chem. Soc. - 2008. - 130, 8094-8100.

Brunetti F. G. [et al.] Reversible Microwave-Assisted Cycloaddition of Aziridines to Carbon Nanotubes, J. Am. Chem. Soc.. - 2007. - 129, 14580-14581.

Chen Z. [et al.] Soluble Ultra-Short Single-Walled Carbon Nanotubes, J. Am. Chem. Soc.. - 2006. - 128, 10568-10571.

Coleman K. S. [et al.] Functionalization of Single-Walled Carbon Nanotubes via the Bingel Reaction, J. Am. Chem. Soc.. - 2003. - 125, 8722-8723.

Colomer J.-F. [et al.] Microwave-Assisted Bromination of Double-Walled Carbon Nanotubes, Chem. Mater. - 2009. - 21, 4747-4749.

Dai H. [et al.] Controlled Chemical Routes to Nanotube Architectures, Physics, and Devices, J. Phys. Chem. B. - 1999. - Vol. 103. - 11246-11255.

Darmstadt H [et al.] Surface spectroscopic analysis of vapour grown carbon fibers prepared under various conditions, Carbon. - 1998. - 36, 1183-1190.

Datsyuk V. [et al.] Chemical oxidation of multiwalled carbon nanotubes, Carbon. - 2008. - 48, 833-840.

de la Hoz A., Diaz-Ortiz Á. and Moreno A. Microwaves in organic synthesis. Thermal and non-thermal microwave effects, Chem. Soc. Rev. - 2005. - 35, 164-178.

Devaux X. [et al.] Covalent Functionalization of HiPco Single-Walled Carbon Nanotubes: Differences in the Oxidizing Action of H2SO4 and HNO3 during a Soft Oxidation Process, ChemPhysChem. - 2015. - Vol. 16. - 2692 – 2701.

Dyke C. A. and Tour J. M. Solvent-Free Functionalization of Carbon Nanotubes, J. Am. Chem. Soc. - 2003. - 125, 1156.

Elving P. J. [et al.] NAD/NADH as a model redox system: mechanism, mediation, modification by the environment, Bioelectrochemistry and bioenergetics. - 1982. - Vol. 141. - 365-378.

Gebhardt B. [et al.] A Novel Diameter-Selective Functionalization of SWCNTs with Lithium Alkynylides Eur. J. Org. Chem. - 2010. - 1484-1501.

Gebhardt J. [et al.] Selective reduction of SWCNTs – concepts and insights, J. Mater. Chem. C. - 2017. - Vol. 5. - 3937--3947.

Georgakilas V. [et al.] Organic Functionalization of Carbon Nanotubes, J. Am. Chem. Soc. - 2002. - 124, 760-761.

Gibson I., Rosen D.W. and Stucker B. Additive Manufacturing Technologies Rapid Prototyping to Direct Digital, page 246 [Book]. - [s.l.] : Springer, 2010.

Giroud F. [et al.] 5,5-Dithiobis(2-nitrobenzoic acid) pyrene derivative-carbon nanotube electrodes for NADH electrooxidation and oriented immobilization of multicopper oxidases for the development of glucose/O2 biofuel cells, Biosensors and Bioelectronics. - 2017. - Vol. 87. - 957-963.

Guo T. [et al.] Catalytic growth of single-walled nanotubes by laser vaporization, Chemical Physiqcs Letters. - 1995. - Vol. 243. - 49-54.

Hamon M. A. [et al.] Effect of Rehybridization on the Electronic Structure of Single-Walled Carbon Nanotubes, J. Am. Chem. Soc.. - 2001. - 123, 11292-11293.

Hodge S.A. [et al.] Unweaving the rainbow: a review of the relationship between single-walled carbon nanotube molecular structures and their chemical reactivity, Chemical Society Reviews. - 2012. - Vol. 41. - 4409–4429.

Holzinger M. [et al.] Functionalization of Single-Walled Carbon Nanotubes with (R-)Oxycarbonyl Nitrenes, J. Am. Chem. Soc.. - 2003. - 125, 8566-8580.

Holzinger M. [et al.] Sidewall Functionalization of Carbon Nanotubes, Angew. Chem., Int. Ed.. - 2001. - 40, 4002-4005.

Hu H. [et al.] Sidewall Functionalization of Single-Walled Carbon Nanotubes by Addition of Dichlorocarbene, J. Am. Chem. Soc.. - 2003. - 125, 14893-14900.

IIjima S. and Ichihashi T. Single-shell carbon nanotubes of 1-nm diameter, Nature. - 1993. - Vol. 363. - 603-605.

IIjima S. Helical microtubules of graphitic carbon, Nature. - 1991. - Vol. 354. - 56-58.

Jang H. [et al.] Performance and early applications of a versatile double aberration-corrected JEOL-2200FS FEG TEM/STEM at Aalto University, Micron. - 2012. - Vol. 43. - 545–550.

Journet C. [et al.] Large-scale production of single-walled carbon nanotubes by the electric-arc technique, Nature. - 1997. - Vol. 388. - 756-758.

Kara P. [et al.] Aptamers based electrochemical biosensor for protein detection using carbon nanotubes platforms, Biosens. Bioelectron. - 2010. - 26, 1715-1718.

Kelly S.M. and Kampe S.L. Microstructural Evolution in Laser-Deposited Multilayer Ti-6Al-4V Builds: Part I. Microstructural Characterization, Metallurgical and materials transactions A. - 2004. - Vol. 35 A.

Khabashesku V. N., Billups W. E. and Margrave J. L. Fluorination of Single-Wall Carbon Nanotubes and Subsequent Derivatization Reactions, Acc. Chem. Res. - 2002. - 35, 1087-1095.

Kong J, Cassell A.M. and Dai H. Chemical vapor deposition of methane for single-walled carbon nanotubes, Chemical Physics Letters. - 1998. - Vol. 292. - 567–574.

Kumar I., Rana S. and Cho J. W. Cycloaddition Reactions: A Controlled Approach for Carbon Nanotube Functionalization, Chem. Eur. J.. - 2011. - 17, 11092-11101.

Lei T., Pochorovski I. and Bao Z. Separation of Semiconducting Carbon Nanotubes for Flexible and Stretchable Electronics Using Polymer Removable Method, Accounts of Chemical Research. - 2017. - Vol. 50. - 1096–1104.

Li X. [et al.] Controlled Doping of Carbon Nanotubes with Metallocenes for Application in Hybrid Carbon Nanotube/Si Solar Cells, Nano Lett.. - 2014. - 14, 3388-3394.

Li Y. [et al.] Comparative study of methylene blue dye adsorption onto activated carbon, graphene oxide, and carbon nanotubes, Chem. Eng. Res. Des.. - 2013. - 91, 361-368.

Liang F. [et al.] A Convenient Route to Functionalized Carbon Nanotubes, Nano Lett.. - 2004. - 4, 1257-1260.

Liu H., Tanaka T. and Kataura H. Optical Isomer Separation of Single-Chirality Carbon Nanotubes Using Gel Column Chromatography, Nano Letters. - 2014. - Vol. 14. - p. 6237−6243.

Liu J. [et al.] Efficient microwave-assisted radical functionalization of single-wall carbon nanotubes, Carbon. - 2007. - Vol. 45. - 885–891.

Liu J. [et al.] Preferential functionalisation of carbon nanotubes probed by Raman spectroscopy, Physica E. - 2008. - Vol. 40. - 2343–2346.

Liu J. [et al.] Sidewall functionalization of single-wall carbon nanotubes (SWNTs) through aryl free radical addition, Chem. Phys. Lett. - 2006. - 430, 93–96.

Loiseau A. and al et Understanding Carbon Nanotubes, from basics to application. Lecture Notes in Physics. [Book] / ed. Loiseau A. [et al.]. - Berlin Heidelberg : Springer, 2006.

Lütjering Gerd and Williams James C. Titanium [Book]. - 2007.

Mamane V. [et al.] Chemi- vs physisorption in the radical functionalization of single-walledcarbon nanotubes under microwaves, Beilstein J. Nanotechnol. - 2014. - 5, 537-545.

Martic S. [et al.] Ferrocene-peptido conjugates: From synthesis to sensory applications, Dalton Trans. - 2011. - 40, 7264-7290.

Monthioux M. Who should be given the credit for the discovery of carbon nanotubes ?, Carbon. - 2006. - Vol. 44. - 1621-1623.

Nish A [et al.] Highly selective dispersion of single-walled carbon nanotubes using aromatic polymers, Nature Nanotechnology. - 2007. - Vol. 2. - 640-646.

Pekker S. [et al.] Hydrogenation of Carbon Nanotubes and Graphite in Liquid Ammonia, J. Phys. Chem. B. - 2001. - 105, 7938-7943.

Perez E.M. [et al.] Supramolecular chemistry of π-extended analogues of TTF and carbon nanostructures, New J. Chem.. - 2009. - 33, 228-234.

Perez-Lopez B. [et al.] Glucose biosensor based on carbon nanotube epoxy composites, J. Nanosci. Nanotechnol.. - 2005. - 5, 1694-1698.

Pumera M. [et al.] Microchip Capillary Electrophoresis with a Single-Wall Carbon Nanotube/Gold Electrochemical Detector for Determination of Aminophenols and Neurotransmitters, Microchim. Acta. - 2006. - 152, 261-265.

Rabti A., Raouafi N. and Merkoçi A. Bio(Sensing) devices based on ferroceneefunctionalized graphene and Carbon Nanotubes, Carbon. - 2016. - 108, 481-514.

Rao C. N. R., Govindaraj A and Satishkumar B. C. Functionalised carbon nanotubes from solutions, Chem. Comm. - 1996. - 1525-1526.

Saleem M. [et al.] Review on synthesis of ferroceneebased redox polymers and derivatives and their application in glucose sensing, Anal. Chim. Acta. - 2015. - 876, 9-25.

Saleh F. S. [et al.] Poly(phenosafranin)-functionalized single-walled carbon nanotube as nanocomposite electrocatalysts: fabrication and electrocatalysis for NADH oxidation, Electrochimica Acta. - 2018. - Vol. 56. - 4916-4923.

Salzmann C. G. [et al.] The role of carboxylated carbonaceous fragments in the functionalization and spectroscopy of a single-walled carbon-nanotube material, Adv. Mater.. - 2007. - 16, 883-887.

Sanchez-Valencia J.R. [et al.] Controlled synthesis of single-chirality carbon nanotubes, Nature. - 2014. - Vol. 512. - 61-65.

Sandgren Hayley R. [et al.] Characterization of fatigue crack growth behavior in LENS fabricated Ti-6Al-4V using high-energy synchrotron x-ray microtomography, Additive Manufacturing, 2016. - 132-141 : Vol. 12.

Schmidt G. [et al.] Mechanism of the Coupling of Diazonium to Single-Walled Carbon Nanotubes and Its Consequences, Chemistry a European Journal. - 2009. - Vol. 15. - 2101 – 2110.

Singh P. [et al.] Organic functionalisation and characterisation of single-walled carbon nanotubes, Chem. Soc. Rev. - 2009. - 38, 2214-2230.

Srivastava D. [et al.] Predictions of Enhanced Chemical Reactivity at Regions of Local Conformational Strain on Carbon Nanotubes: Kinky Chemistry, J. Phys. Chem. B. - 1999. - 103, 4330-4337.

Strano M.S. [et al.] Electronic Structure Control of Single-Walled Carbon Nanotube Functionalization, Science. - 2003. - Vol. 301. - 1519-1522.

Tagmatarchis N. and Prato M. Functionalization of carbon nanotubes via 1,3-dipolar cycloadditions. J. Mater. Chem. - 2004. - 14, 437-439.

Tanaka T. [et al.] Simultaneous Chirality and Enatiomer Separation of Metallic Single-Wall Carbon Nanotubes by Gel Column Chromatography, Analytical Chemistry. - 2015. - Vol. 87. - 9467-9472.

Thess A. [et al.] Crystalline ropes of metallic carbon nanotubes, Science. - 1996. - Vol. 273. - 483-487.

Thomsen C. and Reich S. Raman Scattering in Carbon Nanotubes, Topics in Applied Physics / ed. Cardona M. and Merlin R.. - Berlin Heidelberg : Springer-Verlag, 2007. - Vol. 108. - 115–232.

Toshimitsu F. and Nakashima N. Semiconducting single-walled carbon nanotubes sorting with a removable solubilizer based on dynamic supramolecular coordination chemistry, Nature Communications. - 2014. - Vol. 5. - 5041/1-5041/9.

Tu X. [et al.] DNA sequence motifs for structure-specific recognition and separation of carbon nanotubes, Nature. - 2009. - Vol. 460. - 250-253.

Tu X. and Zheng M. A DNA-Based Approach to the Carbon Nanotube Sorting Problem, Nano Research. - 2008. - Vol. 1. - 185-194.

Usrey M.L., Lippmann E.S. and Strano M.S. Evidence for a two-step mechanism in electronically selective single-walled carbon nanotube reactions, J. Am. Chem. Soc. - 2005. - Vol. 127. - 16129-16135.

Vázquez E. and Prato M. Carbon Nanotubes and Microwaves: Interactions, Responses, and Applications, ACS Nano. - 2009. - 3, 3819-3824.

Wang J. [et al.] Low-potential stable NADH detection at carbon-nanotube-modified glassy carbon electrodes, Electrochem. Commun. - 2002. - 4, 743-746.

Wang Y., Iqbal Z. and Mitra S. Rapidly Functionalized, Water-Dispersed Carbon Nanotubes at High Concentration, J. Am. Chem. Soc. - 2006. - 128, 95-99.

Weisman R.B. Optical spectroscopy of single-walled carbon nanotubes, Contemporary Concepts of Condensed Matter Science. - 2008. - Vol. 3. - 109-133.

Wirth E., Guitteny F. and Mathonat C. Thermogravimétrie [Book]. - [s.l.] : Techniques de l'Ingénieur, 2014. - P1260.

Xu Y. [et al.] Microwave-induced electrophilic addition of single-walled carbon nanotubes with alkylhalides, Appl. Surf. Sci. - 2008. - 254, 2431-2435.

Zhang F. [et al.] Growth of semiconducting single-wall carbon nanotubes with a narrow band-gap distribution, Nature Communications. - 2016. - Vol. 7. - 11160/1-11160/9.

Zhang J. [et al.] Effect of Chemical Oxidation on the Structure of Single-Walled Carbon Nanotubes, J. Phys. Chem. B. - 2003. - 107, 3712-3718.

Zheng M. [et al.] Structure-Based Carbon Nanotube Sorting by Sequence-Dependent DNA Assembly, Science. - 2003. - Vol. 302. - 1545-1548.

A- Physico-chemical study of oxidation processes of carbon nanotubes

Paper number 1.

Carbon 96 (2016) 557–564

Contents lists available at ScienceDirect

Carbon

journal homepage: www.elsevier.com/locate/carbon

Mild covalent functionalization of single-walled carbon nanotubes highlighted by spectroscopic ellipsometry

Yann Battie [a], Manuel Dossot [b, *], Naoual Allali [b, c, d], Victor Mamane [c, 1], Aotmane En Naciri [a], Laurent Broch [a], Alexander V. Soldatov [d, e]

[a] LCP-A2MC, Université de Lorraine, 1 Boulevard Arago – CP 87811, F-57078 Metz Cedex 3, France
[b] LCPME UMR 7564 CNRS-Université de Lorraine, 405 rue de Vandoeuvre, F-54602 Villers-lès-Nancy Cedex, France
[c] SRSMC UMR 7565 CNRS-Université de Lorraine, Faculté des Sciences et Techniques, B.P. 70239, 54506 Vandoeuvre-les-Nancy Cedex, France
[d] LTU, Department of Engineering Sciences and Mathematics, Luleå University of Technology, 971 87 Luleå, Sweden
[e] Department of Physics, Harvard University, Cambridge, MA 02138, USA

ARTICLE INFO

Article history:
Received 18 May 2015
Accepted 17 September 2015
Available online 30 September 2015

ABSTRACT

Single-walled carbon nanotubes (SWCNT) synthesized using the HiPco® process and purified thereafter were submitted to two covalent functionalization processes: i) a mild oxidation in a concentrated HNO_3 solution using microwave irradiation and ii) a radical functionalization to graft methoxyphenyl groups. The samples were analyzed by Raman spectroscopy and spectroscopic ellipsometry in the energy window 0.07–4.96 eV. The complex dielectric function was analytically calculated in order to extract the real (ε_r) and imaginary (ε_i) parts of this function vs. the incident energy of the light. The ellipsometric data in the infrared part of the spectrum revealed that process i) mainly affected the amorphous carbon deposited on the surface of SWCNTs while process ii) strongly changed the electronic nature of the film due to a charge transfer between methoxyphenyl groups and SWCNTs. These results demonstrate the richness of information that spectroscopic ellipsometry is able to bring about on an entire carbon nanotube ensemble compared to Raman spectroscopy, while not suffering from limitation on their electronic structure and/or aggregate state/presence of surfactants.

1. Introduction

Carbon nanotubes (CNT) are nanomaterials with great potential applications owing to their superior mechanical properties [1] and the interesting fact that their metallic or semi-conducting state depends on how the graphene sheet is rolled [2]. Methods that produce CNTs in quantities sufficient for useful applications, such as CVD or electrical arc discharge, furnish samples with a mixture of CNTs having many different chiralities and tube diameters, in spite of the recent progress to restrain this diversity [3,4]. The material is therefore heterogeneous and often difficult to properly analyze. Generally chemistry is required to make CNTs more compatible with a specific medium or to graft new chemical groups on their sidewalls and/or end caps. Chemical modifications made to a heterogeneous starting material obviously lead to samples that are difficult to analyze thoroughly. Many different methods have already been used. Spectroscopic methods include Raman scattering, ultraviolet–visible–near-infrared (UV–vis–NIR) absorption, fluorescence emission, Fourier-transform infrared (FTIR) absorption spectroscopy, X-ray photoelectron spectroscopy (XPS). Thermal and microscopic methods are also used, like thermogravimetric analysis coupled to mass spectrometry (TGA-MS) and high-resolution transmission electronic microscopy (HR-TEM) [5–7]. Spectroscopic methods have the advantage to be non-invasive and they don't modify or destroy the samples, but each method has also some drawbacks. For instance, Raman spectroscopy is very useful for obtaining information on the diameter distribution of CNTs in a sample by monitoring the radial breathing modes (RBM) occurring at low frequencies (ca. 100–300 cm^{-1}). The RBM frequencies are indeed inversely proportional to CNT diameter [8–11]. Furthermore, the ratio of integrated area or intensity between the D-band around 1350 cm^{-1} and the G^+ band around 1590 cm^{-1} is also a rough indicator of the number of covalent defects present in the structure. It is important to note that, Raman

* Corresponding author.
E-mail address: manuel.dossot@univ-lorraine.fr (M. Dossot).
[1] Present address: Institut de Chimie de Strasbourg, UMR 7177, Equipe LASYROC, 1 rue Blaise Pascal, BP 296 R8, 67008 Strasbourg Cedex, France.

http://dx.doi.org/10.1016/j.carbon.2015.09.066
0008-6223/

characterization can be carried out on different sample morphologies (both individual and bundled nanotubes) and much other information can also be retrieved from other Raman-active vibrational modes [10]. Fine analysis of the spectral features obtained leads to information such as charge transfer between the CNT and sorbed molecules or atoms [12]. However, a significant drawback exists for this kind of analysis: the only CNTs in the sample which contribute significantly to the overall Raman spectrum are those for which the excitation laser energy corresponds to the energy difference between singularities in the density of states (van Hove singularities). Though the laser energy can be tuned on some lasers or the laser source can be changed [13], it is presently almost impossible to continuously monitor the whole range of laser energies necessary to account for all the CNTs present in a sample. A similar drawback can exist for instance with fluorescence emission spectroscopy, since the fluorescence emission is quenched for metallic and bundled CNTs [14,15]. Sometimes the problem can arise from the sample preparation. For UV–vis–NIR absorption experiments, the CNTs are generally dispersed in a solvent (often heavy water) using a surfactant [14]. This surfactant is not removed during the analysis to avoid re-bundling of the tubes, which might slightly change the intrinsic optical properties of CNTs due to specific interactions between CNT sidewalls and surfactant molecules [16,17]. Furthermore, background absorption is also present. This background can be dependent on the quantity of residual catalyst particles and amorphous carbon impurities, as well as the number ratio of metallic to semi-conducting nanotubes present and this requires some specific method of analysis to be properly controlled [18].

These examples show that there is room for a new analytical technique that could analyze a significant quantity of CNTs, and would be sensitive to defects introduced in the structure of chemically treated CNTs. This is especially true is the surface density of new chemical groups is low and can lead to ambiguous results with traditional analytical techniques. In the present article, by using two differently functionalized samples, we show that spectroscopic ellipsometry is a method of choice to overcome such kinds of limitation. Spectroscopic ellipsometry has already been used to analyze optical properties of raw CNT films [19–26] but to our knowledge it has not yet been used to collect information about functionalized CNTs.

2. Experimental

The starting material (further in the text referred to as “raw”) was commercially available SWCNTs synthesized by the HiPco® process and highly purified by a proprietary process from Nanointegris, Inc. The purest grade available is designated as “superpure” by the company and it is claimed that there are less than 5% of residual catalytic particles. This sample was indeed found to be quite clean with few carbonaceous impurities. Fig. 1 gives an example of the HRTEM analysis of this starting material. Few residual catalytic particles are embedded within CNT bundles (see yellow arrow in Fig. 1A). Carbonaceous impurities are of nanometric size and deposited along the side-wall of CNT bundles (see yellow arrow in Fig. 1B). In the rest of the text, to avoid the use of the commercial term HiPco®, the symbol of our samples will be written HiPCO.

HiPCO SWCNTs have been modified by two different chemical methods. The first method is indicated in Fig. 2 and corresponds to a rather soft oxidation of CNTs using an acidic medium and microwave irradiation [27]. The sample modified by this process is hereafter referred to as HiPCO-HNO_3. The second method is the radical functionalization of CNTs by *p*-methoxyphenyl radicals indicated in Fig. 3 [28]. This sample is referred to as HiPCO-MeOPh.

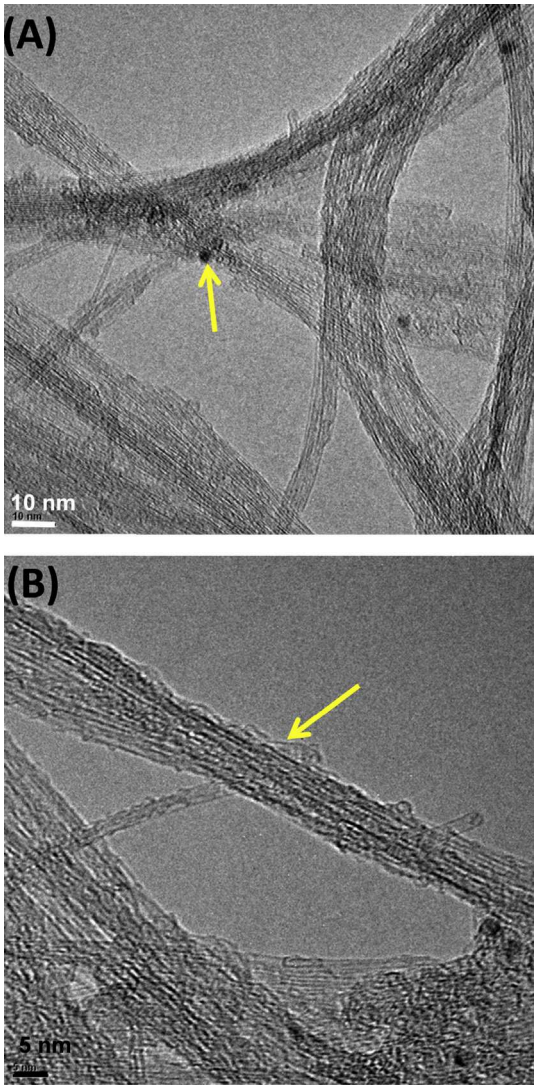

Fig. 1. HR-TEM micrographs of the raw HiPCO material. Arrow in (A) shows a residual catalyst particle, while arrow in (B) shows some carbonaceous impurities covering CNT sidewalls. (A colour version of this figure can be viewed online.)

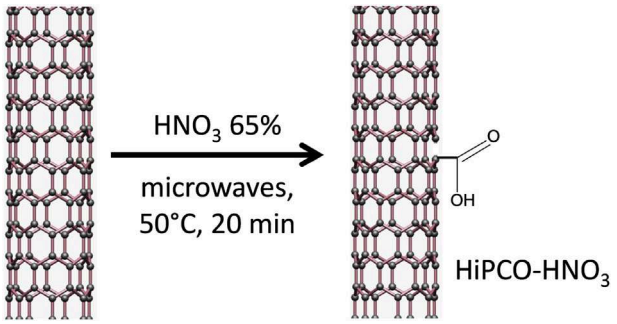

Fig. 2. A micro-wave assisted oxidation treatment. (A colour version of this figure can be viewed online.)

Raman spectroscopy was performed on two different set-ups. The experiments using 532 and 633 nm laser wavelengths were done on a Witec CR200 Raman microspectrometer equipped with an electrically-cooled CCD detector, a grating with 1800 grooves per mm, and a long working distance ×50 objective with a numerical

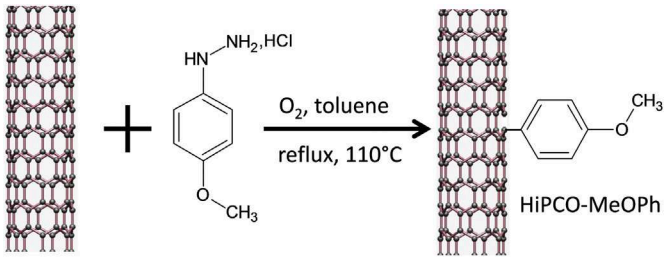

Fig. 3. A radical functionalization process. (A colour version of this figure can be viewed online.)

aperture of 0.55. CNTs were dispersed in tetrahydrofuran (THF) (0.1 mg of CNTs/mL) using sodium deoxycholate (DOC) as a surfactant (5% in weight). A sonication tip was used to make the suspension (90 W for 30 min), the suspension was then spin-coated onto a glass slide. The experiments using 514 nm for raw HiPCO and HiPCO-MeOPh samples were done on a Horiba Jobin-Yvon T64000 Raman microspectrometer equipped with a liquid N_2-cooled CCD detector, an Ar^+ laser working at 514.57 nm and a long working distance × 50 objective with a numerical aperture of 0.55. For both Raman set-ups, the laser irradiance was kept below 1 kW cm^{-2} to avoid any laser heating damage to the samples.

For the ellipsometric measurements, a suspension of 4 mg mL^{-1} of CNTs was realized using a surfactant (sodium cholate, 2% in weight). The suspension was sonicated for 90 min at 240W using a sonic probe. The flask was maintained at 5 °C to avoid heating of the solution. The suspension was then centrifuged at 35000 rpm for 1 h. The supernatant was collected and deposited on a nitrocellulose filter (100 nm pore diameters) using a Büchner filtration set-up. A thick and opaque film of CNTs was obtained, with a thickness of 300–500 nm. The surfactant was removed by washing the film thoroughly with a solution of distilled water until no surfactant was detected in the filtrate. Two ellipsometric spectrometers were used. For the analysis in the NIR-visible-UV range (0.6–4.96 eV), the set-up was a phase modulated ellipsometer (UVISEL, Horiba Jobin Yvon), while in the infrared part (0.07–0.6 eV), a homemade rotating polarizer ellipsometer combined with a Fourier transform infrared spectrometer was used.

3. Results and discussion

Before analyzing the samples with spectroscopic ellipsometry, they were characterized by Raman spectroscopy. Fig. 4 reports the spectra obtained with the two laser wavelengths of 532 and 633 nm for raw HiPCO and HiPCO-HNO_3 samples, while Fig. 5 reports those obtained at 514 nm for the HiPCO-MeOPh sample. Fig. 4 is a typical example of the problem one can be confronted with when analyzing CNTs that have been softly oxidized in an acidic medium. In this case, the acidic conditions can i) partly remove some amorphous carbon deposited on the CNT sidewalls, and ii) removed or heal the already strongly damaged structures that are created during the synthesis and the industrial purification process used by Nanointegris Inc. Both these phenomena (i and ii) can contribute to the decrease of the D-band intensity. On the other hand, the acidic treatment can also add some new sp^3 defects on the nanotube sidewalls by oxidizing carbon bonds. In that case, the D-band intensity would increase. Considering that the two laser wavelengths used in Fig. 4 are sufficiently different to probe different tubes in resonance, the D/G intensity ratio can increase or decrease depending on which phenomenon is preeminent or on whether certain metallic or semi-conducting CNTs are preferentially affected. So Fig. 4A is the kind of result one would expect with

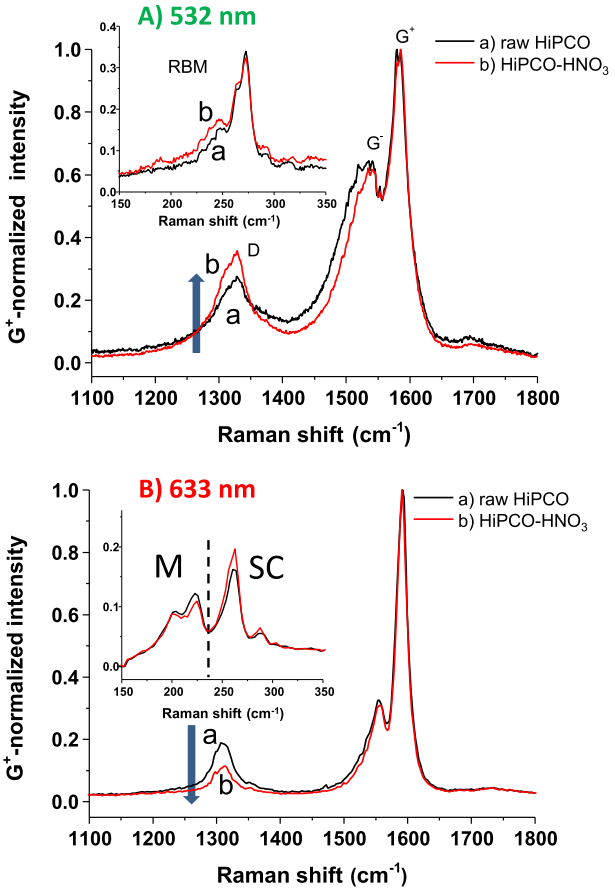

Fig. 4. Raman spectra of raw HiPCO and HiPCO-HNO_3 samples taken using two different laser wavelengths A) 532 nm and B) 633 nm. The spectra have been normalized to the G^+ band intensity. Insets show a detailed view of the radial breathing mode (RBM) region with dash line separating part of the spectrum related to metallic (M) and semiconducting (SC) CNTs. (A colour version of this figure can be viewed online.)

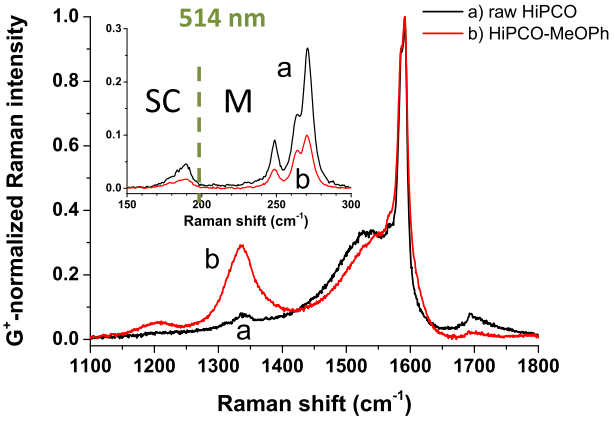

Fig. 5. Raman spectra of raw HiPCO and HiPCO-MeOPh samples taken using a laser wavelength of 514 nm. Spectra have been normalized to the G^+ band intensity. The inset displays RBM region with dash line separating part of the spectrum related to metallic (M) and semiconducting (SC) CNTs. (A colour version of this figure can be viewed online.)

an acidic treatment (increase of the D-band intensity), but Fig. 4B shows exactly the contrary (decrease of the D-band intensity). This example clearly exemplifies that Raman spectroscopy is not a fully adequate method to allow drawing conclusions concerning a mild

oxidation process that does not strongly damage the CNT structure nor introduce many covalent defects. The relative D-band intensity in this case is not an indicator of the number of covalent defects affecting the structural integrity of the CNTs, while one can still conclude that its small intensity change indicates that the oxidation protocol given in Fig. 2 is mild and does not severely affect the CNT bundles. It can be noted that the shape of the G^- band near 1560 cm^{-1} in Fig. 4A is different for the two samples. This certainly arises from the fact that the oxidation process has affected certain metallic nanotubes, which decreases the Breit-Wigner-Fano contribution of the metallic tubes in the G-band, hence a bandwidth that has decreased for HiPCO-HNO_3 sample compared to that of the raw HiPCO. The spectra are normalized to the G^+ band intensity and one can see that the intensity of the RBM modes is not so different between raw HiPCO and HiPCO-HNO_3 samples. Therefore the electronic resonance of the tubes probed at this wavelength has not been affected by any significant charge transfer process. Note that at these photon energies (2.33 and 1.96 eV) and using the typical diameter distribution of HiPCO nanotubes (0.7–1.2 nm), the Kataura plot indicates that we essentially probe metallic CNTs (see Fig. S1 of the supporting information) at 532 nm (2.33 eV) and a mixture of metallic and semiconducting tubes at 633 nm (1.96 eV). This is another difficulty using Raman spectroscopy: the sampling is different when the laser wavelength is changed due to the difference in electronic character of the CNTs in good electronic resonance with the incident photons. While the G^- band is changed due to a loss of metallic CNTs in Fig. 4A, the RBM profile has not so significantly changed. A possible explanation is that all the metallic tubes are affected in a similar way, and the resonance condition and RBM frequencies are not strongly modified.

The Raman spectra of Fig. 5 reveal on the contrary that the radical functionalization process described in Fig. 3 affects substantially the structural integrity of the HiPCO tubes by introducing a significant number of sp^3 defects in the sidewalls, as shown by the huge increase of the D-band intensity. The intensity of the RBM modes is also strongly affected, indicating that both metallic CNTs and also some semi-conducting CNT are affected. This fact was already reported in a previous study using Raman spectra obtained at other laser wavelengths [29]. This loss of resonance intensity may come from several physical effects, including a possible change in the oscillator strength of the corresponding van Hove singularities. Ellipsometric measurements will confirm this hypothesis (see below).

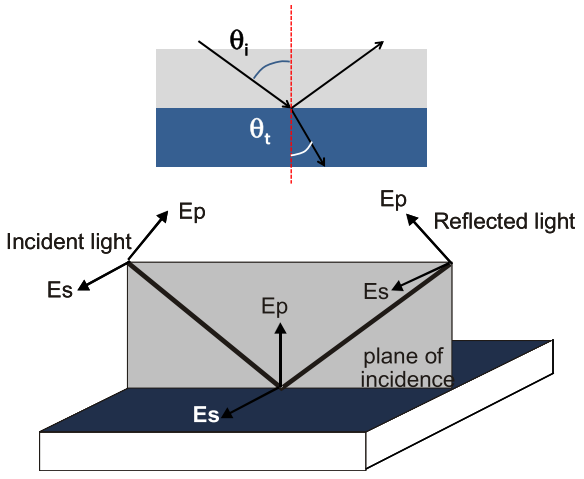

Fig. 6. Definition of the ellipsometric parameters. (A colour version of this figure can be viewed online.)

Fig. 6 sketches the principle of ellipsometry and defines the notations used in the subsequent equations. The electric field of the incident light is decomposed into two perpendicular components usually designated Es and Ep. Ep is parallel to the plane of incidence while Es is perpendicular. The incident light angle is noted θ_i, the transmitted light in the analyzed material is refracted with an angle θ_t.

Considering the CNT film to be a semi-infinite isotropic substrate, the Fresnel reflection coefficients r_s ad r_p are defined by Eqs. (1) and (2), and the ellipsometric angles Ψ and Δ are given by Eq. (3). In these equations, n_i and n_t are the indices of refraction of air and the CNT film, δ_S and δ_p are the differences in path length between the incident and the reflected beams.

$$r_s = \left(\frac{E_r}{E_i}\right)_s = \frac{n_i \cos\theta_i - n_t \cos\theta_t}{n_i \cos\theta_i + n_t \cos\theta_t} = |r_s| e^{j\delta s} \tag{1}$$

$$r_p = \left(\frac{E_r}{E_i}\right)_p = \frac{n_i \cos\theta_i - n_t \cos\theta_t}{n_t \cos\theta_i + n_i \cos\theta_t} = |r_p| e^{j\delta p} \tag{2}$$

$$\rho = \frac{E_p^r / E_p^i}{E_S^r / E_S^i} = \frac{r_p}{r_S} = \frac{|r_p|}{|r_S|} e^{j(\delta_p - \delta_S)} = \tan(\Psi) e^{j\Delta} \tag{3}$$

Spectroscopic ellipsometry consists in monitoring the values of the ellipsometric angles (Ψ,Δ) versus the energy of the incident light. The energy range in our case was varied from 0.07 eV (infrared region) to 4.6 eV (UV region) for an angle of incidence

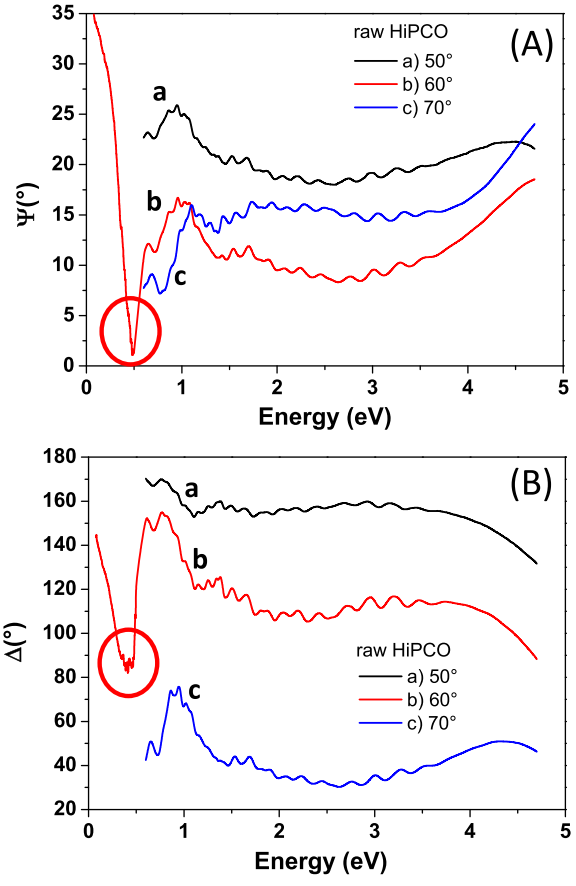

Fig. 7. Spectroscopic ellipsometric angles Ψ and Δ for raw HiPCO CNTs at three different incident angles. The red circles indicate the connecting points of IR and NIR-visible-UV data. (A colour version of this figure can be viewed online.)

$\theta_i = 60°$. The angle of incidence θ_i was also varied (see below) to test a hypothesis on the model used to analyze the data. Fig. 7 reports the measurements made on the raw HiPCO film, at three angles of incidence. The curve at 60° shows that the ellipsometric data collected in the IR part (0.07–0.6 eV) are consistent with the data collected with the second set-up in the NIR-visible-UV (0.6–4.96 eV) part of the spectrum. Indeed the data are consistent at 0.6 eV while no specific adjustment was necessary. From the ellipsometric angles, the dielectric function of the CNT film can be retrieved. To do so, we model our film as an isotropic medium of semi-infinite thickness, as already reported in Refs. [24] and [30]. This model is reasonable since our CNT films were completely opaque to the visible and infrared parts of the spectrum, and the CNTs were found to be randomly oriented. Indeed, the CNT films have a spaghetti-like structure (not shown). Using this model, the analytical expression given in equation (4) allows calculating the complex dielectric function ε, at each energy point.

$$\varepsilon = \sin^2\theta_i \left(1 + \left(\frac{1 - \tan\Psi e^{j\Delta}}{1 + \tan\Psi e^{j\Delta}}\right)^2 \tan^2\theta_i\right) \quad (4)$$

Fig. 8 reports the real part ε_r and the imaginary part ε_i of the dielectric function of the raw CNT film for the three incidence angles. The three curves are superposed and no deviation is observed between the three angles, which is a strong argument to validate the model used. In other words, the film roughness is sufficiently small to be neglected and the CNTs are sufficiently misaligned and absorbent to consider the CNT film as an isotropic semi-infinite medium. The agreement found in Fig. 8 indicates that the assumed model is appropriate and the obtained results are reliable. Making use of different angles of incidence is an excellent mean to verify the reliability of results and the validity of the model itself, since the optical indices should be independent on the angle of incidence.

The same kind of treatment was done for the two functionalized samples HiPCO-HNO_3 and HiPCO-MeOPh. The data are shown in Fig. 9. Several interesting observations can be made: i) the imaginary dielectric function perfectly reveals the van Hove singularities of the raw and HiPCO-HNO_3 sample. The S_{11}, S_{22}, M_{11} and S_{33} transitions can be properly assigned as in more conventional absorption spectroscopy. The bands associated with the transitions between the van Hove singularities of the raw HiPCO are more structured than those of the HiPCO-HNO_3. The substructures are the optical signature of the individual chiralities present in the film. Though expected, this result is interesting since: i) the data pertain to the entire set of carbon nanotubes forming the film and not only to those CNTs in electronic resonance with the incident photon energy as in Raman spectroscopy; ii) in the UV part of ε_i, the π-plasmon band is observed, which is characteristic of the metallic tubes present in the sample; iii) the real dielectric function is negative in the infrared part for raw and HiPCO-HNO_3 samples, while this is not the case for the HiPCO-MeOPh sample; iv) there

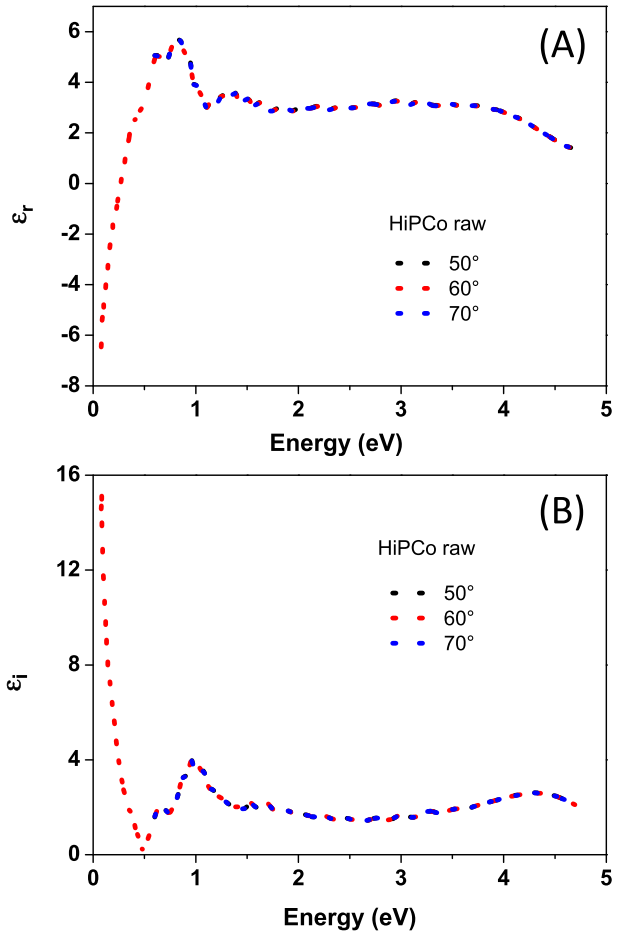

Fig. 8. (A) Real part ε_r and (B) imaginary part ε_i of the dielectric function of raw HiPCO CNTs measured at three different incident angles vs. the beam energy. (A colour version of this figure can be viewed online.)

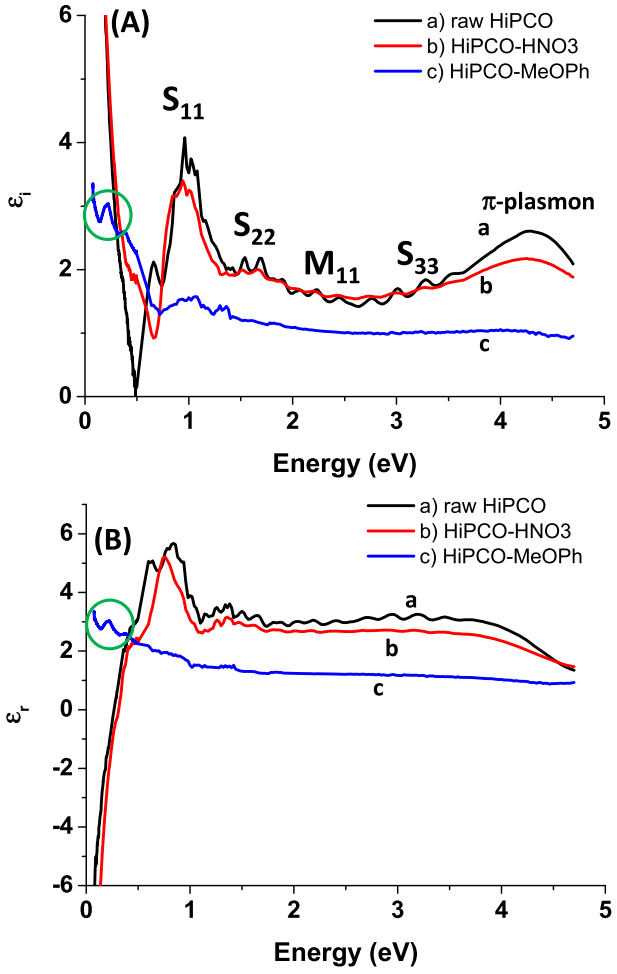

Fig. 9. (A) Imaginary part ε_i and (B) real part ε_r of the dielectric function of the three samples vs. the beam energy using an angle of incidence of 60°. (A colour version of this figure can be viewed online.)

are two unexpected peaks in the IR part of the dielectric functions at 0.2 eV and 0.38 eV for the HiPCO-MeOPh sample (green circles in Fig. 9).

The complex dielectric function contains much useful information for analyzing CNT samples. Its imaginary part ε_i reveals the van Hove singularities for semi-conducting and metallic nanotubes, and the π-plasmon band. One can see in Fig. 9A that the intensity of the van Hove singularities is affected by the covalent defects introduced in the CNT structure. For HiPCO-HNO_3 sample, Raman spectroscopy has shown that the number of defects is low and the conditions of electronic resonance with the laser wavelength are little affected. The ellipsometric data of Fig. 9A confirm this conclusion since the van Hove singularities are still present for this sample as in the raw sample, though their intensity and sharpness are decreased. For the HiPCO-MeOPh sample, ε_i is strongly affected, the intensity of the van Hove singularities is decreased so much that only the S_{11} transition remains slightly visible. This is in line with the Raman spectra of Fig. 5 showing strong effects of the functionalization process on the RBM, D and G bands.

A similar conclusion can be drawn from the analysis of the π-plasmon band. The intensity of this band is related to the electronic transitions between the electronic π bound states to the π* excited states of the carbon atoms of the rolled graphene sheet of the CNTs. If sp^3 defects are introduced into the CNT structure, the number of C=C double bonds is decreased. Some electronic density is localized on the sp^3 C atoms created during the chemical treatment and forming the covalent defects. The overall number of available free π electrons and the oscillator strength associated with the plasmon band are decreased. Consequently, the intensity of this band is an indicator of the number of defects. Indeed, the decrease of its intensity between raw HiPCO, HiPCO-HNO_3 and HiPCO-MeOPh in Fig. 9A indicates that the number of defects is highest for the HiPCO-MeOPh sample. This result confirms the fact that the microwave-assisted oxidation of HiPCO CNTs does not damage the essential electronic properties of the nanotubes, a conclusion that agrees with what has been reported for multi-walled CNTs [31].

The infrared part of the ellipsometric data between 0.07 eV and 0.6 eV is also very informative. For both ε_r and ε_i, the peaks at 0.2 eV (i.e. 1610 cm^{-1}) and 0.38 eV (i.e. 3060 cm^{-1}) can be respectively attributed to the infrared absorption bands of the aromatic ring vibration and the C–H stretching mode of the methoxyphenyl groups grafted at the surface of the chemically treated CNTs. This is certainly one of the most useful results obtained in this study: the infrared ellipsometric set-up is very convenient to directly detect the functional groups covalently grafted on CNT sidewalls, provided that the number of grafted groups is sufficient. Moreover, ε_r is negative for raw and HiPCO-HNO_3 samples in this infrared region, while it is positive for the HiPCO-MeOPh sample. A negative real dielectric function suggests that the CNT films are conductive. This conductivity comes from both i) semi-conducting CNTs doped by O_2 molecules sorbed at the surface, which created holes as charge carriers, and ii) metallic tubes. This conductivity disappears with the HiPCO-MeOPh sample, in agreement with the Raman spectra of Fig. 5 that show a preferential attack of metallic tubes and a loss of electronic resonance with the laser energy for these tubes [29].

The infrared part of the dielectric function for raw SWCNTs and HIPCO–HNO3 sample therefore can be analyzed using the Drude model:

$$\varepsilon = \varepsilon_\infty - \frac{\omega_p^2}{\omega(\omega + i\gamma)} \tag{5}$$

where ω, ω_p et γ are the photon energy, the plasma frequency and the damping parameter of free charge carriers, respectively. ε_∞ is the dielectric function of the film at high energy. The measured dielectric functions in the 0.07 eV–0.5 eV are fitted by adjusting ε_∞, ω_p et γ. As shown in Fig. 10, the Drude model reproduces the experimental data.

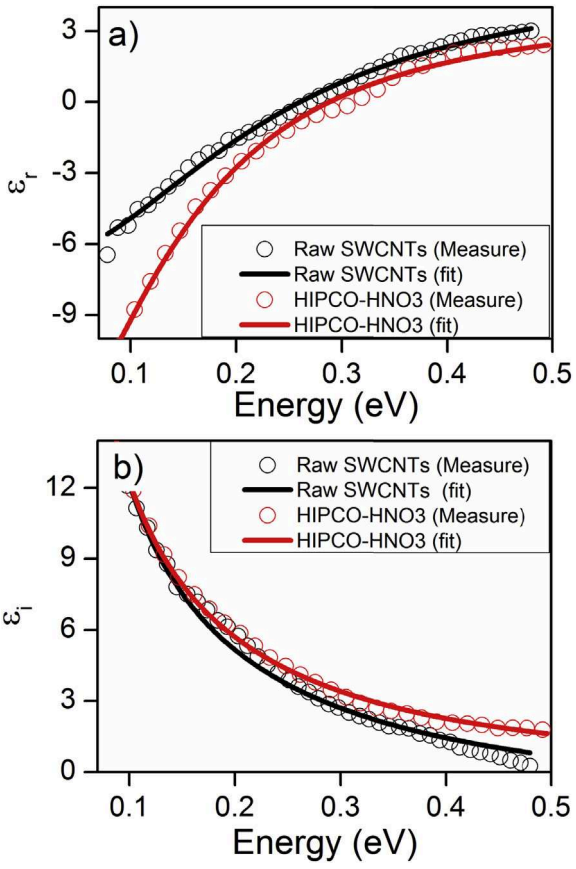

Fig. 10. Comparison between the measure (empty dots) and the fit (solid lines) of the (a) Real part and (b) the imaginary part of the dielectric function of raw and HIPCO–HNO3 SWCNTs. (A colour version of this figure can be viewed online.)

ω_p is estimated at 0.51 ± 0.01 eV and 0.45 ± 0.09 eV for raw and HIPCO–HNO3 SWCNTs, respectively. These values are in the same order of magnitude than the previously reported ones [32]. The charge carrier concentration n is defined by:

$$n = \frac{m\varepsilon_0\omega_p^2}{e^2} \tag{6}$$

where e and m are the elementary charge and the effective mass of charge carriers. By assuming a parabolic band structure, the effective mass of free charge carrier of SWCNT can be calculated from:

$$m = \frac{4\hbar^2}{tad3\sqrt{3}} \tag{7}$$

where d = 0.95 nm is the average SWCNT diameter in our sample, t = 2.8 eV the electronic transfer integral and a = 0.246 nm the SWCNT lattice parameter. The charge carrier concentrations of raw and HIPCO–HNO3 SWCNTs, estimated from Eq. (6) are $1.7 \times 10^{19} \pm 7 \times 10^{17}$ cm^{-3} and $1.4 \times 10^{19} \pm 3 \times 10^{17}$ cm^{-3}, respectively. Despite HNO_3 is considered as an electron acceptor [33,34], it has a negligible effect on the charge carrier concentration. Indeed, as pointed out by Chandra et al. [35], the charge carrier concentration remains stable because HNO_3 is easily desorbed in air.

In Eq. (5), γ is related to the average time τ between two subsequent collisions of free charge carriers. The time τ of raw and HIPCO–HNO3 SWCNTs is respectively 4.3 ± 0.2 fs and 7.1 ± 0.2 fs, corresponding to 3.8 ± 0.2 nm and 6.2 ± 0.2 nm charge carrier mean free path. Despite a ballistic micrometer length transport was reported for individual SWCNTs [36], the mean free path of charge carrier is here in the nanometre range. The charge carrier mean free path is related to the scattering events and potential barriers that occur in the conduction channel. The films are composed of highly entangled SWCNTs. The potential barrier at the junction between two SWCNTs drastically reduces the mean free path of carriers. In addition, the mean free path is also affected by SWCNT defects, amorphous carbon and catalyst. Since in our HIPCO sample there are very few residual catalyst particles, the increase of the mean free path of charge carriers can be attributed to the removal of the amorphous carbon deposited on the SWCNT sidewall.

The DC optical conductivity σ_{dc} of SWCNT films can be extracted from the Drude model:

$$\sigma_{dc} = \frac{\varepsilon_0 \varepsilon_\infty \omega_p^2}{\gamma} \quad (8)$$

The value of σ_{dc} of raw HIPCO is ca. 224 ± 15 Ω^{-1} cm^{-1}. In agreement with Shin et al. [33], the microwave-assisted HNO_3 treatment of Fig. 2 induces in fact an increase of σ_{dc} up to 295 ± 11 Ω^{-1} cm^{-1}. Since the charge carrier concentration of HIPCO–HNO3 is close to the charge carrier concentration of raw SWCNTs, the evolution of σ_{dc} can be attributed to the improvement of the mean free path of HIPCO–HNO3 charge carriers due to amorphous carbon removal from CNT sidewalls.

The results obtained by the analysis of the IR part of the dielectric function enable to understand the change of D band intensity between raw and HIPCO–HNO3 samples for the Raman spectra reported in Fig. 4. Depending on the relative quantity of SWCNTs that are in electronic resonance with the incident laser energy compared to the amorphous carbon deposited on SWCNT sidewall, the D-band intensity can be higher or lower after the mild oxidation by HNO_3. Using a laser wavelength of 532 nm (Fig. 4A), metallic SWCNTs are probed almost exclusively and their diameter is below ~1 nm (see the Kataura plot of Fig. S1). It is known that nanotubes of small diameter are more sensitive to thermal acid oxidation processes [37]. Therefore, the D-band intensity is increased for the HIPCO–HNO3 sample since it essentially reflects the increase of sp^3 defects in the small part of the sample concerned by the resonant metallic nanotubes probed at this wavelength. Using the 633 nm laser wavelength, a more statistically significant part of the sample is probed and includes both metallic and semiconducting nanotubes. Therefore the decrease of the D-band intensity observed for HIPCO–HNO3 sample is essentially the result of the amorphous carbon removal by this chemical treatment and the decrease of the spectral contribution of this amorphous carbon in the overall spectrum.

4. Conclusion

Raman spectroscopy showed that HiPCO-HNO_3 had almost the same D band intensity as that of raw CNTs, while HiPCO-MeOPh gave a quantitative increase of this band. The ellipsometric measurements showed very interesting complementary results. The dielectric function of the films was independent of the incident angle, confirming a posteriori the hypothesis of a homogeneous and isotropic medium. Raw and HiPCO-HNO_3 nanotubes showed a negative ε_r function in the infrared spectrum, which corresponds to a metallic behavior due to holes as charge carriers. This metallic behavior was lost with HiPCO-MeOPh. This can be explained by a partial electron transfer from grafted groups towards CNTs, leading to a decrease of the number of holes and an increase of the CNT Fermi level. The covalent grafting also decreased the intensity of the π-plasmon band at 4.5 eV and the peaks due to van Hove singularities. The mild oxidation process of Fig. 2 also mainly removed amorphous carbon from CNT sidewall but did not introduce new sp^3 defects in their structure in a significant amount. The microwave irradiation is therefore very useful to control the number of defects, to change already existing defects in oxidized ones, and to clean CNT sidewalls. These conclusions agree with and go beyond those obtained from Raman spectroscopy. Our results exemplify the fact that spectroscopic ellipsometry is a powerful method to obtain precious information on the electronic effects resulting from the covalent functionalization of SWCNTs. Most importantly, this technique probes the whole population of CNTs present in the analyzed sample (even non Raman-resonant) irrespective of whether they are in bundled or individual state which gives the method a substantial advantage over fluorescence and absorption spectroscopies commonly used in characterization of functionalized carbon nanotubes.

Acknowledgment

The authors acknowledge colleagues at the ENS Cachan for enabling the carbon nanotube film deposition. Xavier Devaux is acknowledged for HR-TEM analysis of the raw HiPCO CNTs. Maxime Noël is acknowledged for assistance in the Raman measurements performed on the Witec setup. Dr. Edward McRae is kindly acknowledged for his careful reading of the manuscript. This work has been supported by the French National Research Agency (ANR), project ANR-10-BLAN-0819-01-SPRINT.

Appendix A. Supplementary data

Supplementary data related to this article can be found at http://dx.doi.org/10.1016/j.carbon.2015.09.066.

References

[1] M.M. Shokrieh, R. Rafiee, A review of the mechanical properties of isolated carbon nanotubes and carbon nanotube composites, Mech. Compos. Mater. 46 (2010) 155–172.
[2] C. Wang, K. Takei, T. Takahashi, A. Javey, Carbon nanotube electronics – moving forward, Chem. Soc. Rev. 42 (2013) 2592–2609.
[3] Y. Chen, J. Zhang, Chemical vapor deposition growth of single-walled carbon nanotubes with controlled structures for nanodevice applications, Acc. Chem. Res. 47 (2014) 2273–2281.
[4] F. Yang, X. Wang, D. Zhang, J. Yang, D. Luo, Z.W. Xu, et al., Chirality-specific growth of single-walled carbon nanotubes on solid alloy catalysts, Nature 510 (2014) 522–524.
[5] M. Burghard, Electronic and vibrational properties of chemically modified single-wall carbon nanotubes, Surf. Sci. Rep. 58 (2005) 1–109.
[6] P. Singh, S. Campidelli, S. Giordani, D. Bonifazi, A. Bianco, M. Prato, Organic functionalisation and characterisation of single-walled carbon nanotubes, Chem. Soc. Rev. 38 (2009) 2214–2230.
[7] K.A. Wepasnick, B.A. Smith, J.L. Bitter, D.H. Fairbrother, Chemical and structural characterization of carbon nanotube surfaces, Anal. Bioanal. Chem. 396 (2010) 1003–1014.
[8] J. Maultzsch, H. Telg, S. Reich, C. Thomsen, Radial breathing mode of single-walled carbon nanotubes: optical transition energies and chiral-index assignment, Phys. Rev. B (2005) 72, 205438/1-205438/16.
[9] R. Saito, M. Hofmann, G. Dresselhaus, A. Jorio, M.S. Dresselhaus, Raman spectroscopy of graphene and carbon nanotubes, Adv. Phys. 60 (2011) 413–550.
[10] R. Graupner, Raman spectroscopy of covalently functionalized single-wall carbon nanotubes, J. Raman Spectrosc. 38 (2007) 673–683.
[11] P.T. Araujo, P.B.C. Pesce, M.S. Dresselhaus, K. Sato, R. Saito, A. Jorio, Resonance Raman spectroscopy of the radial breathing modes in carbon nanotubes, Phys. E 42 (2010) 1251–1261.
[12] M. Mases, M. Noël, G. Mercier, M. Dossot, B. Vigolo, V. Mamane, et al., Effects on Raman spectra of functionalisation of single walled carbon nanotubes by nitric acid, Phys. Status Solidi B 248 (2011) 2552–2555.
[13] N. Stürzl, S. Lebedkin, S. Klumpp, F. Hennrich, M.M. Kappes, Novel micro-

Raman setup with tunable laser excitation for time-efficient resonance Raman microscopy and imaging, Anal. Chem. 85 (2013) 4554–4559.
[14] M.J. O'Connell, S.M. Bachilo, X.B. Huffman, V.C. Moore, M.S. Strano, E.H. Haroz, et al., Band gap fluorescence from individual single-walled carbon nanotubes, Science 297 (2002) 593–596.
[15] A. Jorio, C. Fantini, M.A. Pimenta, D.A. Heller, M.S. Strano, M.S. Dresselhaus, et al., Carbon nanotube population analysis from Raman and photoluminescence intensities, Appl. Phys. Lett. (2006) 88, 023109/1-023109/3.
[16] H.-Z. Geng, D.S. Lee, K.K. Kim, G.H. Han, H.K. Park, Y.H. Lee, Absorption spectroscopy of surfactant-dispersed carbon nanotube film: modulation of electronic structures, Chem. Phys. Lett. 455 (2008) 275–278.
[17] A.J. Blanch, J.G. Shapter, Surfactant concentration dependent spectral effects of oxygen and depletion interactions in sodium dodecyl sulfate dispersions of carbon nanotubes, J. Phys. Chem. B 118 (2014) 6288–6296.
[18] A.V. Naumov, S. Ghosh, D.A. Tsyboulski, S.M. Bachilo, R.B. Weisman, Analyzing absorption backgrounds in single-walled carbon nanotube spectra, ACS Nano 5 (2011) 1639–1648.
[19] W.A. de Heer, W.S. Bacsa, A. Châtelain, T. Gerfin, R. Humphrey-Baker, L. Forro, D. Ugarte, Aligned carbon nanotube films: production and optical and electronic properties, Science 268 (1995) 845–847.
[20] T.M. Barnes, J. van de Lagemaat, D. Levi, G. Rumbles, T.J. Coutts, C.L. Weeks, et al., Optical characterization of highly conductive single-wall carbon-nanotube transparent electrodes, Phys. Rev. B 75 (2007) 235410/1–235410/10.
[21] G. Fanchini, S. Miller, B.B. Parekh, M. Chhowalla, Optical anisotropy in single-walled carbon nanotube thin films: implications for transparent and conducting electrodes in organic photovoltaics, Nano Lett. 8 (2008) 2176–2179.
[22] H. Soetedjo, M.F. Mora, C.D. Garcia, Optical properties of single-wall carbon nanotube films deposited on Si/SiO(2) wafers, Thin Solid Films 518 (2010) 3954–3959.
[23] Y.R. Park, W.-J. Kim, M.J. Ko, N.K. Min, C.J. Lee, Investigation of ultraviolet optical properties of semiconducting-enriched and metal-enriched single-walled carbon nanotube networks using spectroscopic ellipsometry, Nanoscale 4 (2012) 6532–6536.
[24] Y. Battie, D. Jamon, A. En Naciri, J.-S. Lauret, A. Loiseau, Chirality distribution in single walled carbon nanotube films by spectroscopic ellipsometry, Appl. Phys. Lett. (2013) 102, 091909/1-091909/5.
[25] Y. Battie, D. Jamon, J.-S. Lauret, A. En Naciri, L. Broch, A. Loiseau, Optical anisotropy of single walled carbon nanotubes investigated by spectroscopic ellipsometry, Carbon 50 (2012) 4673–4679.
[26] Y. Battie, D. Jamon, J.-S. Lauret, Q. Gu, M. Gicquel-Guézo, A. En Naciri, et al., Confinement in single walled carbon nanotubes investigated by spectroscopic ellipsometry, Thin Solid Films 571 (2014) 395–398.
[27] N. Allali, V. Urbanova, V. Mamane, J. Waldbock, M. Etienne, M. Mallet, et al., Covalent functionalization of few-wall carbon nanotubes by ferrocene derivatives for bioelectrochemical devices, Phys. Status Solidi B-Basic Solid State Phys. 249 (2012) 2349–2352.
[28] J. Liu, M. Rodriguez i Zubiri, B. Vigolo, M. Dossot, Y. Fort, J.-J. Ehrhardt, et al., Efficient microwave-assisted radical functionalization of single-wall carbon nanotubes, Carbon 45 (2007) 885–891.
[29] J. Liu, M. Dossot, D. Olevik, V. Mamane, B. Vigolo, D. Abrahamsson, et al., Preferential functionalisation of carbon nanotubes probed by Raman spectroscopy, Phys. E 40 (2008) 2343–2346.
[30] R.M.A. Azzam, N.M. Bashara, Ellipsometry and Polarized Light, Elsevier, North-Holland Personal Library, Amsterdam, 1988.
[31] P. Ciambelli, D. Sannino, M. Sarno, C. Leone, Wide characterisation to compare conventional and highly effective microwave purification and functionalization of multi-wall carbon nanotubes, Thin Solid Films 519 (2011) 2121–2131.
[32] Y. Battie, L. Broch, A.E. Naciri, J.S. Lauret, M. Guézo, A. Loiseau, Diameter dependence of the optoelectronic properties of single walled carbon nanotubes determined by ellipsometry, Carbon 83 (2015) 32–39.
[33] D.W. Shin, J.H. Lee, Y.H. Kim, S.M. Yu, S.Y. Park, J.B. Yoo, A role of HNO_3 on transparent conducting film with single-walled carbon nanotubes, Nanotechnology 20 (2009) 475703.
[34] W. Zhou, J. Vavro, N.M. Nemes, J.E. Fischer, F. Borondics, K. Kamaras, et al., Charge transfer and Fermi level shift in p-doped single-walled carbon nanotubes, Phys. Rev. B (2005) 71, 205423.
[35] B. Chandra, A. Afzali, N. Khare, M.M. El-Ashry, G.S. Tulevski, Stable charge-transfer doping of transparent single-walled carbon nanotube films, Chem. Mat. 22 (2010) 5179–5183.
[36] A. Bachtold, M.S. Fuhrer, S. Plyasunov, M. Forero, E.H. Anderson, A. Zettl, et al., Scanned probe microscopy of electronic transport in carbon nanotubes, Phys. Rev. Lett. 84 (2000) 6082–6085.
[37] M.N. Tchoul, W.T. Ford, G. Lolli, D.E. Resasco, S. Arepalli, Effect of mild nitric acid oxidation on dispersability, size, and structure of single-walled carbon nanotubes, Chem. Mater 19 (2007) 5765–5772.

Mild covalent functionalization of single-walled carbon nanotubes highlighted by spectroscopic ellipsometry.

Yann Battie,[&] *Manuel Dossot*[*], [‡] *Naoual Allali,* [‡,§,#] *Victor Mamane,* [§,†] *Aotmane En Naciri,*[&] *Laurent Broch* [&] *and Alexander V. Soldatov* [#,a]

[&] LCP-A2MC, Université de Lorraine, 1 Boulevard Arago - CP 87811, F-57078 Metz cedex 3, France.

[‡] LCPME UMR 7564 CNRS-Université de Lorraine, 405 rue de Vandoeuvre, F-54602 Villers-lès-Nancy Cedex, France.

[§] SRSMC UMR 7565 CNRS-Université de Lorraine, Faculté des Sciences et Techniques, B.P. 70239, 54506 Vandoeuvre-les-Nancy Cedex, France.

† Institut de Chimie de Strasbourg, UMR 7177, Equipe LASYROC, 1 rue Blaise Pascal, BP 296 R8, 67008 Strasbourg Cedex, France (present address)

[#] LTU, Department of Engineering Sciences and Mathematics, Luleå University of Technology, 971 87 Luleå, Sweden.

[*] **Corresponding Author.** Tel : +333 83 68 52 49. E-mail: manuel.dossot@univ-lorraine.fr

[a] Department of Physics, Harvard University, Cambridge, MA-02138, USA

SUPPORTING INFORMATIONS

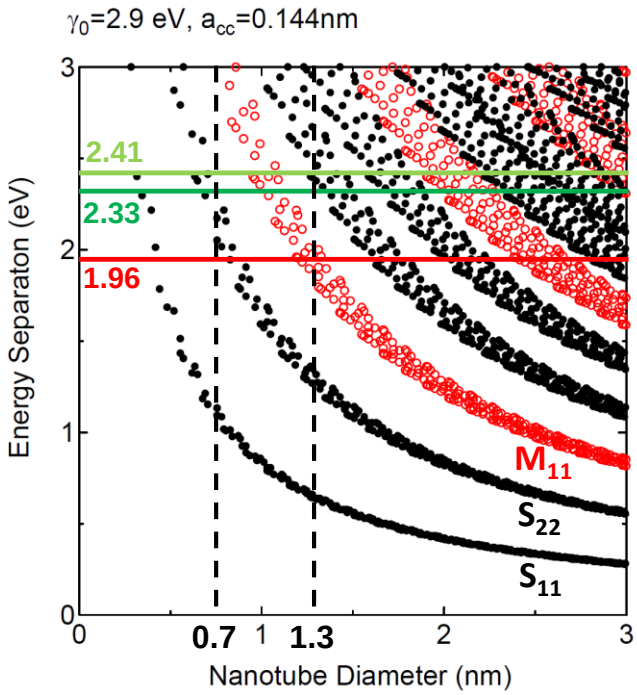

FIGURE S1: The Kataura plot showing the resonance energy in the van Hove singularities of semiconducting (black) and metallic (red) CNTs versus their diameter (nm). The diagram was taken from http://www.photon.t.u-tokyo.ac.jp/~maruyama/kataura/kataura.html and completed to indicate the laser energies (wavelengths) used in this paper at 1.96 (633 nm), 2.33 (532 nm) and 2.41 eV (514 nm) as well as the estimated diameter range of our HiPCO sample (0.7-1.3 nm) obtained from HR-TEM experiments (data not shown).

Paper number 2

ChemPubSoc Europe

DOI: 10.1002/cphc.201500248

CHEMPHYSCHEM Articles

Covalent Functionalization of HiPco Single-Walled Carbon Nanotubes: Differences in the Oxidizing Action of H_2SO_4 and HNO_3 during a Soft Oxidation Process

Xavier Devaux,[a] Brigitte Vigolo,[a] Edward McRae,[a] Fabrice Valsaque,[a] Naoual Allali,[b, d, f] Victor Mamane,[b, c] Yves Fort,[b] Alexander V. Soldatov,[d, e] Manuel Dossot,[f] and Svetlana Yu. Tsareva*[a]

The results of a study on the evolution of HiPco single-walled carbon nanotubes during the oxidizing action of H_2SO_4 and HNO_3 are presented. The process conditions used have been chosen so as to avoid any significant damage to the nanotube structure. The type and level of functionalization, the location of the grafted functions on the surface of the nanotube and the changes in morphological characteristics of the samples were examined by using a wide and complementary range of analytical techniques. We propose an explanation for the differences in the oxidizing action of sulfuric and nitric acids. The combined results allow us to suggest possible reaction mechanisms that occur on the surface of the nanotube.

1. Introduction

Carbon nanotubes (CNTs) and perhaps especially single-walled CNTs (SWCNTs) are attractive because of their potential use in a variety of applications such as electronics devices, composite materials, energy storage devices, sensors and in medicine.[1–6]

[a] Dr. X. Devaux, Dr. B. Vigolo, Dr. E. McRae, Dr. F. Valsaque, Dr. S. Y. Tsareva
Institut Jean Lamour
UMR 7198 CNRS-Université de Lorraine
Faculté des Sciences et Technologies
Boulevard des Aiguillettes
BP 70239, 54506 Vandœuvre-lès-Nancy (France)
E-mail: svetlana.tsareva@univ-lorraine.fr

[b] N. Allali, Dr. V. Mamane, Prof. Y. Fort
Laboratoire de Structure
et Réactivité des Systèmes Moléculaires Complexes
UMR 7565 CNRS-Université de Lorraine
Faculté des Sciences et Techniques
Boulevard des Aiguillettes
BP 70239, 54506 Vandœuvre-lès-Nancy (France)

[c] Dr. V. Mamane
Institut de Chimie de Strasbourg
UMR 7177, Equipe LASYROC
Université de Strasbourg
1 rue Blaise Pascal BP 296 R8
67008 Strasbourg (France)

[d] N. Allali, Prof. A. V. Soldatov
Luleå University of Technology
Department of Engineering Sciences and Mathematics
SE-97187, Luleå (Sweden)

[e] Prof. A. V. Soldatov
Department of Physics
Harvard University
Cambridge MA 02138 (USA)

[f] N. Allali, Dr. M. Dossot
Laboratoire de Chimie Physique
et Microbiologie pour l'Environnement
UMR 7564, CNRS-Université de Lorraine
405 rue de Vandœuvre
54601 Villers-lès-Nancy (France)

One hindrance, however, to all these potential uses is that as-grown SWCNTs rarely feature the characteristics required for certain specific applications. To transform these ideas into real-world devices, one or several stages of chemical modification are required.[1–7] A covalent modification or a covalent attachment of chemical functional groups is one way to realize this. A grafting of different functional groups is easier on an active oxygen-containing group such as -OH or -COOH on the CNT surface than directly on the graphene-like CNT sidewall.[7,8] Such groups can be generated by an oxidative process,[7–13] which could involve heating in air or in an O_2 atmosphere or through treatment with an acid. Two commonly used acids are H_2SO_4 and HNO_3 as well as their mixtures in different ratios.[7,9,11,12,14–16] The level of functionalization can be quite different according to the treatment conditions and the structural properties of the CNTs.[17] Even if it is considered that carboxylic groups are prevalent on the surface of the CNT after an oxidative process, in reality, there is always a variety of different oxygen-containing groups with a ratio that can be quite different from one process to another.[7,10,13–16] The exact mechanism that defines the preferential destination sites of oxygen-containing groups as well as the ratio between these groups remain open to question. CNTs are the most reactive at the tips, in the curved regions, and in the connecting regions between different bundles.[18] Structural defects promote oxidation and favor the formation of certain functional groups.[10] During the acid treatment used, the electrophilic reagent first attacks some of the C=C bonds, producing hydroxyl groups that, in turn, can be converted into quinone groups, and finally into carboxylic acid groups.[19] These last groups can form dimmers,[19] which, under certain conditions (thermal treatment, for example), may transform into anhydrides.[19] Given that the formation of oxygen-containing functional groups is

stepwise (-C–H→-C–OH→-C=O→-COOH→…) and the reactivity of the CNT surface is very heterogeneous, there is always a variety of different oxygen-containing groups after an oxidative process. The abundance and the ratio between the different functional groups depend on the nature of the oxidant.[20] In the case of a strong oxidant or when the oxidative process is applied for a long time, there are more functional groups on the CNT surface and the carboxyl groups predominate. The use of a very soft oxidation process in which the acids react with already-existing defect sites without damaging the sidewall of the CNT further, could help to increase our understanding of the difference in the oxidizing action of different oxidants. However, it is a real challenge to define the ratio between the number of the different grafted groups and their localization on the CNT surface, especially when low levels of functionalization are present.

To verify the presence and number of grafted functional groups, analytical methods such as infrared spectroscopy,[4,8,13–16] X-ray photoelectron spectroscopy (XPS)[8] and thermogravimetric analysis coupled with mass spectrometry (TGA-MS)[6,12,15,21] are commonly used. This list could be complemented with Raman spectroscopy, which allows the kinds of SWCNTs most affected during treatment to be determined.[4,6,14–17,21] Transmission electron microscopy (TEM) and scanning transmission electron microscopy (STEM) allow the level of damage to CNTs as well as the evolution of sample morphology to be assessed.[4,6,8,9,14,15,17,21] In fact, there is no single method of analysis that gives complete information about the level of functionalization, the ratio between different grafted groups and their localization or the degree of sample damage caused by the process used. Only by using a combination of complementary methods can sufficient information be obtained that can shed more light on the interactions of CNTs with different oxidants.

In this study we have compared the oxidizing action of H_2SO_4 and HNO_3. The concentration of the acids and the choice of the other process conditions used have been made so as to carry out "soft" oxidation to avoid damage to the CNT structure. It is known that the acids can react with impurities such as amorphous carbon, hollow carbon shells, or catalyst particles; therefore, HiPco Super Pure Tubes were used because their high levels of purity simplified data interpretation.

We have used a whole battery of analytical techniques including TEM, STEM, energy-dispersive X-ray spectroscopy (EDS), TGA-MS, diffuse reflectance infrared Fourier transform (DRIFT) spectroscopy, rare-gas adsorption volumetry, and Raman spectroscopy, which collectively allow sufficient information to be obtained regarding the type and level of functionalization, the distribution of the different grafted functional groups on the CNT surface, and the changes in morphological characteristics of the samples. The combined results allow us to put forward an explanation for the difference in the oxidizing action of H_2SO_4 and HNO_3.

2. Results and Discussion

2.1. Raman Scattering and DRIFT Spectroscopy

The resonance Raman spectra of pure-SWCNTs, oxH_2SO_4-SWCNTs, and oxHNO_3-SWCNTs are presented in Figure 1. These

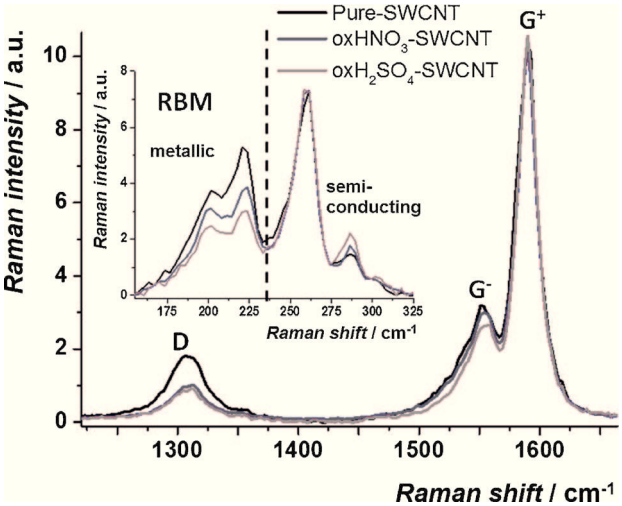

Figure 1. Raman spectra taken at 1.96 eV (633 nm) for the samples of pure-SWCNTs, oxH_2SO_4-SWCNTs, and oxHNO_3-SWCNTs. The intensities have been scaled to that of the G^+ peaks. In the inset at the top of the image: the RBM spectra taken for the same samples. The intensities of RBM have been scaled to that of the 264 cm^{-1} band.

spectra show the radial breathing modes (RBM) at low wavenumbers (150–325 cm^{-1}) (in the inset), the graphene sheet-derived modes (the G-band) around 1590 cm^{-1}, and the defect band (D-band) around 1300 cm^{-1}. The latter is indicative of both the covalent defects on carbon nanotube side-walls and the carbonaceous impurities present in the sample.[22] Given that the HiPco SuperPureTubes sample was purified by the manufacturer after synthesis, we attribute the D-band mostly to these treatment-induced defects within the tubes. The acid treatments seem to have preserved the CNT structural integrity and the relative D-band intensity decreases slightly after treatment with either of the acids. For the nanotubes that resonated with the laser wavelength used, it was observed that the RBM band intensity for all metallic SWCNTs decreased, whereas that of the semiconducting band centered at 287 cm^{-1} increased slightly upon the acid treatment. Metallic SWCNTs are generally more sensitive to chemical treatment. Importantly, smaller diameter tubes of both types (metallic and semiconducting) are more influenced by functionalization than tubes with larger diameter, as evidenced by the RBM profiles. The G^- component of the G-band exhibits the same trend as the RBM spectrum; that is, there is a stronger impact of the H_2SO_4 treatment on the resonance conditions. Specifically, both the G^- contribution from metallic nanotubes—the broad Breit–Wigner–Fano peak at approximately 1530 cm^{-1}—and the G^- peak from the semiconducting CNTs near 1550 cm^{-1} decrease in intensity, as shown in Figure 1. Furthermore, functionaliza-

tion of the semiconducting CNTs alters the resonance conditions to a greater extent and has a higher impact on the G-band than on the RBM part of the spectrum.

The interpretation of experimental results obtained from Raman spectroscopic analysis of SWCNT bundles is difficult. It is impossible to distinguish between the contribution to the D-band from amorphous carbon and that coming from defective nanotubes. However, defect formation in the SWCNT sample during the oxidizing process changes the intensity of all the Raman features and line shapes for the D-, G-, and the G′-Raman bands, and the lower frequency G^- part of the G-mode is reduced in intensity more significantly than the higher frequency G^+ part.[23,24] We can therefore suggest that the observed decrease in D-band intensity accompanied by a decrease in the G^- band intensity is a sign of the oxidation of both disordered carbon and nanotubes. Even if the number of functionalized SWCNTs increased after acid treatments, some amorphous carbon was probably eliminated from the samples during the oxidizing procedures. This results in a slight decrease of the D-band intensity of the two oxidized samples. Similar D-band behavior has been described elsewhere.[22]

The infrared spectrum of pure-SWCNTs, shown in Figure 2, reveals a very small, broad band derived from hydroxyl groups

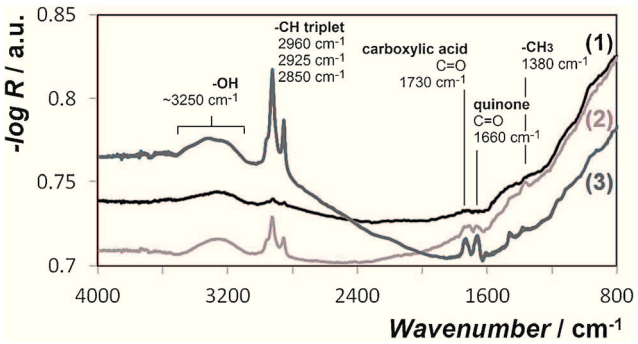

Figure 2. DRIFT spectra of 1) pure-SWCNT, 2) oxH_2SO_4-SWCNT, and 3) $oxHNO_3$-SWCNT samples.

as well as a very low intensity triplet at 2900 cm^{-1}. The latter is identified with C-H_n functional groups,[25] which probably come from the purification procedure, which often involves an acid treatment to remove metal catalyst impurities. The IR spectra of oxH_2SO_4-SWCNT and $oxHNO_3$-SWCNT samples are also presented in Figure 2. The main features of these samples are assigned to two bands characteristic of carboxylic acid (at 1730 cm^{-1}) and quinone (at 1660 cm^{-1}) groups. A very broad band with a maximum near 3250 cm^{-1} can be identified with -OH from the carboxylic acid and the phenol groups attached to SWCNTs. A triplet at approximately 2900 cm^{-1} (2960, 2925 and 2850 cm^{-1}) arising from C-H_n functional groups can also be observed, as can a band at 1380 cm^{-1}, which is associated with the -CH_3 groups. The intensity from all functionalities for the two oxidized samples is higher than that in the spectrum of pure-SWCNTs. The band intensities of the $oxHNO_3$-SWCNT sample are higher than those of the oxH_2SO_4-SWCNT sample. Given that the amount of SWCNT in the samples diluted in KBr was approximately the same for all samples, the intensity of the bands can be associated with the density of functionalities.

We can thus conclude that more functional groups were created upon HNO_3 treatment than upon H_2SO_4 treatment. However, in both cases, the oxidizing treatment was very soft. As mentioned above, the formation of carboxylic acid groups passed through an intermediate stage of producing hydroxyl groups, which can be converted into quinone and then into carboxylic groups.[19] Quinone groups may therefore be considered as intermediates in the oxidation process.[19] The ratio between the peak heights at 1730 and 1660 cm^{-1} corresponds to the ratio between carboxylic and quinone groups. As the oxidation proceeds, the ratio between the groups increases. For our two oxidized samples, the ratio between carboxylic acid and quinone groups is approximately the same.

2.2. TGA-MS

In the thermal analyses, weight loss of the samples was recorded upon heating to 1000 °C under helium. The oxygen-containing functional groups, expected to be added through the two applied oxidative treatments, decompose, leading to release of CO and/or CO_2 depending on the nature of the attached group.[26] Release of CO and CO_2 was complete below 800 °C, therefore TGA-MS data are included herein up to this temperature.

Thermograms of pure-SWCNT and the two oxidized SWCNT samples are shown in Figure 3 (a). The pure-SWCNT undergoes a continuous weight loss as the temperature rises to reach 15.2 wt.% loss at 800 °C. The TG curves of the two oxidized samples are dissimilar. Below 700 °C, the weight loss of oxH_2SO_4-SWCNT is almost identical to that of pure-SWCNT but above 700 °C there is an additional weight loss. For $oxHNO_3$-SWCNT, above 150 °C the functions are eliminated with a more pronounced rate of weight loss. The treatment using H_2SO_4 thus introduced fewer functions compared with that involving HNO_3. The total weight loss at 800 °C reaches approximately 18 wt.% for oxH_2SO_4-SWCNTs and approximately 21 wt.% for $oxHNO_3$-SWCNTs, which indicates a low level of functionalization for both acids.

For pure-SWCNTs, the results of MS analysis (Figure 3 (b)) show the emission of $^{\bullet}CH_3$ (*m/z* 15) and $^{\bullet}C_2H_2$ (*m/z* 26) fragments in the 100–600 °C temperature range. The observed emission could come from the defect sites (the dangling bonds or hydrogen saturated carbon bonds) at the SWCNT surface. Mass fragments at *m/z* 12 (carbon atoms) and *m/z* 28, corresponding to release of CO (*m/z* 12 being the fragment corresponding to carbon from CO), show a prominent increase in intensity at approximately 660 °C. CO emission may come from phenol functions introduced by the purification treatment. That would mean that functional groups and defects are present on the surface of the purified SWCNTs before the oxidation treatments are carried out. This result correlates well with IR spectroscopy data, which have shown the presence of groups containing -C-H_n and -OH in the pure-SWCNT sample.

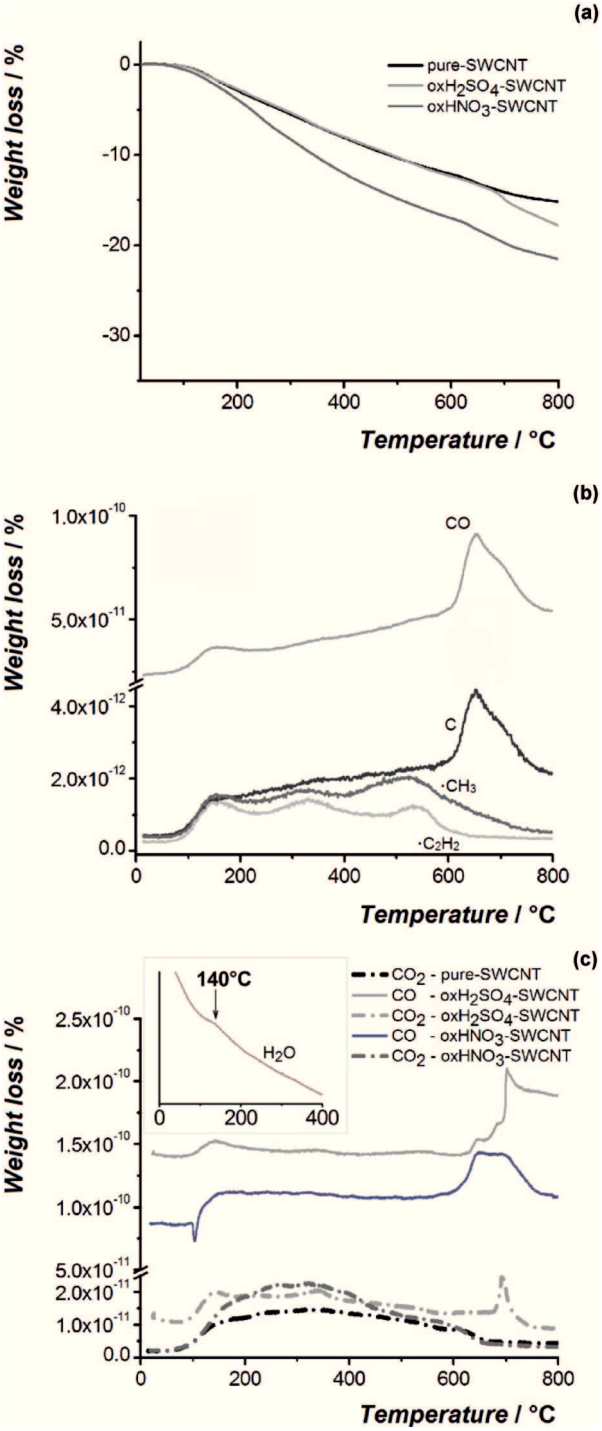

Figure 3. Thermograms taken under helium and the associated MS curves: a) TGA curves of pure-SWCNT, oxH_2SO_4-SWCNT, and $oxHNO_3$-SWCNT; b) MS curves of C (*m/z* 12), $^{\bullet}CH_3$ (*m/z* 15), $^{\bullet}C_2H_2$ (*m/z* 26), and CO (*m/z* 28) for pure-SWCNTs; c) MS curves of CO (*m/z* 28) and CO_2 (*m/z* 44) for pure-SWCNTs, oxH_2SO_4-SWCNT, and $oxHNO_3$-SWCNT; insert: MS curve of H_2O (*m/z* 18) for oxH_2SO_4-SWCNT.

Regarding the nature of the oxygen-containing functions introduced during acid treatment, MS signals recorded for *m/z* 44 (CO_2) (Figure 3(c)) show an increase with a bump around 140 °C for oxH_2SO_4-SWCNT, whereas the intensity of the signal for $oxHNO_3$-SWCNT slowly increases in the range 150–650 °C. For both samples, CO_2 emission detected in the 150–650 °C temperature range indicates the presence of carboxylic acid functions grafted at the SWCNT surface.[26] Loss of CO_2 is higher in this temperature range for $oxHNO_3$-SWCNT, in agreement with the greater weight loss for this sample compared with that of oxH_2SO_4-SWCNT (Figure 3(a)). Pure-SWCNTs emit a negligible amount of CO_2 in this temperature range, which can signify the presence of few carboxylic groups on the SWCNT surface. This is probably why they were not detected by IR spectroscopic analysis.

Between 600 and 750 °C, loss of CO is found for both samples (Figure 3(c)), which is related to the departure of phenol groups. For oxH_2SO_4-SWCNT, an additional peak around 700 °C is observed. Moreover, unlike $oxHNO_3$-SWCNTs or pure-SWCNTs, for oxH_2SO_4-SWCNTs the peak for *m/z* 44 (CO_2) is also detected at around 700 °C (Figure 3(c)). Simultaneous emission of CO and CO_2 at this temperature is a characteristic of the anhydride groups.[26] The IR spectrum of oxH_2SO_4-SWCNT does not, however, show the presence of anhydride groups (Figure 2). Feng et al.[18] showed that the carboxylic acid functionalities change drastically during thermal annealing. Based on FTIR measurements they proved that the anhydride may form from the coupling of two carboxylic groups with the loss of H_2O (dehydrolysis) at a relatively low temperature (423 K). For the oxH_2SO_4-SWCNT, sample we have verified that there is a signal for *m/z* 18, which is the main mass expected for water. There is a noticeable bump added to a continuous release during heating around 140 °C (Figure 3(c), inset). Therefore, the excess water detected at 140 °C is probably produced by the formation of anhydride functions from the coupling of two carboxylic acids. However, in the case of $oxHNO_3$-SWCNTs, in spite of having detected a greater number of carboxylic acid groups, we did not record the same dehydrolysis. Zhang et al.[19] showed that the efficiency of forming hydrogen bonds between -COOH groups is linked with their abundance; that is, with their mutual proximity. So, we can suppose that the carboxylic acid functions are located differently for the two acid treatments. Indeed, although there are fewer grafted functions in the oxH_2SO_4-SWCNT sample, they nevertheless form dimers that transform into the anhydride functions during thermal treatment. This might be possible if the carboxylic acid groups are densely located, for example, at the end of the bundles.

A precise quantitative analysis is unfortunately not possible with such systems because of the low level of functionalization containing a variety of functional groups that can react together and be released over quite a large temperature range.

2.3. TEM and STEM Examination

As has been described elsewhere,[27] detailed TEM/STEM examinations show that the pure-SWCNTs are combined into small bundles, comprising on average 25–30 nanotubes. There is also a significant number of isolated SWCNTs and very small bundles of two or three tubes. The bundles appear to be loosely bound and are some micrometers in length. The SWCNT diameters are heterogeneous, approximately 0.7–1.6 nm, with a consequential range of interstitial channel

shapes and sizes, some of which are large. Triangular-shaped channels defined by three closely-packed tubes are observed, but there are other bigger channels defined by four tubes. Analysis of HRSTEM images shows that the distance between adjacent tubes is variable.[27] Most of the SWCNTs are closed. There are a few scattered metallic particles or carbon impurities. The carbon impurities comprise hollow carbon shells of 4–5 nm in diameter and small hollow spherical or ellipsoid structures of approximately 0.7–1.2 nm in size. These last hollow carbon "particles" are composed of one layer of carbon and might be fullerenes.

Detailed TEM-STEM examination of oxH_2SO_4-SWCNT and oxHNO_3-SWCNT show that treatment with neither of the acids led to a significant increase in the number of opened SWCNTs and that the typical SWCNT lengths are similar to those of the pure-SWCNTs. A very small increase in the number of carbon impurities was observed in both cases. The morphologies of oxH_2SO_4-SWCNT and oxHNO_3-SWCNT were, however, different. As can be seen in Figure 4(a,b), the bundle structure of oxH_2SO_4-SWCNT is similar to that of pure-SWCNTs but, in the case of oxHNO_3-SWCNT, the morphology changes through a certain alignment of the bundles (Figure 4(c)). Based on DRIFT analysis, we know that there are the same functional groups on the SWCNT bundle surface of the two samples. TGA-MS shows that the density of functionalities in the oxHNO_3-SWCNT is slightly higher than that of the oxH_2SO_4-SWCNT. TGA-MS also established a difference between the two oxidized samples regarding the thermal stability of the carboxylic acid groups that allow a difference in the functional group localizations on the SWCNT surface to be supposed. If we assume that in the case of oxHNO_3-SWCNT the carboxylic acid groups are uniformly dispersed on the side faces of the bundles, we can explain the alignment of the bundles by an electrostatic attraction between different bundles. This could be due to the formation of weak hydrogen bonds between functional groups on the CNT surface. The bundles in the oxH_2SO_4-SWCNT would then not be aligned because there are fewer -COOH groups on the side faces of the bundles; they are probably densely located mainly at the ends of SWCNT bundles.

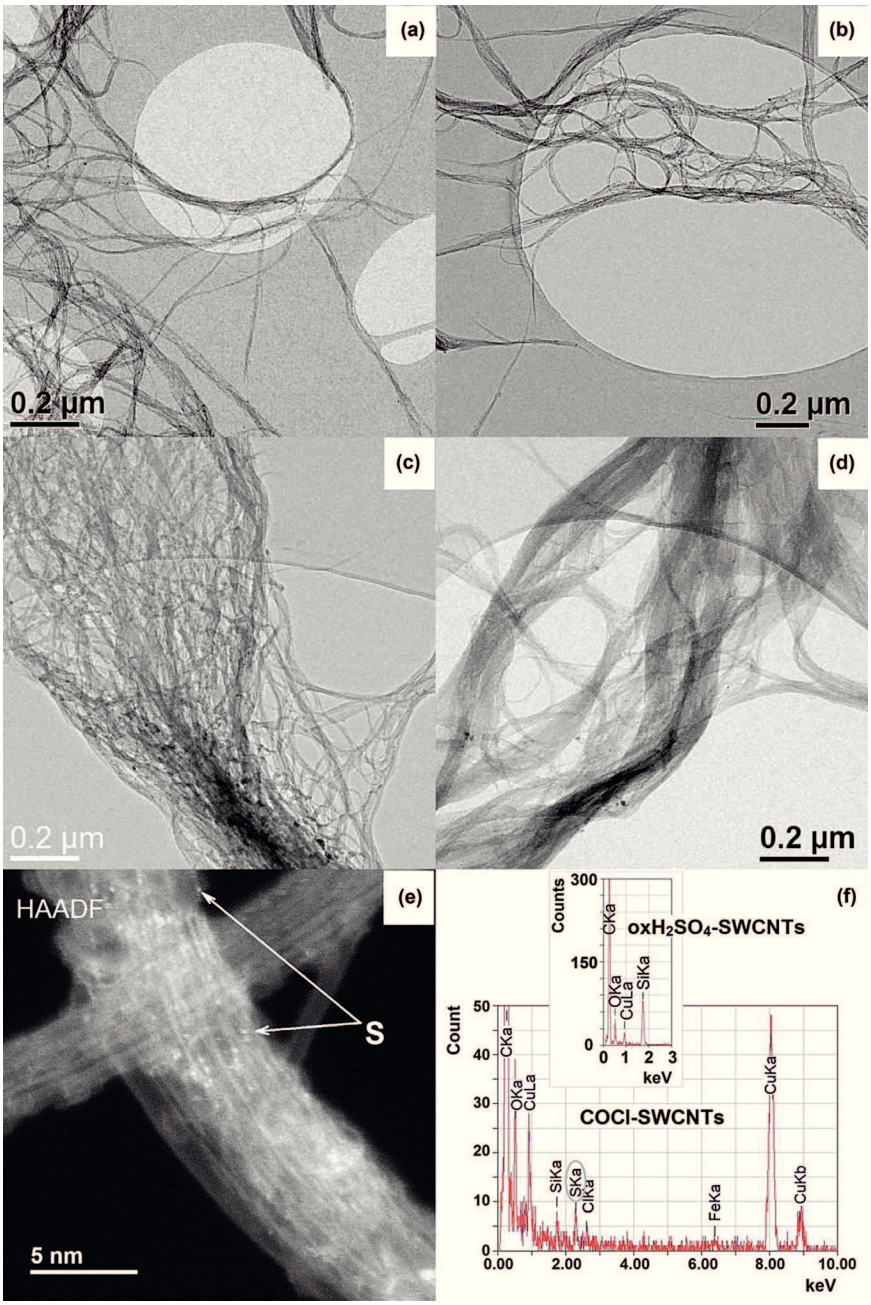

Figure 4. TEM (a–d), High-angle annular dark-field (HAADF) (e) images of a) pure-SWCNTs, b) oxH_2SO_4-SWCNTs, c) oxHNO_3-SWCNTs, d,e) COCl-SWCNTs. f) EDS spectra of COCl-SWCNTs and oxH_2SO_4-SWCNTs (inset). The C, O, S, Si, Cl, Fe signals come from SWCNT samples, the copper signal comes from the sample grid.

Subsequent to the H_2SO_4 treatment, chlorination increases the bundle size (Figure 4(d)). HAADF images (i.e. Figure 4(e)) of the SWCNT bundle surface reveal white points that correspond to atoms heavier than carbon. The EDS spectra show the presence of S and Cl (Figure 4(f)). The sulfur appeared on the SWCNT bundle surfaces only after chlorination; it was no

longer detected in the oxH_2SO_4-SWCNT. An EDS spectrum taken from the side face of a oxH_2SO_4-SWCNT bundle, shown in the inset of Figure 4(f), shows the presence of Si (in the form of Si or SiO_2) on the surface of SWCNT bundles, but not sulfur. It should be noted that a Si signal was detected in all samples, even in pure-SWCNTs, and could come from the laboratory glassware used during purification or oxidation treatment. The question of how the sulfur or chlorine might promote enlargement or consolidation of the bundles will be discussed below.

2.4. Volumetric Adsorption Studies

Rare-gas adsorption isotherms of SWCNT bundles generally have two inclined steps as the relative equilibrium pressure progressively increases.[28,29] The lower pressure step represents adsorption on higher binding energy sites. These are the grooves separating two adjacent outer tubes (G), the inner channels of the tubes (T) and the bundle interstitial channel (IC) sites. The higher pressure step corresponds to the exohedral adsorption on the external surface of the bundles (E). Being grafted on the SWCNT surface, functions can influence the adsorption site availability, so this analytical technique can furnish information about changes that might have occurred during chemical treatments.

As has been described elsewhere,[27] 77 K krypton adsorption isotherms on the pure-SWCNT sample used here have adsorptive dosing (AD) dependent characteristics of the low-pressure region (LPR) of the isotherm. This results from adsorption on the IC-sites that can be seen as subnanoscale pore channels with alternating enlargements (voids) and constrictions (necks) along the tube axes. An equilibrium pressure drop with increasing AD is noted by using the increased adsorptive dosing (IAD) protocol, which we have explained by the formation of metastable adsorbed phases inside the IC-sites or by intrapore blocking. In measurements using the constant adsorptive dosing (CAD) protocol, the exact position of the first step is AD-dependent. It is located between approximately 0.0007 and 0.05 Pa. The branches obtained by using the CAD protocol for the four indicated doses of Kr are presented in Figure 5(a). There is no continuous step shift to the right as AD increases; rather, the increasing AD influences the isotherm in a cyclic manner. The second step extends from near 0.3 to approximately 3 Pa. Its position is independent of the protocol used and of the chosen AD value.

A soft acid treatment will graft oxygen-containing functions on the already-existing defect sites of a SWCNT sample without causing extensive damage to the CNT sidewall. Kuznetsova et al.[30] showed that, upon such an acid treatment, the grafted quinone or carboxylic acid groups block the entry ports into the individual nanotubes (T-sites). The bundle ends are the sites at which the concentration of carboxylic acid functions can be maximal after acid treatment.[31] They are also the entry ports to the ICs and opened SWCNTs. This means that if in the case of a pure-SWCNT sample, AD-dependent adsorption takes place in the IC-sites (and possibly T-sites of a few opened nanotubes), subsequent acid treatment presumably blocked the entry ports to these sites, leading to suppression of the branches, substeps and branch switching in the low-pressure region of the isotherm. Indeed, the 77 K adsorption curve of

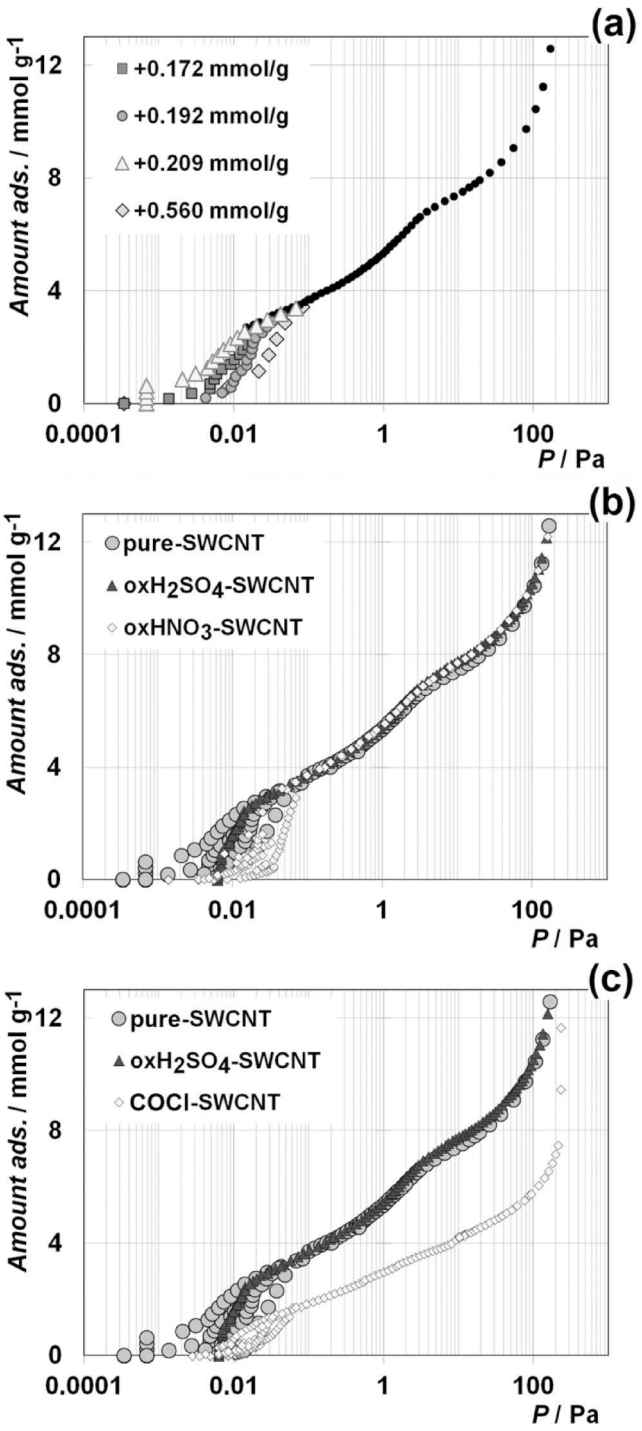

Figure 5. a) 77 K isotherm of Kr adsorbed on pure-SWCNTs. In the LPR the branches obtained by using the CAD protocol for the four indicated doses of Kr are presented. b) 77 K isotherm of Kr adsorbed on pure-SWCNTs, oxH_2SO_4-SWCNT, and $oxHNO_3$-SWCNT samples. c) 77 K isotherm of Kr adsorbed on pure-SWCNTs, oxH_2SO_4-SWCNT, and COCl-SWCNTs. The adsorption curve of oxH_2SO_4-SWCNT has AD-independent behavior. For $oxHNO_3$-SWCNT and COCl-SWCNT samples, the branches in the LPR were obtained by using the CAD protocol for some different values of AD comparable with the indicated doses of Kr for pure-SWCNT sample.

oxH$_2$SO$_4$-SWCNT has the "usual" AD-independent behavior (Figure 5(b)). There are no branches or equilibrium pressure drops with either the CAD or the IAD protocol. The first step extends from approximately 0.005 to approximately 0.02 Pa; that is, it is much narrower than for pure-SWCNTs. The reason underlying this change might be that the grafted functional groups such as quinone or carboxylic acid moieties are located at the ends of the SWCNT bundles so they block the entry ports for Kr adsorption into the channel sites.

However, the adsorption curve of the oxHNO$_3$-SWCNT sample maintains an AD-dependent behavior. The branches in the LPR obtained for some different values of AD are shown in Figure 5(b).

This is a very surprising result. The data obtained from IR spectroscopy and TGA-MS show that both acid treatments lead to the introduction of the same carboxylic acid groups on the SWCNT surface but, in the case of HNO$_3$, the number of -COOH groups is slightly greater than that for samples treated with H$_2$SO$_4$. Given that the tips of SWCNTs are among the most reactive sites of SWCNT bundles, one can expect a localization of the same number of -C=O and -COOH groups here as in oxH$_2$SO$_4$-SWCNT sample, resulting in blocking of the entry ports to IC-sites for Kr adsorption. However, this is not the case for the oxHNO$_3$-SWCNTs.

The volumetric adsorption study has thus established a difference between the two oxidized samples regarding the number of carboxylic acid groups on the tips of the SWCNTs. For both oxidized samples, the second part of the overall isotherm coincides with that of the pure-SWCNT sample (Figure 5(b)), implying that the number of functions on the surface is insufficient to influence the Kr adsorption on the external surface of the bundles.

Regarding the COCl-SWCNT sample, the 77 K Kr adsorption curve has AD-dependent behavior (Figure 5(c)). This suggests that the entry ports to the IC-sites at the bundle ends that were closed by the H$_2$SO$_4$ treatment are reopened by the chlorination treatment. The chlorination passes through the reaction SWCNT-COOH + SOCl$_2$ → SWCNT-COCl.[6] The chlorocarbonyl groups stay in the same places as the -COOH groups. The question then arises: Why in this case are the entry ports of the IC-sites opened for the Kr adsorption? One possible reason might be a breaking of the hydrogen bonds between two -COOH functions when they are transformed into -COCl groups. So, we can postulate that the grafted functional groups such as quinone or carboxylic acid at the ends of the bundles block the IC entry ports of the bundles only if they form dimers. If there are not enough adjacent functions to form dimers (the case of oxHNO$_3$-SWCNT sample) or the nature of the functions do not allow them to form hydrogen bonds, as in the case of -COCl groups, then they block such entry ports only partially through decreasing the size of the canal; thus, the quantity of gas that can be adsorbed, then decreases.

The adsorption curve of COCl-SWCNT in the second step region is lower; that is, the sample adsorbs less on the external sites. This could be explained by the bundle size increase. TEM micrographs (Figure 4(d)) show a rise in the bundle size, so part of the initially external surface is "transformed" into an internal surface of the larger bundles; that is, the total outer surface has diminished. In the HAADF image (Figure 4(e)) one can see on the SWCNT surface some atoms heavier than carbon. The EDS spectra show the presence of S and Cl (Figure 4(f)). The Cl signal arises from the chlorocarbonyl groups. They do not form the dimers. So, if the presence of Cl can be eliminated as an explanation, then S must be the reason for the bundle consolidation. In fact, during H$_2$SO$_4$ treatment on the SWCNT surface, not only were carboxylic acid and quinone functions created, but also phenol -OH groups (Figure 2). If the bundle ends are occupied by the carboxylic acid and quinone functions, the phenol groups might be distributed over the side faces of the bundles. They do not form dimers like carboxylic acid and quinone functions, thus explaining why they probably do not promote bundle alignment. Nevertheless, during the chlorination they can react with thionyl chloride forming sulfite ester functions linking two adjacent bundles: SWCNT-OH + SOCl$_2$ → SWCNT-O-(S=O)-O-SWCNT.

2.5. Possible Reaction Mechanisms that Occur on the Nanotube Surface

Let us summarize the obtained results. Firstly, all of the analytical techniques that were used clearly show that the level of functionalization for the two oxidized samples is very low. In the case of oxHNO$_3$-SWCNTs, the number of oxygen-containing functionalities is slightly higher than in the oxH$_2$SO$_4$-SWCNTs sample. The oxygen-containing groups are the same in the two samples: the phenol -OH, the quinone -C=O and the carboxylic acid -COOH groups. Nevertheless, the morphology of the two samples is different. TEM/STEM examinations show an oxHNO$_3$-SWCNT morphology change through alignment of the bundles. However, the morphology of oxH$_2$SO$_4$-SWCNT is similar to that of pure-SWCNT. We hypothesize that, in the case of the HNO$_3$ treatment, more functional groups such as quinone and carboxylic acids were uniformly located on the side faces of the bundles. The alignment might be due to an electrostatic attraction between different bundles because of the formation of weak hydrogen bonds between functional groups on the CNT surface. The post-chlorination of oxH$_2$SO$_4$-SWCNT sample leads to an increase in the average bundle size. STEM examination and EDS analysis show the presence of S on the SWCNT bundle surface, which is introduced as a result of a reaction between thionyl chloride and phenol groups distributed on the SWCNT surface. As a result, the sulfite ester functions linking two adjacent bundles are formed. We can therefore suggest that there are phenol groups on the side faces of the bundles in the oxH$_2$SO$_4$-SWCNT sample.

Given that the formation of oxygen-containing functions is stepwise,[20] the first hypothesis that occurs to us is that the nitric acid is simply more reactive and is able to further oxidize the CNT sidewalls. It is known that the ends of the nanotubes are among the most reactive sites.[10,18] So, they react the first with the acids. If that is the case, then there should not be any difference in the number of -COOH groups at the ends of the nanotube of the two oxidized samples, and the only difference

would be the number of functionalities along the nanotube length. This hypothesis can explain the difference in morphology between the two oxidized samples. However, it cannot explain the difference regarding the results of TGA-MS or of the volumetric adsorption study. It cannot explain why the same carboxylic acid groups located at the ends of SWCNT bundles transform into the anhydride functions during thermal treatment in the oxH_2SO_4-SWCNT sample and not in the oxHNO_3-SWCNTs. Furthermore it cannot explain why -COOH groups block the entry ports to the IC and T-sites for Kr adsorption in the oxH_2SO_4-SWCNT sample and not in the oxHNO_3-SWCNT.

If, however, we hypothesize that the number of -COOH functional groups at the ends of the SWCNT bundles in the two oxidized samples is different, we can explain all the obtained results, including those of TGA-MS and volumetry. The -COOH groups, which are located densely at the end of bundles in the oxH_2SO_4-SWCNT sample, form the dimers between two adjacent groups. The dimers block the entry ports to the interstitial channels and to the opened tubes for Kr adsorption. During the thermal treatment, they transform into anhydride functions. In the oxHNO_3-SWCNT sample there are few -COOH groups (or maybe even none) at the tips of the nanotubes; that is, there are no dimers of -COOH. For this reason, the IC and T-sites stay opened for Kr adsorption. For the same reason, there is no transformation of the dimers of -COOH groups into the anhydride groups during the thermal treatment.

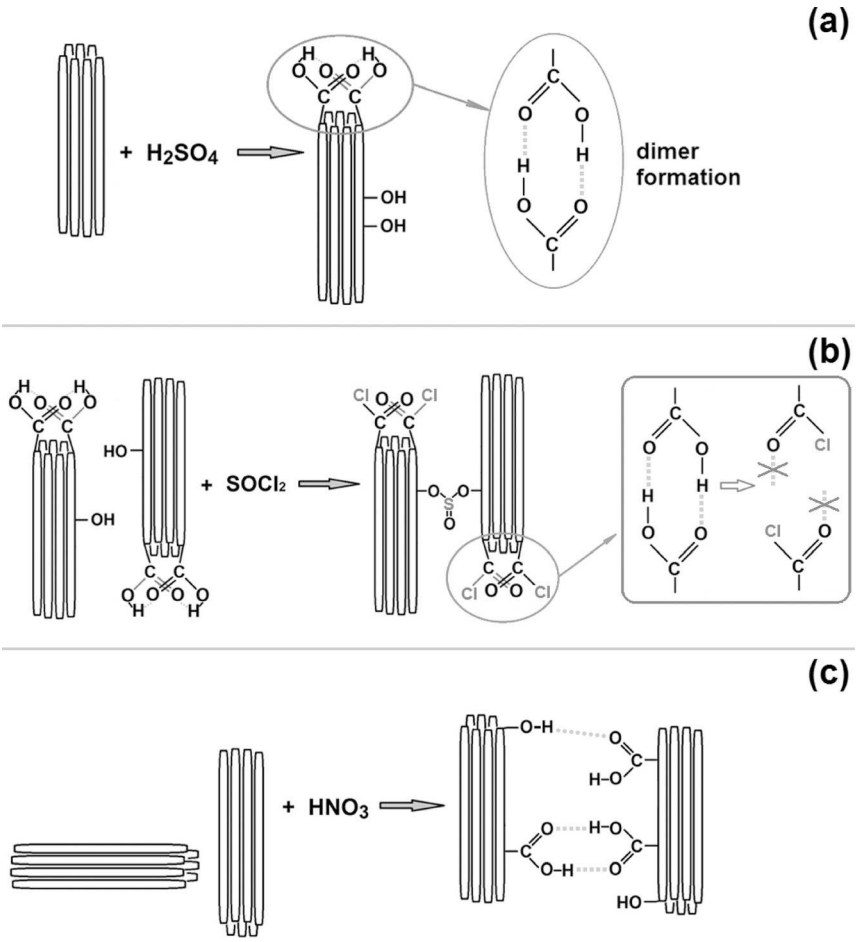

Figure 6. Schematic illustration of possible reaction mechanisms occurring on the nanotube during: a) H_2SO_4 treatment; b) subsequent chlorination using $SOCl_2$; c) HNO_3 treatment. Dashed lines show the formation of weak hydrogen bonds between different functions. The weak bonds between two groups located on two different bundles, are not strong enough to force the adjacent bundles to form any stable structure, but they can promote an alignment of bundles as noted by TEM/STEM examination.

Possible reaction mechanisms occurring on the nanotubes are presented in Figure 6. Clearly, the presented images are only schematic; they illustrate the localization of the reactions taking place and the organization of functionalities on the CNT surfaces. These include (1) dimer formation between two adjacent -COOH groups at the bundle ends, (2) the formation of "bridge" functionalities linking two adjacent bundles, and (3) the bundle alignment due to an electrostatic attraction owing to formation of weak hydrogen bonds between functional groups on the CNT surface.

We do not know the true reason leading to this difference in the oxidizing action of the two acids. We can only suppose that the reason might be in a different oxidizing force of the two acids. Probably, nitric acid is more effective, stronger, i.e. it forms more oxygen-containing functionalities on the nanotube surface than H_2SO_4. Its higher reactivity means that it probably reacts immediately with all the reactive sites. However, it remains unclear why, during the HNO_3 treatment, the transformation of phenol groups into carboxylic acids at the nanotube tips was not realized in contrast to the side faces of the bundles. We believe that this difference in the number of -COOH groups at the bundle ends in the two oxidized samples is characteristic of a soft oxidation process. A unique aspect of the current study is in the realization of a very soft oxidation. This is probably why we have observed this phenomenon. The use of a wide and complementary range of analytical techniques has allowed the difference between some properties of oxidized samples resulting from different numbers of -COOH groups at the nanotube ends to be determined.

3. Summary and Conclusions

We have presented the results of a study on the covalent functionalization of HiPco SWCNTs. The analytical techniques that have been employed, including TEM/STEM, EDS, TGA-MS, Raman scattering, DRIFT spectroscopy, and rare-gas volumetric adsorption, have allowed much information to be obtained about the level of functionalization, the type of functional groups, and their location on the nanotube surface.

Both H_2SO_4 and HNO_3 treatments lead to the introduction of the same functions on the SWCNT bundle surfaces, but the number of -COOH groups at the end of SWCNT bundles is different, resulting in significant differences in the properties. In the oxH_2SO_4-SWCNT sample, quinone or carboxylic acid groups grafted at the bundle ends can block the entry ports into the inner channels of opened tubes or into the interstitial channels of bundles through dimer formation. In the case of the oxHNO_3-SWCNT sample, the -COOH functions are well dispersed on the SWCNT surface and can form weak bonds either with -COOH, or with other groups such as -OH or quinone=O located on adjacent bundles. These interactions result in an alignment of the bundles.

Subsequent chlorination of the oxH_2SO_4-SWCNT sample transforms -COOH groups into the chlorocarbonyl groups COCl-. The -OH groups are distributed over the SWCNT surface, and can react with thionyl chloride with formation of sulfite ester functions, which can link the adjacent bundles. This results in an increase in bundle size.

Experimental Section

Samples

The SWCNTs used in this study were HiPco SuperPureTubes produced by NanoIntegris. According to the manufacturer, the diameter range is 0.8–1.2 nm with individual CNT lengths up to 1 μm; they contain $<5\%$ of metal catalyst impurities. The SWCNTs are bundled.

Oxidation of SWCNTs Using Acids: HiPco SuperPureTubes (10 mg) were placed in a 10 mL vial and 3 mL of concentrated HNO_3 (70% w/w which corresponds to 15 M) or 2.5 M H_2SO_4 was added. The vial was closed with a Teflon cap and irradiated under microwaves at 50 °C for 20 min (15 psi, 100% power with a 300 WCEM Discover). After cooling, the SWCNTs were submitted to three centrifugation/decanting cycles in deionized water (10 mL for each cycle). The SWCNT acid suspensions were neutralized by adding a sodium hydroxide solution (2 M, 4 mL) and washed extensively with water using sonication to eliminate the salts of sodium. Final rinsing was performed with ethanol to remove all traces of water. The Ox-SWCNTs were dried overnight in an oven at 80 °C and stored in closed vials at RT.

Treatment of SWCNTs with $SOCl_2$: Thionyl chloride (10 mL) was added to ox-SWCNT (10 mg) and the mixture was heated to reflux at 70 °C for 24 h under an argon atmosphere. The thionyl chloride was removed under vacuum at ambient temperature, then the SWCNTs were washed several times with anhydrous tetrahydrofuran (THF) using three sonication/filtration cycles (20 mL THF for each cycle). The COCl-SWCNTs were dried under vacuum for 5 h. The COCl-SWCNTs can be stored under argon at −20 °C for several days.

Due to the instability of chlorocarbonyl functional groups at ambient temperature in air, some methods of analysis that would have required long manipulations under these conditions, were not carried out.

Hereafter for HiPco SuperPureTubes we will use the term "pure-SWCNT", for SWCNTs oxidized with H_2SO_4 - "oxH_2SO_4-SWCNT", for those oxidized with HNO_3 - "oxHNO_3-SWCNT", and finally for oxH_2SO_4-SWCNT chlorinated with $SOCl_2$ the term "COCl-SWCNT".

Raman Spectroscopy

Raman scattering experiments using a He-Ne laser excitation (633 nm wavelength) were performed with a Witec CRM200 confocal Raman microscope equipped with an electrically-cooled CCD detector, a grating with 1800 grooves per mm (spectral resolution 1 cm^{-1}), and a long working distance ×50 objective with a numerical aperture of 0.55. CNTs were dispersed in THF (0.1 mg of CNTs/mL) using sodium deoxycholate (DOC) as a surfactant (5% in weight). A tip sonication method was used to make the suspension (90 W for 30 min) which was then spin-coated onto a glass slide. The laser irradiance was kept below 1 kW cm^{-2} to avoid damage to the samples caused by heating. To strengthen the statistical significance of the Raman data, more than 40 spectra were collected at various locations on the sample, and we report the average spectra for each sample.

Diffuse Reflectance Infrared Fourier Transform (DRIFT) Spectroscopy

Infrared powder diffuse reflectance data were collected with a Harrick Praying Mantis attachment and a high-temperature reaction chamber that allowed the sample to be analyzed up to 100 °C under nitrogen flow. Spectroscopic grade KBr was used as background. The diffuse reflectance R_s of the sample and R_r of potassium bromide, used as a nonabsorbing reference powder, were measured under the same conditions. The sample was prepared by mixing the SWCNT with KBr (SWCNT mass fraction of 0.001 in KBr), without compaction. The reflectance is defined as $R=R_s/R_r$. The spectra are shown on a pseudoabsorbance ($-\log R$) scale.

Thermogravimetric Analysis Coupled with Mass Spectrometry (TGA-MS)

A Setaram Setsys Evolution 1750 Thermal Gravimetric Analyzer coupled with a Pfeiffer GSD 301C Vacuum OmniStar mass spectrometer allowed the nature of the products formed by detachment of the groups from the SWCNT surface and their release into the TGA system to be studied. Approximately 3–4 mg of raw or functionalized sample were placed in an alumina crucible in the TGA chamber and the temperature was raised at a rate of 3 °C min^{-1} from RT to 1000 °C under a helium (Air Liquide Alphagaz 2) flux of 20 mL min^{-1}. The parameters used for the mass spectrometer apparatus ensured that most of the species undergo single ionization, meaning that the charge $z=1$ for the detected mass-to-charge ratio m/z; thus, m/z or mass will be employed interchangeably in the text. TGA-MS characterizations were performed on at least two samples for any given batch to guarantee reproducible results.

Electron Microscopy

Samples were dispersed in absolute ethanol then deposited on a holey carbon film supported by a 300 mesh copper grid. Some of the high-resolution transmission electron microscopy (HRTEM) observations were performed with a Philips CM200 operating at 200 kV. The other HRTEM and STEM images, were performed with a JEOL ARM 200F equipped with a cold field emission gun, a probe Cs-corrector (correction of the spherical aberration) and with a JEOL SD30Gv detector for EDS spectroscopy. The microscope was operated at 80 kV to avoid damaging the SWCNTs. High-angle annular dark-field (HAADF) STEM images were obtained for collection semi-angles of 45–180 mrad, and a pixel time of 40 μs (1024×1024 pixels).

Volumetric Measurements

The physisorption studies were carried out by using an apparatus with two capacitive pressure gauges, allowing measurement between 10^{-3} and 1100 Pa (i.e. over the full range of the isotherms) with a resolution of 0.003% of full scale and a precision of 0.5% (in the range 10^{-3}–1 Pa) and of 0.2% (in the range 1–1100 Pa) of the reading. The raw isotherms were corrected for the thermal transpiration effect.[32] A liquid N_2 bath temperature stabilization method was used to maintain a constant temperature (77 K) of the sample cell containing the adsorbent under study. The other part of the apparatus (including pressure gauges, inlet manifold, gas reservoir, etc, except the pumps) isolated from the cell by a valve, was stabilized at 30.0±0.5 °C. Krypton was first introduced into this latter part and then into the adsorption cell by opening the valve. Upon adsorption, the cell pressure thus decreases and reaches a limiting value at equilibrium. Equilibration times ranged from 0.3 to 1 h per dose and were chosen experimentally. Our experimental setup was optimized so that small mass samples—but with large specific surface areas—could be accurately examined. The samples (typically 10 mg) were initially outgassed outside the adsorption chamber for 7 days at 100 °C to a pressure lower than 10^{-4} Pa. After installation in the adsorption setup, they were additionally outgassed for 1 day at 100 °C to a pressure lower than 5.10^{-5} Pa. Further isotherm measurements always started with outgassing of the sample at RT (20 °C) for 16 h to a pressure of $<5.10^{-5}$ Pa. Krypton (≥99.998%, Fluka Analytical) was purified by pumping on the condensed phase inside the apparatus. The experiments were carried out with use of two adsorptive dosing (AD) protocols. These are designated IAD (increased adsorptive dosing) if the dose is increased from one injection to another or CAD (constant adsorptive dosing) if the dose is constant.

Acknowledgements

The French Agence Nationale de la Recherche (ANR) (grant ANR-10-BLANC-0819–01-SPRINT) and the Région Lorraine (grant 30031172) are acknowledged for financial support. The authors thank Professor C. Carteret and Dr. S. Fontana for fruitful discussions and Dr. J.-F. Marêché for important technical assistance.

Keywords: nanostructures · nanotubes · oxidation · surface analysis · surface chemistry

[1] S. Kruss, M. P. Landry, E. V. Ende, B. M. A. Lima, N. F. Reuel, J. Zhang, J. Nelson, B. Mu, A. Hilmer, M. Strano, *J. Am. Chem. Soc.* **2014**, *136*, 713–724.
[2] W. Xu, J. Zhao, L. Qian, X. Han, L. Wu, W. Wu, M. Song, L. Zhou, W. Su, C. Wang, S. Nie, Z. Cui, *Nanoscale* **2014**, *6*, 1589–1595.
[3] N. Terasawa, I. Takeuchi, *Electrochim. Acta* **2014**, *123*, 340–345.
[4] B. He, Q. Tang, J. Luo, Q. Li, X. Chen, H. Cai, *J. Power Sources* **2014**, *256*, 170–177.
[5] Y. Hashida, H. Tanaka, S. Zhou, S. Kawakami, F. Yamashita, T. Murakami, T. Umeyama, H. Imahori, M. Hashida, *J. Controlled Release* **2014**, *173*, 59–66.
[6] N. Allali, V. Urbanova, V. Mamane, J. Waldbock, M. Etienne, M. Mallet, X. Devaux, B. Vigolo, Y. Fort, A. Walcarius, M. Noël, A. V. Soldatov, E. McRae, M. Dossot, *Phys. Status Solidi B* **2012**, *249*, 2349–2352.
[7] D. Tasis, N. Tagmatarchis, A. Bianco, M. Prato, *Chem. Rev.* **2006**, *106*, 1105–1136.
[8] L. Meng, C. Fu, Z. Fei, Q. Lu, P. J. Dyson, *Inorg. Chim. Acta* **2010**, *363*, 3926–3931.
[9] P.-X. Hou, C. Liu, H.-M. Cheng, *Carbon* **2008**, *46*, 2003–2025.
[10] A. Barinov, L. Gregoratti, P. Dudin, S. La Rosa, M. Kiskinova, *Adv. Mater.* **2009**, *21*, 1916–1920.
[11] A. M. Da Silva Jr., H. F. Dos Santos, P. Giannozzi, *Chem. Phys. Lett.* **2013**, *582*, 123–128.
[12] H. Hu, B. Zhao, M. E. Itkis, R. C. Haddon, *J. Phys. Chem. B* **2003**, *107*, 13838–13842.
[13] D. B. Mawhinney, V. Naumenko, A. Kuznetsova, J. T. Yates Jr., *J. Am. Chem. Soc.* **2000**, *122*, 2383–2384.
[14] S. Fogden, R. Verdejo, B. Cottam, M. Shaffer, *Chem. Phys. Lett.* **2008**, *460*, 162–167.
[15] A. G. Osorio, I. C. L. Silveira, V. L. Bueno, C. P. Bergmann, *Appl. Surf. Sci.* **2008**, *255*, 2485–2489.
[16] A. Kukovecz, Ch. Kramberger, M. Holzinger, H. Kuzmany, J. Schalko, M. Mannsberger, A. Hirsch, *J. Phys. Chem. B* **2002**, *106*, 6374–6380.
[17] B. Liu, H. Jiang, A. V. Krasheninnikov, A. G. Nasibulin, W. Ren, C. Liu, E. I. Kauppinen, H.-M. Cheng, *Small* **2013**, *9*, 1379–1386.
[18] X. Feng, C. Matranga, R. Vidic, E. Borguet, *J. Phys. Chem. B* **2004**, *108*, 19949–19954.
[19] J. Zhang, H. Zou, Q. Qing, Y. Yang, Q. Li, Z. Liu, X. Guo, Z. Du, *J Phys Chem. B* **2003**, *107*, 3712–3718.
[20] K. A. Wepasnick, B. A. Smith, K. E. Schrote, H. K. Wilson, S. R. Diegelmann, D. H. Fairbrother, *Carbon* **2011**, *49*, 24–36.
[21] V. Mamane, G. Mercier, J. A. Shukor, J. Gleize, A. Azizan, Y. Fort, B. Vigolo, *Beilstein J. Nanotechnol.* **2014**, *5*, 537–5345.
[22] R. Saito, M. Hofmann, G. Dresselhaus, A. Jorio, M. S. Dresselhaus, *Adv. Phys.* **2011**, *60*, 413–550.
[23] M. Kalbac, Y.-P. Hsieh, H. Farhat, L. Kavan, M. Hofmann, J. Kong, M. S. Dresselhaus, *Nano Lett.* **2010**, *10*, 4619–4626.
[24] S. Osswald, E. Flahaut, Y. Gogotsi, *Chem. Mater.* **2006**, *18*, 1525–1533.
[25] U. J. Kim, X. M. Liu, C. A. Furtado, G. Chen, R. Saito, J. Jiang, M. S. Dresselhaus, P. C. Eklund, *Phys. Rev. Lett.* **2005**, *95*, 157402.
[26] J. L. Figueiredo, M. F. R. Pereira, M. M. A. Freitas Órfão, *Carbon* **1999**, *37*, 1379–1389.
[27] S.Yu. Tsareva, E. McRae, F. Valsaque, X. Devaux, *Adsorption* **2015**, *21*, 217–227.
[28] M. Muris, N. Dupont-Pavlovsky, M. Bienfait, P. Zeppenfeld, *Surf. Sci.* **2001**, *492*, 67–74.
[29] M. R. Johnson, S. Rols, P. Wass, M. Muris, M. Bienfait, P. Zeppenfeld, N. Dupont-Pavlovsky, *Chem. Phys.* **2003**, *293*, 217–230.
[30] A. Kuznetsova, D. B. Mawhinney, V. Naumenko, J. T. Yates Jr., J. Liu, R. E. Smalley, *Chem. Phys. Lett.* **2000**, *321*, 292–296.
[31] X. Li, J. Niu, J. Zhang, H. Li, Z. Liu, *J. Phys. Chem. B* **2003**, *107*, 2453–2458.
[32] T. Takaishi, Y. Sensui, *Trans. Farad Soc* **1963**, *59*, 2503–2514.

Received: March 21, 2015
Revised: May 29, 2015
Published online on July 1, 2015

B- Functionalization of purified single-walled carbon nanotubes

Paper number 3.

Electrocatalytic effect towards NADH induced by HiPco single-walled carbon nanotubes covalently functionalized by ferrocene derivatives

Journal:	*2012 MRS Fall Meeting*
Manuscript ID:	Draft
Manuscript Type:	Symposium YY
Date Submitted by the Author:	n/a
Complete List of Authors:	Allali, Naoual; LCPME UMR 7564 CNRS-Lorraine University, ; SRSMC UMR 7565 CNRS-Lorraine University, ; Lulea University of Technology, Department of Engineering Sciences and Mathematics Urbanova, Veronika; LCPME UMR 7564 CNRS-Lorraine University, Etienne, Mathieu; LCPME UMR 7564 CNRS-Lorraine University, Mallet, Martine; LCPME UMR 7564 CNRS-Lorraine University, Devaux, Xavier; IJL UMR 7198 CNRS-Lorraine University, P2M Vigolo, Brigitte; IJL UMR 7198 CNRS-Lorraine University, CP2S Fort, Yves; SRSMC UMR 7565 CNRS-Lorraine University, Walcarius, Alain; LCPME UMR 7564 CNRS-Lorraine University, Noël, Maxime; Lulea University of Technology, Department of Engineering Sciences and Mathematics McRae, Edward; IJL UMR 7198 CNRS-Lorraine University, CP2S Soldatov, Alexander; Lulea University of Technology, Department of Engineering Sciences and Mathematics Dossot, Manuel; LCPME UMR 7564 CNRS-Lorraine University, Mamane, Victor; SRSMC UMR 7565 CNRS-Lorraine University,
Keywords:	C, nanostructure, chemical reaction

Electrocatalytic effect towards NADH induced by HiPco single-walled carbon nanotubes covalently functionalized by ferrocene derivatives

Naoual Allali[1, 2,5], Veronika Urbanova[1], Mathieu Etienne[1], Martine Mallet[1], Xavier Devaux,[3] Brigitte Vigolo[4], Yves Fort[2], Alain Walcarius[1], Maxime Noël[5], Edward McRae[4], Alexander V. Soldatov[5], Manuel Dossot[1,*], Victor Mamane[2].

1. Laboratoire de Chimie Physique et Microbiologie pour l'Environnement, UMR 7564 CNRS-Université de Lorraine, F-54602 Villers-les-Nancy, France.
2. Laboratoire de Structure et Réactivité des Systèmes Moléculaires Complexes, UMR 7565 CNRS-Université de Lorraine, F-54506 Vandoeuvre-les-Nancy, France.
3. Département P2M, Institut Jean Lamour, UMR 7198 CNRS-Université de Lorraine, Ecole des Mines, F-54042 Nancy, France.
4. Département CP2S, Institut Jean Lamour UMR 7198 CNRS-Université de Lorraine, F-54506 Vandoeuvre-les-Nancy, France.
5. Department of Engineering Sciences and Mathematics, Lulea University of Technology, SE-97187 Lulea, Sweden.

ABSTRACT

The present work reports the covalent functionalization of single-walled carbon nanotubes (SWCNTs) by ferrocene derivatives with polyethyleneglycol linkers. A very clean initial sample was chosen to avoid any residual catalyst and carbon impurities. Functionalized SWCNTs (f-CNTs) are deposited on the surface of a glassy carbon electrode (GCE) and this modified electrode is used for oxidizing the cofactor NADH (dihydronicotinamide adenine dinucleotide) in the presence of diaphorase. A clear electrocatalytic effect is evidenced, which can only be attributed to the f-CNTs.

INTRODUCTION

For electrochemical applications, several properties render carbon nanotubes (CNTs) very attractive including the diameter-dependent metallic or semi-conducting behavior, the high aspect ratio and the high specific surface area [1-3]. Chemical functionalization of CNTs is often used to attach electroactive molecules that can play the role of an electron shuttle (also known as redox mediators). Mediators react with the redox center of a protein or can be used to electrochemically detect the NADH cofactor. They can be covalently grafted or simply sorbed on the CNT surface [3]. If the envisaged applications concern biosensors or bioreactors, it is preferable that the mediator be covalently linked to the CNT surface to avoid any diffusion of the molecule in the analyzed medium or the reactor solution. Covalent functionalization therefore increases the lifetime of the electrochemical device but the functionalization step has to be sufficiently controlled to avoid degradation of the initial electronic properties of the CNTs. Many pioneering studies using CNTs for electrochemical devices employed multi-walled CNTs (MWCNTs) [1-3]. These are indeed cheaper and produced in higher quantities than SWCNTs; the chemistry on MWCNTs has been well explored and many reactions have been used to introduce oxidized defects on their side-walls [4,5]. This strategy allows increasing the interaction with polar solvents and notably water, and it seems that oxidized functions may help

to increase the electrochemical signals [6], while other authors have challenged this conclusion [7]. Nevertheless, MWCNTs have a broad diameter distribution and their surface chemistry is more difficult to characterize; smaller diameter SWCNTs are generally more reactive and can be properly separated from amorphous carbon impurities and residual catalyst particles [5]. Covalent functionalization processes on SWCNTs can be more controlled and characterized at each step of the process.

Deposited on the electrode surface, CNTs are thought to enhance electron transfer efficiency through electrocatalytic effects [1-3]. This has recently been challenged by several studies and may involve residual catalytic particles or other carbonaceous species that might be present [7-9]. In order to address this controversy, we have used a very clean HiPco SWCNT sample made and purified by NanoIntegris. We have covalently functionalized these tubes by ferrocene derivatives using a three step process (Scheme 1) that involves i) oxidation in an acidic medium using micro-wave irradiation to control the number of defects on the CNT side-walls, ii) a chlorination step using $SOCl_2$ and iii) the grafting of ferrocene derivatives using polyethyleneglycol linkers of various chain lengths. This procedure ensures both grafting enough groups to obtain a good electrochemical signal and retaining the intrinsic electronic properties of the tubes. It has already been successfully employed on the covalent functionalization of few-walled CNTs [10]. The ferrocene electroactive group is chosen as the redox mediator and the polyethylene glycol spacer is used to promote the dispersion of the f-CNTs in water (necessary for modifying the GCE). Spectroscopic, thermal and microscopic techniques are used to collect complementary data on the functionalization process and to quantify the number of grafted ferrocene derivatives per C atom of the CNTs. Finally, an electrochemical biosensor is made by modification of glassy carbon electrode surface by f-CNTs, which is then tested for diaphorase-catalyzed oxidation of NADH cofactor.

EXPERIMENTS

Materials and methods

All chemical compounds used for the functionalization steps (Scheme 1) were of high purity grade and used as received. HiPco SWCNTs were of "super purified" grade from Nanointegris and are claimed by the manufacturer to contain less <5% of residual catalyst particles and to have a diameter distribution between 0.8 and 1.2 nm. They were dispersed in nitric acid (65% in weight) and submitted to a microwave irradiation for 20 min at 50°C. Then, the COOH functions were converted to COCl using a $SOCl_2$ treatment at 70°C for 24h. The ferrocene derivatives noted as Fc-ETG-n in Scheme 1 were reacted through their alcohol function with the COCl groups to covalently attach the redox mediator to the CNT side-walls. The corresponding f-CNTs are noted as HiPco-FcETGn. We studied ethylene glycol spacers of two different chain lengths: n=1 and n=7. The f-CNTs were studied using Raman scattering (laser wavelength 514 nm), visible-near infrared (vis-NIR) absorption and X-ray photoelectron spectroscopy (XPS), high resolution transmission electron microscopy (HRTEM) coupled to energy dispersive X-Ray spectroscopy (EDS) analyses, and thermogravimetric analysis (TGA) coupled to mass spectrometry (MS). The f-CNTs were suspended in water using chitosan molecules and co-deposited on the surface of GCE with diaphorase enzyme for recycling NADH molecules. The cyclic voltammetry measurements were performed in a three-electrode cell configuration, including the film modified GCE as working electrodes, an Ag/AgCl (3M KCl

internal electrolyte) and platinum wire auxiliary electrode. All measurements were recorded in Tris-HCl buffer (pH 9.0) at a scan rate of 5 mV s^{-1}.

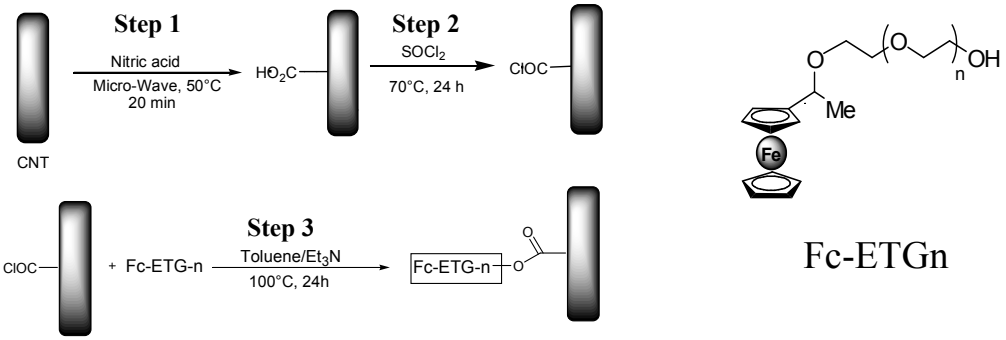

Scheme 1: The three-step process for functionalizing HiPco SWCNTs by ferrocene derivatives.

RESULTS AND DISCUSSION

Figure 1 shows representative HRTEM micrographs of the raw HiPco sample, which contains few metallic impurities as well as almost no carbon onions or nanographite impurities. Some amorphous carbon layers may be visible on the outer tubes of the bundles but this may be produced under the electron beam in the microscope.

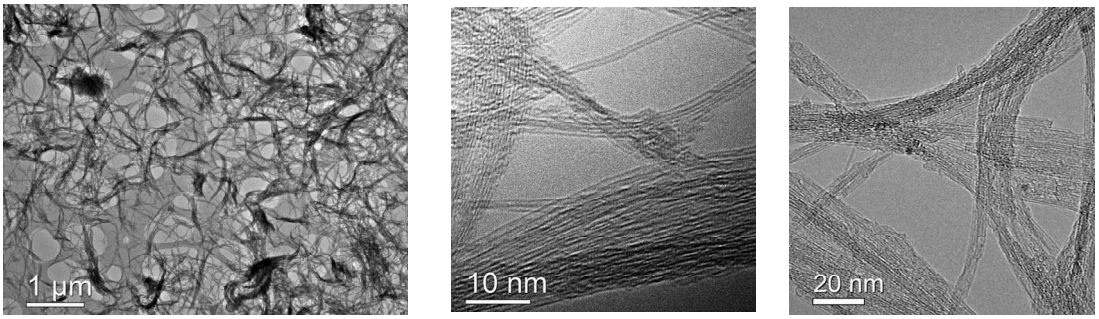

Figure 1: HRTEM images of the raw HiPco sample.

Figure 2 reports the results of TGA experiments under helium gas for raw HiPco, HiPco oxidized by HNO_3 (step 1 of Scheme 1) and HiPco-FcETG1 sample. The raw sample shows a monotonic weight loss up to 1000°C related to the desorption of existing chemical functions (e.g. alcohol, quinone groups) on its surface or sorbed solvent molecules coming from the manufacturer's purification process. For the oxidized HiPco sample, the slope of the weight loss curve is a little more pronounced between 200 and 300°C, and then almost parallel to that of the raw sample. The oxidation treatment by concentrated HNO_3 under 20 minutes of microwave irradiation does not introduce many new defects, contrary to thermal oxidation processes using several hours of treatment [5]. Assuming that the weight loss difference between curves (a) and (b) arises from the desorption of COOH functions, ca. 1 COOH function is formed per 120 C atoms. For HiPco-FcETG1, the rate of the weight loss is strongly increased between 200 and 600°C. We attribute this significant weight loss to the desorption of the ferrocene compounds grafted on CNT side-walls. MS coupled to TGA analyses confirmed that iron atoms and 1,3-cyclopentadiene groups are desorbed between 200°C and 500°C (Figure 2 right). Assuming that the weight loss difference between curves b and c comes from the ferrocene derivative, one can

calculate that 1 C per 130 is grafted by the FcETG1 group. Therefore, ca. 92% of the COOH functions are grafted by ferrocene derivatives under these hypotheses. Obviously this conversion rate might be a little overestimated but it is clear that steps 2 and 3 are quite efficient for HiPco CNTs.

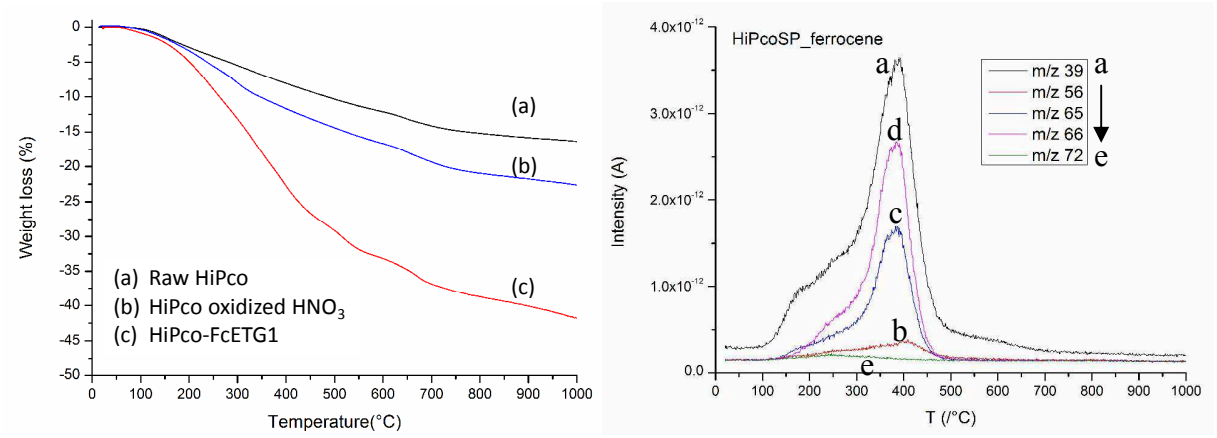

Figure 2: Left: TGA analyses of a) raw HiPco sample, b) HiPco oxidized in step 1 of Scheme 1 and c) HiPco-FcETG1 functionalized sample. Right: MS channels vs. temperature for detachment of 1,3-cyclopentadienyl moieties and iron atoms for HiPco-FcETG1 sample.

To corroborate the TGA conclusions, we performed XPS analyses of the raw HiPco, oxidized and the two functionalized HiPCo samples. Table 1 summarizes the quantification (in weight %) of C, O and Fe atoms obtained with these samples. Iron atoms of the residual catalyst particles are not detected by XPS for raw or oxidized samples due to carbon layers covering the particles, as previously reported [10]. Therefore, iron atoms detected for functionalized samples come from the grafted ferrocene groups, a fact that confirms the functionalization of CNTs by ferrocene derivatives.

	%C	%O	%Fe
Raw HiPco	92.9	7.1	0
Oxidized HiPco	87.3	12.7	0
HiPco-FcETG1	78.0	19.1	2.9
HiPco-FcETG7	74.9	24.0	1.1

Table 1: XPS quantification of elements (Fe, O, C) in the HiPco samples.

Figure 3 shows the HR-TEM micrograph of the HiPco-FcETG7 sample and the corresponding EDS spectrum taken on a spot located at the middle of a CNT bundle. The EDS spectrum clearly evidences the presence of iron atoms, and since no catalytic particle is visible in the HR-TEM image, we can attribute this signal to the ferrocene moieties grafted all along CNT side-walls. This is in agreement with the calculations derived from TGA-MS analyses: if only grafting at tube ends occurred, the yield of Fe atom per C atom would not be as high as 1 per 130. Figure 4 reports the vis-NIR absorption and Raman scattering spectra obtained for the samples in suspension in heavy water with sodium deoxycholate (DOC) as surfactant. The van Hove singularities of CNTs are clearly visible on absorption spectra (from metallic E^{m}_{11} and semiconducting E^{sc}_{11} and E^{sc}_{22} CNTs). Functionalized samples clearly show a decrease of intensity for the van Hove singularities of both metallic and semi-conducting CNTs. This is a strong indication of the covalent nature of the functionalization process, in agreement with TGA,

XPS and EDS analyses. Concerning Raman spectra, the D band intensity, related to covalent defects, does not change much among the different samples. The oxidation process by micro-wave irradiation in conc. HNO_3 did not introduce many new defects, which agrees well with the TGA curves of Figure 2. This chemical treatment certainly favors the conversion of existing defects to COOH functions but does not strongly cut CNTs neither destroyed the side-walls. After normalization at 270 cm^{-1}, low frequency radial breathing modes (RBM) also don't change much despite the decrease of electronic resonance in absorption spectra. No preferential functionalization between metallic or semiconducting CNTs is observed.

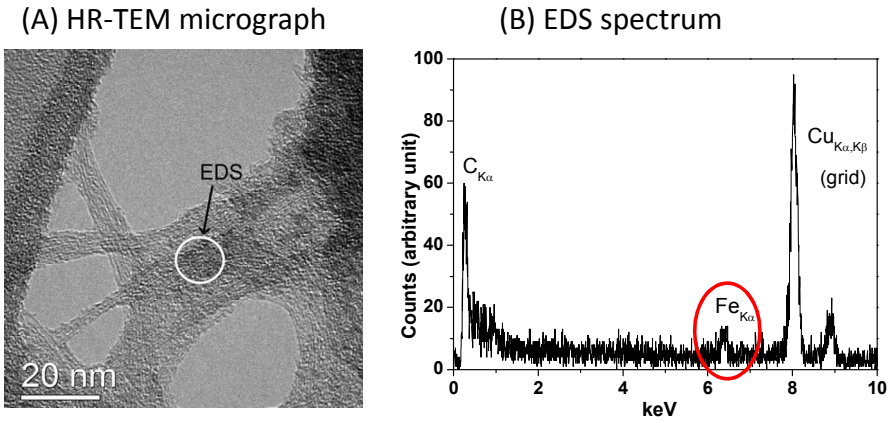

Figure 3: (A) HR-TEM images of HiPco-FcETG7 sample (the white circle corresponds to the location of the EDS analysis); (B) The corresponding EDS spectrum.

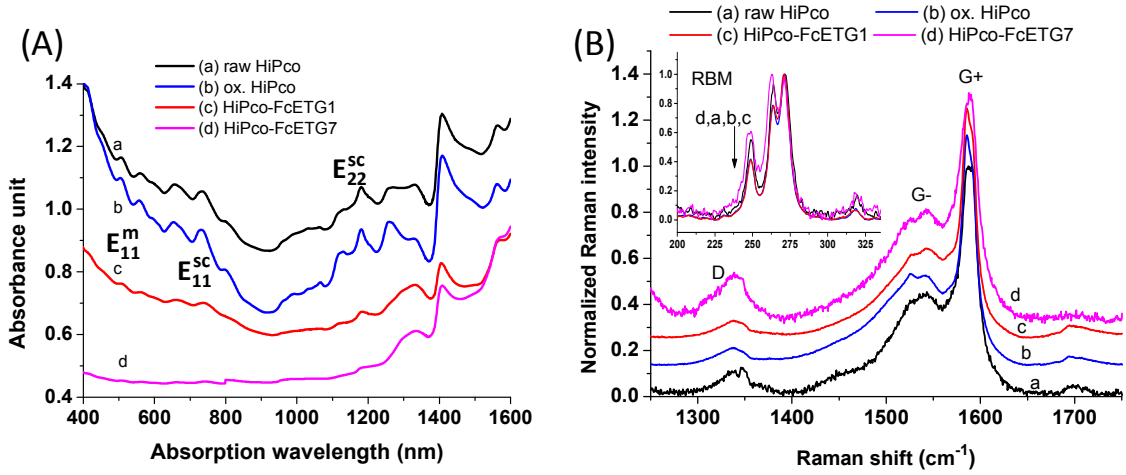

Figure 4: (A) Vis-NIR absorption spectra and (B) Raman spectra of raw, oxidized and functionalized HiPco samples.

Finally, Figure 5 reports the evolution of cyclic voltammograms obtained with oxidized and functionalized HiPco samples deposited at the GCE in the presence of increasing amounts of NADH molecules in solution. The oxidized HiPco sample only gives rise to a strong capacitive current and no electrocatalytic effect, while for both HiPco-FcETG1 and HiPco-FcETG7 samples, the oxidation peak significantly increases with progressive addition of NADH indicating an effective electrocatalytic behavior. Since the oxidized HiPco sample does not

produce any electrocatalytic effect towards NADH, we claim that the covalently modified HiPco samples do lead to electrocatalytic effects towards NADH in solution. In our case, oxygen atoms at the edges of CNTs are not responsible for the electrocatalytic effect, as suggested recently by Pumera et al. [9].

CONCLUSIONS

Covalent functionalization of clean HiPco CNTs by ferrocene derivatives has been done and confirmed by a set of complementary analyses. Cyclic voltammetry of GCE modified by these f-CNTs in the presence of NADH has undoubtedly evidenced a clear electrocatalytic effect of these covalently modified CNTs towards the oxidation of NADH. The role of impurities or only oxidized edges at CNT ends can be ruled out to explain this effect.

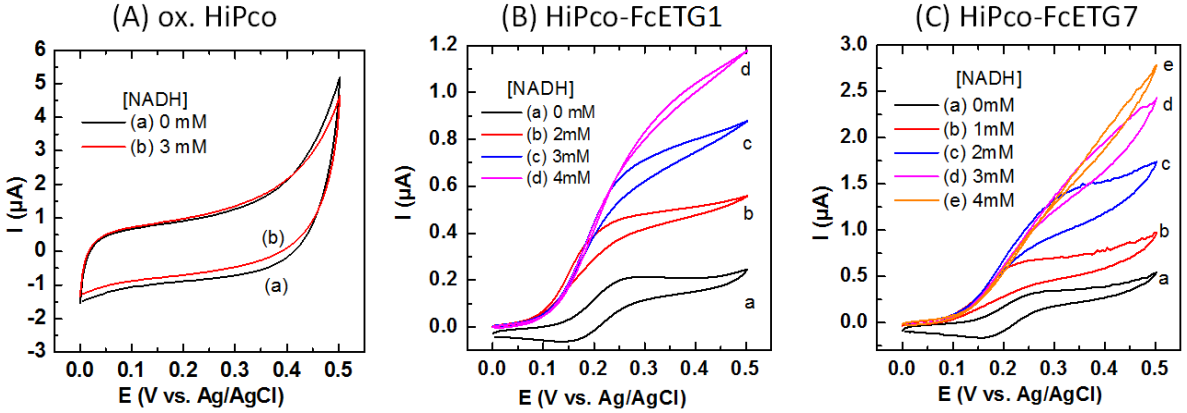

Figure 5: Cyclic voltammetry responses to NADH concentrations measured at GCE modified with (A) oxidized HiPco sample and (B),(C) functionalized HiPco samples.

ACKNOWLEDGMENTS

This work has been supported by the French National Research Agency (ANR), project ANR-10-BLAN-0819-01-SPRINT.

REFERENCES

1. S. K. Vashist, D. Zheng, K. Al-Rubeaan, J. H. T. Luong and F.S. Sheu, *Biotechnol. Adv.*, **29**, 169 (2011).
2. C. B. Jacobs, M. J. Peairs and B. J. Venton, *Anal. Chim. Acta*, **662**, 105 (2010).
3. I. Dumitrescu, P. R. Unwin and J. V. Macpherson, *Chem. Commun.*, **45**, 6965 (2009).
4. P.-X. Hou, C. Liu and H.-M. Cheng, *Carbon*, **46**, 2003 (2008).
5. D. Tasis, N. Tagmatarchis, A. Bianco and M. Prato, *Chem. Rev.*, **106**, 1105 (2006).
6. A. Chou, T. Böcking, N. K. Singh and J. J. Gooding, *Chem. Commun.*, **7**, 842 (2005).
7. M. Pumera, *Chem. Eur. J.*, **15**, 4970 (2009).
8. M. Pumera, *Chem. Rec.*, **12**, 201 (2012).
9. R. Scipioni, M. Pumera, M. Boero, Y. Miyahara and T. Ohno, *J. Phys. Chem. Lett.*, **1**, 122 (2010).
10. N. Allali, V. Urbanova, V. Mamane, J. Waldbock, M. Etienne, M. Mallet, X. Devaux, B. Vigolo, Y. Fort, A. Walcarius, M. Noël, A. V. Soldatov, E. McRae and M. Dossot, *Phys. Status Solidi B-Basic Solid State Phys.*, 2012 (Ahead of Print).

Paper number 4.

Journal of Electroanalytical Chemistry 707 (2013) 129–133

Contents lists available at ScienceDirect

Journal of Electroanalytical Chemistry

journal homepage: www.elsevier.com/locate/jelechem

Functionalized carbon nanotubes for bioelectrochemical applications: Critical influence of the linker

Veronika Urbanová [a], Naoual Allali [a,b], Wissam Ghach [a], Victor Mamane [b], Mathieu Etienne [a,*], Manuel Dossot [a], Alain Walcarius [a]

[a] CNRS and Université de Lorraine, LCPME, UMR7564, 405 rue de Vandoeuvre, F-54600 Villers-lès-Nancy, France
[b] CNRS and Université de Lorraine, LSRSMC, UMR7565, BP 70239, F-54506 Vandoeuvre-lès-Nancy, France

ARTICLE INFO

Article history:
Received 24 February 2013
Received in revised form 21 August 2013
Accepted 29 August 2013
Available online 7 September 2013

Keywords:
Covalent carbon nanotube functionalization
Ferrocene
Poly(ethylene glycol) spacer
NADH
Sol–gel
Glucose dehydrogenase

ABSTRACT

A series of covalently bonded ferrocene derivatives to carbon nanotubes via either alkyl or poly(ethylene glycol) (PEG) spacers has been prepared and deposited onto glassy carbon electrodes using chitosan as a binder. Evaluation of the effect of spacer arms revealed that the hydrophilic and flexible PEG chain greatly facilitates electron transfer reactions. When adding diaphorase in the composite, effective electrocatalytic oxidation of NADH was achieved. The PEG spacer also permitted an efficient dispersion of the functionalized carbon nanotubes, without additives. In this way, they can be easily incorporated in water-based sol–gel matrices, as illustrated for bioelectrochemical applications with co-immobilized glucose dehydrogenase, diaphorase and NAD^+ cofactor.

1. Introduction

The efficient electron transfer communication between an electrode surface and the enzyme active centres is a prerequisite for constructing amperometric biosensors and biofuel cell elements. To this end, the use of electron relay units that transport the electrons between the enzyme redox centre and the conducting surface is essential [1,2]. One could anticipate two general approaches to establish such electronic communication [3]. The first one comprises of so-called "electroenzymes", in which the protein itself is modified by covalently bonded redox mediators. Chemical modification of proteins by electron relay has been successfully applied in oxidative pathway, e.g., with glucose oxidase or dehydrogenase and lactate oxidase [4–6]. A second approach concerns the covalent attachment of the redox mediator via a long and flexible spacer arm leading to electrical wiring between an enzyme active site and the electrode surface [3,7], and hence effective mediated electron transfer can be expected [8].

Electrochemical oxidation of nicotinamide adenine dinucleotide (NADH) has received considerable attention due to its significance for designing novel biosensors because NAD-dependent dehydrogenases constitute one the largest group of redox enzymes [9]. Both direct electrochemical NADH oxidation and NAD^+ reduction reactions require the application of high overpotentials, often leading to electrode poisoning; moreover, the direct electrochemical reduction of NAD^+ leads to non-enzymatically active species [10,11]. These drawbacks can be overcome by using electron transfer mediators as the electrocatalysts that are able to lower the overpotentials usually observed for the NADH/NAD^+ redox couple. Diaphorase (DI) is an enzyme utilized to enhance electron transfer reaction rates and is a suitable counterpart in bioelectrocatalysis for the oxidation of NADH and for the reduction of NAD^+ in presence of a suitable redox mediator [12–14]. A variety of redox mediators, such as quinones, methylviologen, and flavinic compounds [12,14–17] have been used for this purpose. Hence, diaphorase-catalysed oxidation of NADH is an interesting example of mediated electron transfer for development of electrochemical devices based on NADH recycling, e.g. biofuel cells or for electrosynthesis [18,19].

Carbon nanotubes (CNTs) are widely used to improve the electron transfer between enzyme redox sites and an electrode surface and they also constitute promising platforms for immobilization of various redox mediators [20,21]. CNTs have received growing interest in the field of biosensors owing to their attractive features in terms of enhancing the sensitivity and/or selectivity towards chemical or biological compounds [22,23]. The study of the oxidation of nicotinamide adenine dinucleotide using CNTs has been the subject of numerous studies related to the development of amperometric biosensors [24–27]. For example, glassy carbon electrodes modified with CNT coatings (dispersed in a solution of

* Corresponding author. Tel.: +33 3 83 68 52 50; fax: +33 3 83 27 54 44.
E-mail address: mathieu.etienne@univ-lorraine.fr (M. Etienne).

1572-6657/$ - see front matter © 2013 Elsevier B.V. All rights reserved.
http://dx.doi.org/10.1016/j.jelechem.2013.08.029

concentrated sulfuric acid) revealed decrease in the overvoltage for the NADH oxidation (490 mV) and also eliminated surface fouling effects [26]. Facilitation of NADH oxidation at CNTs treated by microwaving has been described by Wooten and Gorski [27].

One has to be aware that carbon nanotubes tend to aggregate together in almost all kind of aqueous or organic solutions due to the van der Waals forces between the tubes. This fact imposes strong difficulties in preparing homogenous CNTs dispersions and thus greatly hampers electrochemical studies and their electroanalytical applications [21,28–30]. In general, getting an electrochemical sensor modified with a CNT-dispersion consists of casting the electrode, usually glassy carbon or gold, with a drop of the given dispersion, followed by a drying step under appropriate conditions. Different media (solutions/binders) such as dimethylformamide (DMF) [31], nafion [21,32], chitosan [33], polyethylenimine [34] or surfactants [35–37] have been used for CNTs dispersion. Significant progress has also been made in covalent and non covalent functionalization of CNTs since those strategies can improve solubilizing the CNTs and further facilitating their manipulation [38,39]. However, methods for the preparation of CNTs-modified electrodes from an electrochemical point of view are still needed [21].

Ferrocene derivatives are often employed to modify bioelectrodes since they act as redox mediator between the electrode and the redox active centre of an enzyme [40]. To prevent any loss of mediator in solution, different matrices for ferrocene encapsulation (e.g., chitosan, conducting polymers, hydrogels, sol–gel, etc.) have been used in literature [41–44]. Besides, some attempts of covalent or non-covalent attachment of ferrocene derivatives to CNTs have been described [45–49]. In general, π-stacking or aryldiazonium reduction were used to modify either single-walled or multi-walled carbon nanotubes.

In this work, we have followed an original strategy for covalent bonding of ferrocene derivatives to carbon nanotubes (CNTs-Fc) via either alkyl (CNT-$(CH_2)_n$-Fc) or poly(ethylene glycol) (CNT-$(EtG)_n$-Fc) linkers (Figs. 1B and 1C) and we have studied their behaviour towards the electrocatalytic oxidation of NADH. To the best of our knowledge, the role of a linker between CNTs and ferrocene (CNTs-Fc) on its electrochemistry connected with an enzymatic reaction was not considered so far in the literature. At first, glassy carbon electrodes modified by CNTs-Fc (in a chitosan matrix) were tested for diaphorase-catalyzed NADH oxidation. In a second step, CNTs-Fc were successfully incorporated in silica-based gels for co-immobilization with glucose dehydrogenase, diaphorase and NAD^+ cofactor, in the goal to evaluate their interest in reagentless bioelectrochemical devices.

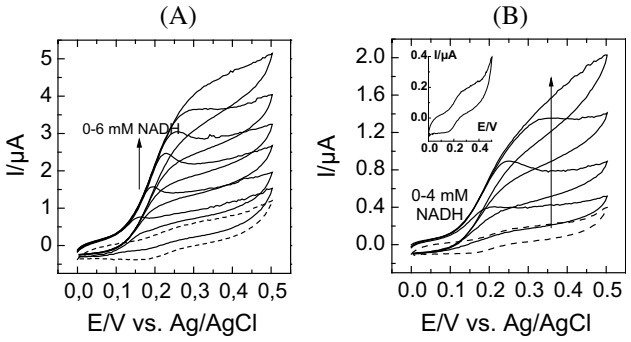

Fig. 2. Cyclic voltammetry responses to NADH measured at GCE modified with (A) chitosan/CNT-$(EtG)_2$-Fc and chitosan/DI overlayer and (B) chitosan/CNT-$(EtG)_8$-Fc and chitosan/DI overlayer. Inset in (A) shows the electrochemical response measured with CNT-$(EtG)_8$-Fc in the absence of NADH. All measurements have been performed in 0.1 M Tris–HCl buffer (pH 9.0) at a scan rate of 20 mV s^{-1}.

2. Experimental

2.1. Chemicals and materials

Carboxylic acid-functionalized single-walled carbon nanotubes (D1.5L1-5-COOH) were purchased from Nanolab. Diaphorase (DI, from *Bacillus stearothermophilus*, 1020 units mg^{-1}, Unitika, Japan.), ß-nicotinamide adenine dinucleotide, reduced dipotassium salt (NADH, 97 wt%, Sigma), ß-nicotinamide adenine dinucleotide (NAD^+, 98 wt%, Sigma), D-glucose (99 wt%, Acros), glucose dehydrogenase (GDH, from *Pseudomonas* sp., 200 units mg^{-1},

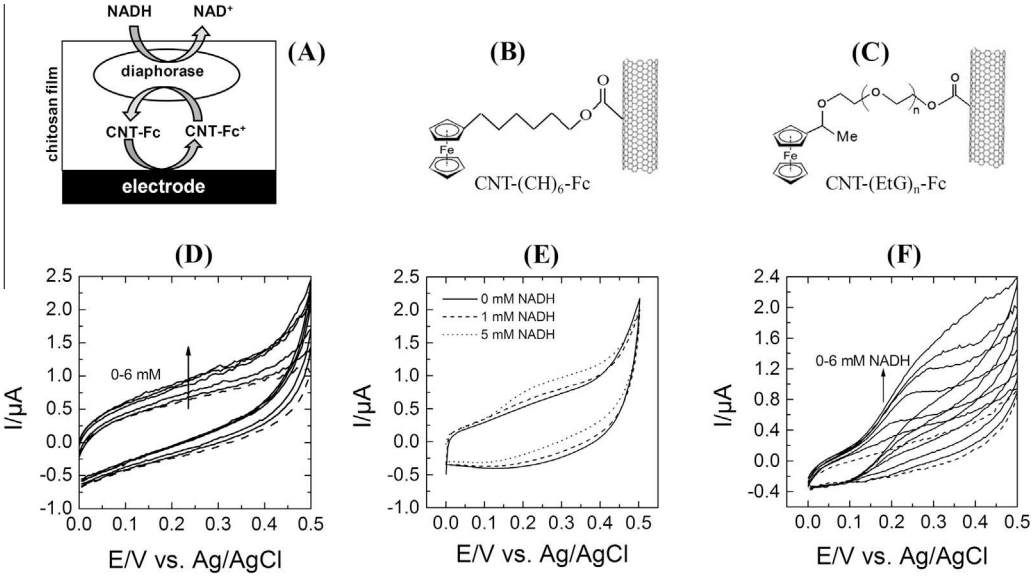

Fig. 1. (A) Schematic illustration of glassy carbon electrode (GCE) modified by chitosan/CNTs-Fc with chitosan/diaphorase overlayer for NADH oxidation. (B) Pictorial representation of carbon nanotubes covalently modified with ferrocene via alkyl: $(CH_2)_6$. (C) Pictorial representation of carbon nanotubes covalently modified with ferrocene via polyethylene glycol: $(EtG)_n$ linker. (D) Cyclic voltammetry responses to NADH measured at GCE modified with chitosan/CNT and chitosan/DI overlayer. (E) Cyclic voltammetry responses to NADH measured at GCE modified with chitosan/CNT-$(CH_2)_6$-Fc and chitosan/DI overlayer. (F) Cyclic voltammetry responses to NADH measured at GCE modified with chitosan/CNT-(EtG)-Fc, and chitosan/DI overlayer. All measurements have been performed in 0.1 M Tris–HCl buffer (pH 9.0) at a scan rate of 20 mV s^{-1}.

Sigma–Aldrich), chitosan (Aldrich), tris(hydroxylmethyl)-amino-methane (Tris, Sigma), HCl (36%, Prolabo), 3-glycidoxypropyl-trimethoxysilane (GPS, Sigma), tetraethoxysilane (TEOS, 98%, Alfa Aesar) and polyethylenimine (PEI, Sigma) were of analytical grade and used without further purification. All solutions were prepared with high-purity water (from a Millipore Milli-Q purification system).

2.2. Synthesis of ferrocene derivatives and CNT functionalization

The synthesis of ferrocene derivatives modified with the proper linker was performed according to a recently published procedure [50]. Their covalent binding was achieved through the carboxylate groups of oxidized CNTs. The resulting CNTs-Fc were characterized by physico-chemical techniques (TGA, Raman spectroscopy) in order to confirm the covalent functionalization [51].

2.3. Electrode preparation

Glassy carbon electrodes (GCE, 5 mm in diameter) were polished with alumina slurry (1 and 0.05 μm particles), sequentially, and then washed with water. 0.5 wt% chitosan solution was prepared by dissolving chitosan in 1% acetic acid. 2 mg of ferrocene-functionalized CNTs (CNTs-Fc) and 1 mL of the above chitosan solution were mixed together under stirring overnight. 5 μL of chitosan/CNTs-Fc suspension was deposited onto GCE surface to get a stable thin film after drying. Chitosan films containing either DI or GDH and DI were prepared by mixing 10 μL of 0.5 wt% chitosan solution with 5 μL of DI (5 mg mL^{-1}) or 15 μL of 0.5 wt% chitosan with 10 μL of GDH (1000 U mL^{-1}) and 5 μL of DI (5 mg mL^{-1}). Afterwards, 5 μL of this mixture was deposited onto chitosan/CNTs-Fc modified GCE and allowed drying at ambient temperature.

A typical bio-doped silica sol–gel layer was prepared according to a previous report [52] by dissolving 0.18 g TEOS, 0.13 g GPS, 0.5 mL of water and 0.625 mL of 0.01 M HCl, which were stirred for 12 h and then diluted 15 times with water for further use. NAD-GPS solution was typically prepared by mixing 6 mg NAD^+ and 37.5 mg GPS in 100 μL Tris–HCl buffer solution (pH 7.5) under stirring for 14 h. Finally, 7.5 μL of TEOS/GPS sol was mixed with 7.5 μL CNTs-Fc, 2.5 μL of PEI (10 wt%, pH 9.0), 5 μL NAD-GPS solution, 7.5 μL of GDH (1000 U mL^{-1}) and 5 μL of DI (5 mg mL^{-1}) and drop-coated onto the electrode surface.

2.4. Electrochemical measurements

All electrochemical experiments were carried out using a PGSTAT-12 Autolab potentiostat (EcoChemie) monitored by the GPES Software. Measurements were performed in a three-electrodes cell, including the film modified GCE as working electrode, an Ag/AgCl reference electrode (3 M KCl internal electrolyte), and a platinum wire auxiliary electrode.

3. Results and discussion

3.1. Alkyl versus poly(ethylene glycol) spacer arm

Since dehydrogenase-based biosensors operate on the basis of the detection of enzymatically generated NADH, we have first investigated the electrocatalytic behaviour of the CNTs-Fc towards NADH oxidation in the presence of a DI/chitosan overlayer as shown schematically in Fig. 1A. In our case, diaphorase is expected to enhance electron transfer reaction rate of NADH oxidation in the presence of ferrocene as redox mediator grafted onto carbon nanotubes with an alkyl (Fig. 1B) or a poly(ethylene glycol) spacer (Fig. 1C). As oxidized carbon nanotube can catalyze the electrochemical oxidation of NADH [24–27], a first experiment was performed with carboxylic acid-functionalized single-walled carbon nanotubes before the modification by ferrocene moieties (Fig. 1D). As it can be observed on the successive cyclic voltammograms only a limited current increase was observed between 0.2 and 0.3 V upon addition of 1–6 mM NADH, with no evidence of well-defined redox peak.

Fig. 1F shows the cyclic voltammograms obtained at GCE modified by CNT-(EtG)-Fc and DI upon continuous addition of NADH. As one can see, the oxidation peak rises significantly with increasing NADH concentration (solid lines), indicating an effective electrocatalysis. The Fc/Fc^+ oxidation peak (at 0.25 V versus Ag/AgCl) corresponds to the mediated oxidation of NADH. As it will be discussed in Section 3.2., such good electrocatalytic behaviour was also observed for all EtG arms tested here. On the other hand, very low anodic currents were observed using GCE modified by CNT-$(CH_2)_6$-Fc (i.e., an alkyl arm) in the presence of NADH (Fig. 1E), and such poor result was obtained independently on the alkyl chain length. The amount of ferrocene moieties grafted to CNTs was estimated by X-ray photoelectron spectroscopy (XPS). XPS experiments have been performed on the raw, oxidized and functionalized CNTs [51]. As expected, elemental iron was detectable only for ferrocene functionalized carbon nanotubes and these measurements revealed its concentration around 1%. Besides, termogravimetric analysis (TGA) and Raman spectroscopy have been performed to confirm the covalent functionalization of carbon nanotubes [51]. Moreover, the stability of the ferrocene attachment was evaluated by multicyclic voltammetry experiments and no significant loss in the electrochemical response was found.

The effect of spacer arm on the electrocatalytic response can be explained by different hydrophobic/hydrophilic balance. The hydrophobic alkyl spacer might hinder the proper mobility of Fc-moieties between the electrode surface and/or the active centre of diaphorase. By contrast, poly(ethylene glycol) is known as a flexible and biocompatible linear polymer with excellent solubility in water and thus PEG spacers offer to Fc-moiety more freedom which allows sweeping electrons from larger volume which, in turn, increase the frequency of electron transfer reactions with the redox centres of diaphorase.

3.2. Influence of the length of poly(ethylene glycol) spacer arm

In order to evaluate the effect of PEG spacer length on the electrochemical response of CNTs-$(EtG)_n$-Fc as well as their water dispersion efficiency, six different lengths of PEG chain have been synthesized, i.e., mono, di-, tri-, tetra-, penta- and octaethylene glycol (n = 1, 2, 3, 4, 5, 8). Fig. 2 reports the electrochemical responses

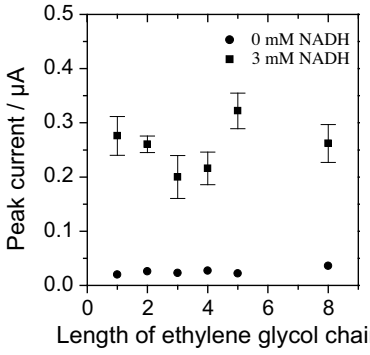

Fig. 3. Influence of ethylene glycol arm length on electrochemical response to 0 mM (●) or 3 mM (■) NADH in solution. All measurements have been performed in 0.1 M Tris–HCl buffer (pH 9.0) at a scan rate of 5 mV s^{-1}.

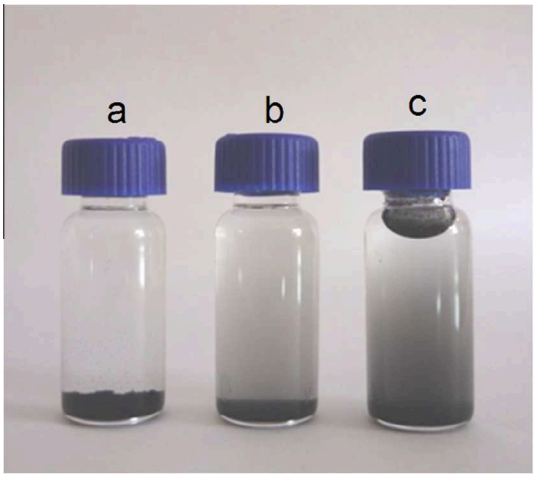

Fig. 4. Water dispersion of different CNTs after 48 h (a) pristine CNTs, (b) CNT-$(CH_2)_6$-Fc and (c) CNT-$(EtG)_8$-Fc.

measured by cyclic voltammetry with PEG chain of two (Fig. 2A) and eight ethylene glycol (Fig. 2B). While the electrochemical response of the ferrocene group in the absence of NADH was poorly defined in the experiment reported in Fig. 1F, an increase in the chain length led here to a better electrochemical response with clearly visible oxidation and reduction peaks of the ferrocene respectively located at 0.26 and 0.16 V versus Ag/AgCl.

Fig. 3 illustrates the influence of ethylene glycol arm length on the electrochemical response to 3 mM NADH. One can see that the various chain lengths of the PEG linker resulted in comparable electrocatalytic behaviour and the number of ethylene oxide units does not seem to dramatically influence the current intensity for NADH oxidation. It could have been expected that electron transfer processes would have been influenced by the distance between the electrode and immobilized redox probes, but the PEG linkers seem to keep comparable flexibility independently on their length. Only small differences have been observed between the various chain lengths, which can be explained by the small differences in the amount of ferrocene grafted on the carbon nanotubes (e.g., 0.78% Fe in CNT-$(EtG)_5$-Fc and 0.55% Fe in CNT-$(EtG)_8$-Fc, note again that the iron content was obtained from XPS analysis). On the other hand, water dispersion efficiency of functionalized CNTs was found to be dependent on the CNT surface state, with the best results obtained for long PEG linkers (Fig. 4). This is particularly attractive in view of using such functionalized nanotubes as potential biomedical materials since PEG chain extended their biocompatibility [53].

3.3. Application to the bioelectrocatalytic oxidation of glucose

With respect to possible application of CNTs-Fc modified electrode as a component of an electrochemical biodevice, glucose dehydrogenase (GDH) has been chosen to examine the bioelectrocatalytic oxidation of glucose in the presence of NAD^+ cofactor. GDH oxidizes ß-D-glucose to D-glucono-δ-lactone while reducing NAD^+ to NADH [54]. The produced NADH is reoxidized to NAD^+ by diaphorase with the concomitant reduction of the ferrocene bearing CNTs which in turn is regenerated at the electrode surface (Fig. 5). One of the most challenging aspects in development of dehydrogenase-based biosensors is the immobilization of all components enabling biocatalysis (i.e., enzymes, cofactors and mediators) in a durable and active form on the electrode surface. In this context, silica matrixes prepared by sol–gel processing have emerged as a promising platform for bioencapsulation [52]. Difficulties with solubility of CNTs in common solvents impose serious limitations of their use within a sol–gel matrix. Herein, thanks to the hydrophilic character of PEG arms, CNTs-$(EtG)_n$-Fc have been incorporated in a sol–gel thin film to co-immobilize all the necessary components for electroenzymatic reaction (Fig. 5). Note that the chain length should not influence the electrocatalytic activity of the bioelectrode. Some study, not shown here, using D-sorbitol dehydrogenase (DSDH) (but immobilized in chitosan, not in the sol–gel silica matrix) has been done in the presence of 4 mM D-sorbitol and no significant improvement in the electrocatalytic current response could be observed when using different PEG length.

In this experiment, CNTs functionalized by ferrocene via octa(ethylene glycol) linker (CNT-$(EtG)_8$-Fc) have been chosen because such long PEG linker ensures the best dispersion efficiency in the sol–gel matrix compared to pristine CNTs. SEM analysis of the film deposited on glassy carbon electrode shows that texture was homogeneous with no evidence of CNT aggregation, which is a good indication of a good dispersion of f-CNT in the sol–gel layer (Fig. 6). Typical response of this reagentless device to increasing concentration of glucose is shown in Fig. 7A. These results clearly demonstrate that the electrocatalytic oxidation of NADH to NAD^+ takes place fluently via mediated electron transfer in such multi-components system.

Since the direct electrocatalytic behaviour of pristine CNTs towards NADH oxidation was described in the literature [26,27], it was important to perform a control experiment in order to evaluate the real effect of ferrocene and to confirm that electron transfer is indeed carrying out via this mediator. Fig. 7B shows typical electrochemical responses to D-glucose additions using the same electrode configuration mentioned above (Fig. 5) but with unmodified CNTs instead of CNTs-Fc. As shown, the unmodified CNTs did not reveal any noticeable electrochemical response towards glucose and thus one can conclude that ferrocene plays clearly the role of mediator in our suggested system.

While the selectivity of the biosensor is guaranteed by the redox proteins used to oxidize the substrate to be detected, its sensitivity should be improved as it seems to be limited by the number of ferrocene moieties grafted on the CNT surface. We are currently exploring some routes to increase the quantity of groups to be grafted on CNT, which would also improve the dispersion of the material in water solution.

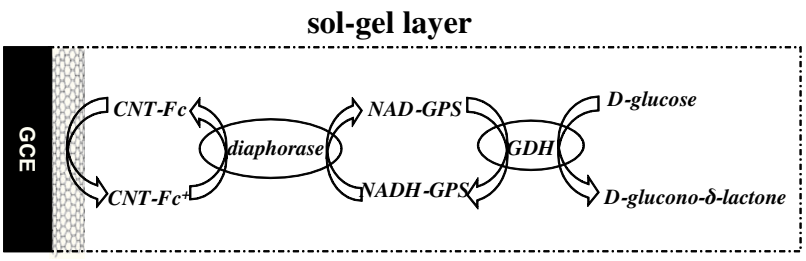

Fig. 5. Schematic illustration showing electrode configuration for glucose sensing.

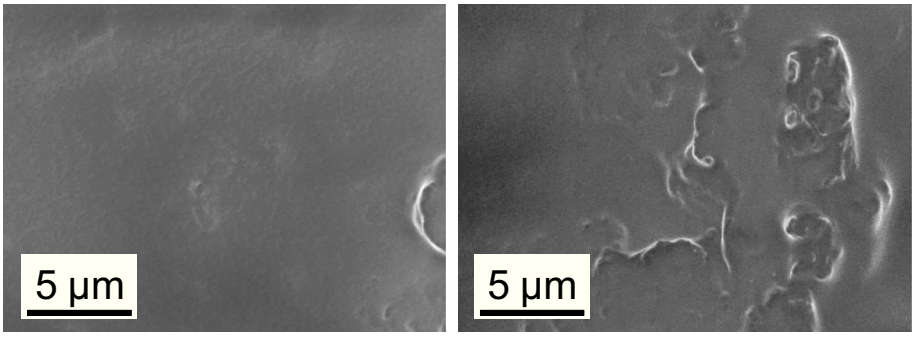

Fig. 6. SEM images of a glassy carbon electrode modified by a the sol–gel layer (TEOS-GPS/CNT-$(EtG)_8$-Fc/PEI/NAD-GPS/DI/GDH) similar as the one characterized electrochemically in Fig. 7A.

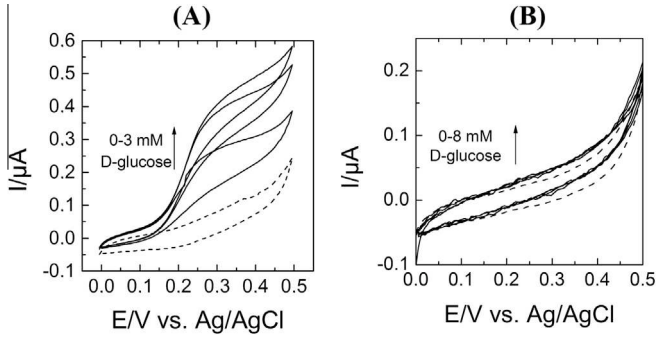

Fig. 7. (A) Cyclic voltammetry responses to D-glucose measured at GCE modified with TEOS-GPS/CNT-$(EtG)_8$-Fc/PEI/NAD-GPS/DI/GDH. (B) Cyclic voltammetry responses to D-glucose measured at GCE modified with TEOS-GPS/CNT/PEI/NAD-GPS/DI/GDH. All measurements have been performed in 0.1 M Tris–HCl (pH 9.0) at a scan rate 5 mV s^{-1}.

4. Conclusion

In this work, we have shown the interest of poly(ethylene glycol) linkers for the functionalization of carbon nanotubes with mediator moieties (Fc in this case). It allows effective wiring of diaphorase for the electrocatalytic oxidation of NADH. The good dispersion of the functionalized carbon nanotubes in water-based sols permits their incorporation in sol–gel-based bioelectrocatalytic devices including glucose dehydrogenase, diaphorase and linked NAD^+. Such strategy for covalent functionalization of carbon nanotubes should be useful for the design of a variety of other devices such as biosensors, biological fuel cells or bioreactors.

Acknowledgement

This work has been supported by Project ANR-2010-BLAN-0819-04-SPRINT and by the Institut Jean Barriol (FR 2843, CNRS – Université de Lorraine).

References

[1] M. Zayats, B. Willner, I. Willner, Electroanalysis 20 (2008) 583–601.
[2] A. Heller, Curr. Opin. Chem. Biol. 10 (2006) 664–672.
[3] I. Willner, N. Lapidot, A. Riklin, R. Kasher, E. Zahavy, E. Katz, J. Am. Chem. Soc. 116 (1994) 1428–1441.
[4] A. Heller, J. Phys. Chem. 96 (1992) 3579–3587.
[5] P.N. Bartlett, R.G. Whitaker, M.J. Green, J. Frew, J. Chem. Soc. Chem. Commun. (1987) 1603–1604.
[6] S. Reiter, K. Eckhard, W. Schuhmann, Analyst 126 (2001) 1912–1918.
[7] F. Mao, N. Mano, A. Heller, J. Am. Chem. Soc. 125 (2003) 4951–4957.
[8] E.J. Calvo, R. Etchenique, C. Danilowicz, L. Diaz, Anal. Chem. 68 (1996) 4186–4193.
[9] P.N. Bartlett, E. Simon, C.S. Toh, Bioelectrochemistry 56 (2002) 117–122.
[10] P.N. Bartlett, P. Tebbutt, R.G. Whitaker, Prog. React. Kinet. 16 (1991) 55–155.
[11] W. Schuhmann, Microchim. Acta 121 (1995) 1–29.
[12] K.M. Shin, S.I. Kim, I. So, S.J. Kim, Electrochim. Acta 54 (2009) 3979–3983.
[13] Y. Kashiwagi, T. Osa, Chem. Lett. 22 (1993) 677–680.
[14] Y. Ogino, K. Takagi, K. Kano, T. Ikeda, J. Electroanal. Chem. 396 (1995) 517–524.
[15] T. Miyake, M. Oike, S. Yoshino, Y. Yatagawa, K. Haneda, H. Kaji, M. Nishizawa, Chem. Phys. Lett. 480 (2009) 123–126.
[16] K. Takagi, K. Kano, T. Ikeda, J. Electroanal. Chem. 445 (1998) 211–219.
[17] V. Urbanová, M. Etienne, A. Walcarius, Electroanalysis 25 (2013) 85–93.
[18] R. Antiochia, L. Gorton, Biosens. Bioelectron. 22 (2007) 2611–2617.
[19] K. Miki, T. Ikeda, S. Todoriki, M. Senda, Anal. Sci. 5 (1989) 269–274.
[20] J. Wang, Electroanalysis 17 (2005) 7–14.
[21] K. Gong, Y. Yan, M. Zhang, L. Su, S. Xiong, L. Mao, Anal. Sci. 21 (2005) 1383–1393.
[22] A. Le Goff, M. Holzinger, S. Cosnier, Analyst 136 (2011) 1279–1287.
[23] D. Tasis, N. Tagmatarchis, A. Bianco, M. Prato, Chem. Rev. 106 (2006) 1105–1136.
[24] M. Tominaga, A. Iwaoka, D. Kawai, S. Sakamoto, Electrochem. Commun. 31 (2013) 76–79.
[25] C.E. Banks, R.G. Compton, Analyst 130 (2005) 1232–1239.
[26] M. Musameh, J. Wang, A. Merkoci, Y. Lin, Electrochem. Commun. 4 (2002) 743–746.
[27] M. Wooten, W. Gorski, Anal. Chem. 82 (2010) 1299–1304.
[28] V. Georgakilas, N. Tagmatarchis, D. Pantarotto, A. Bianco, J.-P. Briand, M. Prato, Chem. Commun. (2002) 3050–3051.
[29] J. Chen, Science 282 (1998) 95–98.
[30] G.A. Rivas, M.D. Rubianes, M.C. Rodríguez, N.F. Ferreyra, G.L. Luque, M.L. Pedano, S.A. Miscoria, C. Parrado, Talanta 74 (2007) 291–307.
[31] J. Wang, M. Li, Z. Shi, N. Li, Z. Gu, Anal. Chem. 74 (2002) 1993–1997.
[32] J. Wang, M. Musameh, Y. Lin, J. Am. Chem. Soc. 125 (2003) 2408–2409.
[33] Y. Liu, X. Qu, H. Guo, H. Chen, B. Liu, S. Dong, Biosens. Bioelectron. 21 (2006) 2195–2201.
[34] M.D. Rubianes, G.A. Rivas, Electrochem. Commun. 9 (2007) 480–484.
[35] J. Tkac, T. Ruzgas, Electrochem. Commun. 8 (2006) 899–903.
[36] Z. Wang, S. Xiao, Y. Chen, J. Electroanal. Chem. 589 (2006) 237–242.
[37] R.R. Moore, C.E. Banks, R.G. Compton, Anal. Chem. 76 (2004) 2677–2682.
[38] J. Pinson, F. Podvorica, Chem. Soc. Rev. 34 (2005) 429–439.
[39] C.-S. Lee, S.E. Baker, M.S. Marcus, W. Yang, M.A. Eriksson, R.J. Hamers, Nano Lett. 4 (2004) 1713–1716.
[40] S.L. Brooks, R.E. Ashby, A.P.F. Turner, M.R. Calder, D.J. Clarke, Biosensors 3 (1987) 45–56.
[41] Y. Miao, L.S. Chia, N.K. Goh, S.N. Tan, Electroanalysis 13 (2001) 347–349.
[42] J. Tkáč, I. Voštiar, P. Gemeiner, E. Šturdik, Bioelectrochemistry 55 (2002) 149–151.
[43] H.-Z. Bu, S.R. Mikkelsen, A.M. English, Anal. Chem. 70 (1998) 4320–4325.
[44] J. Li, L.S. Chia, N.K. Goh, S.N. Tan, H. Ge, Sens. Actuators. B 40 (1997) 135–141.
[45] A. Le Goff, F. Moggia, N. Debou, P. Jegou, V. Artero, M. Fontecave, B. Jousselme, S. Palacin, J. Electroanal. Chem. 641 (2010) 57–63.
[46] E. Nazaruk, K. Sadowska, J.F. Biernat, J. Rogalski, G. Ginalska, R. Bilewicz, Anal. Bioanal. Chem. 398 (2010) 1651–1660.
[47] Y. Wang, X. He, K. Wang, X. Ni, J. Su, Z. Chen, Biosens. Bioelectron. 32 (2012) 213–218.
[48] B. Fabre, C. Samorì, A. Bianco, J. Electroanal. Chem. 665 (2012) 90–94.
[49] F. Pepi, A. Tata, S. Garzoli, P. Giacomello, R. Ragno, A. Patsilinakos, M. Di Fusco, A. D'Annibale, S. Cannistraro, C. Baldacchini, G. Favero, M. Frasconi, F. Mazzei, J. Phys. Chem. C 115 (2011) 4863–4871.
[50] N. Allali, V. Mamane, Tetrahedron Lett. 53 (2012) 2604–2607.
[51] N. Allali, V. Urbanova, V. Mamane, J. Waldbock, M. Etienne, M. Mallet, X. Devaux, B. Vigolo, Y. Fort, A. Walcarius, M. Noël, A.V. Soldatov, E. McRae, M. Dossot, Phys. Status Solidi B 249 (2012) 2349–2352.
[52] Z. Wang, M. Etienne, F. Quilès, G.-W. Kohring, A. Walcarius, Biosens. Bioelectron. 32 (2012) 111–117.
[53] M. Shim, N.W. Shi Kam, R.J. Chen, Y. Li, H. Dai, Nano Lett. 2 (2002) 285–288.
[54] F. Sato, M. Togo, M.K. Islam, T. Matsue, J. Kosuge, N. Fukasaku, S. Kurosawa, M. Nishizawa, Electrochem. Commun. 7 (2005) 643–647.

Paper number 5.

BEILSTEIN JOURNAL OF NANOTECHNOLOGY

Accurate control of the covalent functionalization of single-walled carbon nanotubes for the electro-enzymatically controlled oxidation of biomolecules

Naoual Allali[1,2,3], Veronika Urbanova[1], Mathieu Etienne[1], Xavier Devaux[4], Martine Mallet[1], Brigitte Vigolo[5], Jean-Joseph Adjizian[6], Chris P. Ewels[6], Sven Oberg[3], Alexander V. Soldatov[3], Edward McRae[5], Yves Fort[2], Manuel Dossot[*1] and Victor Mamane[*2,7]

Full Research Paper

Open Access

Address:
[1]LCPME, UMR CNRS-Université de Lorraine 7564, 405 rue de Vandoeuvre, F-54602 Villers-lès-Nancy, France, [2]SRSMC, UMR CNRS-Université de Lorraine 7565, Campus Victor Grignard, Faculté des Sciences et Technologies, F-54506 Vandoeuvre-lès-Nancy, France, [3]Department of Engineering Sciences and Mathematics, Lulea Technical University, Sweden, [4]IJL, UMR CNRS-Université de Lorraine 7198, Parc de Saurupt - CS 50840, 54011 Nancy Cedex, France, [5]IJL, UMR CNRS-Université de Lorraine 7198, Campus Victor Grignard, Faculté des Sciences et Technologies, 54506 Vandoeuvre-lès-Nancy Cedex, France, [6]IMN, UMR CNRS-Université de Nantes 6502 and [7]New address: Institut de Chimie de Strasbourg, UMR CNRS-Université de Strasbourg 7177

Email:
Manuel Dossot[*] - manuel.dossot@univ-lorraine.fr; Victor Mamane[*] - vmamane@unistra.fr

* Corresponding author

Keywords:
biosensing; carbon nanotubes; covalent functionalization; electrocatalysis; ferrocene

Beilstein J. Nanotechnol. **2018,** *9,* 2750–2762.
doi:10.3762/bjnano.9.257

Received: 28 May 2018
Accepted: 10 October 2018
Published: 26 October 2018

Associate Editor: J. J. Schneider

Abstract

Single-walled carbon nanotubes (SWCNTs) were functionalized by ferrocene through ethyleneglycol chains of different lengths (FcETGn) and the functionalized SWCNTs (f-SWCNTs) were characterized by different complementary analytical techniques. In particular, high-resolution scanning electron transmission microscopy (HRSTEM) and electron energy loss spectroscopy (EELS) analyses support that the outer tubes of the carbon-nanotube bundles were covalently grafted with FcETGn groups. This result confirms that the electrocatalytic effect observed during the oxidation of the reduced form of nicotinamide adenine dinucleotide (NADH) co-factor by the f-SWCNTs is due to the presence of grafted ferrocene derivatives playing the role of a mediator. This work clearly proves that residual impurities present in our SWCNT sample (below 5 wt. %) play no role in the electrocatalytic oxidation of NADH. Moreover, molecular dynamic simulations confirm the essential role of the PEG linker in the efficiency of the

bioelectrochemical device in water, due to the favorable interaction between the ETG units and water molecules that prevents π-stacking of the ferrocene unit on the surface of the CNTs. This system can be applied to biosensing, as exemplified for glucose detection. The well-controlled and well-characterized functionalization of essentially clean SWCNTs enabled us to establish the maximum level of impurity content, below which the f-SWCNT intrinsic electrochemical activity is not jeopardized.

Introduction

Carbon nanotubes (CNTs) have been recognized as interesting candidates for developing electrochemical sensors for almost two decades [1-3]. They have been used to modify electrodes (e.g., glassy carbon electrodes, GCEs) in order to decrease the overpotential value, increase sensitivity and reduce the occurrence of electrode fouling by degradation of the analyzed (bio)molecules [4]. They can increase the electron transfer rate between electrode and target molecules and decrease electrode response time [3,5]. We and others have reported some interesting electrocatalytic effects when using CNT-modified GCEs for the voltamperometric detection of (bio)molecules [6-14].

Two major hurdles have to be tackled when designing CNT-modified GCEs as biosensors: the water solubility and the cleanliness of employed CNTs in order to avoid misinterpreted results.

The solubility of CNTs in water, a usual solvent for biosensors, is quite low. The strategies used to increase their water solubility have been either i) to chemically modify them by putting oxidative defects on their sidewalls and extremities to decrease their hydrophobicity, ii) to use non-covalent interaction with hydrophilic biomolecules or surfactants [15-18] or iii) to use covalently grafted polyethyleneglycol (PEG) linkers, as described by us [9,11,12].

Many studies use multiwall CNTs (MWCNTs) as a rather cheap source of CNTs. They are often mixed with an electron mediator that interacts non-covalently with the CNT sidewalls. The electron mediator is used as an electron shuttle towards biologically relevant molecules, such as enzymes or co-factors, especially nicotinamide adenine dinucleotide hydride (NADH) [6,8,13,19]. The CNTs and mediator are co-deposited on the GCE using a polymer. Chitosan is often used as a cheap biodegradable biopolymer with good compatibility with CNTs for making adequate suspensions before deposition on the GCE [20]. The main problem arising from the non-covalent interaction between CNTs and the electron mediator is that the latter may diffuse inside the analyzed medium, resulting in a progressive decrease of the sensor efficiency. A good alternative is therefore to covalently graft an electron mediator onto the CNT sidewalls. While CNT chemistry is now well developed, it can still remain somewhat challenging depending on the quality of the nanotube sample. Indeed, if the sample contains many carbonaceous impurities, these can also be functionalized and contribute to the final electrochemical signal. Several studies have underlined the role of residual metallic and carbonaceous impurities present in CNT samples on the electrocatalytic effects often reported in the literature [21-26]. The presence of such impurities may modify the reactivity of the CNTs themselves and can make it difficult to qualify and quantify the covalent functionalization of the CNTs. If one wants to control the chemistry made on the tubes at each step, it is absolutely mandatory to start from a very clean sample. Purified HiPco® SWCNTs are now commercially available at reasonable prices and constitute such a clean sample.

In our previous work, we have described the synthesis of covalently functionalized HiPco SWCNTs (f-SWCNTs) with ferrocene through PEG linkers, which presented good electrochemical efficiency for NADH oxidation [12]. However, two questions remained open regarding: i) the role of the PEG linker, besides its ability to increase the water solubility of f-SWCNTs and ii) the influence of metallic and/or carbonaceous impurities that may be present in the CNT sample.

In this article, by using advanced and complementary analytical techniques, we fully confirm the covalent nature of the chemical grafting. In particular, high-resolution scanning electron transmission microscopy (HRSTEM) and electron energy loss spectroscopy (EELS) analyses strongly supports the role of ferrocene in the observed electrocatalytic effect for NADH oxidation and rule out the hypothetic role of metallic and carbonaceous impurities. Moreover, the role of the PEG linker in the good electrochemical response was studied by molecular dynamics, which show that favorable interaction between the ETG units and water molecules prevents π-stacking of the ferrocene unit on the surface of the CNTs, therefore allowing for a good electron transfer. Figure 1 summarizes the context of this study.

Results and Discussion

Source of clean SWCNTs and strategy of functionalization

A HiPco SWCNT sample was purchased from Nanointegris Inc. of the purest grade ("super purified grade", less than 5% of residual catalytic particles, http://www.nanointegris.com/en/hipco, accessed August 2016). Figure 2a gives an example of the HRTEM image of this starting material. A small amount of

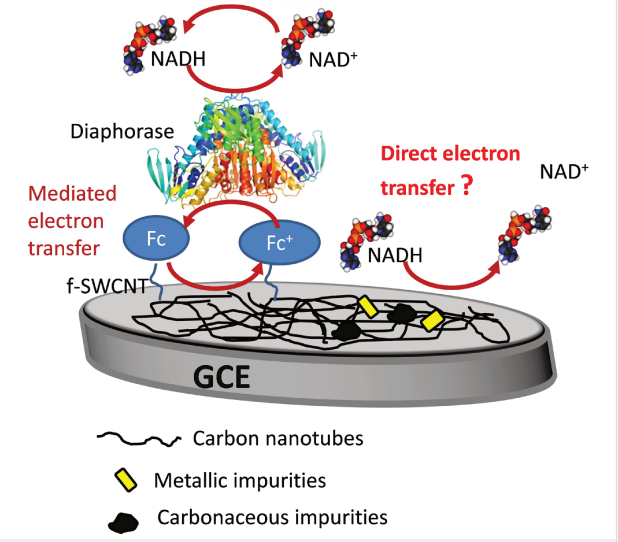

Figure 1: A working electrode (WE) incorporating the f-SWCNTs deposited on the GCE surface.

residual iron catalyst is visible (dark particles pointed out by red arrows). Carbonaceous impurities are mainly present in the form of carbon remains of nanometric size deposited along the CNT sidewalls and on the bundles (see red arrows in HRSTEM BF image presented in Figure 2b) but they are in very small amounts and the sample is clearly quite clean. In the rest of the text, to avoid the use of the commercial term HiPco, the symbol of our samples will be written HIPCO.

The SWCNTs were oxidized in acidic media using microwave irradiation to control the number of oxidized groups created on the CNT sidewalls [9,11]. Several microwave irradiation times were investigated but an optimum was found at around 20 min. Two different acidic media were tested: a quite conventional concentrated HNO_3 solution (65% w/w) and a rather diluted H_2SO_4 solution (2.5 mol·L^{-1}). The latter medium is greener and safer than a concentrated HNO_3 solution. Reaction with $SOCl_2$ was further realized and then ferrocene moieties coupled to linkers were added to the chlorinated CNTs for covalently attaching the ferrocene electron shuttle to the nanotube sidewalls. The principle of our strategy is indicated in Figure 3.

Oxidation of SWCNTs using concentrated HNO_3 (65% w/w, 14.3 M) or 2.5 M H_2SO_4, and subsequent treatment with $SOCl_2$ were realized following the previously described protocols [9,27,28]. We obtained COCl-SWCNT samples that were then used to covalently graft ferrocene derivatives on the CNT sidewalls.

Oxidation and chlorination steps

Figure 3 indicates that the first step needed to subsequently graft ferrocene moieties onto SWCNTs is to create oxidative

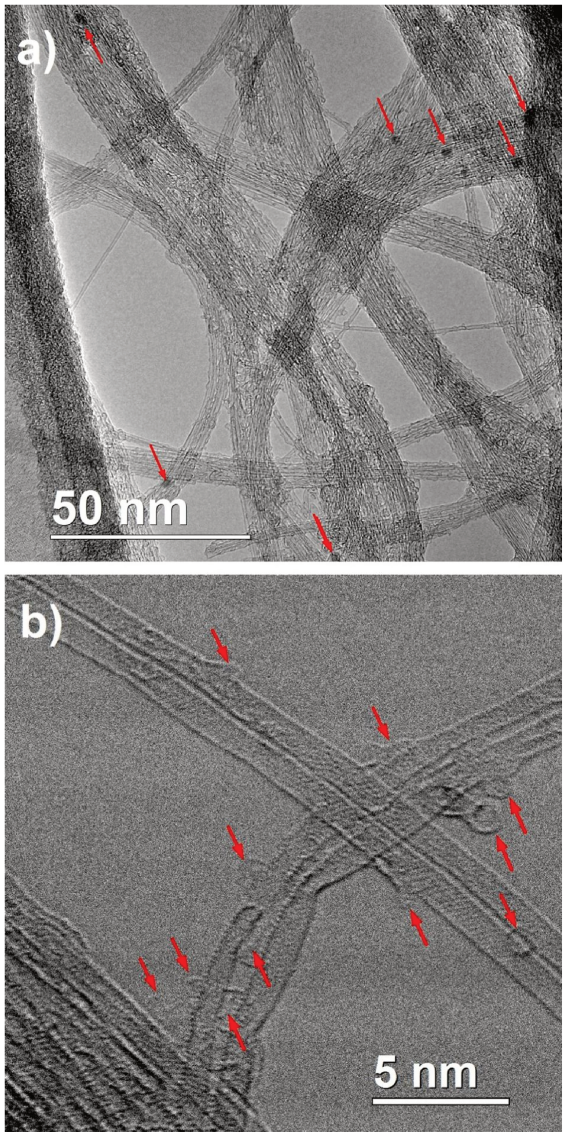

Figure 2: a) HRTEM micrographs of the raw HIPCO material. The arrows point out residual iron nanoparticles. b) HRSTEM BF image showing carbonaceous impurities at the surface of SWCNTs.

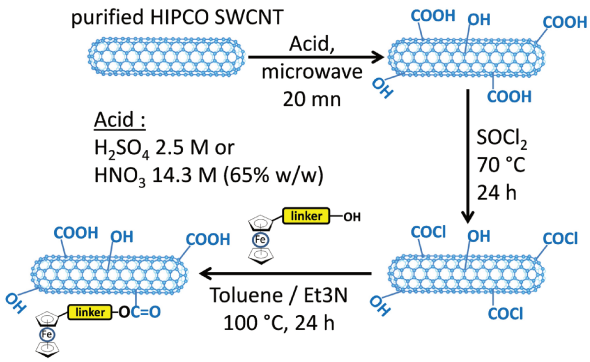

Figure 3: Three-step covalent functionalization of HIPCO SWCNTs using different acidic conditions for step 1.

defects on their sidewalls. In the literature, this is often done by heating under reflux the CNT sample in a strong acidic medium for several hours or days. Doing so, many oxidized functions are introduced but the nanotubes are also cut and shortened. Since we intended to retain the essential electronic properties of the CNTs in the aim of making an electrochemical biosensor, we performed the oxidation step using microwave irradiation. Microwaves indeed promote oxidation through a fast thermal activation, which enables performing the oxidation step in only a few minutes and allows one to roughly control the number of defects introduced by tuning the irradiation time. A few milligrams of the corresponding oxidized SWCNTs were analyzed in each case before proceeding to step 2. At this stage, the samples were protected under argon gas to avoid any moisture contamination and directly analyzed by HRTEM, XPS and TGA-MS. Once opened to air, the samples were analyzed by Raman spectroscopy.

Functionalization by ferrocene derivatives

Ferrocene derivatives were grafted onto CNT sidewalls by reacting the alcohol group of the ferrocene linkers to the COCl groups present after step 2 on the CNT sidewalls. We investigated several linkers, in order to see if the chemical nature of the linker and/or its length might influence the electrochemical response of our final device. An alkyl chain and polyethylene glycol linkers with various chain lengths were used in this study (Figure 4). The corresponding ferrocene derivatives, FcAlkyl and FcETGn, were prepared according to known procedures [29,30].

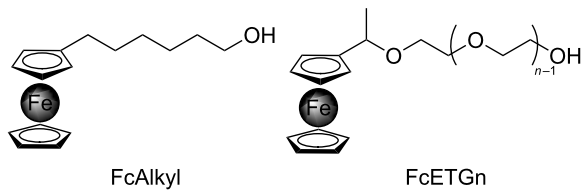

Figure 4: Ferrocene derivatives (FcAlkyl and $FcETG_n$) with different linkers.

Nomenclature of the samples will indicate the oxidation process (HNO_3 or H_2SO_4) and for grafted samples, the nature of the grafted group (FcAlkyl or $FcETG_n$). For instance, HIPCO-HNO_3-$FcETG_8$ means that the SWCNTs were oxidized in HNO_3 65% and grafted with the $FcETG_8$ ferrocene derivative.

After step 3 of the functionalization process, we used a set of complementary techniques to determine the success of the covalent functionalization of the CNT samples. XPS analyses were realized on CNT powders to see if the ferrocene groups were indeed present at the surface of the bundles, using the Fe 2p signal as a marker of the grafted groups (Figure S1A, Supporting Information File 1). Table 1 reports the atomic percentages found on raw, oxidized and functionalized HIPCO samples, as well as the spectral components of the C 1s signal obtained by spectral decomposition using four components for the oxidized/functionalized samples. The component at 284 eV is attributed to sp^2-hybridized carbon atoms, while that at 284.6–284.8 eV is assigned to sp^3-hybridized carbon atoms. Oxidized carbon atoms gave two signals at 286 eV (probably C–OH or ether groups) and 288 eV (lactone or COOH groups). Since these two peaks correspond to oxygenated functions, their areas have been added and Table 1 reports the sum of these two components. Two examples of spectral decomposition are reported in Figure 5, one for the raw HIPCO sample (Figure 5A) and one for HIPCO-HNO_3-$FcETG_8$ (Figure 5B).

After oxidizing SWCNTs under acidic conditions under microwave irradiation, the atomic ratio of oxygen to carbon (%O/%C) is increased for both HNO_3 and H_2SO_4 conditions. Furthermore, the number of oxygenated functions, quantified by the percentage of the C–O/C=O components contributing to the C 1s signal, has also doubled. Oxidation step 1 has therefore increased the number of oxidized defects on CNT sidewalls and

Table 1: Atomic percentages and C 1s contributions deduced from XPS analyses of raw, oxidized and functionalized samples.

sample	atomic concentrations						
	atom % Fe	atom % O	atom % C	atom % O/ atom % C	atom % C sp^2 (284 eV)	atom % C sp^3 (284.6–284.8 eV)	atom % C (C–O/C=O) (286/288 eV)
HIPCO Raw	0	6.6	86.3	0.076	75	17.3	7.7
HIPCO-HNO_3	0	13.7	84	0.163	68.6	16.7	14.7
HIPCO-HNO_3-FcAlkyl	1.3	13.9	84.4	0.165	56.2	23	20.8
HIPCO-HNO_3-$FcETG_2$	1.9	14.4	62	0.232	72.3	14.1	13.6
HIPCO-HNO_3-$FcETG_8$	0.8	19.1	59.6	0.32	29.9	25	45.1
HIPCO-H_2SO_4	0	10.4	75	0.139	70.4	14.8	14.8
HIPCO-H_2SO_4-$FcETG_2$	1.8	15.4	63.1	0.244	69.8	10.1	20.1
HIPCO-H_2SO_4-$FcETG_5$	1.2	16.5	69.5	0.237	60.1	18.4	21.5

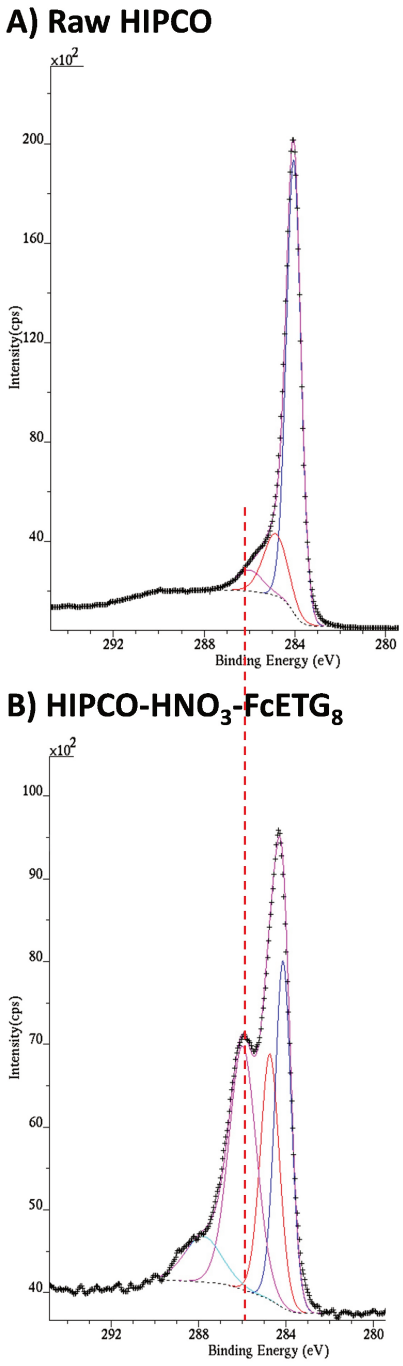

Figure 5: Detailed C 1s spectra of A) raw HIPCO and B) HIPCO-HNO_3-$FcETG_8$. The binding energies of the Fe 2p components were always at 720.4 eV and 706.5 eV for the $2p_{1/2}$ and $2p_{3/2}$ components, respectively, which are typical values for the Fe(II) oxidation state in ferrocene compounds [31].

extremities, at least at the surface of the bundles, which was probed by XPS. It should be pointed out that our raw HIPCO sample has already been submitted to unknown chemical treatments by Nanointegris to reach the claimed degree of purity indicated on their website. It is therefore not surprising to already find oxygenated functions in the raw sample, these defects having certainly been introduced by the chemical treatment.

We also underline the fact that no iron or other metals are visible by XPS spectroscopy, while TEM micrographs have shown some residual catalyst particles embedded in carbonaceous remains or inside CNT bundles, as shown in Figure 2a. These carbon shells certainly hide the metallic species from the XPS analysis, which is essentially a surface-specific method. The clear Fe 2p signal obtained for functionalized samples and reported for instance in Figure S1B (Supporting Information File 1) for the HIPCO-$FcETG_2$ sample arises exclusively from the grafted groups. The binding energies of the Fe 2p components were always at 720.4 eV and 706.5 eV for $2p_{1/2}$ and $2p_{3/2}$ components, respectively, which are typical values for the Fe(II) oxidation state in ferrocene compounds [31].

Table 1 indicates that around 1–2 atom % Fe is detected in the samples functionalized with ferrocene derivatives (entries 3, 4, 5, 7 and 8), which is a low level of functionalization. It also reports an increase of the oxygen content after grafting $FcETG_n$ groups and this is particularly true for the HIPCO-HNO_3-$FcETG_8$ sample (entry 5). The change in the detailed C 1s spectrum if compared to that of the starting material is quite obvious, as shown in Figure 5B. The PEG linker is quite long in this sample, and the surface-specific sensitivity of the XPS technique means that the detected signal is dominated by the contribution of the linker. Another interesting observation is that for the HIPCO-HNO_3-FcAlkyl sample, there is a significant increase of the sp^3 contribution in the detailed C 1s spectrum, also coming from the linker (entry 3). Therefore, the use of very clean HIPCO samples enables detecting by XPS both the tagging Fe atom of ferrocene derivatives and the contributions of the linkers.

XPS analyses prove the presence of ferrocene derivatives at the surface of CNT bundles, but they cannot confirm the covalent nature of the functionalization process. To do this, we have performed TGA-MS analyses of our samples under an inert gas (He). Figure 6A gives an example of the TGA curves obtained for raw, HIPCO-HNO_3 and HIPCO-HNO_3-$FcETG_2$ samples.

The mass spectrometer coupled to the TGA system allowed for the examination of the nature of the departing groups. Compared to the raw sample (curve a), the TGA curve after oxidation clearly shows an increase of weight loss above 300 °C for the oxidized sample due to additional oxygenated functions on the nanotube surface (curve b). A greater increase of weight loss was observed for the HIPCO-HNO_3-$FcETG_2$ sample indicating that FcETG2 functions were covalently grafted (curve c). This is consistent with the greater number of oxidized defects

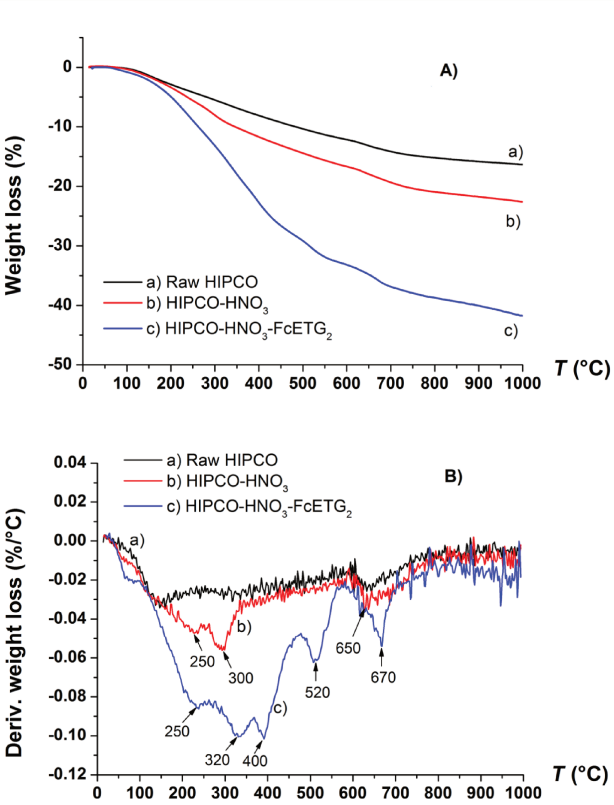

Figure 6: A) TGA curves obtained under He for three samples. B) Derivative curve of the weight loss for the same three samples. Arrows indicate the main peaks in temperature associated with departure of some chemical groups attached to SWCNT sidewalls.

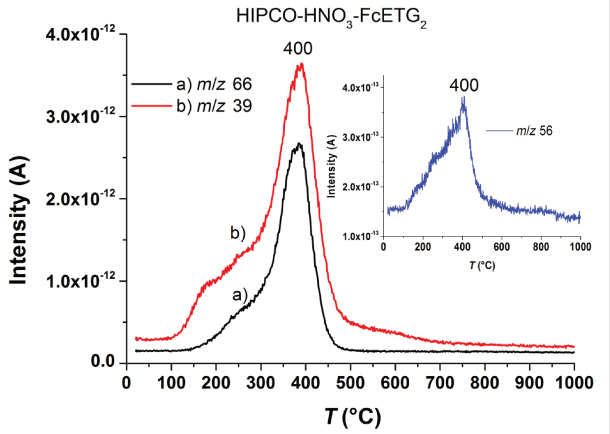

Figure 7: Mass spectrometry channels used to show the departure peaks of the cyclopentadienyl group and its main fragments at m/z = 66 and m/z = 39. Inset: the departure peak of the iron atoms of the ferrocene groups.

Table 2: Percentages of weight loss and temperature of the main desorption peaks measured in TGA-MS for raw, oxidized and functionalized HIPCO samples.

sample	weight loss (in %) at 1000 °C	temperatures of main departures peaks (°C)
HIPCO raw	16	150, 650
HIPCO-HNO_3	22	250, 300, 650
HIPCO-HNO_3-$FcETG_2$	42	250–400, 520, 670

detected by XPS as well as the presence of ferrocene derivatives in the sample. Moreover, cyclopentadienyl groups, which are expected from the decomposition of ferrocenes, can be followed by detecting the main fragments expected for cyclopentadienyl, i.e., at *m*/*z* 66 and at *m*/*z* 39. Figure 7 reports the current intensity corresponding to these fragments, which were evacuated between 150 and 450 °C; the majority being detected around 370–400 °C. The detection of iron ions at *m*/*z* 56 was also found, as shown in the inset of Figure 7.

Figure 7 also indicates that the ferrocene groups are detached mainly above 300 °C, a temperature that is too high to correspond to physisorbed molecules. TGA-MS experiments therefore confirm the covalent grafting of the ferrocene derivatives on the CNTs. Table 2 summarizes the global weight losses and the main departure peaks corresponding to the data plotted in Figure 6.

Figure S2 (Supporting Information File 1) reports the departure of CO and CO_2 fragments at *m*/*z* 28 and *m*/*z* 44, respectively, for the HIPCO-HNO_3 and HIPCO-HNO_3-$FcETG_2$ samples. For HIPCO-HNO_3, CO_2 fragments are mainly evacuated between 150 and 500 °C, while a significant loss of CO is visible around 650 °C. These peaks correspond to the evacuation of oxidized functions introduced by the microwave-assisted oxidation process. For the HIPCO-HNO_3-$FcETG_2$ sample, additional peaks around 340 and 675 °C are visible for both CO and CO_2 fragments. They are due to the fragmentation of the polyethylene glycol linkers, confirming that ferrocene derivatives are covalently attached to CNT sidewalls.

XPS and TGA-MS experiments thus show that oxidized defects can be detected for samples having undergone the oxidation and functionalization steps. Raman spectroscopy is a method of choice to observe the creation of sp^3 defects in carbon nanostructures, due to the presence in the Raman spectrum of a dispersive defect-induced band, called the D band, around 1350 cm^{-1}. Figure 8 reports the Raman spectra of raw, oxidized and functionalized samples using a laser wavelength of 514 nm. In Figure S3 (Supporting Information File 1), some Raman spectra obtained for the samples using a laser at 458 nm are also reported. The data for each sample correspond to the average spectrum obtained from 20 spectra, and they are therefore statistically significant.

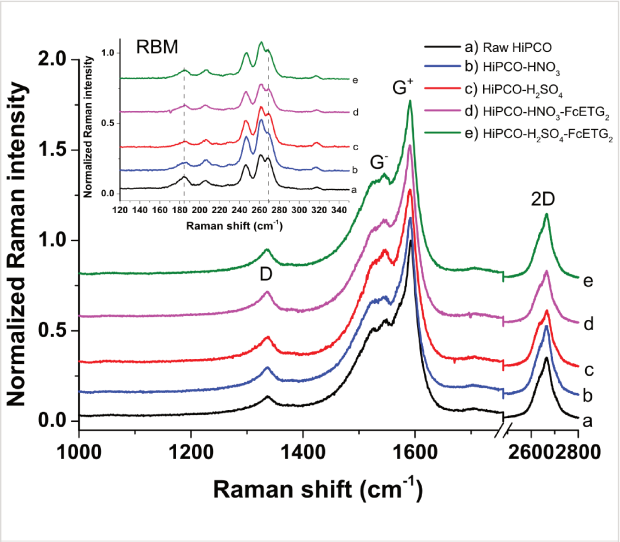

Figure 8: Raman data of raw and f-SWCNTs taken with a laser at 514 nm.

Surprisingly, the intensity of the D band at 1350 cm^{-1}, associated with the presence of structural defects, remains essentially constant if compared to the G^+ and G^- bands for all samples. The radial breathing modes (RBM) shown in the inset are also barely affected by the chemistry steps. The structural integrity of the CNTs in resonance with the laser energies used in this study (514 and 458 nm) remains quite good. That is, the number of sp^3 defects that have been created by the chemical processes is low enough to keep the intensity of the D band almost constant. However, XPS and TGA-MS experiments have shown an increased number of oxidized functions, which generally involve the creation of sp^3-hybridized carbon atoms in the CNT sidewalls. To solve this apparent contradiction, we can make the hypothesis that microwave irradiation in acidic media mainly converts already-existing sp^3 defects in the raw CNTs into oxidized functions such as alcohol and carboxylic acid functions, but does not introduce many new defects as does the purely thermal process (heating under reflux). Moreover, our functionalization process uses bundles of CNTs, and probably most of the inner tubes within the bundles are not affected by the chemical processes. Raman spectroscopy also probes these inner tubes, which may explain the lack of significant change of the D-band intensity in the spectra. This explanation is indeed coherent with the low value of the Fe atomic percentage detected in XPS (Table 1). We have put a small number of ferrocene functions on the surface of our HIPCO bundles, and the integrity of the carbon structure is essentially preserved. This is a very interesting observation since it validates our global approach of using microwave irradiation rather than more conventional thermal routes. Retaining the structural integrity of CNTs (and therefore their electronic properties) is essential in our case to obtain a good electrochemical signal.

HRSTEM and EELS analyses confirm the presence of ferrocene derivatives on the surface of the bundles. Figure 9 shows a HAADF micrograph of the HIPCO-HNO_3-$FcETG_2$ sample.

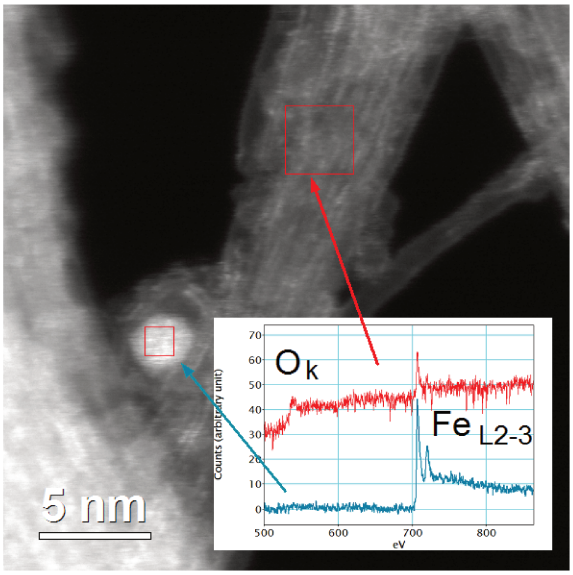

Figure 9: An example of a STEM HAADF image of the HIPCO-HNO_3-$FcETG_2$ sample. Inset: EELS spectra of the catalyst particle (blue arrow) and of the bundle recorded in the area of the red square.

In HAADF the intensity of the signal is linked to the average "*Z*" value of the atoms. On the image presented in Figure 9, the zones that contain atoms heavier than carbon appear as white areas and the thickest area also appears brighter. One residual catalyst particle can be easily identified in Figure 9 as a bright spot with a diameter close to 2.5–3.0 nm. On the bundle some small white dots can also be seen. EELS spectra were recorded of the catalytic particle and in the middle of the bundle, in the area where white dots are visible (Figure 9 inset). On the particle, only a Fe_{L2-3} signal could be detected, typical of iron in its metallic state. From the bundle, both O_K and Fe_{L2-3} signals are clearly visible. These signals are compatible with the presence of ferrocene groups grafted through ETG linkers.

In the HAADF images taken at a high magnification, bright spots at the end of short grey lines can be seen on the sidewalls of isolated tubes or on external tubes of the bundles. A second less bright spot is systematically seen at the other end of these objects. The length of this kind of object was systematically measured between 1.2 and 1.4 nm, which agrees with the presence of a $FcETG_2$ grafted group. Figure 10 illustrates this fact by presenting typical micrographs of high-resolution STEM images recorded on the HIPCO-HNO_3-$FcETG_2$ sample. In the HAADF micrograph (Figure 10a) the arrows point to the two sides of the typical object. The structure of the CNT that is

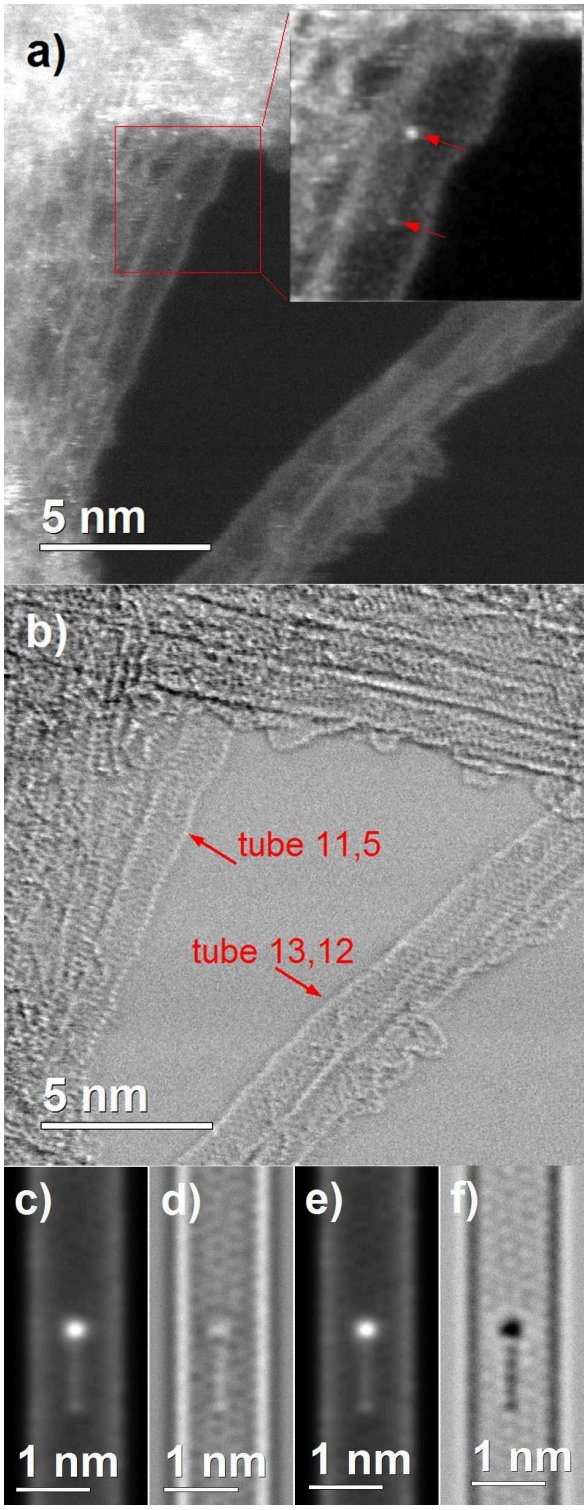

Figure 10: HIPCO-HNO_3-$FcETG_2$ sample analyzed by STEM: a) HAADF image. The inset focuses on the FcETG molecule, the top arrow points to the ferrocene and the bottom arrow to the ester link. b) BF image simultaneously recorded for chiral index assignment. c–f) Simulated images of HAADF (c and e) and BF (d and f) of a 11,6 SWCNT grafted with a $FcETG_2$ molecule for over-focus of 1.7 nm (c and d) and under-focus of −6.3 nm.

present at the outer edge of a bundle was determined from the fast Fourier transform (FFT) of the BF image presented in Figure 10b. The chiral indices (11,5) can be unambiguously assigned to this tube.

To strengthen the interpretation of the images obtained on the small object lying at the surface of the tube, image simulations were done for a SWCNT grafted with a $FcETG_2$ group. A structural model of a SWCNT with (11,6) chiral indices was used for the simulation (structure and diameter close to that of (11,5)). The $FcETG_2$ molecule grafted at the surface of the SWCNT model was oriented to simulate a ferrocene group in a π-stacking interaction (see below the molecular dynamics simulation) since the analysis is done in ultra-high vacuum. The distance between the tube and the cyclopentadiene was fixed at 0.35 nm. Simulations were carried out in steps of 1 nm for focuses from −12 nm to 12 nm for the HAADF and BF detectors. For HAADF simulations the contrast obtained matches well with that experimentally detected (Figure 10c and Figure 10d, compared to the inset of Figure 10a). The bright dot corresponds to the ferrocene group, the gray line to the polyethylene glycol linker, and the less bright dot at the other extremity to the ester link between the CNT and the linker. The contrast obtained is not sensitive to the focus (in the focus range used). For BF images, the contrast obtained depends strongly on the focus and contrast inversion can occur as seen in Figure 10d and Figure 10f.

The image simulation can be used to estimate the focus of the images by comparing the recorded image to simulations for different focuses. For example the focus of the BF image presented in Figure 10b was estimated slightly over-focused by 1 or 2 nm. Numerous STEM images were analyzed for different samples, and the functionalization of the sidewalls was observed for both metallic and semiconducting tubes oxidized with either HNO_3 or H_2SO_4 acidic conditions. Therefore, these results strongly support the hypothesis that outer tubes of the bundles were covalently grafted with FcETGn groups.

As a conclusion to this analytical part, we have succeeded in covalently grafting ferrocene derivatives on HIPCO SWCNTs, to a sufficiently small extent that we have preserved the structural integrity of the nanotubes. The complete set of data is consistent with the oxidation of pre-existing defects under microwave irradiation in acidic media. Isolated CNTs or those constituting the outer tubes of the bundles are functionalized covalently by ferrocene derivatives on their sidewalls. Both acidic conditions give similar results. The diluted H_2SO_4 condition is therefore quite interesting since it avoids the use of a concentrated acid solution. Using H_2SO_4 with microwave irradiation therefore represents a fast, green, safe and energy effi-

cient process if one is interested in development on a semi-industrial scale.

These functionalized samples were then used to modify a GCE in the bioelectrochemical device presented in Figure 1, to test their capability in electrochemical devices.

Electrochemical measurements

The electrochemical response of oxidized SWCNTs, i.e., before their functionalization with Fc, was tested first. The electrode was prepared by dispersing the carbon material in a 0.5 wt % chitosan solution. A layer of this chitosan composite was deposited on the GCE and a second layer of chitosan containing diaphorase was additionally deposited on the top. The GCE was used as the working electrode in a conventional three-electrode setup (see Figure S4 in Supporting Information File 1). Diaphorase can catalyze the oxidation of NADH but only in the presence of a mediator (electron shuttle) transferring electrons from the flavin mononucleotide cofactor to the electrode surface. Figure 11A reports the electrochemical response of the oxidized SWCNTs in the absence and in the presence of 3 mM of NADH in the solution. Both curves are very similar, characterized by a large capacitive current (due to the high surface area of the electrode modified with SWCNTs). The lack of any current increase after addition of NADH in solution indicates that these oxidized clean HIPCO SWCNTs do not exhibit any direct electrocatalytic properties toward NADH oxidation.

While previous reports attributed the catalytic properties of CNTs mainly to their impurities [21-26], the small amount of residual impurities in our HIPCO samples are not electroactive. Oxidized CNTs were used as a blank sample (Figure 11A) in order to verify that the oxidation process has not activated residual impurities nor generated electroactive groups such as quinones [6] at the CNT surface. This was not the case in our experiments. Moreover, this experiment confirms that no direct electron transfer can be achieved between diaphorase and the electrode, even in the presence of SWCNTs.

The functionalization of SWCNTs with ferrocene groups allowed for observing by cyclic voltammetry a quasi-reversible electrochemical signal at +0.215 V vs Ag/AgCl as is illustrated in curve a) of Figure 11B for sample HIPCO-H_2SO_4-FcETG$_2$. All samples functionalized with Fc showed this pair of redox peaks. Some variation in capacitive current was observed between the different samples that must be related to the ease of f-SWCNT dispersion and the resulting different 3D textures after their immobilization at the GCE surface. For example, it was found that the H_2SO_4 oxidation process produced a more porous SWCNT assembly, and long polyethylene glycol linker ($n > 4$) favored dispersion of the nanotubes in water-based solutions. In spite of these differences, all oxidation processes and FcETG$_n$ linkers gave the kind of curves reported in Figure 11B.

Cyclic voltammetry was then performed with f-SWCNTs in the presence of NADH (curve b) in Figure 11B. The electrochemical response was dramatically modified, with the disappearance of the cathodic peak and the large increase in intensity of the anodic peak. This response is due to the electrocatalytic oxidation of NADH by diaphorase, during which the flavin mononucleotide cofactor is oxidized by ferrocenium produced at the electrode surface. No clear trend was observed that could have related the mode of oxidation (HNO_3 or H_2SO_4) or the linker size for the ETG$_n$ spacer with the electrocatalytic response. The

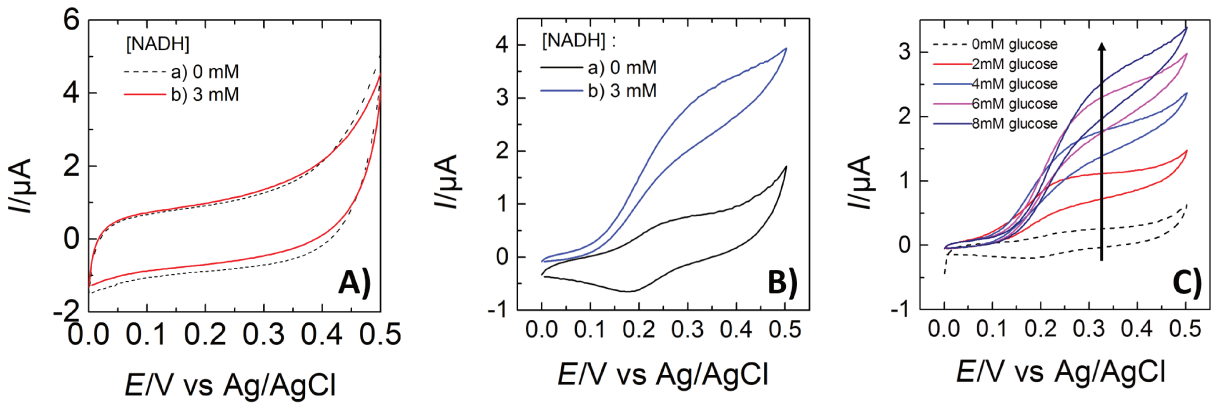

Figure 11: Cyclic voltammograms obtained of GCEs modified with A) HIPCO-H_2SO_4 immobilized with diaphorase; B) HIPCO-H_2SO_4-FcETG$_2$ immobilized with diaphorase; C) HIPCO-H_2SO_4-FcETG$_2$ immobilized with diaphorase, NADH and glucose dehydrogenase (GDH) molecules. In A and B, NADH was added to the analyzed solution; in C, glucose was added to the solution. The modified GCE electrodes were used as working electrodes in a conventional three-electrode setup. The scan rate was 5 mV·s^{-1}. Arrows in B indicate the anodic and cathodic wave of the grafted ferrocene groups.

electrochemical response was most probably controlled by the availability of Fc on the surface, which mainly depended on the dispersion of the tubes in the chitosan layer. Previous analyses of the electrocatalytic properties of f-SWCNTs performed with less pure SWCNTs have shown that the size of the linker does not influence the NADH electrocatalytic current [11]. Contrary to these conclusions with polyethylene glycol linkers, functionalization with alkyl-ferrocene only showed a very poor electrocatalytic response (Figure S5 in Supporting Information File 1). The alkyl spacer certainly favored the folding of the chain in an aqueous solution and prevented the ferrocene group from efficiently exchanging electrons with diaphorase molecules.

In order to illustrate an application of these f-SWCNTs in biosensing, the electrode was further modified with HIPCO-H_2SO_4-FcEtG$_2$, diaphorase, NADH and glucose dehydrogenase (GDH). Upon addition of glucose into the solution, the molecules were oxidized by GDH in gluconolactone and NADH cofactor was simultaneously produced. NADH was then oxidized by diaphorase, mediated by ferrocene moieties. Figure 11C shows the electrochemical response in the absence of glucose (dashed curve, 0 mM of glucose). The reversible electrochemical signal of ferrocene can be distinguished as in curve a) of Figure 11B. After addition of glucose, the electrochemical current increases dramatically, showing again the typical shape of an electrocatalytic response.

Electrochemical characterization by variation of the potential scan rate shows moreover that the current response varied linearly with the scan rate (Figure S6 in Supporting Information File 1). This means that the electrochemical process is confined at the surface, not determined by diffusion of ferrocene into the solution. So the mobility of ferrocene is just sufficient for efficient mediation of the electron flow from the flavin mononuclotide cofactor to the electrode surface.

The fact that the alkyl linker is completely inefficient for the mediated electron transfer process, while the polyethylene glycol spacers are efficient regardless of their length (in the range examined in this work) was puzzling, so we decided to investigate the role of the linker by molecular dynamics computation. The samples were used in an aqueous medium. The alkyl linker being hydrophobic while PEG linkers are hydrophilic strongly suggests also modelling the interaction between the functionalized nanotubes and the water molecules. The corresponding results are reported in the next paragraph.

Determining the role of the PEG linker via molecular dynamics calculations

The influence of the linker length on the resultant enzymatic reactivity of the ferrocene unit was explored using the molecular dynamics package LAMMPS [32,33] to simulate both FcETG$_2$ and FcETG$_8$ when covalently attached to the surface of a (10,0) carbon nanotube (radius typical for HIPCO samples). A tube length of 4.17 nm was chosen (440 carbon atoms) placed in a cubic unit cell of the same length creating an infinite tube in one direction and enough "vacuum" for the PEG chain to relax without constraint. The calculations were performed using a ReaxFF potential [34]. The runs were carried out for 6 ns with a time step of 0.1 fs. Time integration (10 fs) was used on Nosé–Hoover [35,36] style non-Hamiltonian equations of motion, designed to generate positions and velocities sampled from the canonical (npt) method (constant pressure and temperature). All calculations were carried out at room temperature and under atmospheric pressure. Calculations were done both with and without the presence of water (1967 water molecules distributed uniformly initially within the box, giving a net water density of 1.01 g·cm^{-3} without HIPCO-FcETG$_8$ and around 0.800 g·cm^{-3} with HIPCO-FcETG$_8$). Any water molecule within a distance of less than 3.0 Å from the tube was removed (Figure 12).

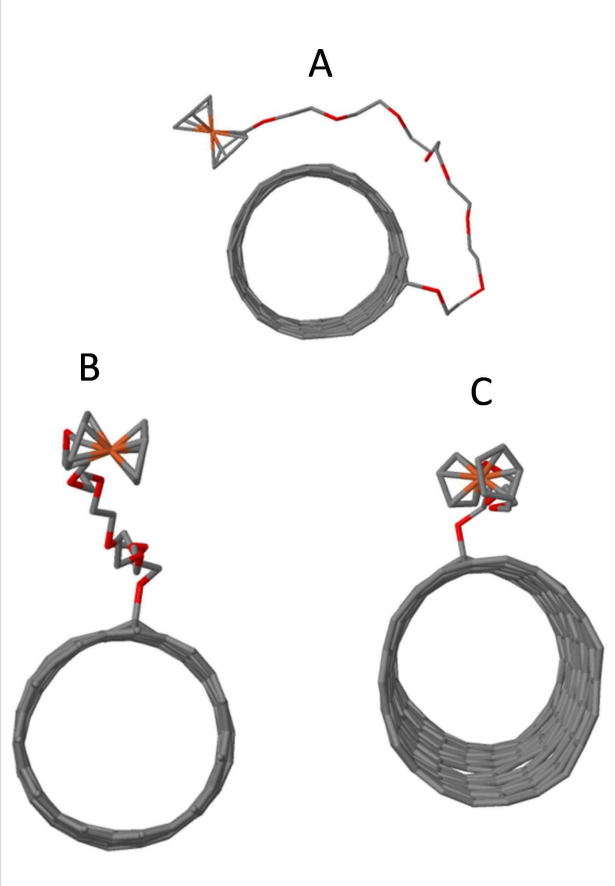

Figure 12: Molecular-dynamics simulated structures after 6 ns: A) HIPCO-FcETG$_8$ without the presence of water, B) HIPCO-FcETG$_8$ and C) HIPCO-FcETG$_2$ in the presence of water (not shown for clarity).

In the absence of water, with both HIPCO-FcETG$_8$ (Figure 12A) and HIPCO-FcETG$_2$ after only 2 ns the ETG chain flexed to go around the tube following a zig-zag path on the CNT surface, allowing the ferrocene unit to π-stack on the nanotube where it remained for the rest of the simulation. We used this very useful information in our HRSTEM simulation in vacuum by placing the ferrocene unit in a π-stacking with the tube, in the results shown in Figure 10c–f. In such a configuration, a ferrocene electron transfer may occur between the ferrocene unit and the CNT surface instead of interacting freely with the diaphorase biomolecule. As a result, this would quench the enzymatic activity of the modified GCE. To explain why and how our device can work, we then simulated the effect of water.

Once water was added, van der Waals and dipolar interactions between the water molecules and the ETG chain effectively blocked chain flexion and maintained the ferrocene unit at a distance of over 6.41 Å from the tube surface throughout the simulation (Figure 12B). Even for HIPCO-FcETG$_2$, while the water–ETG interactions are considerably reduced, which allowed for some chain flexion and more interaction with the surface (Figure 12C), the ferrocene unit is not π-stacked on the CNT surface and therefore the electron-transfer step with diaphorase is still possible. The simulations confirm the essential role of the PEG linker in the efficiency of the bioelectrochemical device in water, due to the favorable interaction between the ETG units and water molecules, which prevents π-stacking of the ferrocene unit on the surface of the CNTs.

Conclusion

This work has clearly established the interest of using covalently functionalized SWCNTs for making electrochemical devices. Using a very clean sample, a complementary set of analytical techniques, including advanced microscopy analyses, has firmly confirmed the covalent nature of the functionalization process. We have shown that residual impurities in the case of mediated electron transfer play no role in the oxidation of NADH, contrary to what has been presented in the literature for other systems. We also underline the interest of using molecular dynamics simulations to evaluate the important role of the linker, which certainly depends on the solvent used for doing electrochemistry. The results of the present study therefore lead us to claim that, while many people are now working with graphene, CNTs are indeed useful for well-designed electrocatalytic devices, thus being a viable alternative to graphene-based sensors provided that the samples used are sufficiently clean so that the function is not controlled by the presence of residual impurities that may lead to unreproducible measurements.

Experimental

General: COCl-SWCNTs were prepared according to [27]. FcETG$_n$ derivatives were synthesized according to [29].

Reaction of COCl-SWCNTs with FcETGn [9]**:** COCl-SWCNTs (10 mg) were suspended in dry toluene (50 mL) under argon. Then, FcETG$_n$ (20–30 mg) and triethylamine (0.1 mL) were added. The mixture was heated to 100 °C and stirred for 24 h under argon. After cooling, the SWCNTs were washed under sonication three times with MeOH (10 mL) and three times with THF (10 mL) in order to remove unreacted FcETGn. After filtration, the HIPCO-Ox-FcETG$_n$ (22–33 mg) were dried under vacuum and stored under argon at room temperature.

Electrode preparation [11]**:** GCEs (3 mm in diameter) were polished with alumina slurry (1 μm and 0.05 μm particles, sequentially) and then washed with water. A 0.5 wt % chitosan solution was prepared by dissolving chitosan in 1% acetic acid. 2 mg of ferrocene-functionalized CNTs (HIPCO-Fc) and 1 mL of the above chitosan solution were mixed together under stirring overnight. 5 μL of chitosan/HIPCO-Fc suspension were deposited onto the GCE surface to obtain a stable thin film after drying. Chitosan films containing either diaphorase (DI) or glucose dehydrogenase (GDH) and DI were prepared by mixing 10 μL of 0.5 wt % chitosan solution with 5 μL of DI (5 mg·mL^{-1}) or 15 μL of 0.5 wt % chitosan with 10 μL of GDH (1000 U·mL^{-1}) and 5 μL of DI (5 mg·mL^{-1}). Afterwards, 5 μL of this mixture were deposited onto the chitosan/HIPCO-Fc modified GCE and allowed to dry at ambient temperature.

Analytical techniques: High-resolution transmission electron microscopy (HRTEM) and high-resolution scanning transmission electron microscopy (HRSTEM) were performed using a probe aberration-corrected JEOL ARM200 microscope equipped with a cold field emission gun, a JEOL JED2300T energy dispersive X-ray spectrometer (EDS) and a Gatan GIF Quantum energy filter for electron energy loss spectroscopy (EELS). The microscope was operated at 80 kV in order to minimize knock-on damage to the samples. HRSTEM images were recorded using an electron beam with a probe-size of about 0.12 nm. High-angle annular dark-field (HAADF) and bright-field (BF) images were simultaneously recorded with a semi-angle of collection of respectively 45–180 mrad and 11 mrad for an image resolution of 1024 × 1024 pixels with a dwell-time of 60 μs. STEM-EDS and STEM-EELS experiments were performed with an electron probe of about 0.17 nm and a convergence semi-angle of 24 mrad. The energy resolution was about 0.45 eV. The collection angle of the EELS spectrometer was 30 mrad. The spectroscopic information was obtained using the spectrum-imaging acquisition mode. Samples

were dispersed in absolute ethanol then deposited on a holey carbon film supported by a 300 mesh copper grid. The STEM image simulations were done using the software Nanotube Modeler (JCrystalSoft) and Vesta 3 for the atomic model generation [37] and QSTEM [38] for the STEM image simulations. SWCNT chiral indices were assigned by analysis of the Fourier-transform of the HRSTEM images and by comparing the images to simulations [39,40].

Raman spectra were recorded with a triple subtractive monochromator T64000 spectrometer (Horiba Jobin Yvon) equipped with a confocal microscope (Olympus BH2-UMA; laser wavelengths λ = 514 nm and λ = 458 nm). An 80× objective with a numerical aperture of 0.90 was used to collect the spectra in the backscattering mode. The spectral resolution was 1 cm^{-1}. The laser spot had a diameter of 1 µm and the irradiance was kept below 1 $kW{\cdot}cm^{-2}$ to avoid laser heating of the samples. At least 20 spectra were collected and averaged for each sample to obtain a statistically representative spectrum.

The XPS analysis was performed with a spectrometer equipped with a monochromatized Al Kα X-ray source (hν = 1486.6 eV), run at 150 W power (KRATOS Axis Ultra, Kratos Analytical, UK). Spectra were collected at a normal take-off angle (90°). The analytical area was 700 × 300 μm^2. XPS survey spectra were recorded with a 1.0 eV step and 160 eV analyzer pass energy. Narrow scans were recorded with a 0.05 eV step and 20 eV pass energy. XPS spectra were analyzed with the Vision software from Kratos (Vision 2.2.0) after subtraction of the background (Shirley baseline). Gaussian–Lorentzian (70/30) functions were used for peak decomposition. Charge correction was carried out using the C 1s core line and setting adventitious carbon signal (C sp^3 signal) to 284.6 eV.

For thermogravimetric analyses coupled to mass spectrometry (TGA-MS) experiments, 5–6 mg of the sample powder were placed in an alumina crucible. The TGA-MS instrument included a Setaram Setsys evolution 1750 Thermal Gravimetric Analyser coupled with a Pfeiffer GSD 301C Vacuum OmniStar mass spectrometer. The temperature was ramped at 3 °C/min from room temperature to 1000 °C under helium (flux 20 $mL{\cdot}min^{-1}$) in the TGA chamber. We consider that most of the species undergo one ionization only meaning that z = 1 for the detected m/z values.

All electrochemical experiments were carried out using a PGSTAT12 Metrohm-Autolab potentiostat monitored by the GPES Software. Measurements were performed in a three-electrode cell, including the film-modified GCE as working electrode, an Ag/AgCl reference electrode (3 M KCl internal electrolyte), and a platinum wire auxiliary electrode.

Supporting Information

Includes XPS Fe 2p spectrum for HiPCO-H_2SO_4-$FcETG_2$, supplemental TGA-MS and Raman data, a cartoon of the complete bioelectrochemical device, and additional electrochemical data.

Supporting Information File 1

Additional experimental data.
[https://www.beilstein-journals.org/bjnano/content/supplementary/2190-4286-9-257-S1.pdf]

Acknowledgements

This work has been supported by the French National Research Agency (ANR), project ANR-10-BLAN-0819-01-SPRINT. Aurélien Renard is acknowledged for XPS data collection. We thank Maxime Noël for help in acquiring the Raman spectra.

ORCID® iDs

Veronika Urbanova - https://orcid.org/0000-0003-4499-2235
Mathieu Etienne - https://orcid.org/0000-0003-3166-4072
Brigitte Vigolo - https://orcid.org/0000-0002-1463-0121
Jean-Joseph Adjizian - https://orcid.org/0000-0002-7899-4565
Chris P. Ewels - https://orcid.org/0000-0001-5530-9601
Victor Mamane - https://orcid.org/0000-0001-8996-7880

References

1. Rivas, G.; Rubianes, M.; Rodriguez, M.; Ferreyra, N.; Luque, G.; Pedano, M.; Miscoria, S.; Parrado, C. *Talanta* **2007,** *74,* 291–307. doi:10.1016/j.talanta.2007.10.013
2. McCreery, R. L. *Chem. Rev.* **2008,** *108,* 2646–2687. doi:10.1021/cr068076m
3. Dumitrescu, I.; Unwin, P. R.; Macpherson, J. V. *Chem. Commun.* **2009,** *7345,* 6886–6901. doi:10.1039/b909734a
4. Vashist, S. K.; Zheng, D.; Al-Rubeaan, K.; Luong, J. H. T.; Sheu, F.-S. *Biotechnol. Adv.* **2011,** *29,* 169–188. doi:10.1016/j.biotechadv.2010.10.002
5. Walcarius, A.; Minteer, S. D.; Wang, J.; Lin, Y.; Merkoçi, A. *J. Mater. Chem. B* **2013,** *1,* 4878–4908. doi:10.1039/c3tb20881h
6. Wooten, M.; Gorski, W. *Anal. Chem.* **2010,** *82,* 1299–1304. doi:10.1021/ac902301b
7. Saleh, F. S.; Rahman, M. R.; Kitamura, F.; Okajima, T.; Mao, L.; Ohsaka, T. *Electroanalysis* **2011,** *23,* 409–416. doi:10.1002/elan.201000268
8. Yuan, J.; Chen, J.; Wu, X.; Fang, K.; Niu, L. *J. Electroanal. Chem.* **2011,** *656,* 120–124. doi:10.1016/j.jelechem.2010.12.018
9. Allali, N.; Urbanova, V.; Mamane, V.; Waldbock, J.; Etienne, M.; Mallet, M.; Devaux, X.; Vigolo, B.; Fort, Y.; Walcarius, A.; Noël, M.; Soldatov, A. V.; McRae, E.; Dossot, M. *Phys. Status Solidi B* **2012,** *249,* 2349–2352. doi:10.1002/pssb.201200098
10. Wang, Z.; Etienne, M.; Pöller, S.; Schuhmann, W.; Kohring, G.-W.; Mamane, V.; Walcarius, A. *Electroanalysis* **2012,** *24,* 376–385. doi:10.1002/elan.201100574

11. Urbanová, V.; Allali, N.; Ghach, W.; Mamane, V.; Etienne, M.; Dossot, M.; Walcarius, A. *J. Electroanal. Chem.* **2013,** *707,* 129–133. doi:10.1016/j.jelechem.2013.08.029
12. Allali, N.; Urbanova, V.; Etienne, M.; Mallet, M.; Devaux, X.; Vigolo, B.; Fort, Y.; Walcarius, A.; Noël, M.; McRae, E.; Soldatov, A. V.; Dossot, M.; Mamane, V. *MRS Online Proc. Libr.* **2013,** *1531,* mrsf12-1531-yy06-05-w06-05. doi:10.1557/opl.2013.84
13. Reuillard, B.; Le Goff, A.; Cosnier, S. *Chem. Commun.* **2014,** *50,* 11731–11734. doi:10.1039/c4cc04758c
14. Rabti, A.; Raouafi, N.; Merkoçi, A. *Carbon* **2016,** *108,* 481–514. doi:10.1016/j.carbon.2016.07.043
15. Karousis, N.; Tagmatarchis, N.; Tasis, D. *Chem. Rev.* **2010,** *110,* 5366–5397. doi:10.1021/cr100018g
16. Bekyarova, E.; Sarkar, S.; Wang, F.; Itkis, M. E.; Kalinina, I.; Tian, X.; Haddon, R. C. *Acc. Chem. Res.* **2013,** *46,* 65–76. doi:10.1021/ar300177q
17. Peng, X.; Wong, S. S. *Adv. Mater.* **2009,** *21,* 625–642. doi:10.1002/adma.200801464
18. Tsai, P.-A.; Kuo, H.-Y.; Chiu, W.-M.; Wu, J.-H. *J. Nanomater.* **2013,** 937697. doi:10.1155/2013/937697
19. Lobo, M. J.; Miranda, A. J.; Tuñón, P. *Electroanalysis* **1997,** *9,* 191–202. doi:10.1002/elan.1140090302
20. Zhang, M.; Mullens, C.; Gorski, W. *Anal. Chem.* **2007,** *79,* 2446–2450. doi:10.1021/ac061698n
21. Ambrosi, A.; Pumera, M. *J. Phys. Chem. C* **2011,** *115,* 25281–25284. doi:10.1021/jp209734t
22. Wang, L.; Ambrosi, A.; Pumera, M. *Anal. Chem.* **2013,** *85,* 6195–6197. doi:10.1021/ac4010748
23. Batchelor-McAuley, C.; Wildgoose, G. G.; Compton, R. G.; Shao, L.; Green, M. L. H. *Sens. Actuators, B* **2008,** *132,* 356–360. doi:10.1016/j.snb.2008.01.049
24. Pumera, M.; Ambrosi, A.; Chng, E. L. K. *Chem. Sci.* **2012,** *3,* 3347–3355. doi:10.1039/c2sc21374e
25. Ma, X.; Jia, L.; Zhang, L.; Zhu, L. *Chem. – Eur. J.* **2014,** *20,* 4072–4076. doi:10.1002/chem.201304311
26. Chia, X.; Ambrosi, A.; Pumera, M. *Electrochem. Commun.* **2014,** *38,* 1–3. doi:10.1016/j.elecom.2013.10.016
27. Devaux, X.; Vigolo, B.; McRae, E.; Valsaque, F.; Allali, N.; Mamane, V.; Fort, Y.; Soldatov, A. V.; Dossot, M.; Tsareva, S. Y. *ChemPhysChem* **2015,** *16,* 2692–2701. doi:10.1002/cphc.201500248
28. Battie, Y.; Dossot, M.; Allali, N.; Mamane, V.; Naciri, A. E.; Broch, L.; Soldatov, A. V. *Carbon* **2016,** *96,* 557–564. doi:10.1016/j.carbon.2015.09.066
29. Allali, N.; Mamane, V. *Tetrahedron Lett.* **2012,** *53,* 2604–2607. doi:10.1016/j.tetlet.2012.03.042
30. Li, F.; Diaz, R.; Ito, T. *RSC Adv.* **2011,** *1,* 1732–1736. doi:10.1039/c1ra00471a
31. Woodbridge, C. M.; Pugmire, D. L.; Johnson, R. C.; Boag, N. M.; Langell, M. A. *J. Phys. Chem. B* **2000,** *104,* 3085–3093. doi:10.1021/jp993235+
32. Plimpton, S. *J. Comput. Phys.* **1995,** *117,* 1–19. doi:10.1006/jcph.1995.1039
33. Aktulga, H. M.; Fogarty, J. C.; Pandit, S. A.; Grama, A. Y. *Parallel Comput.* **2012,** *38,* 245–259. doi:10.1016/j.parco.2011.08.005
34. Mattsson, T. R.; Lane, J. M. D.; Cochrane, K. R.; Desjarlais, M. P.; Thompson, A. P.; Pierce, F.; Grest, G. S. *Phys. Rev. B* **2010,** *81,* 054103. doi:10.1103/physrevb.81.054103
35. Nosé, S. *J. Chem. Phys.* **1984,** *81,* 511–519. doi:10.1063/1.447334
36. Hoover, W. G. *Phys. Rev. A* **1985,** *31,* 1695–1697. doi:10.1103/physreva.31.1695
37. Momma, K.; Izumi, F. *J. Appl. Crystallogr.* **2011,** *44,* 1272–1276. doi:10.1107/s0021889811038970
38. Koch, C. Determination of Core Structure Periodicity and Point Defect Density Along Dislocations. Ph.D. Thesis, Arizona State University, Tempe, AZ, U.S.A., 2002.
39. Zhao, Q.; Zhang, J. *Small* **2014,** *10,* 4586–4605. doi:10.1002/smll.201401567
40. Sato, Y.; Yanagi, K.; Miyata, Y.; Suenaga, K.; Kataura, H.; Iijima, S. *Nano Lett.* **2008,** *8,* 3151–3154. doi:10.1021/nl801364g

License and Terms

Supporting Information

for

Accurate control of the covalent functionalization of single-walled carbon nanotubes for the electro-enzymatically controlled oxidation of biomolecules

Naoual Allali[1,2,3], Veronika Urbanova[1], Mathieu Etienne[1], Xavier Devaux[4], Martine Mallet[1], Brigitte Vigolo[5], Jean-Joseph Adjizian[6], Chris P. Ewels[6], Sven Oberg[3], Alexander V. Soldatov[3], Edward McRae[5], Yves Fort[2], Manuel Dossot*[1] and Victor Mamane*[2,7]

Address: [1]LCPME, UMR CNRS-Université de Lorraine 7564, 405 rue de Vandoeuvre, F-54602 Villers-lès-Nancy, France; [2]SRSMC, UMR CNRS-Université de Lorraine 7565, Campus Victor Grignard, Faculté des Sciences et Technologies, F-54506 Vandoeuvre-lès-Nancy, France; [3]Department of Engineering Sciences and Mathematics, Lulea Technical University, Sweden; [4]IJL, UMR CNRS-Université de Lorraine 7198, Parc de Saurupt - CS 50840, 54011 Nancy Cedex, France; [5]IJL, UMR CNRS-Université de Lorraine 7198, Campus Victor Grignard, Faculté des Sciences et Technologies, 54506 Vandoeuvre-lès-Nancy Cedex, France; [6]IMN, UMR CNRS-Université de Nantes 6502, 2 Rue de la Houssiniere, BP32229, 44322 Nantes Cedex, France and [7]New address: Institut de Chimie de Strasbourg, UMR CNRS-Université de Strasbourg 7177, 1 rue Blaise Pascal, F-67000 Strasbourg, France

Email: Manuel Dossot - manuel.dossot@univ-lorraine.fr; Victor Mamane - vmamane@unistra.fr

* Corresponding author

Additional experimental data

Figure S1A. Global XPS survey spectra of raw HIPCO and HIPCO-H_2SO_4-$FcETG_8$ samples deposited on gold surfaces

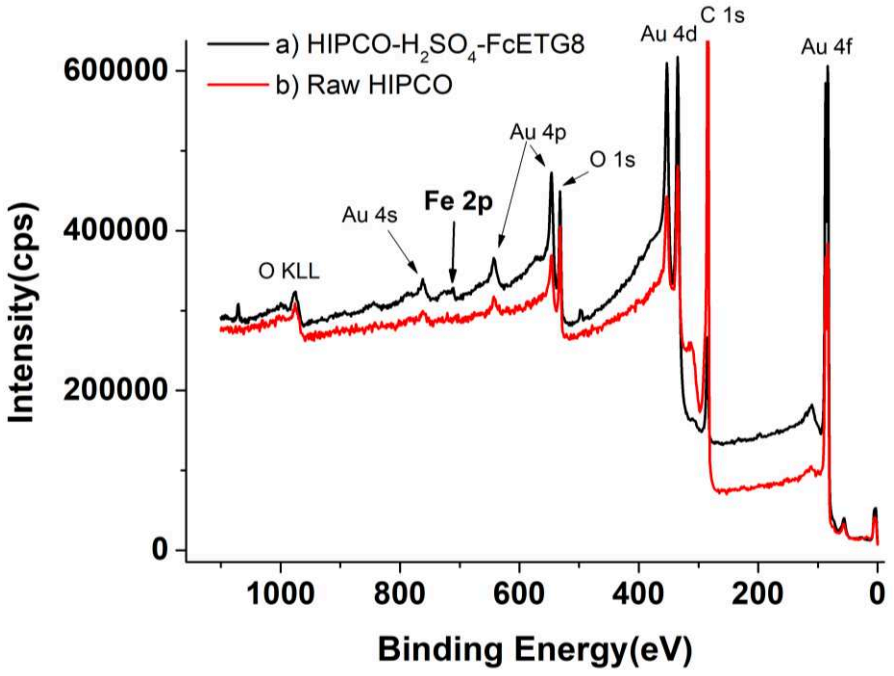

Figure S1B. Detailed XPS spectra in the Fe 2p region for the HiPCO-H_2SO_4-$FcETG_2$ sample

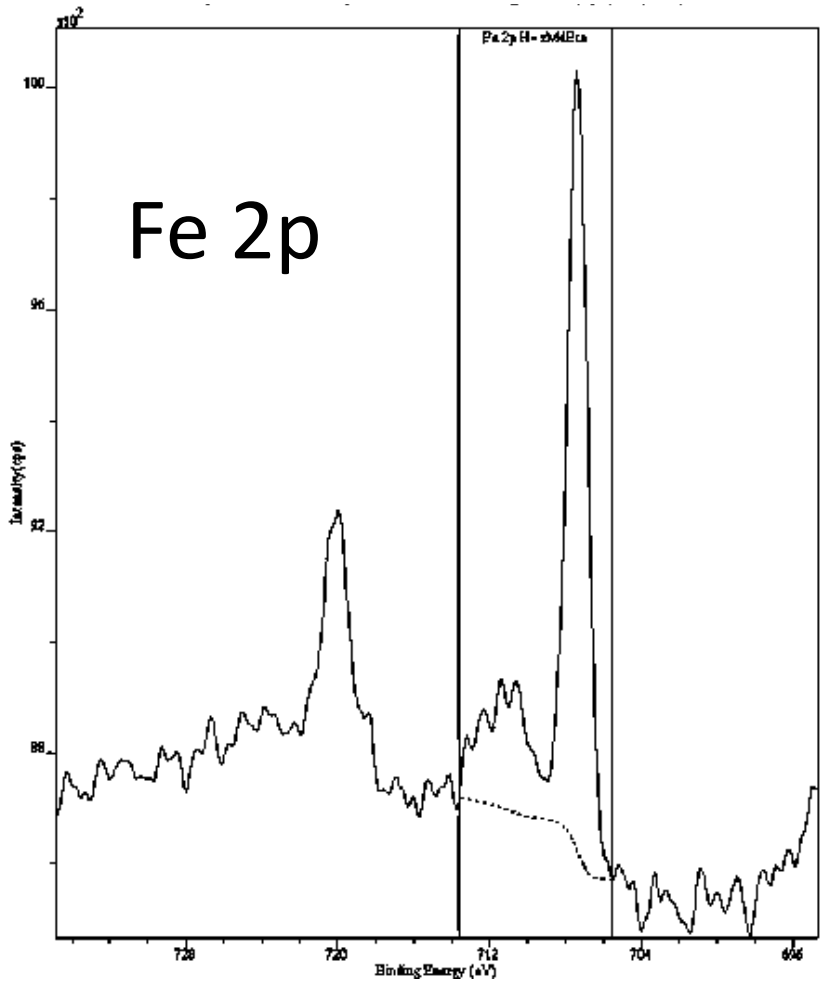

Figure S2. TGA-MS detection of CO and CO2 fragments for A) HIPCO-HNO_3 and B) HIPCO-HNO_3-$FcETG_2$ samples.

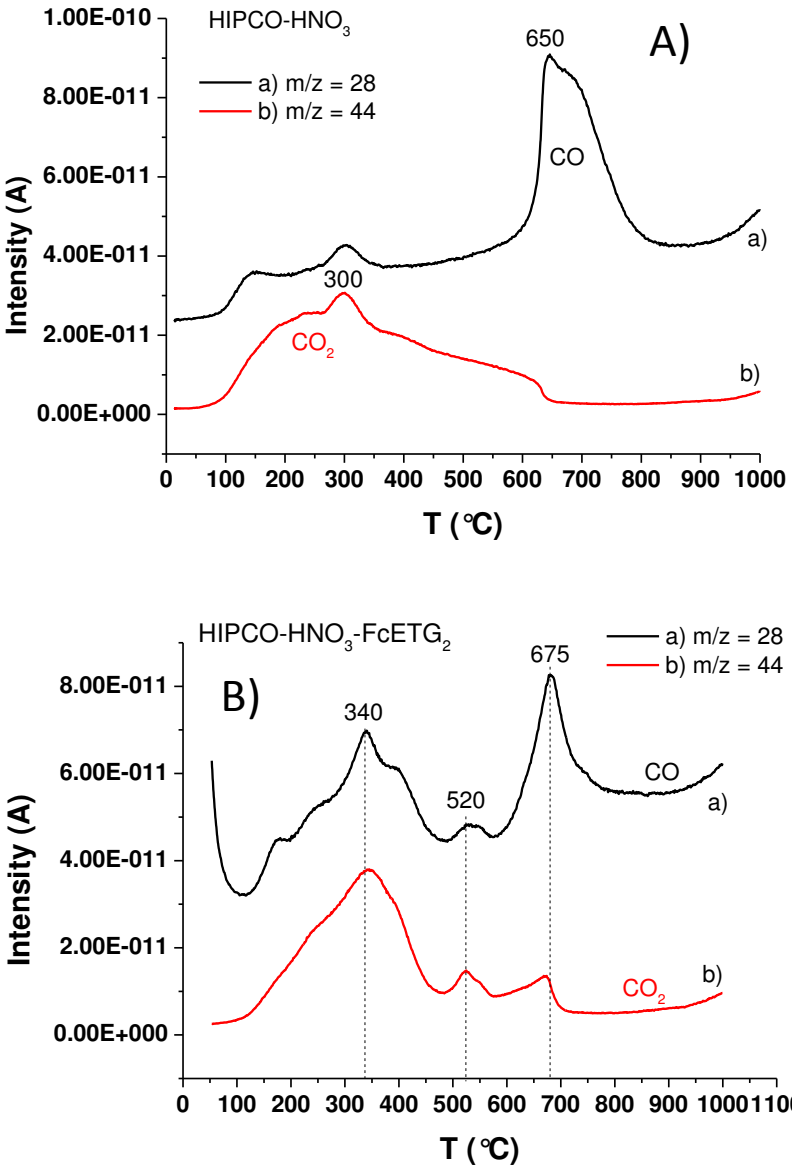

Figure S3. Raman spectra taken using a laser wavelength of 458 nm for samples oxidized by HNO_3 and functionalized with ferrocene derivatives.

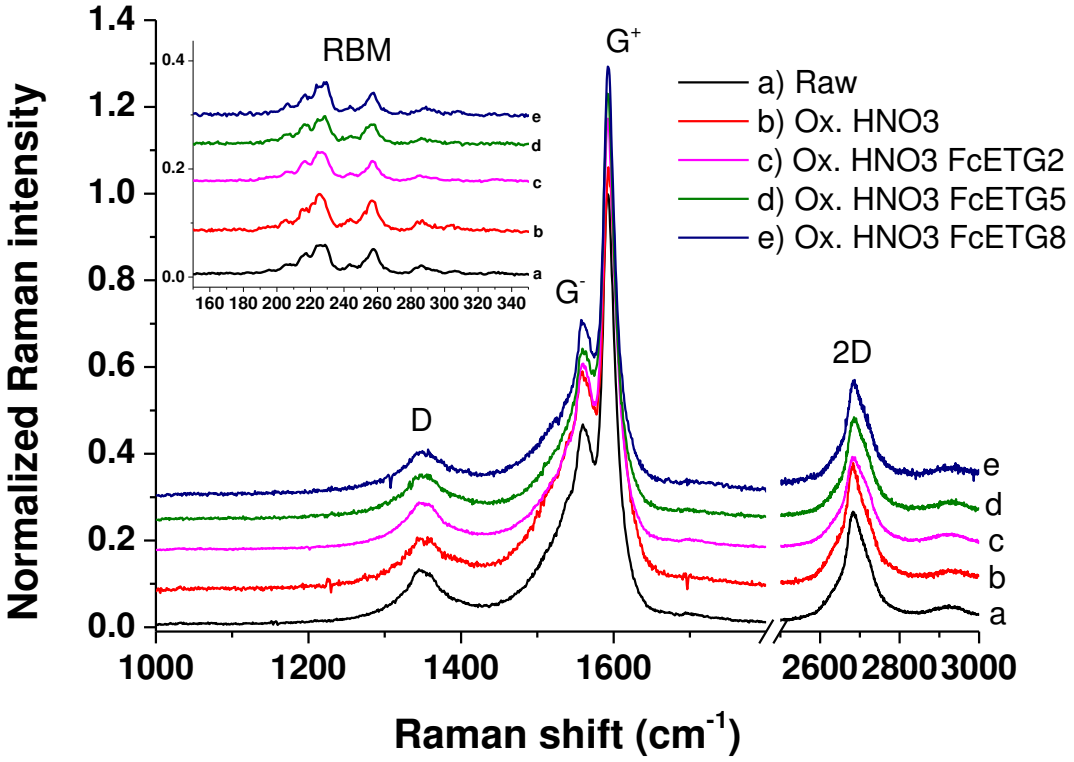

Figure S4. A) Incorporation of the modified GCE in a three-electrode set-up; B) principle of the complete biosensor for glucose detection.

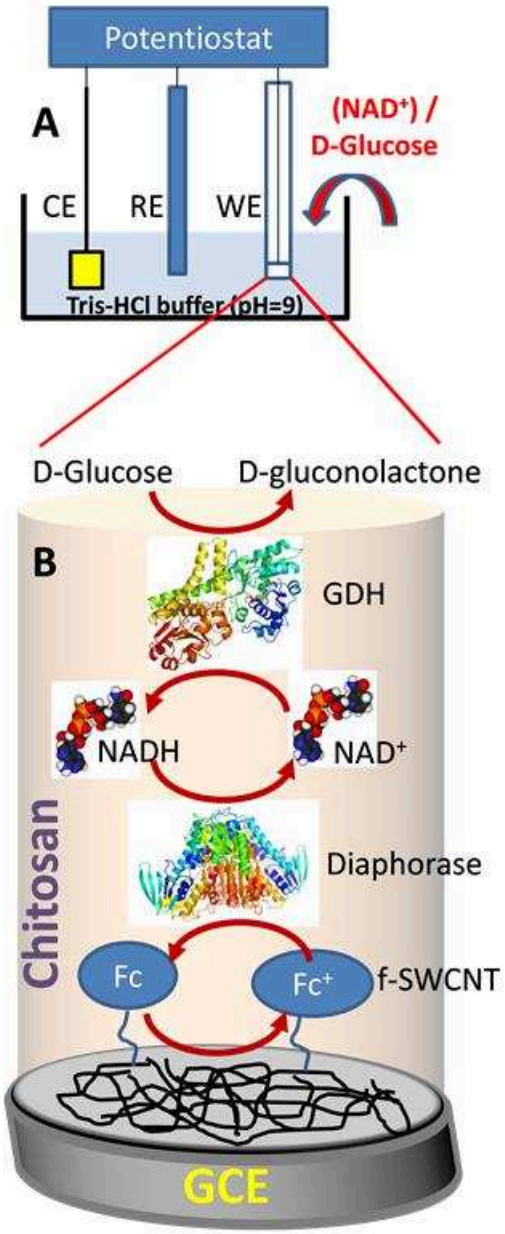

Figure S5. Cyclovoltammogram of HIPCO-HNO_3-FcAlkyl

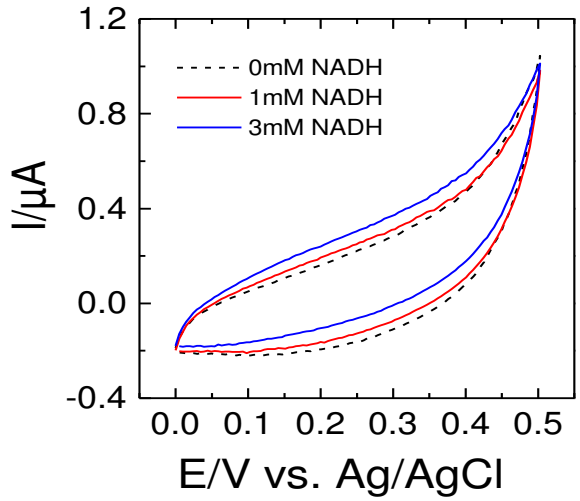

Figure S6. A) Variation of the cyclovoltammogram of HIPCO-H_2SO_4-$FcETG_2$ samples with the scan rate; B) Current intensities of the anodic and cathodic peaks as a function of the scan rate.

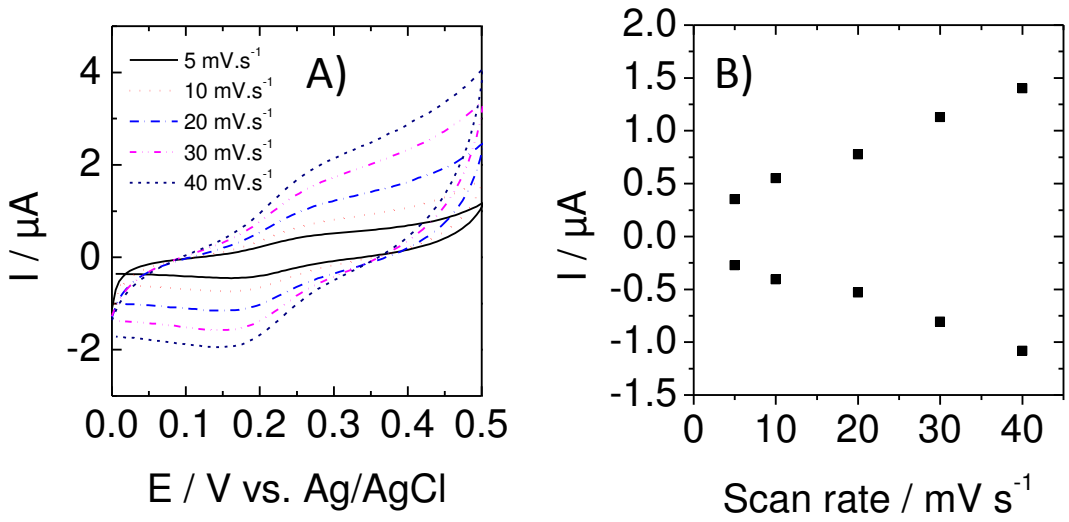

C- Functionalization of multi-walled carbon nanotubes

Paper number 6.

Few-wall carbon nanotubes covalently functionalized by ferrocene groups for bioelectrochemical devices.

Journal:	*2012 MRS Spring Meeting*
Manuscript ID:	MRSS12-1451-DD15-46.R1
Manuscript Type:	Symposium DD
Date Submitted by the Author:	n/a
Complete List of Authors:	Allali, Naoual; SRSMC, Urbanova, Veronika; LCPME, Mamane, Victor; SRSMC, Waldbock, Jérémy; LCPME, Etienne, Mathieu; LCPME, Mallet, Martine; LCPME, Devaux, Xavier; IJL, Vigolo, Brigitte; IJL, Fort, Yves; SRSMC, Walcarius, Alain; LCPME, Noël, Maxime; LTU, Soldatov, Alexander; LTU, McRae, Edward; IJL, Dossot, Manuel; LCPME,
Keywords:	nanostructure, sensor, C

Few-wall carbon nanotubes covalently functionalized by ferrocene groups for bioelectrochemical devices.

Naoual Allali[1, 2,5] , Veronika Urbanova[1], Victor Mamane[2], Jeremy Waldbock[1], Mathieu Etienne[1], Martine Mallet[1], Xavier Devaux[3], Brigitte Vigolo[4], Yves Fort[2], Alain Walcarius[1], Maxime Noël[5], Alexander V. Soldatov[5], Edward McRae[4], Manuel Dossot[1]

1. Laboratoire de Chimie Physique et Microbiologie pour l'Environnement, UMR 7564 CNRS-Lorraine University, F-54602 Villers-les-Nancy, France.
2. Laboratoire de Structure et Réactivité des Systèmes Moléculaires Complexes, UMR 7565 CNRS-Lorraine University, F-54506 Vandoeuvre-les-Nancy, France.
3. Département P2M, Institut Jean Lamour, UMR 7198 CNRS-Lorraine University, Ecole des Mines, F-54042 Nancy, France.
4. Département CP2S, Institut Jean Lamour UMR 7198 CNRS-Lorraine University, F-54506 Vandoeuvre-les-Nancy, France.
5. Department of Engineering Sciences and Mathematics, Lulea Technical University, SE-97187 Lulea, Sweden.

ABSTRACT

The present work reports the covalent functionalization of few-wall CNTs (FWCNTs) by ferrocene derivatives to i) improve their dispersion efficiency in water and ii) to graft electroactive chemical groups on their side-walls in order to promote electron transfer to biomolecules. The functionalized CNTs (f-CNTs) are used to modify a glassy carbon electrode and this modified electrode is used for oxidizing the cofactor NADH (dihydronicotinamide adenine dinucleotide).

INTRODUCTION

Carbon nanotubes (CNTs) are of strong interest for electrochemical applications due to their electronic properties, their high aspect ratio (length/diameter) and their high surface area [1,2]. They have been used in electrochemical devices for bioanalytical applications. In this case, CNTs can be bonded covalently or not to an electron shuttle (also called a mediator) that will be used to react with the electrocatalytic center of a redox protein or to detect electrochemically the NADH cofactor. In this latter case, functionalized CNTs allow reducing overpotentials at the electrodes and can therefore avoid degradation of biomolecules (biofouling) and loss of sensor sensitivity [3-6]. CNTs are also thought to enhance electron transfer efficiency through catalytic effects [1,3,4]. This catalytic effect is still not fully understood and may also involve residual catalytic particles or other carbonaceous species that may be present in the sample [7]. However, it is clear that modifying electrodes with functionalized CNTs, either covalently or non-covalently, strongly increases the sensitivity of the electrochemical devices [3-6]. Multi-walled CNTs (MWCNTs) are often used in the literature due to their lower cost compared to single-wall CNTs [1,2]. However, for MWCNTs the inner tubes may play no role in the electron transfer processes, and single-wall or few-wall (2-4 walls) CNTs (FWCNT) may be a better choice for fundamental studies. The covalent attachment of electroactive groups (electron shuttles) on the side-wall of FWCNTs is a good strategy to avoid any diffusion of the

groups in the analyzed solution. It increases the lifetime of the electrochemical device but the functionalization step has to be controlled enough to avoid destruction of the electronic properties of the functionalized CNTs (f-CNTs). In this work, we report the covalent functionalization of FWCNTs by ferrocene derivatives using a procedure that ensures us to graft enough groups to obtain a good electrochemical signal but also to retain the intrinsic electronic properties of the tubes. The ferrocene electroactive group is chosen as the electron shuttle and is attached to the CNT side-walls through an ethylene glycol spacer of variable chain length. The covalent nature of the functionalization is assessed through the combined use of spectroscopic, thermal and microscopic techniques. An electrochemical biosensor is then made using a glassy carbon electrode incorporating a film of f-CNTs. The electrode is then tested with the $NADH/NAD^+$ redox couple. NADH is indeed the cofactor of more than 300 enzymes of interest and is thus a primary target of interest for bioelectrochemical devices [1].

EXPERIMENTS

Materials and methods

All chemical compounds used for the functionalization steps (scheme 1) were of high purity grade and used as received. A carbon nanotube batch claimed to contain SWCNTs was bought from Nanolabs Inc but HR-TEM experiments have revealed that the sample mainly contained double-walled and three-walled CNTs, few SWCNTs, and few MWCNTs (data not shown). The sample was initially oxidized by Nanolabs through a thermal reflux in concentrated nitric acid solution and sold as containing about 7% of COOH functions. However, our preliminary experiments with this raw batch indicated that this amount was actually less than 2%. This is why a second oxidation process was applied on this sample (step 1 in scheme 1). Briefly, FWCNTs were dispersed in nitric acid (65% in weight) and submitted to a microwave irradiation for 20 min at 50°C. Then, the COOH functions were converted to COCl using a $SOCl_2$ treatment. Finally, the ferrocene derivatives noted as Fc-ETG-n were reacted through their alcohol function with the COCl groups to covalently attach the electron shuttles to the CNT side-walls. The corresponding f-CNTs are noted as CNT-Fc-ETGn. We studied ethylene glycol spacers of different chain lengths from n=0 to n=4. The f-CNTs have been studied using Raman scattering and X-ray photoelectron (XPS) spectroscopies, high resolution transmission electron microscopy (HRTEM) coupled to energy dispersive X-Ray spectroscopy (EDS) analyses, and thermogravimetric analysis (TGA) experiments.

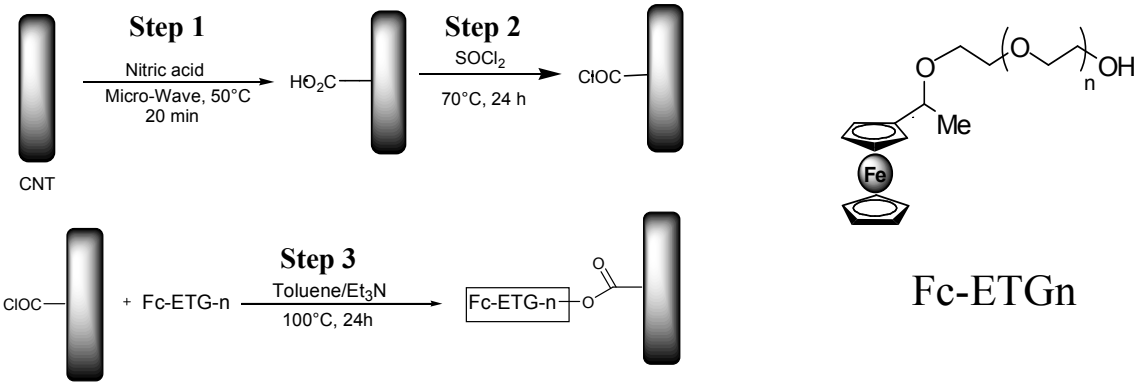

Scheme 1: Functionalization process of FWCNTs by ferrocene derivatives.

RESULTS AND DISCUSSION

Figure 1 shows HRTEM micrographs of the raw CNT sample (a and b) and of the CNTs oxidized by microwave irradiation in nitric acid solution (c). One can see that the oxidative treatment has brought about two detectable effects: a shortening of the tube length (opened tubes are obtained) and also an opening of the CNT walls. The covalent grafting of ferrocene derivatives on oxidized CNTs did not show any obvious difference from the oxidized sample by TEM. EDS analysis has shown that the sample contains some residual catalytic particles of iron covered by carbon layers.

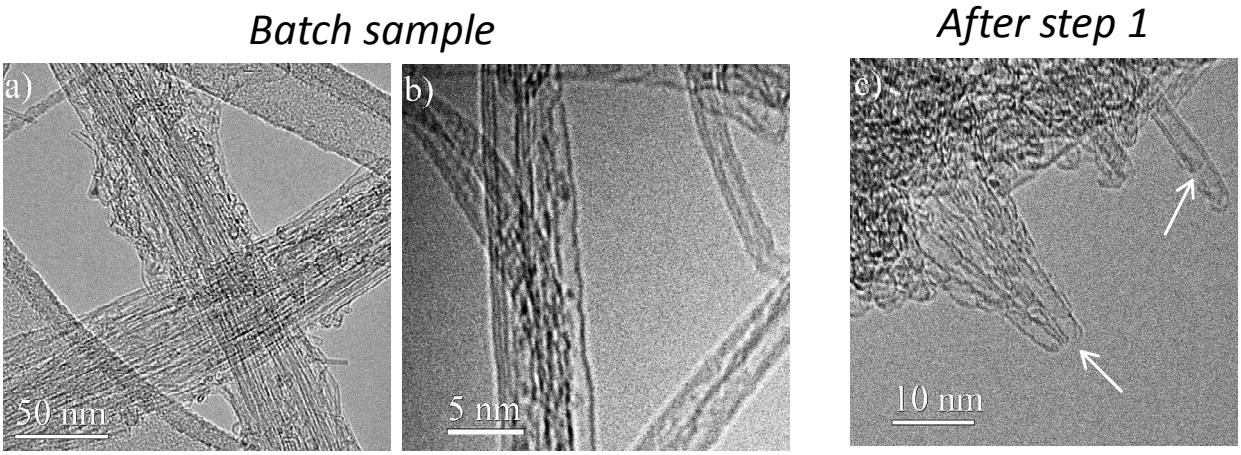

Figure 1: HRTEM images of the raw CNT sample (a, b) and CNTs oxidized through step 1 in scheme 1. Arrows in c) show the opening of CNTs and creation of defects.

Figure 2 reports the results of TGA experiments realized under helium gas for raw, oxidized and functionalized (CNT-Fc-ETG2) samples. The raw sample shows a monotonic loss of weight until 800°C. This can be related to the desorption of existing chemical functions (e.g. alcohol, quinone groups) present on the surface of the raw sample, and maybe residual solvent molecules adsorbed on the surface or inside the bundles (the raw tubes were chemically treated by the manufacturer). For oxidized CNTs, the slope of the weight loss curve is more pronounced between 300 and 500°C, certainly due to a higher number of functional groups, mainly COOH functions created through the oxidation step. The steepest slope is observed around 500°C and above this temperature, the curve is almost parallel to that observed for raw CNTs. For CNT-Fc-ETG2, the rate of the weight loss is strongly increased between 250 and 450°C. We attribute this significant weight loss to the desorption of the ferrocene derivatives. Mass spectrometry coupled to TGA analyses have indeed confirmed that iron atoms and cyclopentadienyl cycles are desorbed in this range of temperatures (data not shown). These results confirm the functionalization of CNTs by ferrocene derivatives. From the weight loss and the quantity of CNT powder used for these experiments, one can estimate the number of COOH groups created during the oxidation step and the number of ferrocene derivatives attached to CNT side-walls. The calculation yields 1 carbon atom per 43 is oxidized to the COOH state and that ca. 1 carbon atom per 118 is functionalized. This means that not all COOH functions have covalently reacted with ferrocene derivative (the value is indeed ca. 100×43/118=36.5%), maybe due to steric hindrance of the grafted groups.

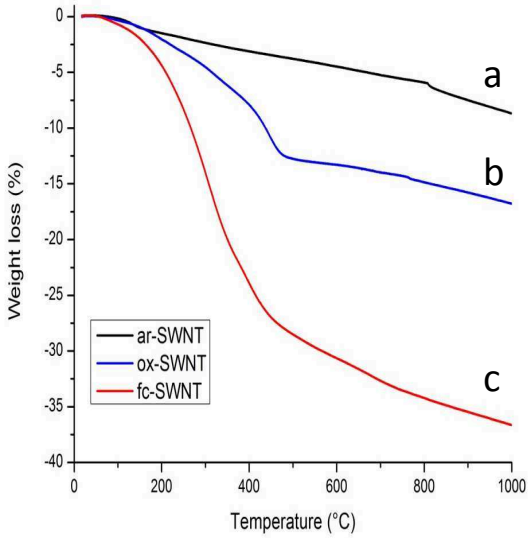

Figure 2: TGA analyses of a) raw FWCNT sample, b) FWCNTs oxidized in step 1 of scheme 1 and c) CNT-Fc-ETG2 functionalized sample.

To corroborate the TGA conclusions, we performed XPS analyses of the raw, oxidized and functionalized CNT samples. Table 1 summarizes the obtained results. It can be seen that the oxidation process increases the number of C-O and HO-C=O functions on tube side-walls in agreement with the TGA observations. Elemental iron is also detectable only for f-CNTs. Since XPS probes only the surface of the CNT bundles, it is not sensitive to the residual catalytic iron particles detected in EDS and buried in carbon layers. Only iron atoms coming from ferrocene derivatives grafted on the surface of CNTs are detected by XPS. The relative atomic ratio of Fe to C (column 5 of Table 1) is maximal for the CNT-Fc-ETG2 sample.

sample	% Fe	%O	%C	100X(%Fe/%C)	C sp2 (284.2 eV)	C sp3 (285 eV)	C-O (286.2 eV)	HO-C=O (288 eV)	C-O + HO-C=O
raw	0.0	4.0	96.0	0.0	74.4	18.1	7.2	0.0	7.2
oxidized µW	0.0	11.7	88.3	0.0	70.5	15.6	11.7	2.3	13.9
CNT-Fc-ETG0	1.1	12.9	86.0	1.2	58.1	24.0	14.6	3.3	17.9
CNT-Fc-ETG2	1.3	21.0	77.7	1.7	57.4	21.4	13.7	7.7	21.4
CNT-Fc-ETG4	0.8	14.0	85.2	0.9	51.6	26.7	17.1	4.6	21.6

Table 1: XPS quantification of elements (Fe, O, C) and C 1s contributions.

To confirm that the CNT structure has not suffered from the oxidation and functionalization steps, Figure 3 shows the Raman spectra in the D and G mode regions for raw, oxidized and CNT-Fc-ETG4 samples taken with a laser wavelength of 514 nm. No significant change of the D/G ratio is observable for these three samples. Same results have been obtained using 458, 488, 532 and 632 nm (data not shown) so that many Raman resonance conditions have been used to probe a large distribution in CNT diameters. These spectroscopic results confirm that oxidized and functionalized CNTs have kept a good structure with negligible increase of the D band. They also indicate that the oxidation process (step 1 in Scheme 1) mainly converts some existing defects to oxidized COOH functions. It is difficult to estimate the quantity of newly created defects due to the nonlinear relationship between the D band intensity and the density of defects, but we can say that the structure has not significantly deteriorated.

Also the grafting of ferrocene derivatives on the COOH functions does not markedly introduce new covalent defects since the D band intensity is not increased if compared to the oxidized sample. This could be expected for a sample containing mainly FWCNTs: the inner tubes are not affected by the functionalization process and maintain their structural and electronic properties.

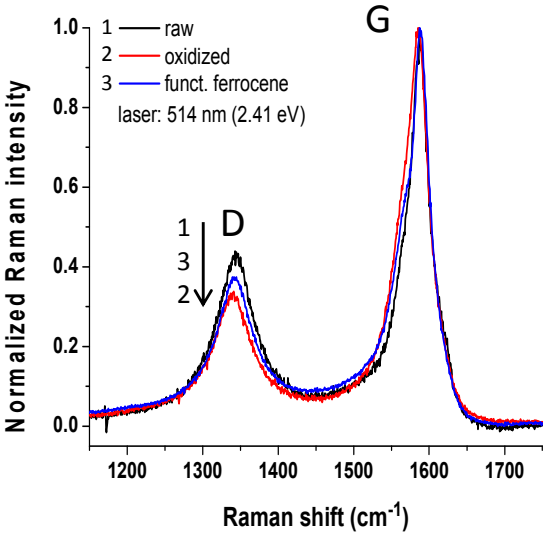

Figure 3: Raman scattering spectra (D and G bands) of raw, oxidized and functionalized (CNT-Fc-ETG4) FWCNTs.

The spectroscopic, thermal and microscopic studies have shown successful functionalization of FWCNTs by ferrocene derivatives. We consequently used these f-CNTs to electrochemically detect NADH. A functional film is deposited on the surface of a glassy carbon electrode (GCE) via the evaporation of a drop of f-CNT suspension mixed with diaphorase and chitosan molecules. Chitosan is a natural biopolymer well-known to ease the dispersion of CNTs in water and to form a durable film on electrodes [4,5,6]. Figure 4 (A) shows ten consecutive cyclic voltammograms of the modified GCE electrode using CNT-Fc-ETG1 sample. The ferrocene electrochemical signal is clearly visible and stable, which indicates that the ferrocene derivatives are immobilized at the CNT surface. We then investigated the electrocatalytic response of the f-CNT modified GCE towards oxidation of NADH. Firstly, we performed a control experiment using oxidized-only CNTs. Figure 4 (B) shows the voltammograms of the GCE electrode modified using these oxidized CNTs without and with 2.5 mM of NADH in solution. Figure 4 (C) shows the same kind of results obtained with CNT-Fc-ETG1 sample and the corresponding evolution of the cyclic voltamograms obtained in the presence of increasing concentrations of NADH in solution. As can be seen the oxidation peak is significantly increased with continuous addition of NADH indicating an efficient electrocatalytic effect with ferrocene-grafted CNTs while for oxidized-only CNTs, no electrocatalytic effect is detected in the wider range of electrode potential explored. The electrocatalytic response of CNT-Fc-ETG1 sample (same results were obtained with the other linkers), in conjunction with the spectroscopic and thermal experiments, confirms that the f-CNTs have been covalently modified by the ferrocene derivatives. Control experiments with non-functionalized CNTs have also shown no detectable signal at this potential in the presence of NADH (data not shown).

CONCLUSIONS

Using a combination of spectroscopic, thermal and microscopic techniques, we have shown that CNTs have been covalently functionalized by ferrocene derivatives. These f-CNTs have been used to modify a glassy carbon electrode and tested towards the oxidation of NADH in aqueous solution. The results demonstrate the usefulness of such covalently-modified CNTs in view of their potential application as a component of an electrochemical biosensor. Future work will be devoted to the realization of a complete bioelectrochemical device including NADH, diaphorase and an enzyme of interest such as glucose dehydrogenase.

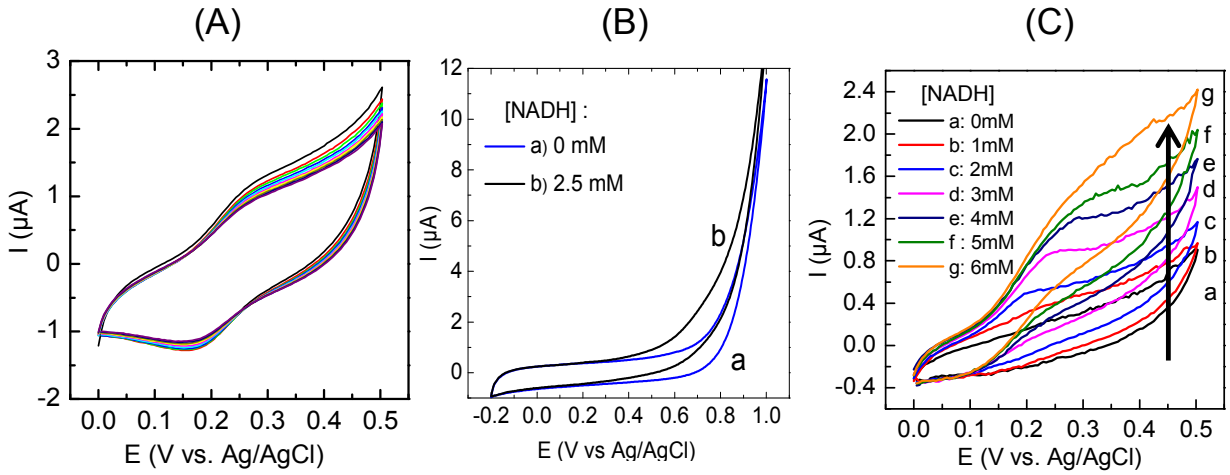

Figure 4: (A) First ten consecutive cyclic voltammograms recorded on a GCE modified with a chitosan/CNT-Fc-ETG1 film (B) Cyclic voltamograms measured on a GCE modified with a chitosan/oxidized FWCNT film without (a) and with (b) 2.5 mM of NADH in the solution (C) Cyclic voltamograms measured on a GCE modified with a chitosan/CNT-Fc-ETG1 film in the presence of increasing concentrations of NADH in the solution. All measurements performed in 0.1 mol L^{-1} tris-HCl buffer (pH = 9) at a scan rate of 20 mV s^{-1}.

ACKNOWLEDGMENTS

This work has been supported by the French National Research Agency (ANR), project ANR-10-BLAN-0819-01-SPRINT.

REFERENCES

1. S. K. Vashist, D. Zheng, K. Al-Rubeaan, J. H. T. Luong and F.S. Sheu, *Biotechnol. Adv.*, **29**, 169 (2011).
2. A. Qureshi, W. P. Kang, J. L. Davidson and Y. Gurbuz, *Diam. Relat. Mater.*, **18**, 1401 (2009).
3. A. Radoi, D. Compagnone, M.A. Valcarcel, P. Placidi,S. Materazzi, D. Moscone and G. Palleschi, *Electrochim. Acta*, **53**, 2161 (2008).
4. Z. Wang, M. Etienne, S. Pöller, W. Schuhmann, G. W. Kohring, V. Mamane and A. Walcarius, *Electroanalysis*, **24**, 376 (2012).
5. M. Wooten and W. Gorski, *Anal. Chem.*, **82**, 1299 (2010).
6. M. Zhang, A. Smith and W. Gorski, *Anal. Chem.*, **76**, 5045 (2004).
7. M. C. Henstridge, L. Shao, G. G. Wildgoose, R. G. Compton, G. Tobias and M. L. H. Green, *Electroanalysis*, **20**, 498 (2008).

Paper number 7.

Phys. Status Solidi B **249,** No. 12, 2349–2352 (2012) / **DOI** 10.1002/pssb.201200098

physica status solidi b
www.pss-b.com
basic solid state physics

Covalent functionalization of few-wall carbon nanotubes by ferrocene derivatives for bioelectrochemical devices

Naoual Allali[1,2,3], Veronika Urbanova[1], Victor Mamane[2], Jeremy Waldbock[1], Mathieu Etienne[1], Martine Mallet[1], Xavier Devaux[4], Brigitte Vigolo[5], Yves Fort[2], Alain Walcarius[1], Maxime Noël[3], Alexander V. Soldatov[3,6], Edward McRae[5], and Manuel Dossot[*,1]

[1] Laboratoire de Chimie Physique et Microbiologie pour l'Environnement, UMR 7564 CNRS–Université de Lorraine, 54602 Villers-les-Nancy, France
[2] Laboratoire de Structure et Réactivité des Systèmes Moléculaires Complexes, UMR 7565 CNRS–Université de Lorraine, 54506 Vandoeuvre-les-Nancy, France
[3] Department of Engineering Sciences and Mathematics, Luleå University of Technology, 97187 Luleå, Sweden
[4] Insitut Jean Lamour, Department P2M, UMR 7198 CNRS–Université de Lorraine, Ecole des Mines, 54042 Nancy, France
[5] Insitut Jean Lamour, Department CP2S, UMR 7198 CNRS–Université de Lorraine, 54506 Vandoeuvre-les-Nancy, France
[6] Department of Physics, Harvard University, Cambridge, MA 02138, USA

Received 29 April 2012, revised 24 July 2012, accepted 14 September 2012
Published online 26 October 2012

Keywords carbon nanotubes, electrochemical sensors, ferrocene, functionalization, NADH

* Corresponding author: e-mail dossot@lcpme.cnrs-nancy.fr, Phone: +0033 383 685 249, Fax: +0033 383 275 444

The present work reports the covalent functionalization of few-wall CNTs (FWCNTs) by ferrocene derivatives to (i) improve their dispersion efficiency in water and (ii) graft electroactive chemical groups on their side-walls in order to promote electron transfer to biomolecules. The functionalized CNTs (f-CNTs) are used to modify a glassy carbon electrode and this modified electrode is used for oxidizing the cofactor NADH (dihydronicotinamide adenine dinucleotide).

1 Introduction Carbon nanotubes (CNTs) are of strong interest for electrochemical applications due to their electronic properties, their high aspect ratio (length/diameter) and their high surface area [1, 2]. They have been used in electrochemical devices for bioanalytical applications. In this case, CNTs can be functionalized (covalently or not) with an electron shuttle (also called a mediator) that can be used to react with the electrocatalytic centre of a redox protein or to detect electrochemically the NADH cofactor. Indeed, functionalized CNTs allow reducing overpotentials at the electrodes and can therefore avoid degradation of biomolecules (biofouling) and loss of sensor sensitivity [3–6]. CNTs are also thought to enhance electron transfer efficiency through catalytic effects [1, 3, 4]. These effects are still not fully understood and may also involve residual catalytic particles or other carbonaceous species that can be present in the sample [7]. However, it is clear that modifying electrodes with functionalized CNTs, either covalently or non-covalently, strongly increases the sensitivity of the electrochemical devices [3–6]. Multi-walled CNTs (MWCNTs) are often used in the literature due to their lower cost compared to single-wall CNTs [1, 2]. However, for MWCNTs the inner tubes may play no role in the electron transfer processes, and single-wall or few-wall (2–4 walls) CNTs (FWCNT) could be a better choice for fundamental studies. The covalent attachment of electroactive groups (electron shuttles) on the side-wall of FWCNTs is a good strategy to avoid any loss of these groups by diffusion in the analysed solution, therefore increasing the lifetime of the electrochemical device. But the functionalization step has to be carefully controlled to avoid destruction of the electronic properties of the CNTs. In this work, we report the covalent functionalization of FWCNTs by ferrocene derivatives using a procedure that ensures us to graft enough groups to obtain a good electrochemical signal but also to retain the intrinsic electronic properties of the tubes. The ferrocene electroactive group is chosen as a model electron shuttle and is attached to the CNT side-walls through a (poly)ethylene

glycol (ETG) spacer of variable chain length. The covalent nature of the functionalization is assessed through the combined use of thermal and spectroscopic techniques. An electrochemical biosensor is then built by depositing a film of functionalized CNTs (f-CNTs) onto the surface of a glassy carbon electrode (GCE). The electrode is tested with the NADH/NAD^+ redox couple. NADH is indeed the cofactor of more than 300 enzymes of interest and is thus a primary target of interest for bioelectrochemical devices [1].

2 Experimental

2.1 CNT sample and grafting method All chemicals used for the functionalization steps (Fig. 1) were of high purity grade and used as received. A CNT batch claimed to contain SWCNTs was bought from Nanolabs, Inc., but HRTEM experiments revealed that the sample mainly contained double- and three-walled CNTs, a few SWCNTs, and a few MWCNTs (data not shown). We refer to this as a "FWCNT sample." As received Nanolabs CNTs were claimed by the manufacturer to contain about 7% (i.e. 7 C atoms per 100) of COOH functions, originating from a thermal reflux in concentrated nitric acid solution, but our preliminary experiments with this raw batch indicated that this amount was actually <2%. This is why a second oxidation process was applied on this sample (step 1 in Fig. 1). Briefly, the FWCNT sample was dispersed in nitric acid (65% in weight) and submitted to a microwave irradiation for 20 min at 50 °C. The COOH functions were converted to COCl using a $SOCl_2$ treatment. Finally, the ferrocene derivatives noted as Fc-ETGn and synthetized according to Ref. [8] reacted through their alcohol function with the COCl groups to covalently attach the electron shuttles to the CNT side-walls. We studied ethylene glycol spacers of different chain lengths from $n = 0$ to $n = 4$.

2.2 Analytical methods Raw (i.e. as received), oxidized and functionalized CNTs have been studied using Raman scattering and X-ray photoelectron (XPS) spectroscopies, high resolution transmission electron microscopy (HRTEM) and thermo-gravimetric analysis (TGA) experiments. They have been also deposited onto GCE for cyclic voltammetry characterization.

3 Results and discussion

Figure 2 reports the results of TGA experiments performed under helium gas for raw, oxidized and functionalized (Fc-ETG2) samples. The raw sample shows a monotonic loss of weight up to 800 °C. This can be related to the desorption of existing chemical functions (e.g. alcohol, quinone groups) present on the surface of the raw sample, and maybe residual solvent molecules adsorbed on the surface or inside the bundles (the raw tubes were chemically treated by the manufacturer). For oxidized CNTs, the slope of the weight loss curve is more pronounced between 300 and 500 °C, certainly due to a higher number of functional groups, mainly COOH functions created through the oxidation step. The steepest slope is observed around 500 °C and above this temperature, the curve is almost parallel to that observed for raw CNTs. For f-CNTs (with Fc-ETG2 ferrocene derivative), the rate of the weight loss is strongly increased between 250 and 450 °C. We attribute this significant weight loss to the desorption of the ferrocene derivatives. Mass spectrometry coupled to TGA analyses have indeed confirmed that iron atoms and cyclopentadienyl cycles are desorbed in this temperature range (data not shown). These results confirm the functionalization of CNTs by ferrocene derivatives. From the weight loss and the quantity of CNT powder used for these experiments, one can estimate the number of COOH groups created during the oxidation step and the number of ferrocene derivatives attached to CNT side-walls. The

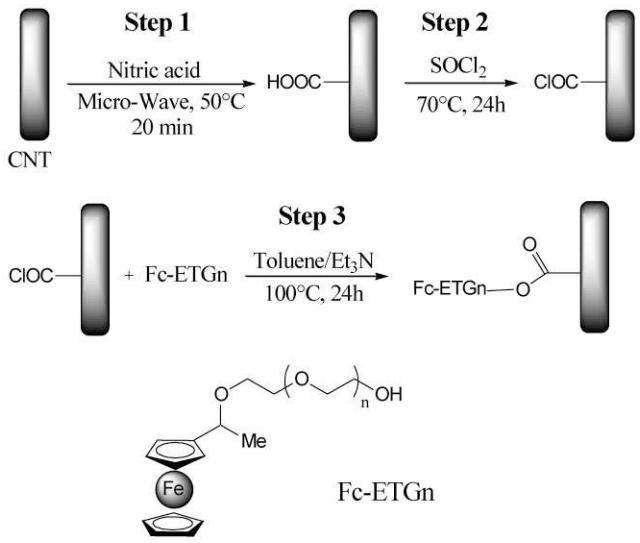

Figure 1 Functionalization process of FWCNT sample by ferrocene derivatives.

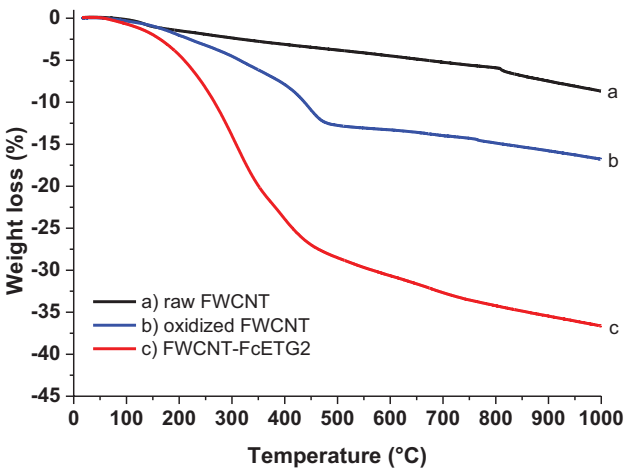

Figure 2 (online colour at: www.pss-b.com) TGA analyses of (a) raw FWCNT sample, (b) FWCNT sample oxidized in step 1 of Fig. 1 and (c) FWCNT sample functionalized by Fc-ETG2 groups.

Table 1 XPS quantification of elements (Fe, O, C) and C 1s contributions.

sample	% Fe	% O	% C
raw	0.0	4.0	96.0
oxidized μW	0.0	11.7	88.3
NTC-Fc-ETG0	1.1	12.9	86.0
NTC-Fc-ETG2	1.3	21.0	77.7
NTC-Fc-ETG4	0.8	14.0	85.2

sample	% C sp^2 (284.2 eV)	% C sp^3 (285 eV)	% C–O + HO–C=O (286.2/288 eV)
raw	74.5	18.2	7.3
oxidized μW	70.5	15.6	13.9
NTC-Fc-ETG0	58.1	24.0	17.9
NTC-Fc-ETG2	57.3	21.3	21.4
NTC-Fc-ETG4	51.6	26.7	21.7

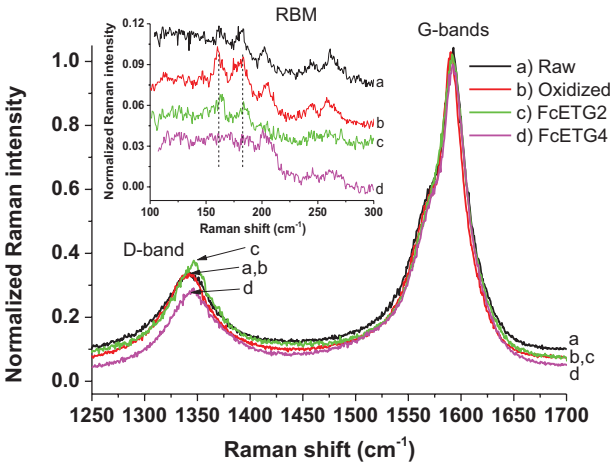

Figure 3 (online colour at: www.pss-b.com) Raman scattering spectra (D, G bands and RBM peaks in inset) of raw, oxidized and functionalized (Fc-ETG2 and Fc-ETG4 groups) FWCNT samples. Laser 514 nm (2.41 eV). Spectra have been normalized to the G band maximal intensity.

calculation yields 1 carbon atom per 43 is oxidized to the COOH state and that ca. 1 carbon atom per 118 is functionalized. This means that not all COOH functions have covalently reacted with ferrocene derivative (the value is indeed ca. $100 \times 43/118 = 36.5\%$), maybe due to steric hindrance of the grafted groups.

To corroborate the TGA conclusions, XPS analyses have been performed on the raw, oxidized and functionalized FWCNT samples. Table 1 summarizes the obtained results. It can be seen that the oxidation process increases the number of C–O and HO–C=O functions on tube side-walls in agreement with the TGA observations. Elemental iron is also detectable only for f-CNTs. Since XPS probes only the outermost surface of the CNT bundles, it is not sensitive to the possible residual catalytic iron particles buried in carbon layers. Only iron atoms coming from ferrocene derivatives grafted on the surface of CNTs are therefore detected by XPS. The slight decrease of iron content in the Fc-ETG4 sample might me due to a more important steric hindrance effect of the grafted groups since the spacer is bigger. More work is currently being done to investigate this possible interesting effect.

To confirm that the CNT structure has not suffered from the oxidation and functionalization steps, Fig. 3 shows the Raman spectra in the D and G mode regions as well as the radial breathing mode (RBM) region for raw, oxidized and f-CNTs (with ETG2 and ETG4 spacers) taken with a laser wavelength of 514 nm. No significant change of the D/G band intensity ratio is observable for the three treated samples. The same conclusion has been obtained from Raman data collected with other laser wavelengths (458, 488, 532 and 632 nm, data not shown) so that many Raman resonance conditions have been used to probe a large distribution in CNT diameters. Some changes can be clearly seen in the RBM region: the oxidation process does not seem to introduce significant changes but for f-CNTs, the intensity of some RBM modes has decreased. These spectroscopic results confirm that (i) oxidized and functionalized CNTs have kept a good structure with negligible increase of the D/G band intensity ratio and (ii) the functionalization process introduces some significant loss of electronic resonance, which is a good hint that the functionalization is covalent. They also indicate that the oxidation process (step 1 in Fig. 1) mainly converts some existing defects to oxidized COOH functions. It is difficult to estimate the quantity of newly created defects due to the absence of any clear linear relationship between the D band intensity and the density of defects, but we can state that the structure has not been significantly deteriorated. Also the grafting of ferrocene derivatives on the COOH functions does not markedly introduce new defects since the D band intensity is not significantly increased if compared to the oxidized sample. This could be expected for a sample containing mainly FWCNTs: the inner tubes are not affected by the functionalization process and maintain their structural and electronic properties. It is worth noting that the RBM modes at low wavenumber (i.e. with bigger diameter) are strongly affected in the Fc-ETG4 sample in Fig. 3: it may indicate that outer tubes (with bigger diameter) are mostly affected by the covalent functionalization process.

Both thermogravimetric analyses and spectroscopic data have proven successful functionalization of FWCNTs by ferrocene derivatives. We consequently used these f-CNTs to electrochemically detect NADH. A functional film was deposited on the surface of a GCE via the evaporation of a drop of f-CNT suspension mixed with diaphorase and chitosan molecules. Diaphorase is used to recycle the created NAD^+ molecules to NADH, while chitosan is a natural biopolymer well-known to ease the dispersion of CNTs in water and to form a durable film on electrodes [4, 5, 6]. Figure 4A shows ten consecutive cyclic voltammograms of the modified GCE electrode using the Fc-ETG1 CNT sample. The characteristic electrochemical signal

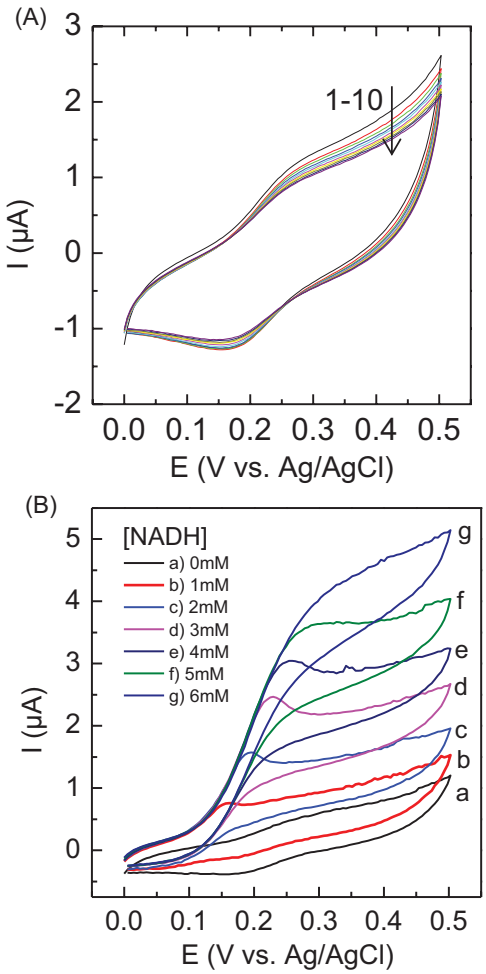

Figure 4 (online colour at: www.pss-b.com) (A) First ten consecutive cyclic voltammograms recorded on a GCE modified with a chitosan/Fc-ETG1 film. (B) Cyclic voltammograms measured on a GCE modified with a chitosan/diaphorase/f-CNTs (Fc-ETG4) film in the presence of increasing concentrations of NADH in the solution. All measurements were performed in 0.1 mol L^{-1} Tris–HCl buffer (pH = 9) at a scan rate of 20 mV s^{-1}.

of the ferrocene/ferricenium couple is clearly visible and stable upon multisweeping, which indicates that the ferrocene derivatives are immobilized at the CNT surface. The same kind of results was obtained for CNTs functionalized with other ETGn groups.

Since the electroactive groups were shown to be grafted to the CNT side-walls, we investigated the electrocatalytic behaviour of the f-CNT (Fc-ETG4) modified GCE towards NADH oxidation. Figure 4B shows the corresponding evolution of the cyclic voltamograms obtained in the presence of increasing concentrations of NADH in solution. As can be seen the oxidation peak significantly increased with progressive addition of NADH indicating an effective electrocatalytic behaviour. This electrocatalytic response, in conjunction with the spectroscopic and thermal experiments, confirms that the f-CNTs have been covalently modified by the ferrocene derivatives. Control experiments with non-functionalized CNTs have revealed no detectable signal at this potential in the presence of NADH (see Figs. S1 and S2 in Supporting Information file).

4 Conclusions Using a combination of thermal and spectroscopic experiments, we have shown that CNTs have been covalently functionalized by ferrocene derivatives. These f-CNTs have been used to modify a GCE and tested towards the oxidation of NADH in aqueous solution. The results demonstrate the usefulness of such covalently modified CNTs in view of their potential application as a durable component of an electrochemical biosensor or bioreactor. Future work will be devoted to the realization of a complete bioelectrochemical device including NADH, diaphorase and an enzyme of interest such as glucose dehydrogenase.

Acknowledgements This work has been supported by the French National Research Agency (ANR), project ANR-10-BLAN-0819-01-SPRINT.

References

[1] S. K. Vashist, D. Zheng, K. Al-Rubeaan, J. H. T. Luong, and F. S. Sheu, Biotechnol. Adv. **29**, 169 (2011).
[2] A. Qureshi, W. P. Kang, J. L. Davidson, and Y. Gurbuz, Diamond Relat. Mater. **18**, 1401 (2009).
[3] A. Radoi, D. Compagnone, M. A. Valcarcel, P. Placidi, S. Materazzi, D. Moscone, and G. Palleschi, Electrochim. Acta **53**, 2161 (2008).
[4] Z. Wang, M. Etienne, S. Pöller, W. Schuhmann, G. W. Kohring, V. Mamane, and A. Walcarius, Electroanalysis **24**, 376 (2012).
[5] M. Wooten and W. Gorski, Anal. Chem. **82**, 1299 (2010).
[6] M. Zhang, A. Smith, and W. Gorski, Anal. Chem. **76**, 5045 (2004).
[7] M. C. Henstridge, L. Shao, G. G. Wildgoose, R. G. Compton, G. Tobias, and M. L. H. Green, Electroanalysis **20**, 498 (2008).
[8] N. Allali and V. Mamane, Tetrahedron Lett. **53**, 2604 (2012).

Summary / Résumé

Bioelectrochemical devices often use the NADH co-factor (nicotinamide adenine dinucleotide) as a biomolecule involved in oxidation-reduction reactions with enzymes of high biochemical interest, such as glucose oxidases or dehydrogenases. It is necessary to use new electrode materials to reduce the over-potentials required for electron transfer with the NADH/NAD^+ system and avoid adsorption of the reaction products to the electrode surface (biofouling). Carbon nanotubes (CNTs) are a conductive material with a large specific surface area that seems promising for modifying the surface of electrodes. This thesis work consisted in developing new methods for covalent grafting of electro-active functional groups with respect to the NADH/NAD^+ system by controlling the various stages of the process with a particularly advanced physico-chemical analysis protocol involving Raman scattering spectroscopy, infrared absorption, X-ray photoelectron spectroscopy, transmission electron microscopy, spectroscopic ellipsometry and thermogravimetric and volumetric adsorption analyses. We have developed a process based on a first step of oxidation of the CNTs by microwave assistance in diluted acid media. This makes it possible to transform existing defects in the wall of the nanotubes (carbon atoms in sp^3 hybridization) into carboxylic acid functions, which will be used in the subsequent steps of the process for covalent grafting of electro-active groups. Thus, the structural integrity of the CNTs, and therefore their excellent electronic and mechanical properties, are preserved. The success of this approach is fully demonstrated in this work both by using purified single-walled nanotubes and multi-walled nanotubes. A clear electrocatalytic effect is obtained with the functional groups derived from ferrocene. The crucial role of the nature of the spacer arm connecting the electro-active units to the wall of the CNTs is also shown. This work made it possible to develop a general method for covalent grafting of CNTs and its step-by-step control. Finally, we show in perspective of this work that it is possible to directly graft the NAD^+ molecule onto the surface of the CNTs.

Les dispositifs bioélectrochimiques utilisent souvent le co-facteur NADH (nicotinamide adénine dinucléotide) comme biomolécule impliquée dans les réactions d'oxydo-réduction avec des enzymes de grand intérêt biochimique, comme par exemple les glucose oxydases ou les déshydrogénases. Il est nécessaire d'utiliser de nouveaux matériaux d'électrode afin de diminuer les sur-potentiels nécessaires au transfert d'électrons avec le système NADH/NAD^+ et éviter l'adsorption des poduits de la réaction à la surface de l'électrode (biofouling). Les nanotubes de carbone (NTCs) constituent un matériau conducteur de grande aire spécifique qui semble prometteur pour modifier ainsi la surface des électrodes. Ce travail de thèse a consisté à développer de nouvelles méthodes de greffage covalent de groupements fonctionnels électro-actifs vis-à-vis du système NADH/NAD^+ en contrôlant les différentes étapes du procédé avec un protocole particulièrement poussé d'analyses physico-chimiques impliquant les spectroscopies de diffusion Raman, d'absorption infrarouge, de photo-électrons X, les microscopies électroniques à transmission, l'ellipsométrie spectroscopique et les analyses thermogravimétriques et de volumétrie d'adsorption. Nous avons développé un procédé reposant sur une première étape d'oxydation des NTCs par assistance micro-ondes dans des milieux acides dilués. Ceci permet de transformer les défauts existant à la paroi des nanotubes (atomes de carbone en hybridation sp^3) pour les convertir en fonction acides carboxyliques, qui serviront dans les étapes ultérieures du procédé au greffage covalent des groupements électro-actifs. Ainsi l'intégrité structurale des NTCs, et donc leurs excellentes propriétés électroniques et mécaniques, sont préservées. Le succès de cette approche est pleinement démontré dans ce travail aussi bien en utilisant des nanotubes monoparois purifiés que des nanotubes multiparois. Un net effet électrocatalytique est obtenu avec les groupes fonctionnels dérivés du ferrocène. On montre également le rôle crucial de la nature du bras espaceur reliant les groupes électro-actifs à la paroi des NTCs. Ce travail a permis de mettre au point une méthode générale de greffage covalent des NTCs et son contrôle étape par étape. On montre enfin en perspective de ce travail qu'il est possible de greffer directement la molécule de NAD^+ à la surface des NTCs.